Investigating the Molecular Mechanisms of CBP/p300 Recruitment by the Transcriptional Regulators MITF and β-catenin

by

Alexandra Dita Rose Brown

Submitted in partial fulfilment of the requirements

for the degree of Doctor of Philosophy

at

Dalhousie University

Halifax, Nova Scotia

July 2023

Dalhousie University is located in Mi'kma'ki, the ancestral and unceded territory of the Mi'kmaq.

We are all Treaty people.

Dedication

To my parents, *Barbara and Andrew*, for always believing in me.

To my sister, *Victoria*, for always being there for me.

To my love, *Nicholas*, for everything else.

Table of Contents

List of Tables

List of Figures

Abstract

CREB-binding protein (CBP) and its homolog p300 (CBP/p300) are sequestered by transcription factors to thousands of promoters and enhancers throughout the human genome, where they modify chromatin structure and enhance gene expression. CBP/p300 also play an important role in the development and progression of human diseases such as cancer, where they stimulate the expression and activity of oncogenic proteins. Utilizing a combination of structural, biophysical, and functional assays I investigate the molecular interactions between CBP/p300 and two oncogenic transcription regulators, Wnt-signaling protein β-catenin and the microphthalmia-associated transcription factor (MITF). With the use of protein pulldown assays, isothermal titration calorimetry, and nuclear magnetic resonance spectroscopy (NMR) I determine that the N-terminal and C-terminal transactivation domains (TAD1 and TAD2, respectively) of MITF and β-catenin are intrinsically disordered and bind with variable affinities to both the transcription adapter zinc finger domains (TAZ1 and TAZ2) of CBP/p300. Using NMR-based chemical-shift perturbation studies I show that the β-catenin TAD1 interacts with TAZ2 at a specific binding interface between helices α-1-α-2-α-3, and that β-catenin TAD2 binds to TAZ2 with extended contacts over α-1-α-4 and to TAZ1 at a hydrophobic groove between α-1-α-2. Mutagenesis studies revealed regions Asp58-Leu103 and Asp750-Leu781 are critical for β-catenin: CBP/p300 binding and for β-catenin transcriptional activation using luciferase-reporter gene assays. I provide the first ever NMR-derived structure of the MITF TAD1 in complex with TAZ2, which was found to form a dynamic ensemble with the hydrophobic TAZ2 surface. I also identify two acidic motifs Arg110-Ala14, Asp334-Asp345, and one serine-rich motif from Ser372-Asp381 integral to maintain MITF: CBP/p300 binding and necessary for MITF transcriptional activity. Furthermore, I develop a peptide inhibitor derived from adenoviral E1A protein that displaces these TAZ2 interactions from MITF and β-catenin *in vitro* and functionally impedes their transcriptional function in cells. Finally, I propose three models in which both β-catenin and MITF TADs may cooperate to recruit CBP/p300 to target gene promoters. These findings provide the high-resolution structural information that would be required to develop targeted therapeutics strategies against CBP/p300 and its interactions in the future.

List of Abbreviations and Symbols Used

δ: Chemical shift

Δδ: Chemical shift change

AC: Adenylate Cyclases

ANOVA: Analysis of Variance

APC: Adenomatous Polyposis Coli

ARM: Armadillo Repeat Domain

Axin: Axis inhibition protein

βCAT: β-catenin

bHLH: Basic helix-loop-helix domain

BRAF: V-raf murine sarcoma viral oncogene homolog B1

BRCA1: Breast cancer gene 1

BRD: Bromodomain

BSA: Bovine Serum Albumin

cAMP: Cyclic Adenosine Monophosphate

CBP: CREB-Binding Protein

ChIP-Seq: Chromatin Immunoprecipitation Sequencing

CITED2: CBP/p300-interacting transactivator with Glu/Asp C-terminal domain 2

CK1α: Casein Kinase 1

CMV: Cytomegalovirus promoter

CR1: Conserved Region 1 domain of E1A

CREB: cAMP-Response Element Binding protein

Cryo-EM: Cryogenic Electron Microscopy

CTERM: C-terminal region

DMEM: Dulbecco's Modified Eagle's Medium

DNA: Deoxyribonucleic Acid

DVL: Disheveled

E1A: Adenoviral Early Region 1 A

FBS: Fetal Bovine Serum

FOXO3: Forkhead Box O3

GB1: B1 domain of *Streptococcus* protein G

GSK-3β: Glycogen Synthase-3

HAT: Histone Acetyltransferase domain

HIF-1α: Hypoxia Inducible Factor 1 subunit α

HPV-16: Human Papillomavirus type 16

HSQC: Heteronuclear Single Quantum Coherence

HTLV-1: T-cell Leukemia Virus type 1

IBiD: IRF-3 Binding Domain

IDP: Intrinsically Disordered Protein

ITC: Isothermal Titration Calorimetry

KIX: Kinase Inducible Domain

LEF: Lymphoid Enhancer Factor

LRP5/6: Lipoprotein Receptor related Protein

MAPK: Mitogen Activated Protein Kinase cascade

MITF: Microphthalmia-associated Transcription Factor

MLL: Mixed Lineage Leukemia

NMR: Nuclear Magnetic Resonance spectroscopy

NOE: Nuclear Overhauser Effect

NRID: Nuclear Receptor Interaction Domain

NTERM: N-terminal region

p300: E1A-binding protein

PAX3: Paired box 3

PDBID: Protein Data Base Identification code

PHD: Plant Homeodomain

PKA: Protein kinase A

Pol II: RNA Polymerase II

RNA: Ribonucleic Acid

SDS-PAGE: Sodium Dodecyl-Sulfate Polyacrylamide Gel Electrophoresis

SOX10: Sry-Box transcription factor 10

SSP: Secondary Structure Propensity

STAT1/2: Signal Transducer and Activator of Transcription

SV40: Simian Virus 40 large T antigen

TAD: Transactivation domain

TAZ: Transcription Adapter Zinc finger domain

TBS-T: Tris-Buffered Saline with 0.1% Tween 20

TCF: T-cell Factor

TFIIB: Transcription factor II B

TFIID: Transcription factor II D

Wnt: Wingless/Integrated

Acknowledgements

This dissertation is a culmination of the past five years I have spent at Dalhousie University, and it would not have been made possible if not for every person who supported me along the way. First and foremost, I would like to express my deepest gratitude to my supervisor David. Thank you for your patience, your time, and your willingness to share your wealth of knowledge with me. Your passion for research is truly admirable and your mentorship has been invaluable, allowing me to grow as both a researcher and an individual. I am confident that this will not be the last of our work together. To my current and former lab mates, Kathleen, Connor, Makenzie, Trilok, Emma, Raymond, Rachael, and Dina, I extend my sincere appreciation. For some of you the efforts of your work are directly presented in the chapters of this thesis, for others you have contributed indirectly by sharing your expertise, but for all of you, you have played an instrumental part in making graduate school so enjoyable for me.

I am grateful for all my committee members, Drs. Denis Dupré, Vanya Ewart, and Paul Liu, for the guidance and support they have given me throughout the course of this project. A significant portion of this work was completed in the lab of Dr. Denis Dupré, I would like to thank him for making me feel welcome and sharing his technical advice with me. Thank you to Dr. Jan Rainey and all the members of the Structural Biology Group for the encouragement and thoughtful feedback they provided me during group meetings. I greatly appreciate Ian Burton from the National Research Council in Halifax for his assistance with NMR data collection, and Dr. Steven Bearne of Dalhousie for the use of his VP-ITC Microcalorimeter.

Furthermore, I would like to acknowledge the Killam Foundation and the Canadian Institutes of Health Research who have made this work possible through their financial support.

Lastly, I want to express my heartfelt thanks to the people who have always been there for me – my family. My sister Victoria is someone who I have always looked up to, and I draw inspiration from seeing her follow her dreams with unwavering determination. My parents Barbara and Andrew encouraged me to pursue this opportunity and provided me with everything I needed to succeed. I thank them for their endless love, their support, and their belief in me. Above all, I could not have undertaken this journey without my partner Nicholas by my side. Through the ups and downs he has been my rock, my confidante, and a steadfast source of laughter and love. Thank you, Nicholas, for keeping me sane throughout this process and for always reminding me to not take life too seriously.

Thank you *all* – your contributions to this work were essential but rest assured that any errors made are entirely my own.

Chapter 1: Introduction

1.1 Intrinsically Disordered Proteins

1.1.1 Definition and Functional Advantages

Prior to the last two decades, the traditional sequence-structure-function model describing proteins remained a central dogma of structural biology. According to this theory, a protein's functionality is dependent on whether it can adopt a stable three-dimensional fold that is encoded by their specific sequence of amino acids (1, 2). The idea that a protein structure is necessary to its function was based on observations that loss of function is often coupled with proteins becoming denatured (3). Nevertheless, large scale genomic studies have predicted that 44% of the human proteome is comprised of polypeptides that do not fold into a well-defined structure, but instead adopt a variety of conformations and remain in a highly dynamic state (4, 5). These proteins are referred to as intrinsically disordered proteins (IDPs) and the discovery that they are able to perform their function while unstructured has led to the emerging disorder-function paradigm, which recognizes that flexibility can be linked to protein function (6).

The study of intrinsic disorder is now a widely discussed and important topic in the field of protein research. IDPs are particularly abundant in cell signaling and regulatory functions such as transcription, translation, and alternative splicing (7). They are well-suited to mediate these biological processes because of their lack of fixed structure, which provides them with certain functional advantages. These advantages include: (i) the accessibility of sites for post-translational modifications

which can help fine tune protein function, (ii) the structural flexibility to bind multiple targets within multi-protein assemblies, (iii) the capability to adopt a variety of binding conformations without steric restrictions to different interaction partners, and (iv) the ability to facilitate interactions with high-specificity but moderate affinity, for rapid association/dissociation in response to cellular stimuli (8, 9).

1.1.2 Prevalence of IDPs in Transcription

Transcription regulation coordinates gene expression by controlling the rate at which DNA sequences are converted into precursor messenger RNA, which can then be processed and translated into proteins (10). In eukaryotes, transcription is governed by a coordinated network of specialized DNA-binding proteins called transcription factors. Initiation of transcription first requires general transcription factors to bind gene promoters adjacent to the coding sequence, which then recruit RNA polymerase II to transcriptional start sites forming the preinitiation complex (11, 12). Only a basal rate of transcription is driven by this preinitiation complex alone. Other specific transcription factors can bind to recognition sequences at promoter or enhancer regions of DNA to influence the transcriptional rate. They do so by recruiting and binding co-activator proteins, which increase the likelihood of a particular gene to be expressed (13).

Transcription regulators are a class of proteins highly enriched in IDPS, with 80-90% of all transcription factors containing extended segments (>30 residues in length) of structural disorder (14). Transcription factors are composed of two major

components, a structured DNA-binding domain which recognizes and binds specific DNA sequences, and disordered transactivation domains (TADs) which contain binding sites for other proteins (15). Transactivation domains are directly linked to transcriptional control, and their unstructured composition allows transcription factors to recruit a variety of co-activators to directly enhance transcription of their target genes (15). In the upcoming section I will discuss a particular transcriptional co-activator CREB-binding protein (CBP) and its closely related homolog p300. CBP/p300 are sequestered by the TADs of numerous different transcription factors to the promoters of over 16,000 genes, where they act as critical transcriptional regulators of the human genome (16).

1.2 Transcriptional Co-activators CBP/p300

1.2.1 Epigenetics and Chromatin Modification

The complexity of human life is not only determined by the billions of base pairs in our genome, but also by the patterns of gene expression that occur without any changes to the nucleotide sequence of our DNA. These fundamental processes are regulated by epigenetics, which control gene activity through chemical modifications at the transcriptional and post-translational levels (17). A critical epigenetic mechanism involves the chemical alteration of DNA following its physical packaging into chromatin, which can render the genome either accessible or inaccessible to the molecular components required for gene expression (18).

Chromatin is made up of repeating units of nucleosomes, which consist of approximately 150 DNA base pairs wrapped around a histone octamer that then form higher orders of chromatin structure (19). Chromatin DNA is repressive to transcription due to its compact structure, which render the genes inaccessible to binding of transcriptional machinery and other co-regulatory proteins (20). However, there are a number of ways in which chromatin can be reversibly modified to influence gene transcription, including the covalent modification of histones through mechanisms of phosphorylation, methylation, and acetylation (21).

Transcription activation is closely associated with histone acetylation, a process that is mediated by histone acetyltransferase enzymes. Histone acetyltransferases catalyze the transfer of an acetyl group from acetyl-CoA to ε-amino groups of conserved lysine residues on histone tails including H3K9, H3K14, H3K18, H4K5, H4K8, and H4K12 (22). This neutralizes the positive charge and weakens histone-DNA interactions, 'relaxing' the chromatin to a more 'open' and transcriptionally active form (22). Two well-known and ubiquitously expressed histone acetyltransferases are CBP and its homolog p300. These two proteins share ~75% sequence similarity, with most of their functional domains located within highly conserved regions (>90% similarity) (23). While in certain circumstances CBP and p300 may take part in distinct cellular roles their structure and function are largely redundant, thus why they are often collectively referred to as CBP/p300 (24, 25).

1.2.2 The Role of CBP/p300 in Transcription

CBP/p300 utilize a variety of methods to carry out their role as transcriptional co-activators. In addition to their primary role as histone modifiers, CBP/p300 can also bind and acetylate DNA-bound transcription factors directly (i.e. CREB, p53, c-Myb, MLL STAT1/2, HIF1-α) modulating their activity (26–31). CBP/p300 also acts as an important scaffold for multi-protein transcriptional complexes, connecting specific transcription factors to the basal transcriptional machinery via direct interactions with general transcription factor II D (TFIID), TFIIB, and RNA polymerase II (32, 33).Through these simultaneous interactions, CBP/p300 bridges the gap between these proteins and stimulates the transcriptional response (Figure 1.1) (34). The critical role of CBP/p300 in gene transcription is further emphasized by the fact that they are a target of many viral oncoproteins including adenoviral early region 1 A (E1A), T-cell leukemia virus type 1 (HTLV-1), human papillomavirus type 16 (HPV-16), and simian virus 40 large T antigen (SV40), which hijack CBP/p300 in order to dysregulate the host's cell cycle (35–38).

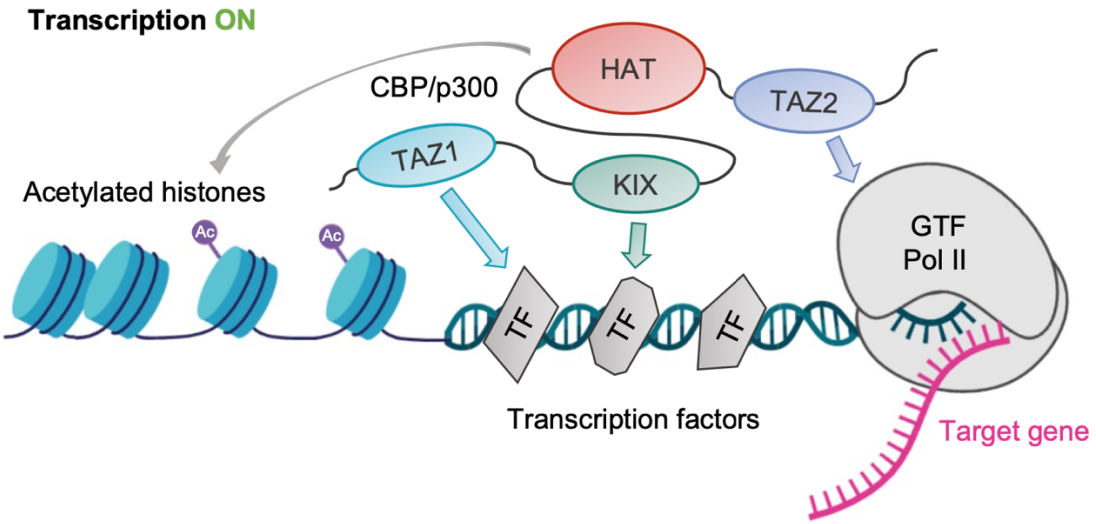

Figure 1.1. Schematic of CBP/p300 gene activation. Transcription co-activation by CBP/p300 is mediated by lysine acetylation on histone tails via its histone acetyltransferase domain (HAT), and by directly linking sequence-specific transcription factors to the basal transcription machinery (a multiprotein complex composed of general transcription factors (GTF) and RNA polymerase II (Pol II)) via interactions with the CBP/p300 protein-binding domains (KIX, TAZ1, TAZ2).

1.2.3 Structure of CBP/p300

CBP/p300 are very large (2442 and 2414 amino acids, respectively) multi-modular proteins that form a hub for protein-protein interactions and have over 300 known binding partners, many of which are cellular transcription factors (39). To facilitate its function, the structure of CBP/p300 is comprised of several folded domains connected by long structurally disordered linker regions. This architecture, which is often referred to as 'beads on a string', allows CBP/p300 the flexibility to bind its diverse array of protein partners and accommodate for differences in spacing between binding sites at gene promoter and enhancers (40).

The catalytic activity of CBP/p300 is conferred by a central histone acetyltransferase (HAT) domain. Near this domain, CBP/p300 also possesses a bromodomain (BRD) that is used to identify acetylated lysine residues on histones and other proteins (41). CBP/p300 can also act as a co-factor for nuclear receptors, and this function is mediated by small motifs in its nuclear receptor interaction domain (NRID) (42). There are four other CBP/p300 protein-binding domains: interferon response binding domain (IBiD), kinase inducible domain (KIX), and two transcriptional adaptor zinc finger domains (TAZ1 and TAZ2) (Figure 1.2). These highly conserved domains facilitate the complex interactions between CBP/p300 and other transcription regulators.

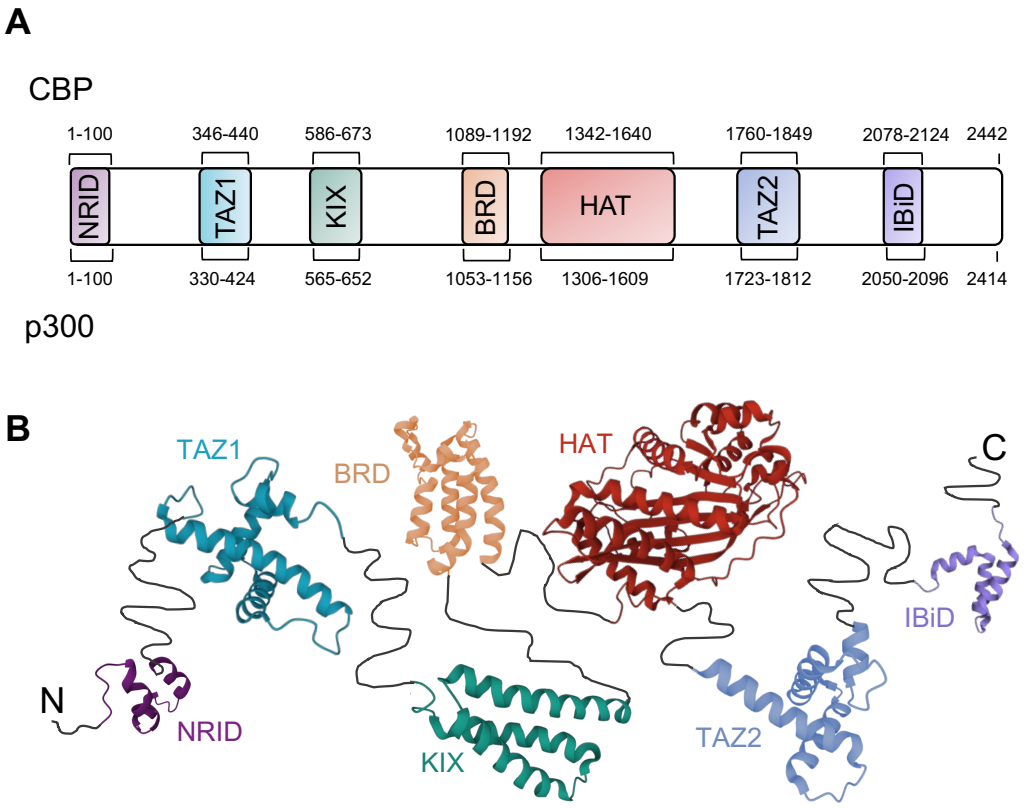

Figure 1.2. Domain architecture of CBP/p300. (A) Diagram of CBP and p300 structure including the nuclear receptor interaction domain (NRID), transcriptional adaptor zinc finger domains (TAZ1 and TAZ2), kinase inducible domain (KIX), bromodomain (BRD), interferon response binding domain (IBiD), and histone acetyltransferase domain (HAT), labelled according to their native amino sequence. (B) Representation of CBP/p300 incorporating nuclear magnetic resonance spectroscopy structures of NRID (43), TAZ1 (44), KIX (45), TAZ2 (46), IBiD (47) combined with x-ray crystal structures of BRD (48) and HAT (49), black lines connecting the domains represent long structurally disordered linker regions.

The KIX domain was initially identified as the region of CBP/p300 that interacts with the transcription factor cAMP response element-binding protein (CREB) to initiate transcription, which led to its previous designation as the CREB-binding domain (50). Since then, structures have been resolved for the KIX domain in complex with numerous other TADs of transcription factors. Structurally, KIX is composed of three α-helices along with two short 3_{10} helices, which bind TADs through several different binding modes (51). The KIX domain interacts using two opposing surfaces, binding sites for TADs of the transcription factors CREB and c-Myb are found on the side of KIX consisting of α1-α3 helices, whereas the mixed lineage leukemia protein (MLL) binds KIX on the opposite side in a groove formed by helices α2-α3 (Figure 1.3A) (28, 45, 52). Interestingly, TADs of MLL and c-Myb are able to bind KIX simultaneously in an allosteric fashion to enhance their interaction (29). Multi-site interactions with this CBP/p300 domain is also demonstrated by transcription factor FOXO3a which contains two TADs that can interact at both KIX binding sites at the same time (Figure 1.3B) (27, 53).

The TAZ domains of CBP/p300 are structurally similar to one another and are each comprise four α-helices (α1-α4) coordinated around three zinc binding sites (54). Both domains adopt a similar fold where the helices are arranged in an irregular tetrahedral shape with a hydrophobic core at the center that provides extra stability and well-defined binding grooves (54). The TAZ domains also share similar surface features and are both highly electropositive, which helps promote long-range electrostatic interactions when forming complexes with transcription factors where they tend to favour binding to acidic TADs (31).

A notable difference between the two domains is the orientation of helix α4, which is positioned in opposing directions. This distinction is thought to play a major role in their binding affinity and selectivity for different TADs (44). Comparatively, the surface of TAZ1 has a rather even charge distribution and, for this reason, TAZ1 often preferentially binds long extended regions of TADs, whereas the charge of TAZ2 is localized to one face of the domain and is often more inclined to bind TADs via short charged motifs (31). Previous structures have been reported for TAZ1 in complex with the TADs of transcription factors including HIF1-α, STAT2, and RelA (Figure 1.3C-E), and for TAZ2 in complex with E2A, STAT1, and p53 (Figure 1.3F-H) (31, 55–58).

In the following sections, I will detail two transcriptional regulators that depend on CBP/p300 to function and were the focus of investigation for this thesis. The first is the transcriptional co-regulator β-catenin. The second is the microphthalmia-associated transcription factor (MITF).

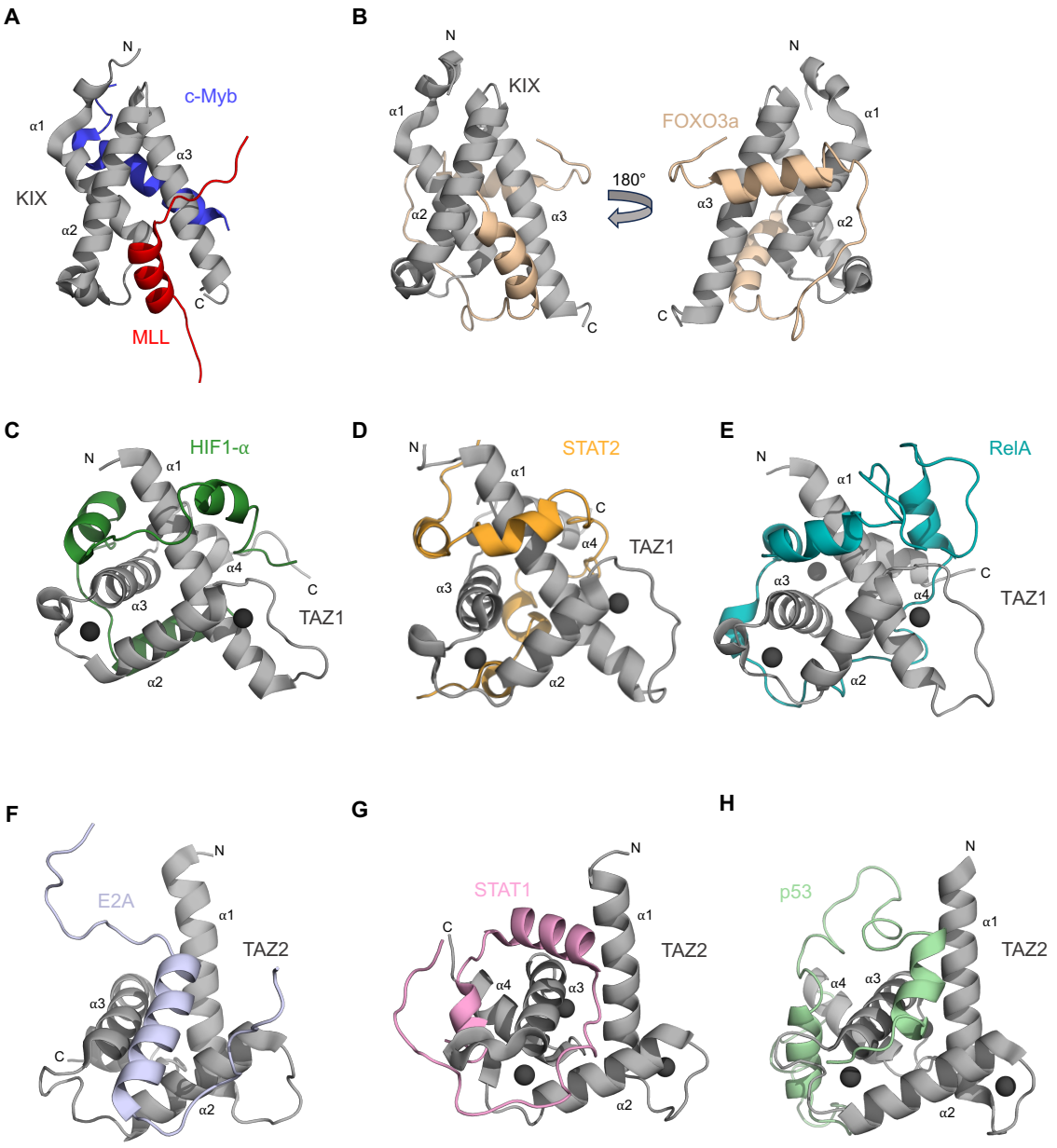

Figure 1.3. Transcription factor TADs in complex with CBP/p300 domains. (A) 3-D cartoon representation of the KIX:MLL:c-Myb ternary complex. KIX is shown in grey, the TADs of MLL and c-Myb are in red and blue, respectively (PDBID: 2AGH) (51). (B) KIX (grey) in complex with both FOXO3a TADs (beige) (PDBID: 2LQH) (53). (C-E) TAZ1 (grey) in complex with TADs of HIF1-α (green), (D) STAT2 (orange), and (E) RelA (teal) (PDBIDs:1L8C, 2KA4, 2LWW, respectively) (31, 56, 59). (F-H) TAZ2 (grey) in complex with TADs of E2A (light purple), (G) STAT1 (pink), and (H) p53 (light green) (PDBIDs: 2MH0, 2KA6, 5HPD, respectively) (31, 57, 58). Zinc ions in TAZ1 and TAZ2 are shown as black spheres. All structures were visualized using PyMOL.

1.3 Wnt-signaling and β-catenin

1.3.1 Overview of Wnt-signaling

The Wnt-signaling pathway is a highly evolutionarily conserved signal transduction cascade found in all groups of metazoans (60). Wnt comprises a diverse group of secreted glycoproteins that regulate an extensive network of cellular processes including embryotic development, cell fate determination, proliferation, and migration (61). Upon binding of extracellular Wnt ligands to the transmembrane receptor Frizzled, the signal is transduced via the cytoplasmic protein disheveled (DVL) into non-canonical and canonical pathways (61). The canonical pathway leads to the regulation of gene transcription and is differentiated based on the involvement of the nuclear effector protein β-catenin.

In the absence of Wnt, cytoplasmic β-catenin is sequestered by the 'destruction complex' comprised of axis inhibition protein (Axin), adenomatous polyposis coli (APC), casein kinase 1 (CK1α), and glycogen synthase-3 (GSK-3β), which target and phosphorylate β-catenin for ubiquitination and proteasomal degradation (62). Activation of the Wnt/ β-catenin pathway allows Frizzled and its co-receptor lipoprotein receptor related protein (LRP5/6) to recruit Axin and DVL, thus dissociating β-catenin from the destruction complex (63). This causes stabilized β-catenin to accumulate in the cytoplasm and translocate to the nucleus where it binds to transcription factors such as T-cell factor and lymphoid enhancer factor (TCF/LEF) and other co-regulators (CBP/p300) to enable the expression of Wnt-related target genes (Figure 1.4).

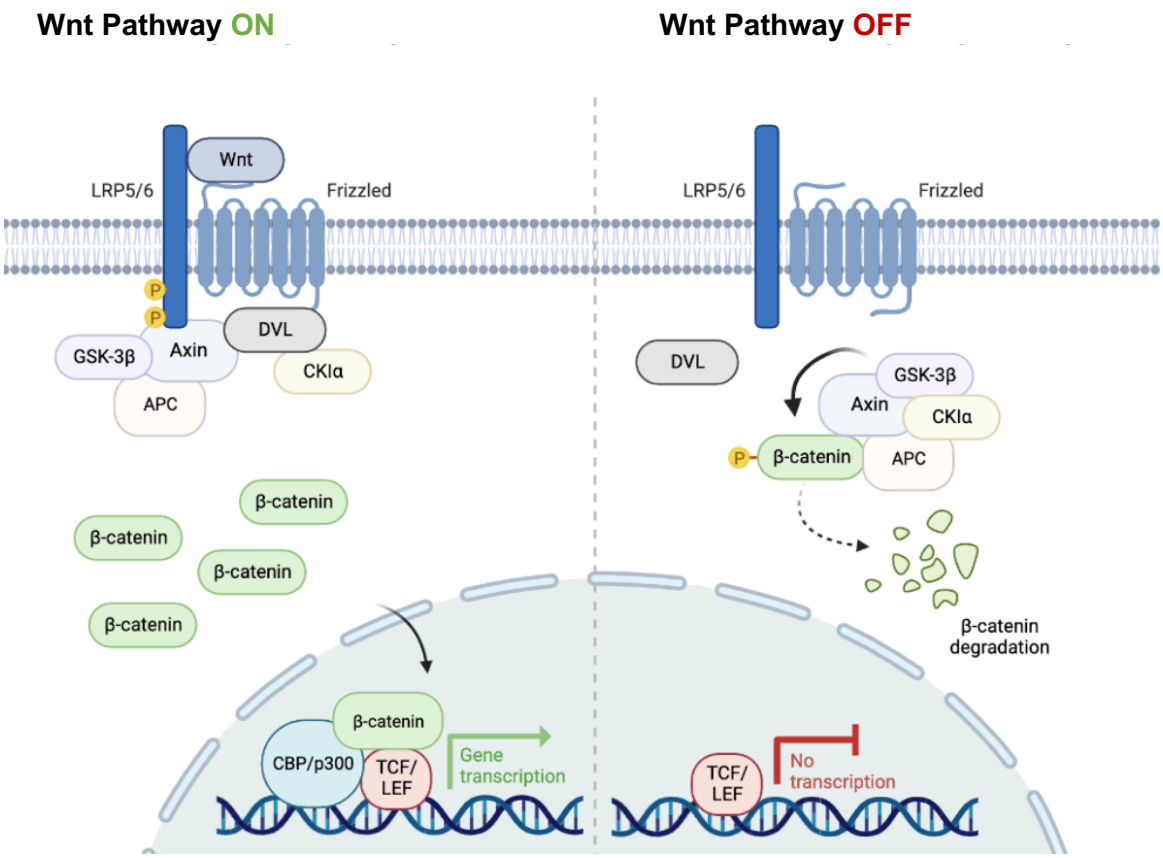

Figure 1.4. The canonical Wnt-signaling pathway. Activation of Wnt-signaling (left) begins with binding of Wnt ligands to the receptor frizzled and its co-receptor lipoprotein receptor related protein (LRP5/6), recruiting Axin and dishevelled (DVL) and releasing β-catenin from the destruction complex (comprised of adenomatous polyposis coli (APC), casein kinase 1 (CK1α), and glycogen synthase-3 (GSK-3β)). β-catenin is then translocated into the nucleus where it enhances the activity of T cell factor and lymphoid enhancer factor (TCF/LEF) transcription factors by recruiting CBP/p300. In the absence of Wnt (right) targeted β-catenin phosphorylation via the destruction complex leads to β-catenin degradation and lack of downstream gene expression. Figure created using BioRender.com.

1.3.2 β-catenin and Cancer

Since its initial discovery as a proto-oncogene in mice, the Wnt/ β-catenin signaling pathway has been recognized as a major causative factor for numerous human diseases including cancer of the breast, colon, and skin (64). β-catenin directly mediates cellular proliferation and differentiation by initiating the transcription of genes including *CyclinD1*, *c-Myc* and *BIRC5*, which in turn drive cell cycle progression and inhibition of apoptosis, but also encode oncoproteins (65, 66). Uncoupling of β-catenin from its normal Wnt control mechanisms is a hallmark of tumorigenesis by driving the expression of these oncoproteins leading to uncontrollable cell division, migration, and overall survival of cancer cells (64).

The role of β-catenin in cancer is emphasized by the fact that its cellular accumulation is found in more than half of all human cancer cases (67). High levels of β-catenin are correlated with poor prognosis and tumor progression in breast cancer and colon cancers, and are also associated with the pro-invasive properties of melanoma skin cancer (68–70). The activity of β-catenin is controlled by numerous protein binding partners that modulate its stability, cellular location, and transcriptional function. Understanding the interactions of β-catenin and its co-regulators could help in the development of targeted therapies for cancers associated with the Wnt/ β-catenin pathway.

1.3.3 Structural Overview of β-catenin

Previous crystal structures have determined that β-catenin is composed of a central repetitive armadillo domain (ARM) made up of 12 tandem repeats each composed of three α-helices (Figure 1.5). Together this ARM domain forms a superhelical positively charged groove that provides the binding interface for interactions with APC of the β-catenin destruction complex and transcription factors TCF/LEF (71, 72). Contrastingly, the β-catenin N-terminus and C-terminus are presumed to be structurally disordered with a net negative charge (Figure 1.5) (73). Within these terminal regions two independent TADs have been identified and are essential for β-catenin transcriptional function (74). While less is known regarding the β-catenin N-terminal region and its interactions, the C-terminal domain of β-catenin is required for mediating binding to chromatin modifying complexes including brahma-related gene-1 (BRG-1) and CBP/p300 (75–77).

CBP/p300 co-localize with β-catenin at gene promoters in cancer cells, where they directly increase transcriptional activity of TCF/LEF mediated Wnt-target genes via histone acetylation (78). CBP/p300 can also directly acetylate the β-catenin ARM domain, modulating its affinity for transcription factors (78, 79). While β-catenin is well-known for being a co-regulator of TCF/LEF, it can also interact with other transcription factors including MITF, which will be discussed further in the next sections.

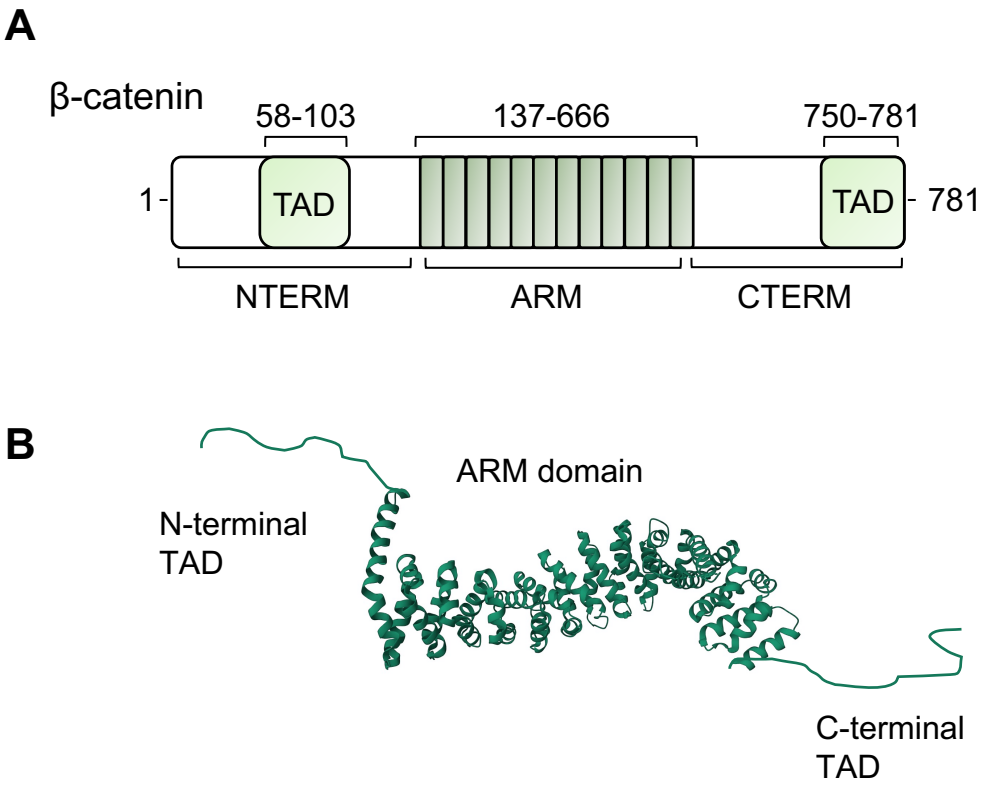

Figure 1.5. Structural domains of β-catenin. (A) Schematic of the functional domains of β-catenin which include a central armadillo repeat domain (ARM) and N-terminal (NTERM) and C-terminal (CTERM) transactivation domains (TAD), annotated according to native amino sequence. (B) Representation of β-catenin incorporating the structurally disordered terminal regions (green lines) and x-ray crystal structure of the ARM domain (PDBID: 2Z6H) (73).

1.4 The Microphthalmia-Associated Transcription Factor

1.4.1 Biological Function

MITF is the 'master regulator' for proper cell development of several cell-lineages including retinal epithelial cells, mast cells, osteoclasts, and melanocytes (80, 81). The first mutation of the *MITF* gene locus was discovered in the progeny of irradiated mice by Paula Hertwig, whose work published in 1942 accounted for the novel recessive gene producing white, small-eyed (microphthalmic) mice (82). The result of her research studying the biological effects of irradiation have since served as invaluable models for investigation of human diseases involving the skin, eyes, ears, and skeleton (83).

In humans, mutation to the *MITF* gene causes the failure of neural crest progenitor cells to properly differentiate, leading to several genetic disorders, notably Waardenburg syndrome type 2 and Tietz syndrome which result in hypopigmentation of the skin and hair, abnormal retinal development, and congenital hearing deficiencies in patients (84, 85). Through the usage of alternative promoters, the *MITF* gene consists of nine different isoforms (MITF-A, MITF-B, MITF-C, MITF-D, MITF-E, MITF-H, MITF-J, MITF-Mc and MITF-M) which differ based on their unique N-terminus and tissue-specific expression patterns (81). The shortest isoform MITF-M is exclusively expressed in melanocytes, the pigment producing cells of the skin. MITF-M has been extensively studied for its critical role in melanocyte biology, where it has been found to directly target and coordinate the expression of hundreds of different melanocyte genes involving numerous biological functions

including melanin pigment synthesis (*TYR, TYRP1, DCT, MLANA*), cell proliferation (*CDK2, TBX2*), migration (*SNAI2, c-MET*), and survival (*BCL2, BIRC7, HIF1α*) (86–90). From here on, reference to MITF refers to the melanocyte specific MITF-M.

1.4.2 MITF and Melanoma

Given the critical role of MITF in melanocyte biology, it is perhaps unsurprising that when deregulated MITF has been linked to the development and progression melanocyte-derived skin cancer, melanoma. MITF is recognized as a lineage specific oncogene of melanoma that drives tumorigenesis and modulates the proliferation and invasiveness of the disease (91). Over the past three decades melanoma has seen the highest annual change in incidence rates above all other cancers (an average increase of ~2.2% per year) and remains a growing health concern amongst Canadians (92). With nearly 9,000 diagnosed cases in 2021, melanoma is one of the top five most common cancers in Canadians between the ages of 15-49 (92). Due to its high metastatic potential, melanoma is also one of the most challenging cancers to treat and results in 80% of all skin cancer related deaths (93). Patients with malignant melanoma have a five-year survival rate of less than 25% and poor prognosis using standard chemotherapy and immunotherapies which demonstrate consistently low response rates (94).

The aggressive and treatment-resistant nature of melanoma cells is in part due to their ability to reversibly transition from highly proliferative to highly invasive states in a process known as phenotypic-switching. These properties are

predominately mediated by MITF, and have led to the previously proposed MITF 'rheostat' model which links the level of MITF activity to melanoma cell phenotype and behavior (95). Quantitative gene analysis of human melanoma cells has shown that MITF expression is heterogenous in tumours and that cell populations can shuttle between high and low MITF expression levels (96). High levels are found to promote differentiation, mid-levels promote proliferation, low-levels promote an invasive phenotype, and the absence of MITF leads to cellular senesce or cell death (97). The considerable variation regarding MITF expression emphasizes the complex and dynamic nature of its regulatory mechanisms.

Upstream of MITF, deregulation of the mitogen activated protein kinase cascade (MAPK) signaling pathway plays a key role in melanoma oncogenesis. Approximately 50% of all melanoma patients carry a mutation to the MAPK kinase BRAF, the most common (~90%) being a V600E substitution in the kinase activation domain (98). This mutation causes constitutive activation of the pathway leading to an increase in MITF activity which promotes cellular growth, anti-apoptotic properties, and evasion of cellular senescence (99). The high frequency of MAPK mutations in melanoma have made them a target for potential therapeutics, and inhibitors developed against both BRAF (vemurafenib and dabrafenib) and MEK (trametinib) have been approved for treatment in adults with unresectable or metastatic melanomas (100).

While suppression of the MAPK signaling pathway and its downstream MITF activity has led to improvements in overall progression-free survival of patients, their effects are unfortunately short-lived, with many patients suffering from acquired drug

resistance to these kinase inhibitors within the first year of treatment (100, 101). Moreover, *MITF* gene amplification has been found in patients who have relapsed from BRAF/MEK therapies, suggesting restoration of MITF function (by gene expression or other methods) as a potential clinical resistance mechanism (102). Given that dysregulation of MITF underlies melanoma development, disease progression, and treatment resistance, as well as its limited role in cell types other than melanocytes, the ability to directly control MITF function could have incredible therapeutic potential for the future treatment of melanoma.

1.4.3 MITF Structure

MITF belongs to the microphthalmia/transcription factor E (MiT/TFE) family, which is composed of four evolutionarily conserved members MITF, TFEB, TFEC, and TFE3 (103). MiT/TFE family members are structurally related and share a common basic helix-loop-helix (bHLH) leucine zipper domain. This leucine zipper allows MiT/TFE proteins to homo- or heterodimerize, while the bHLH region facilitates DNA-binding to consensus E-box (CANNTG) and M-box (TCATGTG) sequences in promoter and enhancer regions (104). The N-terminal region of MITF is thought to be disordered and contain an acidic transactivation domain that is necessary for gene expression. This TAD is present in TFEB and TFE3 which have >90% sequence identity to MITF (105), but is not found in the most divergent family member TFEC (~70% sequence identity), which instead participates in transcriptional inhibition rather than activation (106). Transcription activation by this

domain can be attributed to its ability to facilitate protein-protein interactions with transcriptional co-regulators, and is believed to provide a potential binding-site between MITF and CBP/p300 (107). The C-terminal region of MITF has also been observed to be important for MITF transactivation of the tyrosinase gene, though even less is known regarding this region or its interactions (Figure 1.6) (108).

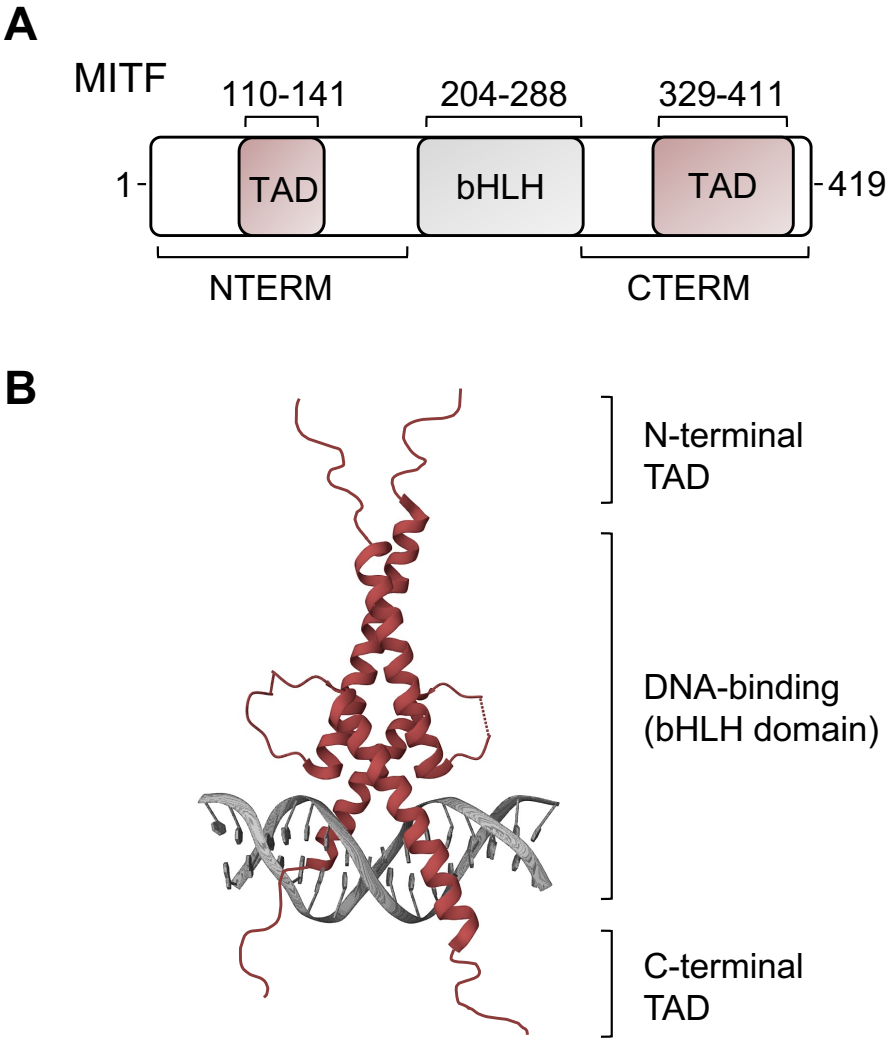

Figure 1.6. Structural domains of MITF. (A) Schematic of the MITF domains, including the N-terminal (NTERM) and C-terminal (CTERM) transactivation domains (TAD), and basic helix-loop-helix (bHLH) leucine zipper DNA-binding domain, annotated according to native amino sequence. (B) Representation of MITF showing the disordered N- and C-termini (red lines) and incorporating the x-ray crystal structure of the MITF bHLH leucine zipper dimer bound to DNA (PDBID: 4ATI) (104).

1.4.4 Expression and Regulation

Multiple signaling pathways are involved in the regulation of MITF expression and activity so that it can properly perform its complex biological role. The MITF promoter is targeted by several transcription factors including PAX3, SOX10, CREB, and TCF/LEF (109, 110). Mutations to *PAX3* fail to transactivate expression of the *MITF* promoter which are responsible for Waardenburg syndrome types 1 and 3, and mutations to *SOX10* for Waardenburg syndrome type 4 (111). CREB and its co-activator CBP/p300 also directly influence *MITF* gene expression (Figure 1.7). Broad inhibition of the catalytic activity of CBP/p300 has been shown to cause senescence in multiple melanoma cell lines, while alternatively, cAMP-induced upregulation of CBP/p300 profoundly stimulates MITF-regulated genes (112).

MITF expression is also induced via Wnt/β-catenin signaling, where activated β-catenin is translocated to the nucleus and interacts with TCF/LEF bound to the *MITF* promoter thereby stimulating transcription (113). β-catenin is not only involved in the regulation of *MITF* gene expression but can also directly interact with MITF itself as a transcriptional co-regulator (Figure 1.7). This interaction is facilitated by the MITF bHLH domain, which binds the β-catenin ARM domain, redirecting β-catenin away from TCF/LEF1 targets to instead enhance the transcription of MITF-specific genes (70). The importance Wnt/β-catenin in melanocyte biology is further emphasized by the fact that activation of this pathway induces MITF expression early in neural crest cell development, promoting cell fate specification towards the melanocyte lineage (114).

MITF activity is also regulated via post-translational modifications. The most well-studied post translational modification is phosphorylation of MITF through the MAPK kinase cascade. Activation of this pathway via extracellular signaling through the c-Kit receptor triggers a cascade of serine-threonine kinases (BRAF-MEK-ERK) and the subsequent phosphorylation of MITF at Ser73, which activates MITF activity (Figure 1.7) (115). Phosphorylation of MITF at this site not only increases its binding affinity for transcriptional co-factors CBP/p300, but also primes MITF for further phosphorylation by the Wnt-pathway related kinase GSK-3β at Ser69 which prevents MITF nuclear export, as well as Ser397, Ser401, and Ser405 which are involved in MITF protein stability (116–118).

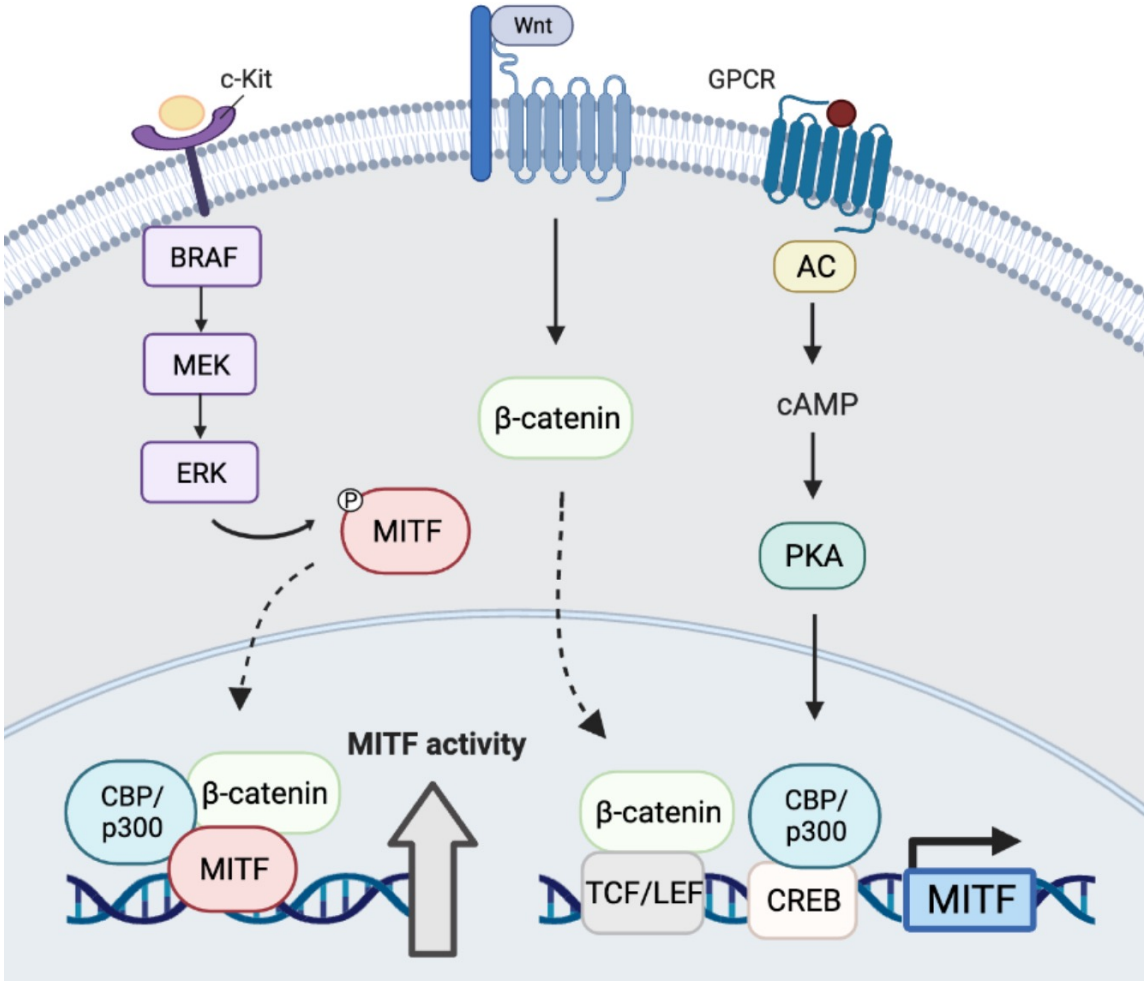

Figure 1.7. Key signaling pathways influencing MITF activity. MITF expression and activity is influenced by multiple upstream signaling pathways including MAPK (left) which upon extracellular binding to c-KIT receptors triggers the mitogen-activated protein kinase (consisting of BRAF, MEK, ERK) to phosphorylate and activate MITF. Activation of Wnt/β-catenin pathway (middle) prevents β-catenin degradation resulting in its stabilization and translocation to the nucleus where it increases *MITF* expression through transcription factors TCF/LEF and acts as a transcriptional co-regulator for MITF target genes. The cAMP signaling pathway (right) is stimulated by ligand binding to G-protein-coupled receptors (GPCR) and activating adenylate cyclases (AC) and protein kinase A (PKA) to phosphorylate CREB, which then recruits CBP/p300 to upregulate MITF and its target genes. Illustration made using BioRender.com.

1.5 Research Objectives

The overall goal of my research is to use a combination of structural, biophysical, and functional studies to understand how the co-activator CBP/p300 is recruited by MITF and β-catenin. Although these proteins are known to work together to coordinate gene expression and their structured domains have been well-defined, molecular details regarding their disordered regions have been limited. Specifically, I set out to characterize the association of CBP/p300 with the MITF and β-catenin transactivation domains and investigate the effect of peptide-based inhibitors on disrupting their function and interaction.

This is a publication-based thesis, and my findings are presented as a collection of manuscripts prepared throughout my PhD. In chapters 2 and 3 I investigate the association of CBP/p300 with the C-terminal and N-terminal transactivation domains of β-catenin, respectively. The focus of chapters 4 and 5 is the interaction of CBP/p300 with the N-terminal and C-terminal transactivation domains of MITF. The insights in this thesis not only improve our fundamental understanding of this transcriptional network, but also expand on our current knowledge of the protein-protein interactions that underlie their role in oncogenesis.

1.6 Using NMR Spectroscopy to Study IDPs

The biological significance of intrinsically disordered proteins in transcription and regulation makes it important to understand more about their structural features and molecular interactions. The most common method for structure determination, x-

ray crystallography, is typically unsuitable to study IDPs due to their conformational heterogeneity, which prevents them from being crystallized. For this reason, disordered regions are often deleted to help facilitate crystallization of many proteins, or left unresolved in their final structures, as seen in the instances of the MITF and β-catenin activation domains (Figures 1.5B and 1.6B) (119). Some IDPs undergo binding-induced folding and are capable of crystallization upon binding partner-molecules, however crystallography may still fail to capture the structural heterogeneity of these dynamic complexes by providing only a static 'snapshot' of the interaction (120).

Another method which has contributed immensely to the field of structural biology is cryogenic electron microscopy (cryo-EM). Cryo-EM can accommodate for moderate differences in protein conformation and composition since it does not require samples to be crystallized, but instead relies on direct images of molecules that are then computationally combined (121). Unfortunately, proteins with high amounts of conformational variability are still poorly resolved using this method, including the previously determined cryo-EM structure of CBP/p300 which is of low resolution (122). Thus, this technique cannot yet yield detailed structural information regarding proteins with extended amounts of intrinsic disorder.

Disordered proteins and their associated 'fuzzy' complexes have instead shown great promise for structural studies using nuclear magnetic resonance (NMR) spectroscopy. NMR spectroscopy provides high resolution atomic-level detail of molecules and is ideally suited to probe the structural propensities of IDPs. Solution state NMR provides an analysis of samples in their native form and represents an

equilibrium averaged across time, making it particularly amenable to study proteins that are highly dynamic by allowing the observation of multiple conformations (120, 123).

NMR signals rely on both the external magnetic field of a spectrometer and specific nuclei that possess spin angular momentum. Atoms like ^{12}C with an even number of both protons and neutrons have no nuclear spin and are not observable by NMR, so one caveat of using this technique is having to incorporate NMR active isotopes such as ^{15}N and ^{13}C into protein samples (124). Each NMR spin active nuclei precess around the external magnetic field at a unique resonance frequency (due to differences in the molecular structure and electron shielding). This resonance frequency is observed by perturbations of the nuclear spins via radiofrequency pulses producing a NMR signal at a specific frequency, which is then converted to chemical shift in reference to a standard compound (124).

The number of NMR active nuclei in a typical polypeptide can cause extensive signal-overlap in a typical one-dimensional NMR spectrum. To resolve this issue, NMR spectra collected for proteins are often correlated between multiple nuclei to increase the dimensionally further resolving the spectrum (125). For instance, in the ^{1}H- ^{15}N heteronuclear single quantum coherence (HSQC) experiment each signal represents only ^{1}H nuclei that are chemically bonded to a ^{15}N nucleus. This means there is only one signal corresponding to the backbone amide of each amino acid residue that has both a ^{1}H and ^{15}N chemical shifts associated with it (Figure 1.8) (125). This concept can then be expanded to a third dimension, for instance experiments which correlate the frequencies from chemically bonded ^{1}H,

^{15}N, and ^{13}C nuclei (125). Coupling these spectra together can then allow for the sequential assignment of resonance peaks to their specific amino acid in the protein sequence and is one of the initial steps to obtaining structural information by NMR.

NMR spectroscopy is a sensitive probe of changes to the molecular environment around each chemically distinct nuclei within a sample, this includes differences of temperature, pH, buffer composition, molecular structure, or ligand binding. In this way, NMR can be used to investigate protein-protein interactions using a method known as chemical shift mapping. Here a series of NMR spectra (commonly ^{1}H-^{15}N-HSQC experiments) are collected in the absence and presence of varying amounts of a binding molecule (126). If an interaction occurs, residues involved in complex formation (from direct impacts of binding or conformationally induced changes) experience a measurable chemical shift change ($\Delta\delta$) from their normal positions in the HSQC spectra, discernable by overlaying the spectra following the titration (Figure 1.8). This mapping can provide invaluable information on the allosteric changes of a protein upon ligand binding and help identify the potential binding interface between two protein molecules (126). This NMR technique has been instrumental to studying IDP interactions, including that of the p53 transactivation domain in complex with CBP/p300 (127), where chemical shift mapping was able to elucidate the multi-site binding taking place based on the linearity and directionality of the peak shift change. In this thesis, I utilize NMR-spectroscopy alongside other biophysical and functional assays, to investigate the structural features of the disordered MITF and β-catenin activation domains, and to study their binding interactions with co-activator CBP/p300.

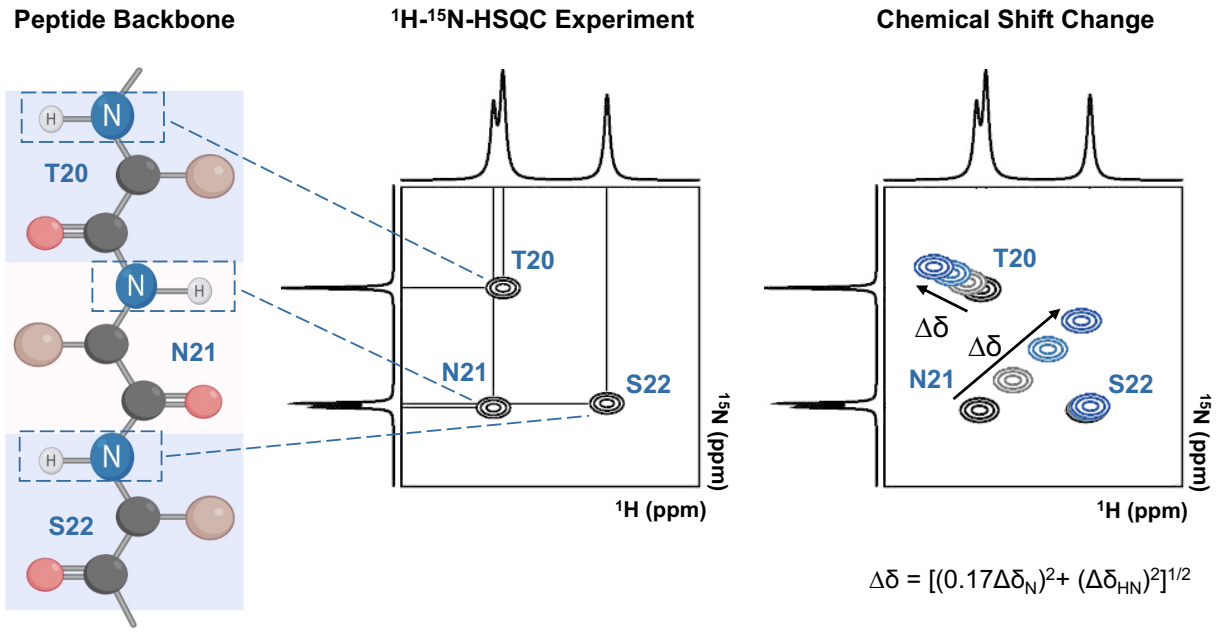

Figure 1.8. Simplified depiction of two-dimensional protein NMR. Representative diagram of ^{1}H-^{15}N-HSQC experiment (middle) showing proton amide resonance peaks of hypothetical peptide (left). Changes to the chemical environment, including the addition of partner molecules can cause a shift (Δδ) in ^{1}H-^{15}N-HSQC peaks (right) represented by a black to blue colour change with directions denoted with arrows. These changes in chemical shift can then be measured as $\Delta\delta = [(0.17\Delta\delta_N)^2 + (\Delta\delta_{HN})^2]^{1/2}$. Figure was created using BioRender.com.

Chapter 2: β-Catenin Interacts with the TAZ1 and TAZ2 Domains of CBP/p300 to Activate Gene Transcription

2.1 Contributions of Authors

This chapter contains the abstract, introduction, methods, results and discussion of the manuscript originally published in the International Journal of Biological Macromolecules: Brown, A. D., Cranstone, C., Dupré, D. J., & Langelaan, D. N. (2023). β-Catenin interacts with the TAZ1 and TAZ2 domains of CBP/p300 to activate gene transcription. *Int. J. Biol. Macromol. 238*, 124155. Connor Cranstone, a previous honours student in the Langelaan lab, prepared NMR samples and collected ITC data in Figures 2.2, 2.4, and 2.9. The conceptualization, execution, and formal analysis of all other experiments were performed by me, as well as the written draft of the original manuscript. Dr. Denis Dupré and Dr. David Langelaan provided materials, support, and editing of the final paper.

2.2 Abstract

The transcriptional co-regulator β-catenin is a critical member of the canonical Wnt signaling pathway, which plays an important role in regulating cell fate. Dysregulation of the Wnt/β-catenin pathway is characteristic in the development of major types of cancer, where accumulation of β-catenin promotes cancer cell proliferation and renewal. β-catenin gene expression is facilitated through recruitment of co-activators such as histone acetyltransferases CBP/p300; however,

the mechanism of their interaction is not fully understood. Here I investigate the interaction between the C-terminal transactivation domain of β-catenin and CBP/p300. Using a combination of pulldown assays, isothermal titration calorimetry, and nuclear resonance spectroscopy I determine the disordered C-terminal region of β-catenin binds promiscuously to the TAZ1 and TAZ2 domains of CBP/p300. I then map the interaction site of the C-terminal β-catenin transactivation domain onto TAZ1 and TAZ2 using chemical-shift perturbation studies. Luciferase-based gene reporter assays indicate Asp750-Leu781 is critical to β-catenin gene activation, and mutagenesis revealed that acidic and hydrophobic residues within this region are necessary to maintain TAZ1 binding. These results outline a mechanism of Wnt/β-catenin gene regulation that underlies cell development and provides a framework to develop methods to block β-catenin dependent signaling.

2.3 Introduction

Wnt signaling is a highly conserved signal transduction pathway that regulates essential cellular processes throughout a person's lifetime (61, 128–130). Binding of the Wnt ligand to its receptor triggers two types of pathways, canonical and non-canonical, which differ based on the involvement of β-catenin (131). The canonical Wnt pathway is dependent on β-catenin to mediate the transcriptional response (132). Upon activation, stabilized β-catenin binds and modulates the actions of DNA-bound transcription factors, including T-cell factor and lymphoid enhancer factor (TCF/LEF), which require β-catenin for Wnt-targeted gene expression (64).

These Wnt/β-catenin-target genes are essential in controlling numerous cellular processes including proliferation, differentiation, and cell survival (6,7). Consequently, mutations to the Wnt/β-catenin signaling pathway are characteristic in many major types of cancer, where enhanced accumulation of nuclear β-catenin leads to tumor formation and cancer progression (68, 135).

β-catenin is composed of a central armadillo repeat domain spanning residues Asn138-Asp665 that is flanked by N- and C-terminal sequences Met1-Val137 (βCAT_{NTERM}) and Lys666-Asp781 (βCAT_{CTERM}), respectively (Figure 2.1) (73). Together these domains allow β-catenin to act as a scaffold for the assembly of multi-protein complexes involved in transcription. The β-catenin armadillo domain consists of 12 helical repeats which together form a positively charged groove that provides the main interaction site for numerous transcription factors (136). βCAT_{NTERM} and βCAT_{CTERM} facilitate protein-protein interactions with transcriptional co-regulators, and are critical to β-catenin function as they each contain potent transactivation domains (TAD1 and TAD2) (72, 137, 138). This in part is attributed to the structurally disordered nature of these domains, which allows β-catenin the flexibility to recruit multiple co-activators to regulatory complexes associated with DNA (139). This includes the homologous histone acetyltransferases CREB-binding protein (CBP) and E1A-binding protein (p300), which directly interact with β-catenin at promoters to enhance gene expression (77, 140, 141). Interactions of CBP/p300 with β-catenin synergistically activate β-catenin/Wnt transcription, whereas lowering CBP/p300 levels inhibits growth and formation of colon carcinomas caused by β-catenin mutation (142).

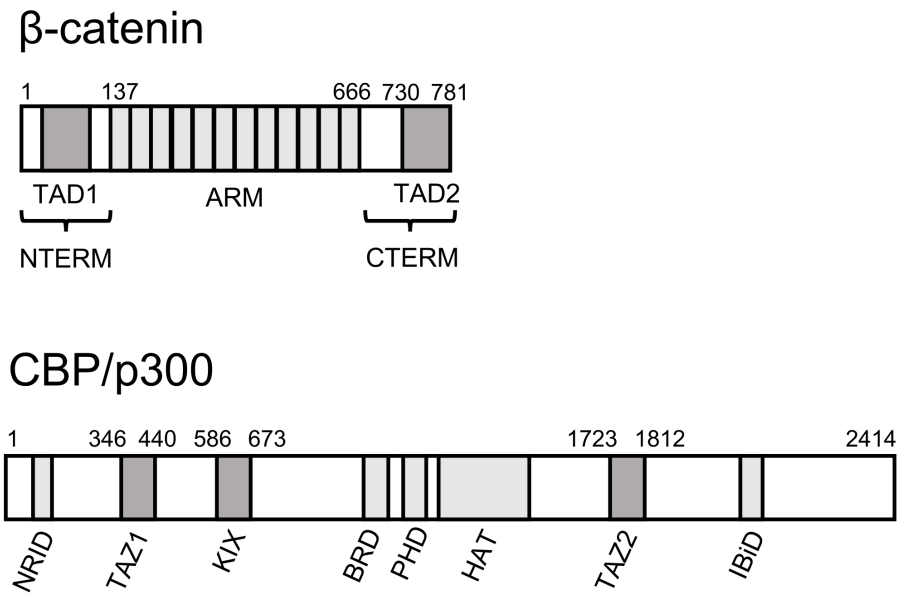

Figure 2.1. Overview of β-catenin and CBP/p300. An illustration of the domains of β-catenin including the central armadillo repeat domain (ARM), N-terminal, and C-terminal transactivation domains (TAD1/2). CBP/p300 contains a nuclear receptor interaction domain (NRID), kinase inducible domain (KIX), bromodomain (BRD), PHD-type zinc finger (PHD), histone acetyltransferase domain (HAT), IRF-3 binding domain (IBiD), and the transcription adapter zinc finger domains TAZ1 and TAZ2. Numbered residues indicate domain boundaries of β-catenin or CBP/p300 used in this study.

Recruitment of CBP/p300 occurs at thousands of different human gene promoters where it forms interaction sites for a large variety of transcription regulators across numerous cellular pathways (143). CBP/p300 enhances target gene expression through histone acetylation, which subsequently enhances DNA transcription (144). CBP/p300 are large proteins with seven globular domains. Outside of the catalytic histone acetyltransferase (HAT) domain, several protein interaction domains allow CBP/p300 to act as an intermediary between transcription factors and transcriptional machinery (Figure 2.1). This includes the kinase inducible domain (KIX), which is recruited by the transactivation domains of transcription factors including MLL, BRCA1 and FOXO3a (52, 53, 145). As well as the transcription adaptor zinc finger domains TAZ1 and TAZ2, which facilitate interactions with the transactivation domains of HIF-1α, CITED2, and STAT1/2 (31, 55, 146).

Despite the importance of Wnt signaling in both health and disease, and considerable evidence that interactions with CBP/p300 mediate Wnt/β-catenin transcription, the molecular mechanisms of this interaction are unclear (76, 77, 147). In this study I characterize a direct interaction between the TAD2 of β-catenin with the TAZ1 and TAZ2 domains of CBP/p300. I identify the residues involved in these interactions using nuclear magnetic resonance spectroscopy (NMR) and quantify their affinities using isothermal titration calorimetry (ITC). Finally, I use mutagenesis studies to evaluate the importance of certain motifs in modulating TAZ1-mediated CBP/p300 recruitment by β-catenin.

2.4 Materials and Methods

2.4.1 Plasmid Preparation

A pET28a plasmid containing full-length human β-catenin was gifted from Randall Moon (Addgene plasmid # 17198) and various fragments of the coding region (residues 1-137 (NTERM), 666-781 (CTERM), 666-729 (CTERMΔTAD2), 730-781 or 750-781 (both referred to as TAD2; 750-781 used in luciferase and NMR mapping involving TAZ1, while 730-781 was used for all other experiments), were amplified by PCR and cloned into a pET21b vector using *Eco*RI, *Bam*HI and *Xho*I restriction enzymes, downstream of sequences encoding for a hexahistidine tag, the B1 domain of *Streptococcus* protein G (GB1), and a tobacco etch virus protease cleavage site to create pGB1-βCAT plasmids. Site-directed mutagenesis of pGB1-βCAT_{CTERM} was performed using sequence and ligation independent cloning (148), where various substitutions (D751A, D761A, D764A, F777A) and deletions (Δ757-761, Δ761-765, Δ776-779) were incorporated into primers. Plasmids used for luciferase transactivation experiments included segments of the β-catenin coding region cloned into pCMV-GAL4 vector gifted by Liqun Luo (Addgene plasmid # 24345) to create pGAL4-βCAT constructs. Expression plasmids of TAZ1, TAZ2, and KIX are the same as those previously used (58).

2.4.2 Protein Purification

BL-21 (DE3) *E. coli* were transformed with pGB1-βCAT plasmids and grown under ampicillin selection. Bacterial cultures were grown at 37 °C in either LB or M9 minimal media (149). Once cultures reached an optical density at 600 nm of 0.8,

isopropyl β-D-1-thiogalactopyranoside was added to 0.5 mM to induce protein expression and cultures were incubated for an additional 4 hours prior to centrifugation. Cell pellets were reconstituted in binding buffer (20 mM Tris-HCl pH 8.0, 250 mM NaCl, 8 M urea), sonicated, and clarified. GB1- βCAT proteins were bound to Ni^{2+} charged resin (IMAC Sepharose, Cytiva), then refolded on-column by washing with binding buffer lacking urea. The eluent was dialyzed against native buffer (20 mM Tris-HCl pH 8.0, 50 mM NaCl, 5 mM βME) at 4 °C overnight. When required, the GB1 affinity tag was removed by the addition of 150 μg of tobacco etch virus protease and βCAT peptides were isolated by Ni^{2+} affinity and ion exchange chromatography (Q Sepharose, Cytiva).

Purification of TAZ2 was carried out in the same manner as GB1-βCAT proteins, with 100 μM $ZnCl_2$ added to all buffers. Following Ni^{2+} affinity chromatography, the eluent was reduced with 50 mM β-mercaptoethanol, supplemented with 1 mM $ZnCl_2$, then cleaved with thrombin protease at 4 °C overnight. After cleavage, samples were isolated using cation exchange resin (SP Sepharose, Cytiva). TAZ1 and KIX purifications took place as previously reported (58), with additional semi-preparative reverse phase high-performance liquid chromatography purification for TAZ1 carried out on a C_8 column using a water: acetonitrile gradient (Zorbax, Agilent Technolgies).

2.4.3 Pulldown Assay

GB1 and GB1-βCAT proteins (20 nmoles) were mixed with IgG agarose beads (20 μL) (Cytiva) in pulldown buffer (20 mM Tris-HCl pH 8, 25 mM NaCl, 5

mM βME, and 10 μM $ZnCl_2$). After two washes with pulldown buffer, purified KIX, TAZ1, or TAZ2 (20 nmoles) was added to the beads for 30 min, following which beads were then washed three more times, resuspended in Laemmli buffer, and analyzed by SDS-PAGE.

2.4.4 Isothermal Titration Calorimetry

All ITC experiments were conducted in 20 mM Tris-HCl pH 8.0, 25 mM NaCl, 5 mM βME, and 1 μM $ZnCl_2$ at 30 °C using a VP-ITC microcalorimeter (MicroCal). The syringe contained 100-400 μM of TAZ1 or TAZ2 which was then injected into matched buffer containing 8-30 μM βCAT peptides. Duplicate experiments were performed using 10 μL injections with 300 sec of equilibration per injection. ITC thermograms were then fit to the appropriate binding model using MicroCal Origin 7.5 software.

2.4.5 NMR Spectroscopy

Unless otherwise noted, all NMR spectra were collected in 20 mM MES pH 6.2, 100 mM NaCl, 5 mM DTT, 5% D_2O, at 25 °C at 700 MHz with a cryogenically cooled probe (Bruker Avance III, NRC-IMB, Halifax, NS). Resonance assignments of $^{13}C/^{15}N$-labelled βCAT_{CTERM} (500 μM) were resolved using ^{1}H-^{15}N HSQC, HNCACB, CBCACONH, H(CCO)NH, (H)C(CO)NH, HNCO, and HN(CA)CO experiments. Chemical shift assignments of backbone resonances for TAZ1 and TAZ2 were determined by interpreting triple resonance spectra that were collected at 600 MHz (Varian INOVA, Queen's University, Kingston ON) from samples of $^{13}C/^{15}N$-labelled protein (TAZ1: 650 μM TAZ1, 20 mM MES pH 6.5, 5 mM βME,

5% D_2O; TAZ2: 358 µM TAZ2, 20 mM MES pH 6.5, 5 mM βME, 100 µM $ZnCl_2$, 5% D_2O) at 25 °C and 15 °C, respectively. NMR data were processed and interpreted using NMRPipe (150) and CcpNmr Analysis (151).

To assess binding between β-catenin and domains of CBP/p300, ^{1}H-^{15}N HSQC spectra were collected of 100 µM ^{15}N-labeled βCAT_{CTERM} or βCAT_{TAD2} in the absence and presence of up to 400 µM unlabelled TAZ1 or TAZ2. Chemical shift changes (Δδ) upon addition of TAZ1 or TAZ2, were quantified for each residue as $\Delta\delta = [(0.17\Delta\delta N)^2 + (\Delta\delta HN)^2]^{1/2}$ (152, 153). For mapping experiments, ^{1}H-^{15}N HSQC spectra were collected of 100 µM ^{15}N-labeled TAZ1 or TAZ2 titrated with up to 400 µM unlabelled βCAT_{TAD2} in NMR buffer with 25 mM NaCl at 35 °C. Residues that experienced Δδ greater than the mean Δδ or mean Δδ + 1 standard deviation, were then mapped onto the surface of the crystal structure of TAZ1 and TAZ2 (PDBID: 1U2N and 1F81, respectively) (154, 155). Figures were created using PyMOL (Schrödinger Inc.) and chemical shift assignments for βCAT_{CTERM} are deposited into the BioMagResBank as accession number 51601 (156).

2.4.6 Luciferase Transcriptional Assays

HEK 293A cells were cultured in Dulbecco's modified Eagle's medium with 10% FBS at 37°C with 5% CO_2. Cells were seeded into 24-well plates, grown to 70-80% confluency and then transfected using jetPRIME reagent. A total of 0.5 µg of plasmid was transfected per well, consisting of 0.35 µg p5xGAL4-luc, 0.05 µg pCMV-Renilla, and 0.1 µg of pGAL4-βCAT expression plasmid. Cell lysate was harvested 18-24 hr after transfection and luminescence was measured using the Dual-

Luciferase Reporter Assay System (Promega). Values shown are triplicate replicates of *Renilla*-normalized luminescence measurements relative to pCMV-GAL4 negative control. Statistical significance was assessed using one-way ANOVA and Dunnett's multiple comparison test compared to GAL4 control.

2.5 Results

2.5.1 The C-terminal Transactivation Domain of β-catenin is Intrinsically Disordered

NMR spectroscopy was first used to investigate the molecular characteristics of βCAT_{CTERM} (residues 666-781). The ^{1}H-^{15}N HSQC spectrum of $^{13}C/^{15}N$-labelled βCAT_{CTERM} was well resolved and had the anticipated number of peaks with narrow chemical shift dispersion of ^{1}H resonances. This is consistent with βCAT_{CTERM} being intrinsically disordered and with the absence of this region from the crystal structure of full-length β-catenin (73). Conventional triple resonance experiments were utilized to manually assign 115/118 residues and 94% of the backbone resonances of βCAT_{CTERM} (Figure 2.2A). Analysis of secondary structure propensity (SSP) (157), indicates that there are no extended regions of sequence with a SSP score magnitude > 0.3, suggesting that βCAT_{CTERM} does not have significant residual α-helix or β-sheet secondary structure (Figure 2.2B).

To better define the boundaries of the C-terminal β-catenin transactivation domain, the ability of various regions of β-catenin to influence transcription was tested using a luciferase-based one-hybrid gene reporter assay. HEK 293A cells were co-transfected with a luciferase reporter and a mammalian expression plasmid

encoding for various regions of β-catenin fused with a GAL4 DNA-binding domain. While some activity was observed for the N-terminal region of β-catenin, the β-catenin C-terminal region demonstrated potent transcription activation of the luciferin reporter with 1500-fold more activation than GAL4 alone (Figure 2.2C). Transfection of pGAL4-βCAT$_{CTERM\Delta TAD2}$ did not induce luciferase expression, indicating the functional importance of the C-terminal 31 amino acids for β-catenin transcription activation.

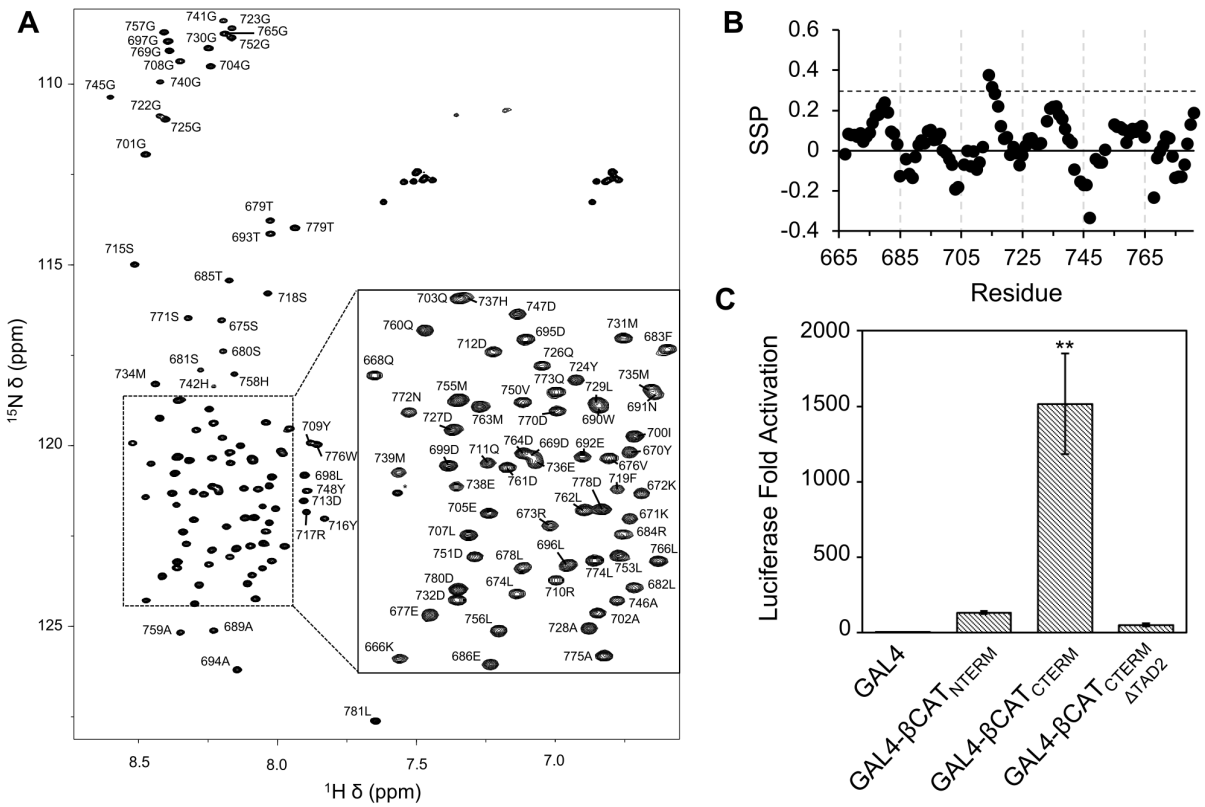

Figure 2.2. The C-terminal transactivation domain of β-catenin is disordered. (A) ^{1}H-^{15}N HSQC of βCAT$_{CTERM}$ with residue assignments of peaks indicated. (B) Secondary structure propensity (SSP) values per residue of βCAT$_{CTERM}$ calculated from Cα and Cβ chemical shifts. (C) Luciferase-based mammalian one-hybrid transactivation assay performed in HEK 293A cells using the indicated pGAL4-βCAT fusion proteins. Statistical significance set at p-value ≤ 0.01** by one-way ANOVA and Dunnett's multiple comparison test compared to pGAL4 control, with standard deviation shown (n=3 technical replicates).

2.5.2 The C-terminal β-catenin Transactivation Domain Interacts with TAZ1 and TAZ2

To identify if the KIX, TAZ1, or TAZ2 domains of CBP/p300 interact with the C-terminal transactivation domain of β-catenin, I completed a pulldown assay involving recombinantly produced and purified GB1-βCAT proteins. SDS-PAGE analysis of total protein following the experiment indicates that βCAT_{CTERM} interacts with isolated TAZ1 and TAZ2 (Figure 2.3). This association with TAZ1 and TAZ2 is maintained for βCAT_{TAD2} but not observed for $\beta CAT_{CTERM\Delta TAD2}$. The KIX domain of CBP/p300 did not interact with any of the β-catenin constructs that were tested.

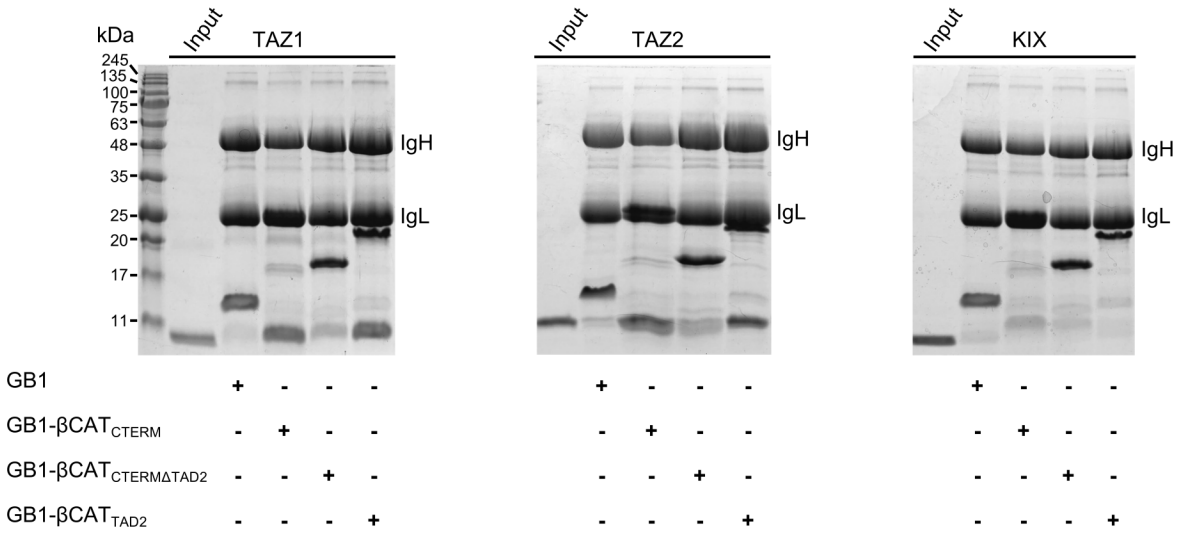

Figure 2.3. βCAT$_{CTERM}$ binds the TAZ1 and TAZ2 domains of CBP/p300. (A) SDS-PAGE analysis of pulldown of the TAZ1, TAZ2, and KIX domains of CBP/p300 by GB1-βCAT fusion proteins. Left lanes show migration of each isolated CBP/p300 domain. IgH and IgL indicate the heavy and light chains of immunoglobulin G, respectively, which originate from the pulldown resin.

2.5.3 Characterization of β-catenin:TAZ1 Binding

To determine what residues of βCAT_{CTERM} are responsible for TAZ1 binding, a ^{15}N-labelled βCAT_{CTERM} sample was prepared and titrated with unlabelled TAZ1 (Figure 2.4A and full spectrum shown in Figure 2.5). ^{1}H-^{15}N HSQC resonance peaks shifted upon addition of TAZ1, indicating that there is a specific interaction between these proteins. Comparisons of chemical shift changes (Δδ, Figure 2.4B) in the absence and presence of TAZ1 show residues Phe683-Ile700 and those C-terminal of Leu729 experience the largest chemical shift changes, with many residues between Asp750-Leu781 undergoing line broadening and not being visible upon addition of TAZ1. These changes indicate that TAZ1 interacts with these regions of β-catenin. ITC revealed that βCAT_{CTERM} and βCAT_{TAD2} both have relatively high-affinity and one-site binding for TAZ1 (K_d 0.26 ± 0.02 μM and 0.38 ± 0.02 μM, respectively; Figures 2.4C, D). Consistent with the pulldown data, $\beta CAT_{CTERM\Delta TAD2}$ weakly interacts with TAZ1 (K_d 67 ± 20 μM; Figure 2.6).

The loss of signal for many residues between Asp750-Leu781 is likely due to chemical exchange induced by interaction with TAZ1. To characterize this interaction, ^{15}N-labelled βCAT_{TAD2} was titrated with unlabelled TAZ1 and chemical shift changes were observed using NMR spectroscopy (Figure 2.7), where Gly757-Asp761 and Trp776-Asp780 experienced the largest chemical shift changes of any residues. This observed binding of motifs within βCAT_{TAD2} to TAZ1 is consistent with deletion of this sequence ablating transactivation by GAL4-βCAT_{CTERM} (Figure 2.2C).

NMR-based chemical shift mapping studies were performed to define where on the TAZ1 surface βCAT_{TAD2} binds (Figure 2.8). Upon addition of βCAT_{TAD2}, a subset of resonances of ^{15}N-labelled TAZ1 shifted, indicative of a specific interaction between these proteins (Figure 2.8A, B). Mapping of the significantly perturbed residues onto the structure of TAZ1 (PDBID: 1U2N) (154), revealed that βCAT_{TAD2} binds to a shallow hydrophobic groove formed by the junction of the α1 and α2 helices of TAZ1 (Figure 2.8C). In contrast, fewer chemical shift changes were observed on the opposing side of TAZ1 or on helices α3 and α4 which could be an effect of allosteric changes to the molecule upon binding.

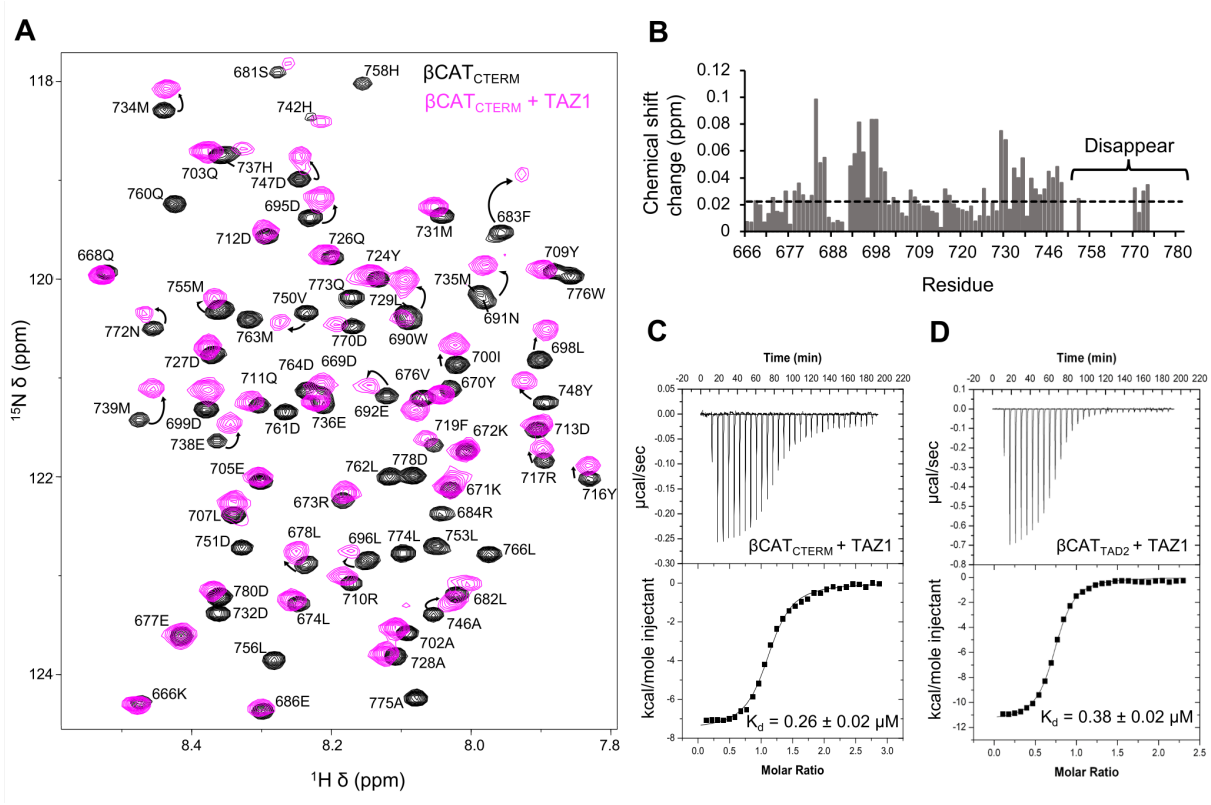

Figure 2.4. βCAT$_{CTERM}$ binds TAZ1 with high affinity. (A) ^{1}H-^{15}N HSQC overlay of ^{15}N-labelled βCAT$_{CTERM}$ in the absence (black) and presence (pink) of a saturating amount of TAZ1 (pink). Annotated arrows indicate residues experiencing chemical shift changes upon addition of TAZ1. (B) Chemical shift changes ($\Delta\delta = [(0.17\Delta\delta_N)^2 + (\Delta\delta_{HN})^2]^{1/2}$) for each residue of βCAT$_{CTERM}$ upon addition of TAZ1. Resonances that disappear due to line-broadening are noted and the dashed line represents the mean Δδ. (C) Isothermal titration calorimetry thermograms of TAZ1 titrated into βCAT$_{CTERM}$ (C) or βCAT$_{TAD2}$ (D) and fit to a one-site binding model (n=2 biological replicates, error reported as SD).

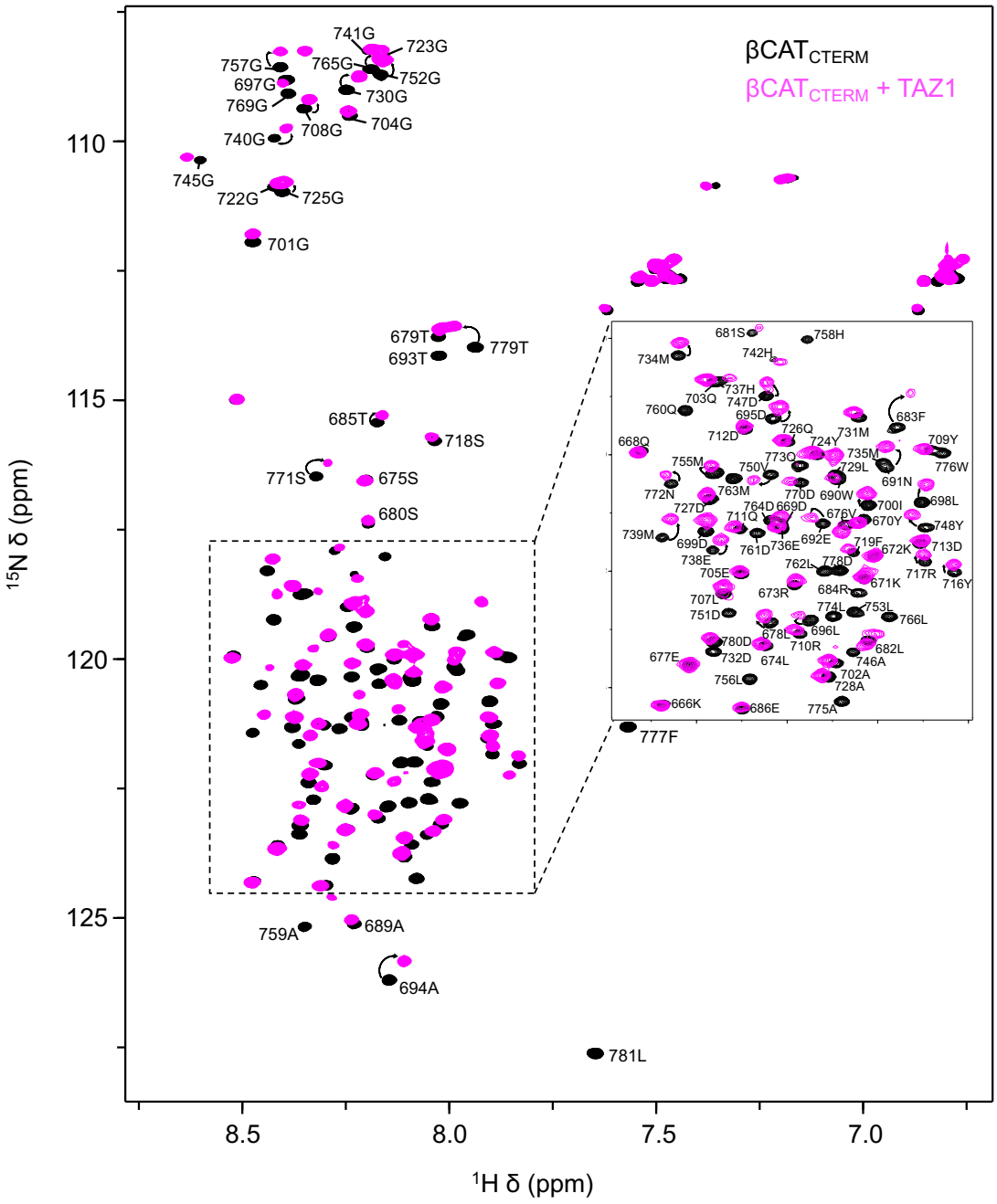

Figure 2.5. HSQC spectra of βCAT$_{CTERM}$ with TAZ1. ^{1}H-^{15}N HSQC spectra of 100 µM ^{15}N-labelled βCAT$_{CTERM}$ overlayed in the absence (black) and presence (pink) of 400 µM unlabeled TAZ1. Resonance assignments and direction of peak movement upon addition of TAZ1 are indicated.

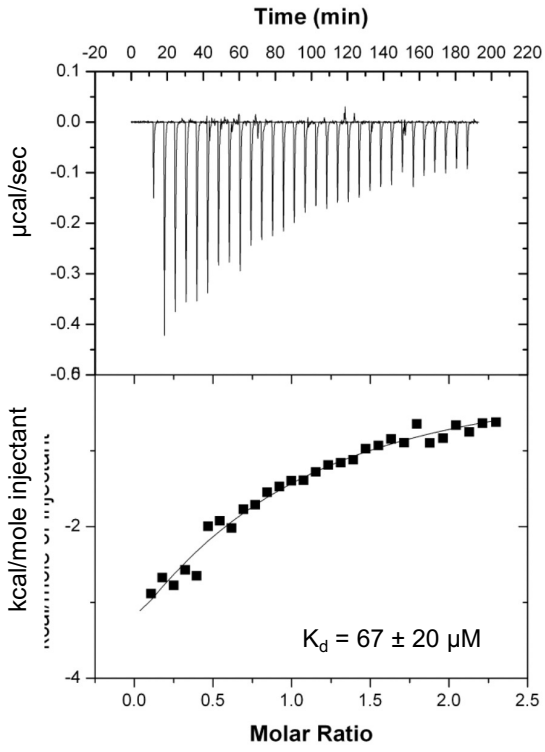

Figure 2.6. ITC analysis of $\beta CAT_{CTERM\Delta TAD2}$ and TAZ1. Isothermal titration calorimetry thermogram of 200 µM TAZ1 titrated into 20 µM $\beta CAT_{CTERM\Delta TAD2}$ (K_d = 67 ± 20 µM).

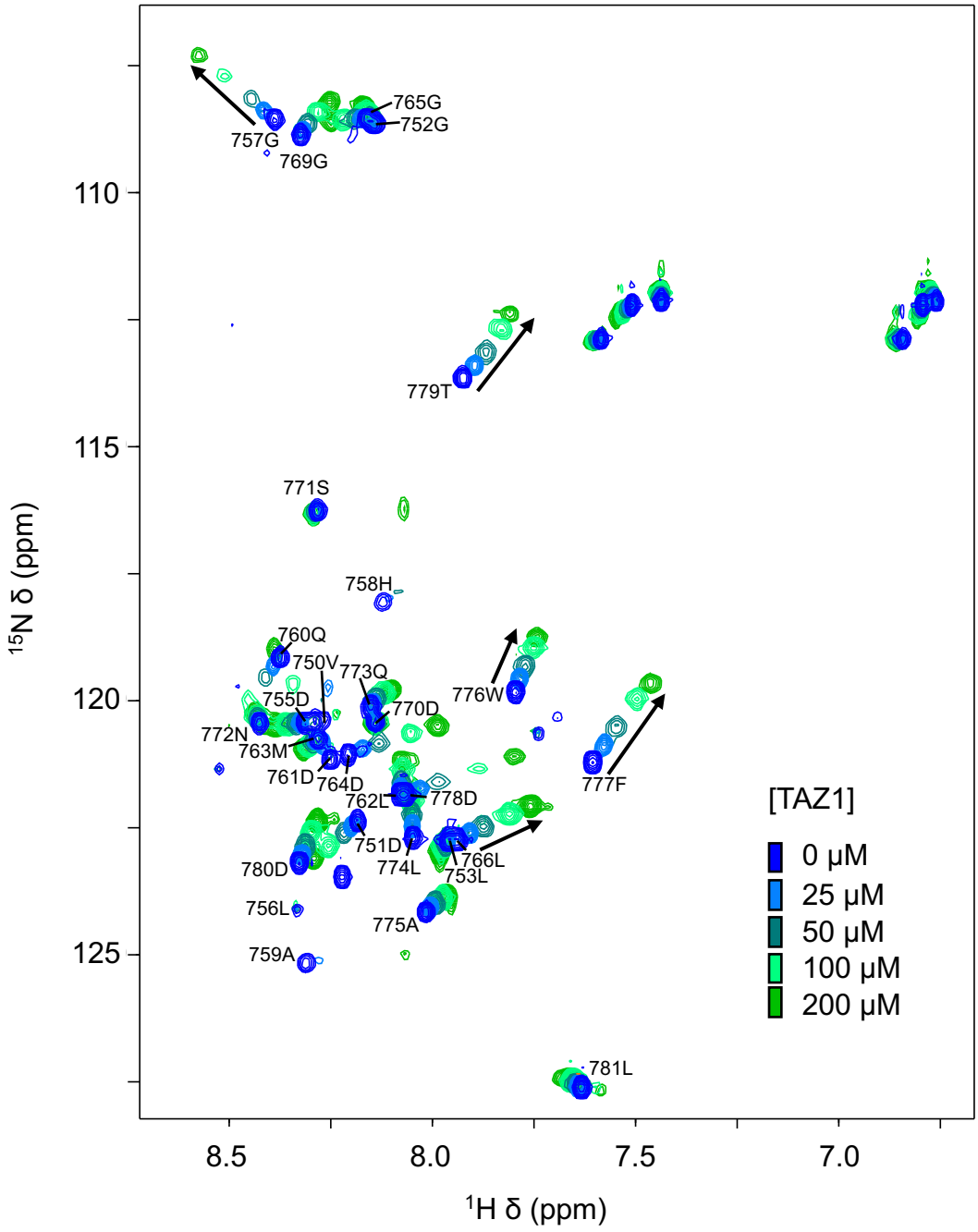

Figure 2.7. HSQC spectra of βCAT_{TAD2} with TAZ1. ^{1}H-^{15}N HSQC of 100 µM ^{15}N-labelled βCAT_{TAD2} (royal blue) titrated with up to 200 µM unlabeled TAZ1 (green). Resonance assignments of βCAT_{TAD2} are annotated and direction of peak movement upon addition of TAZ2 are indicated.

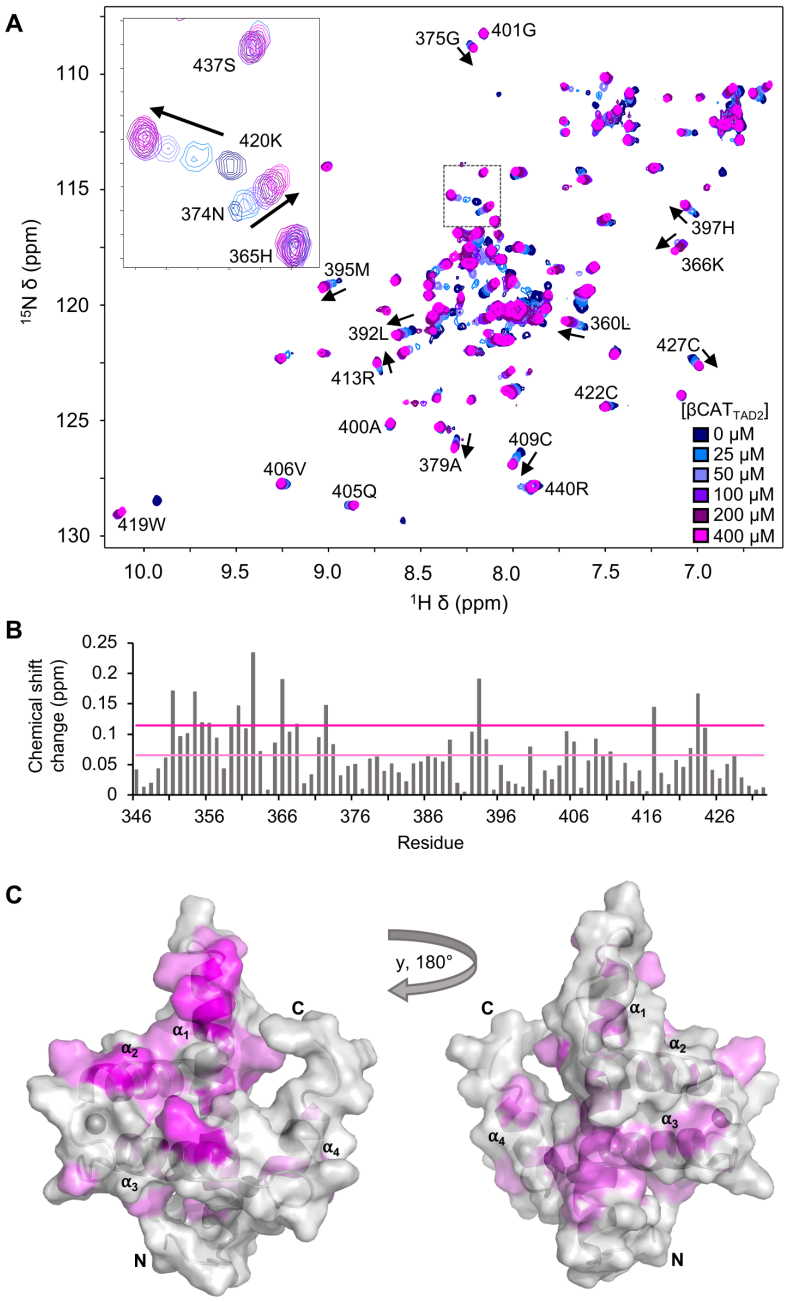

Figure 2.8. βCAT$_{TAD2}$ interaction site mapped onto TAZ1 surface. (A) Overlay of ^{1}H-^{15}N HSQC spectra of 100 μM ^{15}N-labelled TAZ1 titrated with 400 μM of unlabelled βCAT$_{TAD2}$. (B) Chemical shift changes ($\Delta\delta = [(0.17\Delta\delta_N)^2 + (\Delta\delta_{HN})^2]^{1/2}$) that each residue of TAZ1 experienced upon addition of βCAT$_{TAD2}$ are calculated for each residue. (C) Residues with above the mean Δδ (pink) and mean Δδ + standard deviation (magenta) mapped onto a semi-transparent surface of TAZ1 (PDBID: 1U2N). These values are also represented as coloured lines in panel (B).

2.5.4 Characterization of β-catenin:TAZ2 Binding

To characterize the βCAT_{CTERM}:TAZ2 interaction, ^{15}N-labelled βCAT_{CTERM} was titrated with unlabelled TAZ2 and a shift of a subset of β-catenin amide resonances was observed in the ^{1}H-^{15}N HSQC spectra as a function of the addition of TAZ2 (Figure 2.9A and full spectrum shown in Figure 2.10). Quantification of chemical shift perturbations indicate that two regions from residues Pro714-Gly741 and Asp750-Leu781 experienced the largest changes in chemical shift (Figure 2.9B). Unlike TAZ1, ITC analysis indicates that βCAT_{CTERM} binds TAZ2 at two different sites (K_{d1} 0.16 ± 0.04 μM, K_{d2} 7.09 ± 1.4 μM; Figure 2.9C), with βCAT_{TAD2} maintaining high affinity for TAZ2 (K_{d1} 0.65 ± 0.06 μM, K_{d2} 1.18 ± 0.43 μM; Figure 2.9D) these two sites can be close in space or indicative of conformational change.

To determine the binding site of βCAT_{TAD2} on the TAZ2 surface, ^{15}N-labelled TAZ2 was titrated with unlabelled βCAT_{TAD2}, and backbone amide chemical shift changes were monitored (Figure 2.11A, B). Residues experiencing chemical shift changes larger than the average plus one standard deviation were mapped onto a previously determined structure of TAZ2 (PDBID: 1F81) (155). These findings indicate that βCAT_{TAD2} binding is dispersed over the TAZ2 surface with select residues within α1-α4 experiencing large chemical shift changes, which is consistent with our finding that βCAT_{TAD2} interacts with TAZ2 at multiple sites (Figure 2.11C).

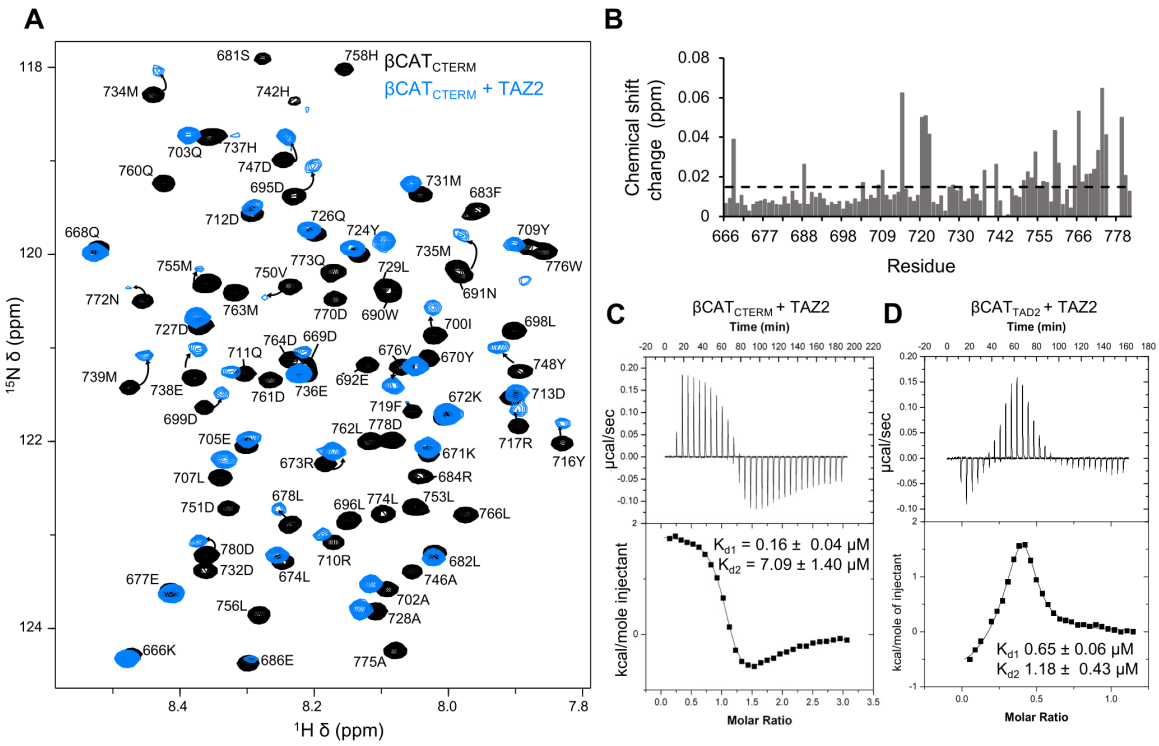

Figure 2.9. βCAT$_{CTERM}$ binds TAZ2. Superposition of ^{1}H-^{15}N HSQC spectra of ^{15}N-labelled βCAT$_{CTERM}$ overlayed in the absence (black) and presence (blue) of saturating amounts of TAZ2 (blue). Annotated arrows indicate residues experiencing chemical shift changes upon TAZ2 addition. (B) Weighted chemical shift changes ($\Delta\delta = [(0.17\Delta\delta_N)^2 + (\Delta\delta_{HN})^2]^{1/2}$) for residues of βCAT$_{CTERM}$ upon addition of TAZ2, the dashed line represents the mean Δδ. (C,D) Isothermal titration calorimetry thermograms of TAZ2 titrated into βCAT$_{CTERM}$ (C) or βCAT$_{TAD2}$ (D). Data were fit to a two-site binding model and dissociation constants are indicated (n=2 biological replicates, error reported as SD).

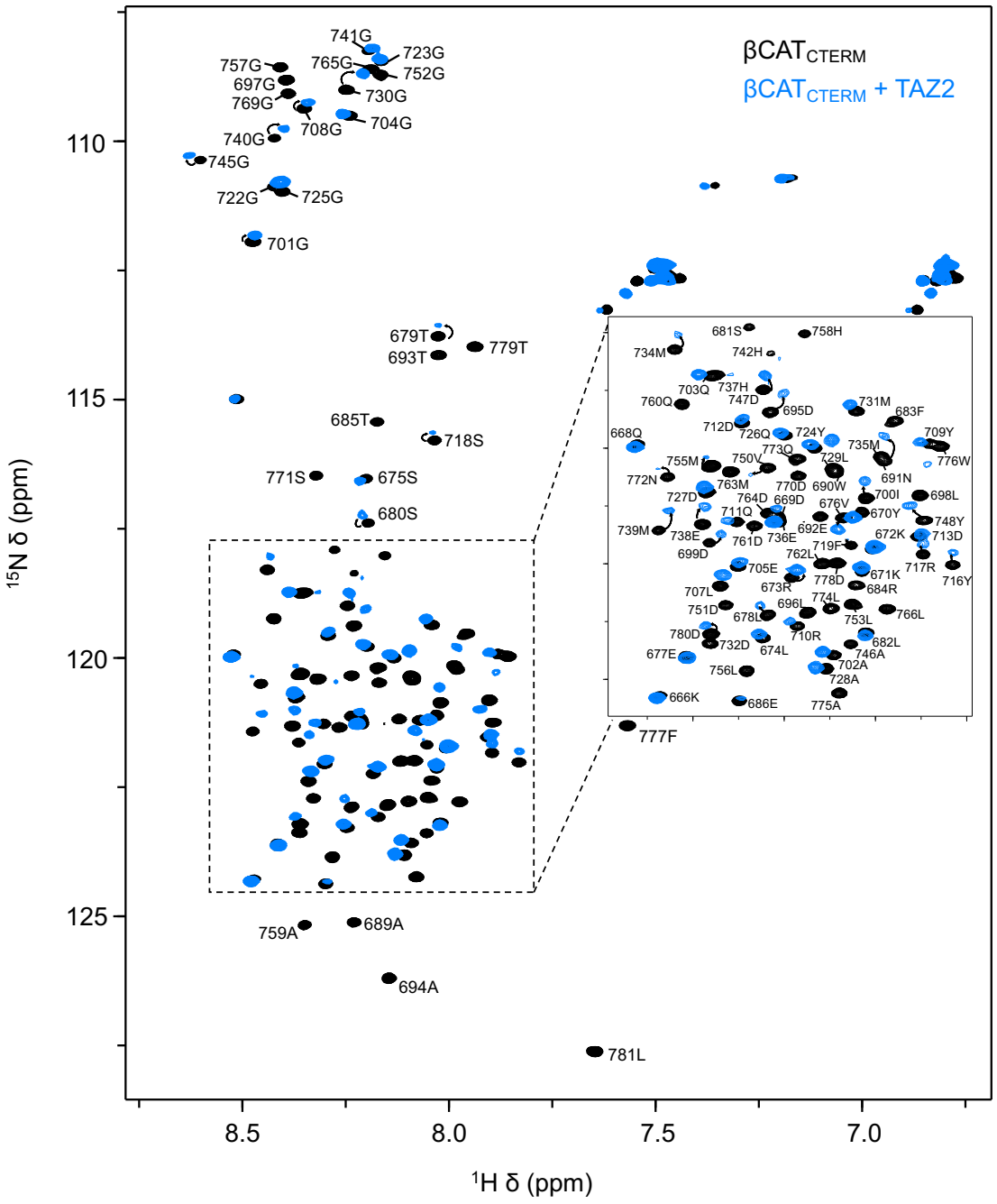

Figure 2.10. HSQC spectra of βCAT$_{CTERM}$ with TAZ2. ^{1}H-^{15}N HSQC of 100 μM ^{15}N-labelled βCAT$_{CTERM}$ overlayed in the absence (black) and presence (blue) of 400 μM unlabeled TAZ2. Resonance assignments and direction of peak movement upon addition of TAZ2 are indicated.

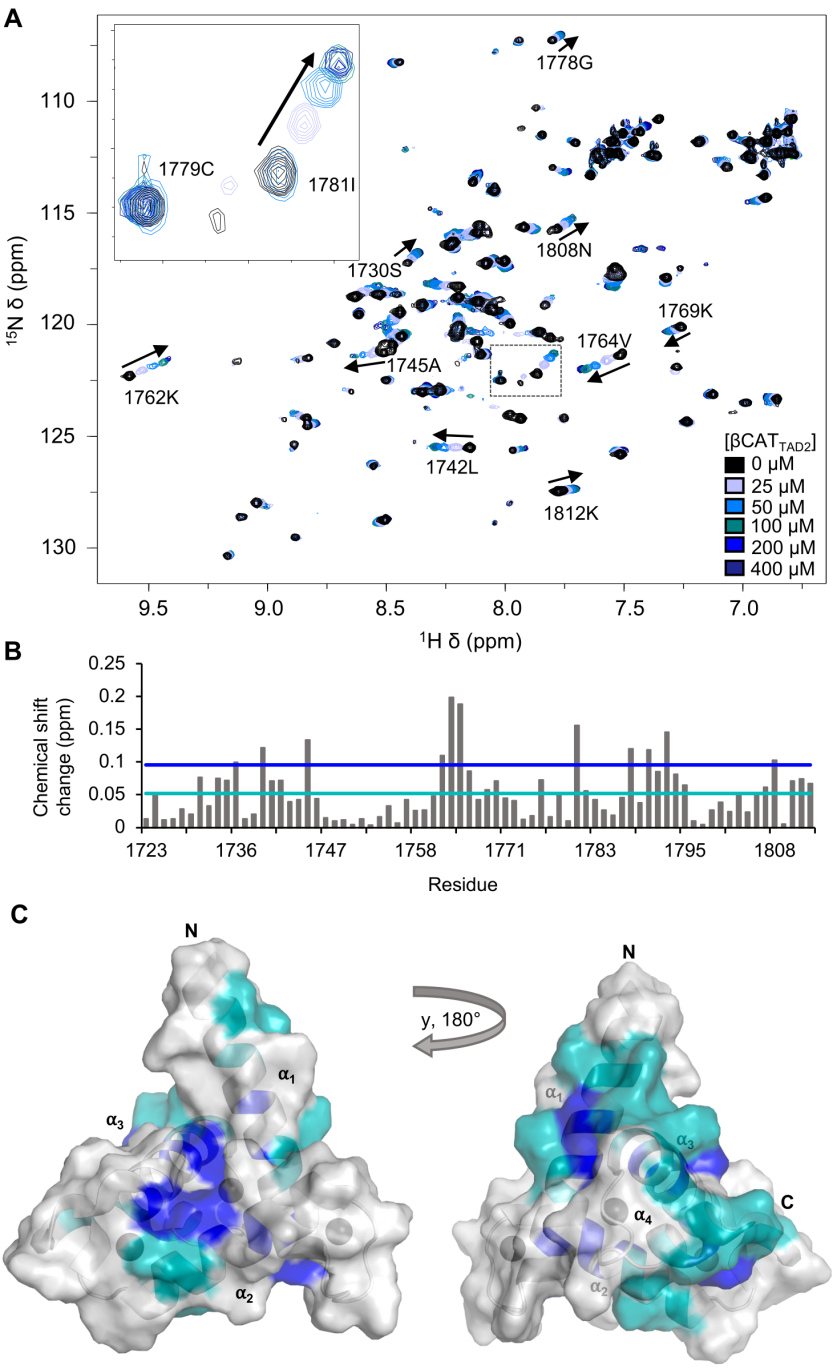

Figure 2.11. βCAT$_{TAD2}$ interaction site mapped onto TAZ2 surface. (A) Overlay of ^{1}H-^{15}N HSQC spectra of 100 μM ^{15}N-labelled TAZ2 titrated with 400 μM of unlabelled βCAT$_{TAD2}$. (B) Chemical shift changes ($\Delta\delta = [(0.17\Delta\delta_N)^2 + (\Delta\delta_{HN})^2]^{1/2}$) that each residue of TAZ2 experienced upon addition of βCAT$_{TAD2}$ were calculated for each residue. (C) Residues with Δδ above the mean Δδ (blue) and mean Δδ + standard deviation (navy) mapped onto a semi-transparent surface representation of TAZ2 (PDBID: 1F81). These values are also represented as coloured lines in panel (B).

2.5.5 Hydrophobic and Acidic Residues Mediate Binding between β-catenin and TAZ1

Since β-catenin interacts more specifically with TAZ1 than TAZ2, I used mutagenesis to investigate which residues of β-catenin mediate this interaction. βCAT_{TAD2} contains acidic and hydrophobic residues that are conserved and often important for binding CBP/p300, and many of these also experience above average shift perturbations upon addition of TAZ1 (Figures 2.12A, B and 2.7). To test if these residues were critical to the β-catenin:TAZ1 interaction, acidic or hydrophobic residues of βCAT_{CTERM} that undergo large chemical shift changes upon TAZ1 binding were substituted for alanine (D751A, D761A, D764A, F777A). ITC experiments determined that these mutants bind TAZ1 only slightly weaker than βCAT_{CTERM}, with measured dissociation constants (K_d) of 0.39 ± 0.03 μM, 0.60 ± 0.06 μM, 0.32 ± 0.02 μM, and 0.55 ± 0.04 μM for D751A, D761A, D764A and F777A, respectively (Figures 2.12C and 2.13). Deletion of small motifs across βCAT_{CTERM} (Δ757-761, Δ761-765, Δ776-779) was sufficient to make binding to TAZ1 undetectable by ITC (Figure 2.14).

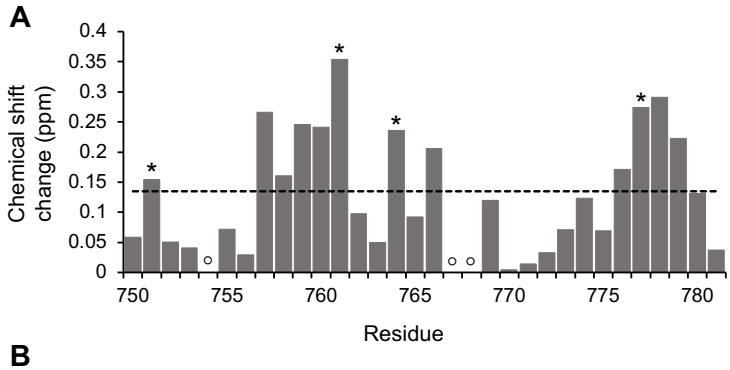

B

```
          *        *  *           *
βCAT_HS   VDGLPDLGHAQDLMDGLPPGDSNQLAWFDTDL
βCAT_CL   VDGLPDLGHAQDLMDGLPPGDSNQLAWFDTDL
βCAT_MM   VDGLPDLGHAQDLMDGLPPGDSNQLAWFDTDL
βCAT_DR   VDGLPDLGHTQDLIDGLPPGDSNQLAWFDTDL
βCAT_XL   VDGLPDLSHAQDLMDGLPPGDSNQLAWFDTDL
```

C

Construct	Ligand	Binding Model	K_d (μM)
βCAT_{CTERM}	TAZ2	Two-site	0.16 ± 0.04, 7.09 ± 1.40
βCAT_{TAD2}	TAZ2	Two-site	0.65 ± 0.06, 1.18 ± 0.43
βCAT_{CTERM}	TAZ1	One-site	0.26 ± 0.02
βCAT_{TAD2}	TAZ1	One-site	0.38 ± 0.02
$\beta CAT_{CTERM\ D751A}$	TAZ1	One-site	0.39 ± 0.03
$\beta CAT_{CTERM\ D761A}$	TAZ1	One-site	0.60 ± 0.03
$\beta CAT_{CTERM\ D764A}$	TAZ1	One-site	0.32 ± 0.02
$\beta CAT_{CTERM\ F777A}$	TAZ1	One-site	0.55 ± 0.04
$\beta CAT_{CTERM\ \Delta TAD2}$	TAZ1	One-site	67.0 ± 20.0
$\beta CAT_{CTERM\ \Delta 757-761}$	TAZ1	No binding	–
$\beta CAT_{CTERM\ \Delta 761-765}$	TAZ1	No binding	–
$\beta CAT_{CTERM\ \Delta 776-779}$	TAZ1	No binding	–

Figure 2.12. βCAT_{CTERM} binds TAZ1 though acidic and hydrophobic residues. (A) Chemical shift changes ($\Delta\delta = [(0.17\Delta\delta_N)^2 + (\Delta\delta_{HN})^2]^{1/2}$) that each residue of βCAT_{TAD2} experienced upon addition of saturating amounts of TAZ1, with the dashed line representing the mean Δδ. Residues that were selected for site-directed mutagenesis are denoted by *, while empty circles indicate proline residues that could not be monitored via ^{1}H-^{15}N HSQC. (B) Sequence alignment of C-terminal activation domains of β-catenin human (HS), dog (CL), mouse (MM), zebrafish (DR) and African clawed frog (XL). Hydrophobic (yellow) and acidic (red) residues are highlighted, and residues selected for site-directed mutagenesis are denoted by *. (C) Summary table of all isothermal titration calorimetry binding models and relative affinities (K_d) of complexes determined in this study (n=2 biological replicates, error reported as SD).

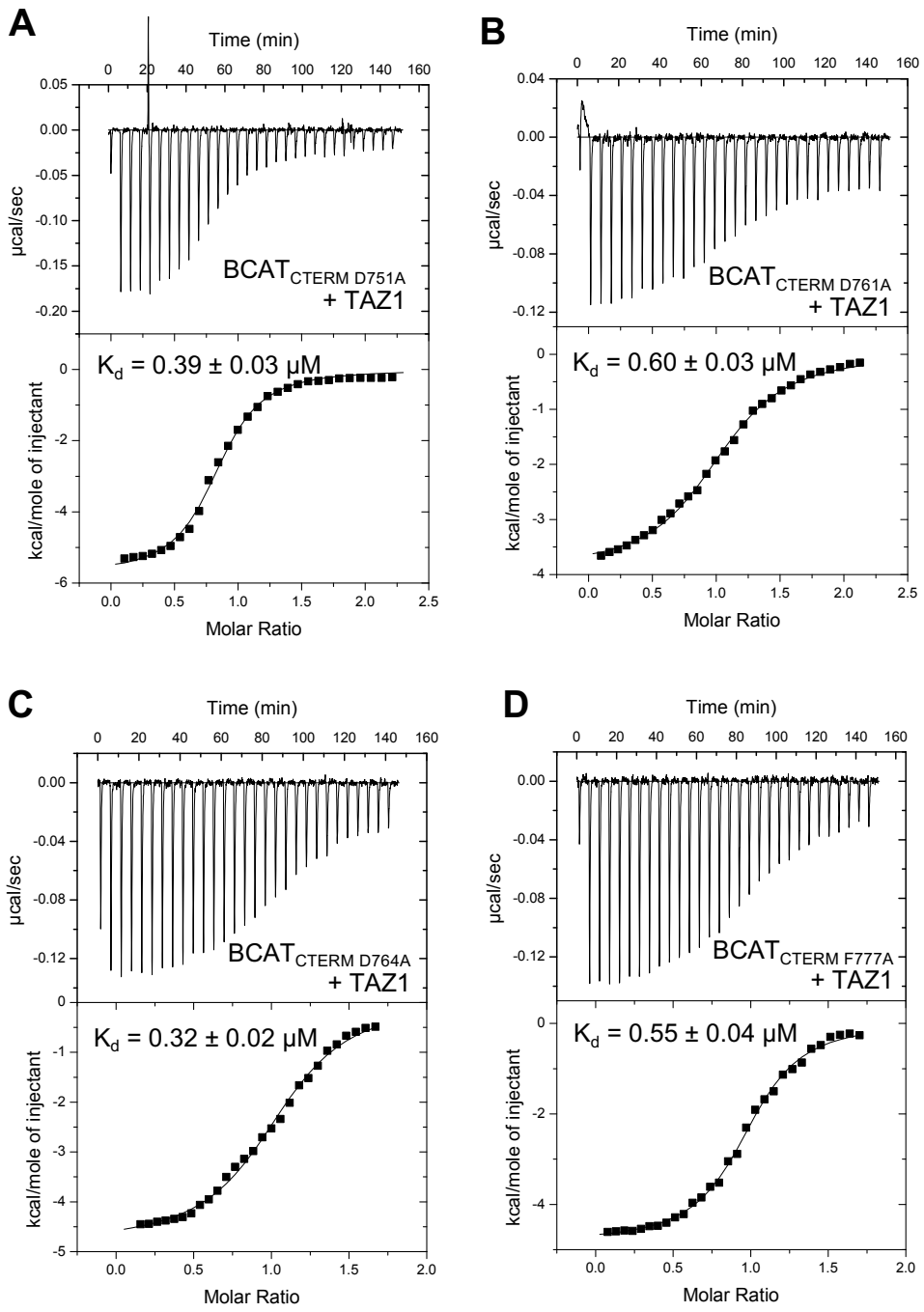

Figure 2.13. ITC of βCAT_{CTERM} alanine mutants with TAZ1. (A-D) Isothermal titration calorimetry thermograms of TAZ1 titrated into βCAT_{CTERM} mutants D751A, D761A, D764A, and F777A, fit to a one-site binding model yielding dissociation constants (K_d) of 0.39 ± 0.03 µM, 0.60 ± 0.03 µM, 0.32 ± 0.02 µM, and 0.55 ± 0.04 µM, respectively (n=2 biological replicates, error reported as SD).

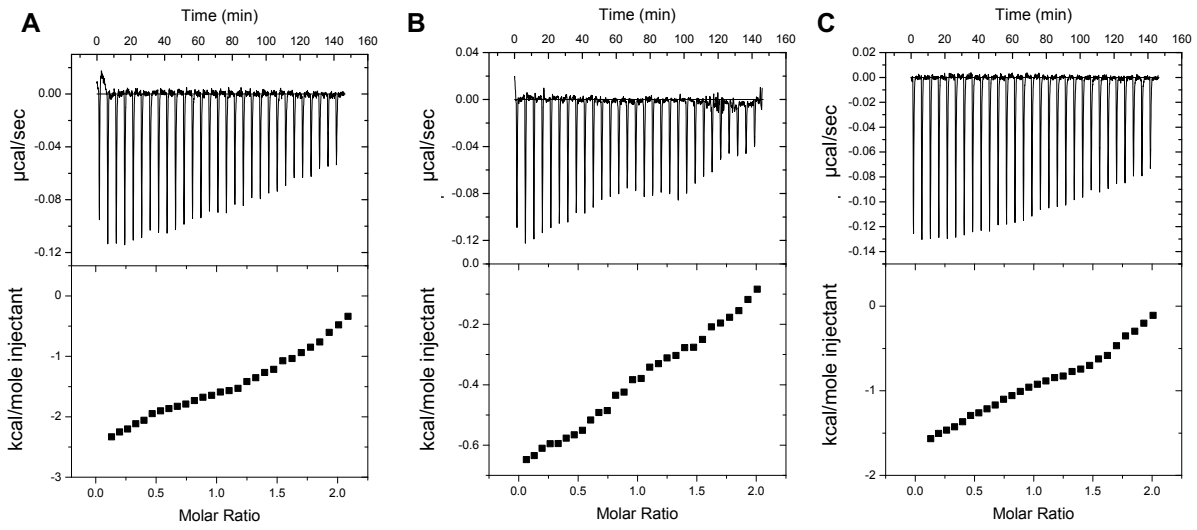

Figure 2.14. ITC of βCAT_{CTERM} deletion mutants with TAZ1. (A) Isothermal titration calorimetry thermograms of 100 µM TAZ1 titrated into 8 µM $\beta CAT_{CTERM\Delta 757\text{-}761}$ (B) $\beta CAT_{CTERM\Delta 761\text{-}765}$ or (C) $\beta CAT_{CTERM\Delta 776\text{-}779}$.

2.6 Discussion

β-catenin is a critical nuclear effector of the canonical Wnt-signaling pathway, however, aberrant activation causing hyperaccumulation of β-catenin is broadly implicated in many major types of cancer (158, 159). Nuclear β-catenin forms transcriptional complexes with co-activators such as CBP/p300, which together enhance the transcription of oncogenes driving cancer initiation and progression (67). Here I examine the recruitment of CBP/p300 by the C-terminal transactivation domain of β-catenin and elucidate fundamental molecular mechanisms of β-catenin-dependent gene transcription. I observe that βCAT_{CTERM} is intrinsically disordered and interacts with both the TAZ1 and TAZ2 domains of CBP/p300 with high affinity. This interaction is mediated by both acidic and hydrophobic amino acids within TAD2 of β-catenin, where mutagenesis of this region ablates transactivation potential and interactions with TAZ1.

Intrinsically disordered regions are abundant in transcription regulators, as their structural flexibility allows them to be highly dynamic and helps to facilitate promiscuous protein-protein interactions with a multitude of different binding partners. Promiscuity in binding of transcription regulators is key to the diversity of transcriptional complexes found at different gene promoters. The KIX, TAZ1, TAZ2 domains of CBP/p300 are candidate interaction sites for disordered transactivation domains of transcription regulators including HIF-1α, CITED2, STAT1/2, E2A, and p53 (27, 31, 55, 58, 146). While some TADs associate with high specificity to particular CBP/p300 domains, others like the TAD of tumor protein p53 have been shown to interact with promiscuity to TAZ1 (K_d 0.9 ± 0.2 μM), TAZ2 (K_d 26 ± 7

nM), and KIX (K_d 22 ± 5 μM) with a broad range of affinity and specificity (57, 160). Our observation that the β-catenin C-terminal transactivation domain interacts with both TAZ1 and TAZ2 in a redundant manner is consistent with this model of CBP/p300 recruitment. The binding promiscuity of the β-catenin C-terminal is also highlighted by its previous implication in binding to the N-terminal interaction domain of CBP/p300 (161). This redundancy, plays an important role in molecular recognition and transcription regulation as it may serve to increase the diversity of interactions that β-catenin can participate in at gene promoters (162).

TAZ1 consists of four α-helices that create three hydrophobic grooves that bind transactivation domains (154). Using NMR-based chemical shift mapping studies, I determined that βCAT_{TAD2} interacts with TAZ1 with relatively high affinity (K_d 0.38 ± 0.02 μM) through an extended interface along helix α1, and in the hydrophobic groove between helices α1 and α2 (Figure 2.8). The unstructured nature of transactivation domains allows for considerable conformational changes upon binding target molecules, thus enabling different TADs with various sequences to bind common partners. Despite their low sequence similarity, TAZ1 interacts with TADs of HIF-1α (K_d 10 ± 5 nM), CITED2 (K_d 13 ± 10 nM), STAT2 (K_d 58 ± 3 nM), and RelA (K_d 57 ± 3 nM) at binding sites corresponding to that of βCAT_{TAD2} with conserved intermolecular contacts at the α1/α2 junction (Figure 2.15) (31, 55, 56, 146). Previous reviews have noted that the presence of hydrophobic residues is a common feature of TADs that bind TAZ1/2 (40). These types of residues are highly conserved within βCAT_{TAD2}, which shares ~90% sequence identity with β-catenin in other vertebrates (Figure 2.12B). These residues likely form extensive hydrophobic

contacts once bound within the grooves of TAZ1, providing overall stability to the transcriptional complex.

TAZ2 adopts a similar structure to TAZ1, but is differentiated by the opposite orientation of helix α4 (29,30). Even though TAZ1 and TAZ2 have similar topology, both domains differ in terms of sequence and binding specificity, with TAZ1 having deeper groves in its surface than TAZ2. Despite this, the flexibility of the β-catenin C-terminal transactivation domain can compensate for differences in topology and bind both TAZ1 and TAZ2 with relatively high affinity. NMR chemical shift mapping indicated that βCAT_{TAD2} binds TAZ2 through extended interactions across multiple helices (Figure 2.11), this is consistent with our ITC data that detected multiple binding sites between βCAT_{TAD2} and TAZ2, and similar to other transactivation domains like those of p53 and STAT1, which wrap around TAZ2 with multiple points of contact (Figures 2.17A, B) (31, 163). Interestingly, p53 has been shown to compete with β-catenin for CBP/p300, which may be occurring through direct competition for TAZ2 domain at gene promoters (164). Similarly, the adenoviral peptide E1A, which directly impairs β-catenin-mediated transcription by competing for CBP/p300, also interacts at one of the βCAT_{TAD2} : TAZ2 binding interfaces (Figure 2.17) (142).

By ITC I observe that one molecule of βCAT_{TAD2} can bind two molecules of TAZ2, while oddly the chemical shift changes observed for both TAZ2 and βCAT_{TAD2} during NMR titrations are linear, which suggests a 1:1 complex and two-state binding. This conflicting result may indicate potential conformational change upon binding or be because the two TAZ2 binding sites present on βCAT_{TAD2} are

sufficiently isolated from each other that they are not affected by binding at the other site. Although in this latter scenario TAZ2 would be in fast exchange between 3 states, the affinities of the binding sites may be similar enough that linear chemical shift changes are still observed. Future studies could work to further delineate these TAZ2 binding sites within βCAT_{TAD2}.

Both TAZ1 and TAZ2 are basic proteins with a strongly electropositive surface that preferentially bind acidic motifs, where electrostatic interactions mediate transactivation domain recognition and specificity (Figures 2.16, 2.18). Our findings demonstrate that deletion of acidic residues within the β-catenin transactivation domain reduces βCAT_{CTERM}:TAZ1 binding, highlighting the importance of electrostatic interactions for TAZ1 recognition. TAZ1-binding favours extended disordered domains with multiple amphipathic motifs, which may explain why β-catenin point mutants that removed a single acidic or hydrophobic contact reduced but did not completely ablate the interaction between βCAT_{CTERM} and TAZ1.

The association of β-catenin with CBP/p300 may also be regulated by post-translational modifications such as acetylation and phosphorylation. CBP/p300-medaited acetylation of β-catenin is frequently disrupted by mutation in thyroid cancers, causing an increase in β-catenin activity (165). Additionally, numerous serine and threonine residues are present in the β-catenin transactivation domain and phosphorylation of C-terminal β-catenin by protein kinase A has been shown to increase both β-catenin transcriptional activity and help facilitate its interactions with CBP/p300 (166, 167). This is similar to the p53 transactivation domains, which modulate interactions with CBP/p300 through phosphorylation (168), as such

modifications may serve to enhance the electrostatic interactions and overall affinity of these domains for TAZ1 or TAZ2.

Overall, I have characterized how the C-terminal TAD of β-catenin binds to both the TAZ1 and TAZ2 domains of CBP/p300, which provides mechanistic understanding of how β-catenin recruits CBP/p300 to mediate Wnt signaling. This work will aid future studies focused on interpreting the interplay between β-catenin and other transcription factors that bind CBP/p300, as well as developing molecules that disrupt the association of β-catenin with CBP/p300.

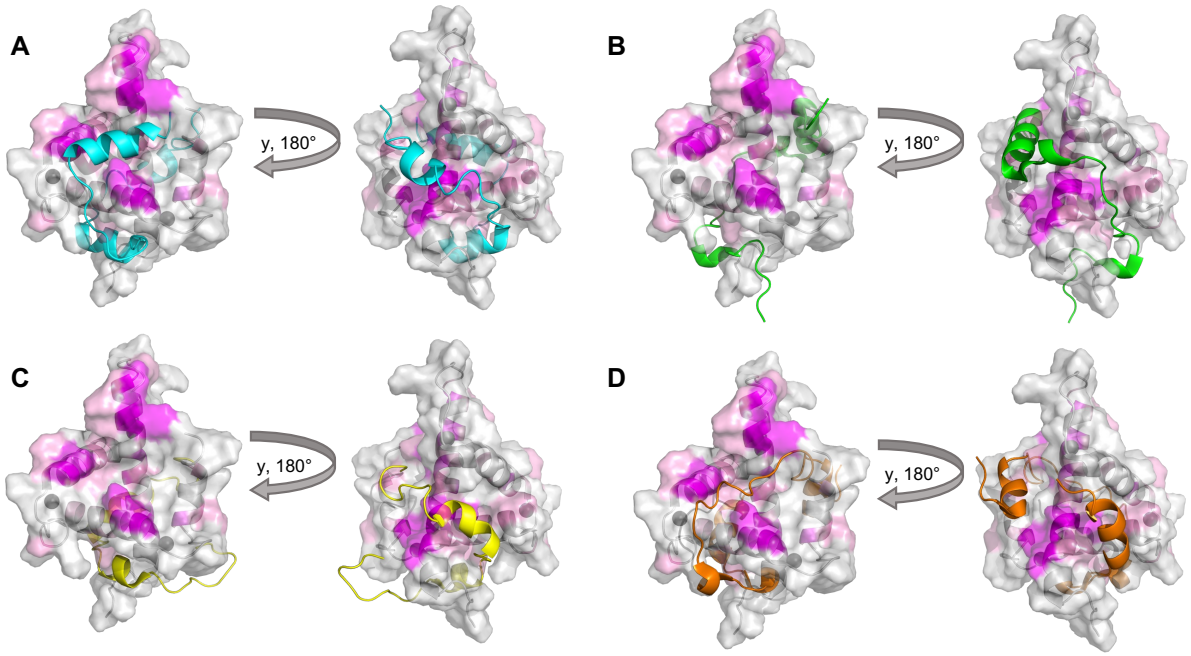

Figure 2.15. Comparison of βCAT$_{TAD2}$: TAZ1 interaction site. Surface representation of TAZ1 (PDBID: 1U2N) showing βCAT$_{TAD2}$ interaction site (magenta) overlayed with bound transactivation domains of (A) HIF-1α (1L8C; teal), (B) CITED2 (1R8U; green), (C) STAT2 (2KA4; yellow), and (D) RelA (2LWW; orange).

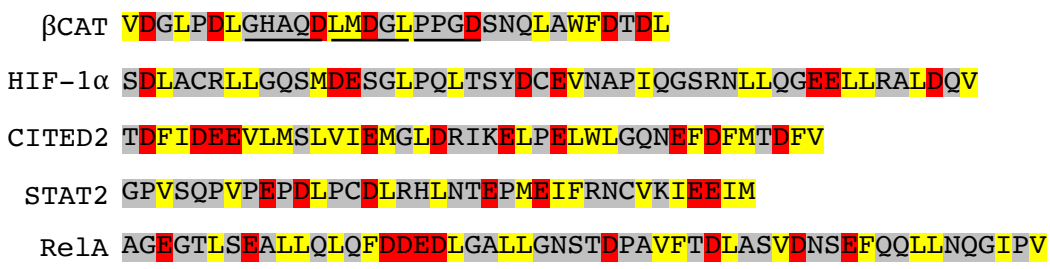

Figure 2.16. Amino acid sequences of TAZ1 binding TADs. TAZ1 binding regions of transactivation domains β-catenin (residues 750-781), HIF-1α (residues 776-781), CITED2 (residues 220-260), STAT2 (residues 780-816), and RelA (residues 431-484) annotated to show the occurrences of acidic (red), hydrophobic (yellow) residues, and regions of β-catenin deleted in mutagenesis studies (underlined).

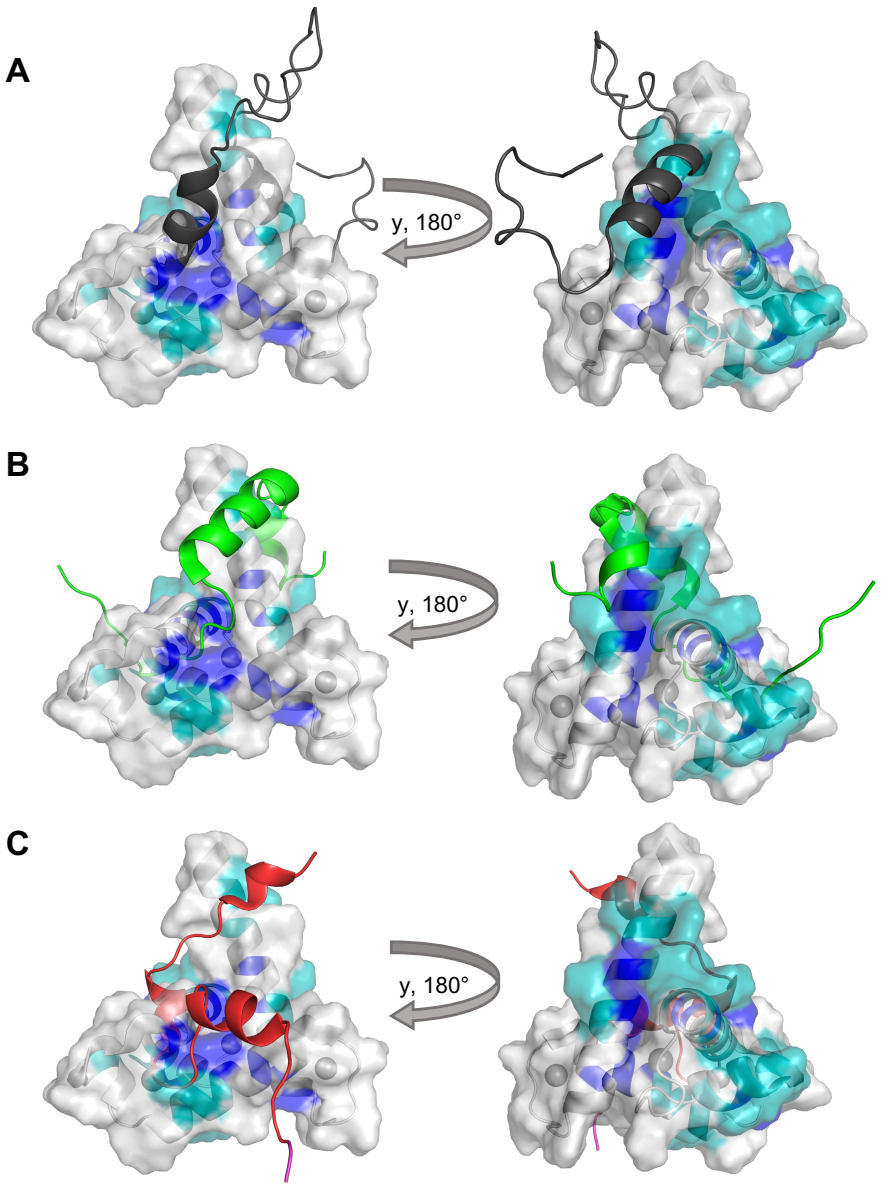

Figure 2.17. Comparison of βCAT_{TAD2}: TAZ2 interaction site. Surface representation of TAZ2 (PDBID: 1F81) showing βCAT_{TAD2} interaction site (blue) overlayed with bound transactivation domains of (A) p53 (5HPD; black), (B) STAT1 (2KA6; green) and (C) E1A (2KJE; red).

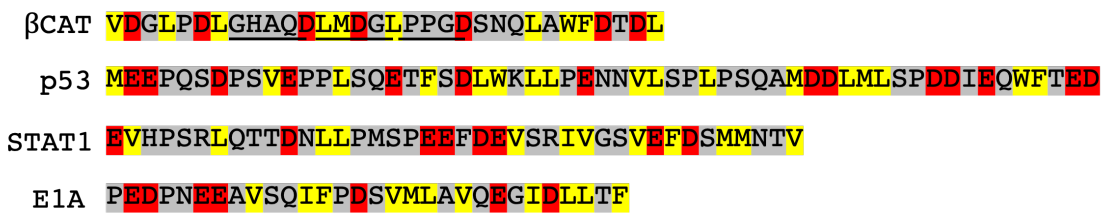

Figure 2.18. Amino acid sequences of TAZ2 binding TADs. Transactivation domains β-catenin (residues 730-781), p53 (residues 1-57), STAT1 (residues 710-750) and adenoviral E1A (residues 54-82) known to bind TAZ2, annotated to show the occurrences of acidic (red), hydrophobic (yellow) residues, and regions of β-catenin deleted in mutagenesis studies (underlined).

Chapter 3: Characterizing the association of co-regulator CBP/p300 with an N-terminal activation domain of β-catenin

3.1 Contributions of Authors

The following chapter contains the Abstract, Introduction, Methods, Results and Discussion sections of a manuscript intended for submission to Protein Science. Brown, A.D., Horner, R., Cranstone, C., Dupré, D.J., Langelaan, D.N. Characterizing the association of co-regulator CBP/p300 with an N-terminal activation domain of β-catenin. Undergraduate student Rachael Horner performed NMR assignments in Figure 3.7A. Connor Cranstone collected the NMR data and completed assignments presented in Figures 3.3A and 3.9. All additional experiments were carried out by me, including writing the first draft of the manuscript. Dr. Denis Dupré provided resources and guidance, and Dr. David Langelaan contributed materials, supervision, and assistance throughout the writing process.

3.2 Abstract

The transcriptional regulator β-catenin drives downstream gene expression of the canonical Wnt signaling pathway, which plays a major role in developmental processes and cancer pathogenesis. To coordinate the transcriptional response, β-catenin binds transcription factors and co-regulators, including the histone acetyltransferases CBP/p300 which enhance β-catenin gene activity. In this study I detail the molecular mechanisms by which the N-terminal β-catenin transactivation

domain (TAD1) interacts with CBP/p300. Using a combination of nuclear magnetic resonance spectroscopy and protein pulldown assays I determine that the structurally disordered N-terminal β-catenin recruits CBP/p300 through promiscuous interactions with the TAZ1 and TAZ2 domains. Characterization of the β-catenin TAD1:TAZ2 interaction by nuclear magnetic resonance spectroscopy shows that they form a high affinity but dynamic complex, with β-catenin TAD1 binding TAZ2 at the intersect of helices α-1, α-2 and α-3. Furthermore, I identify an adenovirus-based peptide inhibitor which can directly compete with β-catenin TAD1 for TAZ2 and can ablate transcription of a β-catenin-dependent luciferase reporter. Finally, I observe that both β-catenin TAD1 and the C-terminal TAD2 are necessary for β-catenin transcriptional function and suggest they may cooperate to recruit CBP/p300 to Wnt-related gene promoters. These findings highlight mechanistic details by which β-catenin sequesters co-activator CBP/p300 to control gene expression and proposes a way these interactions could be targeted to control Wnt/β-catenin signaling in the future.

3.3 Introduction

Wnt signaling is a well-conserved and tightly regulated signal transduction pathway that is critical to development by controlling numerous cellular processes including cell fate, polarity, motility, and survival (61, 169). Downstream gene expression of the canonical Wnt pathway is mediated by the intracellular effector β-catenin (170). Binding of Wnt proteins to their respective cell surface receptor (Frizzled and LRP5/6) activates the Wnt signaling cascade and inhibits the

degradation β-catenin (136). Stabilized β-catenin is then translocated to the nucleus where it coordinates the transcriptional response by binding and modulating the activity of DNA-bound transcription factors such as T-cell factor and lymphoid enhancer factor (TCF/LEF) (136). Given the wide array of cellular processes that Wnt/β-catenin signaling regulates, deregulation of the pathway is a well-known causative factor of many human pathologies including colon, breast, and skin cancers (171–173). In cancer cells, aberrant activation of the Wnt pathway leading to the nuclear accumulation of β-catenin is a key driver for the initiation and progression of the disease, accelerating both cancer cell proliferation and metastasis (174).

β-catenin is composed of a central repetitive armadillo repeat domain, a rigid super helical structure that provides the main interaction site for transcription factors like TCF/LEF (175). Flanking this domain are amino and carboxy terminal regions (residues 1-137 and 666-781, respectively) which are structurally flexible and possess potent transactivation domains (TAD1, residues 58-103; TAD2, residues 750-781) (Figure 3.1A). Once β-catenin is recruited to a transcription factor at a particular target gene promoter, transcription is activated as a result of these transactivation domains and their ability to mediate interactions with transcriptional co-regulators. This includes chromatin remodeling complexes SWI/SNF, as well as CREB-binding protein and its homolog (CBP/p300) which directly interact with β-catenin to promote gene activation (75, 142).

The expression of Wnt/β-catenin target genes is directly correlated with histone acetylation, which enhances the transcriptional response by modifying chromatin structure and allowing for more open and accessible DNA. This reaction is

catalyzed by the histone acetyltransferase proteins CBP/p300. CBP/p300 are large multi-domain proteins that connect transcription factors to the basal transcriptional machinery via direct interactions with general transcription factors and RNA polymerase II, acting as a scaffold for multi-protein transcriptional complexes (176, 177). CBP/p300 interact with hundreds of known binding partners through several interaction domains, namely the nuclear receptor interaction domain (NRID), kinase inducible domain (KIX), and transcription adaptor zinc finger domains (TAZ1 and TAZ2) (Figure 3.1B). CBP/p300 is recruited through the TAZ1 and TAZ2 domains by the C-terminal transactivation domain of β-catenin where it has been shown to mediate Wnt-target gene expression (77, 178). However, the interactions between CBP/p300 and the N-terminal TAD1 of β-catenin have not yet been explored.

In this study I characterize the interaction between the N-terminal β-catenin TAD1 and the TAZ2 domain of CBP/p300. I identify the molecular determinants of their interaction using protein pulldown assays, nuclear magnetic resonance spectroscopy (NMR) chemical shift mapping experiments, and isothermal titration calorimetry (ITC). Furthermore, I derive a peptide that displaces β-catenin TAD1 from TAZ2 and abolishes β-catenin transcriptional activation of a luciferase reporter gene.

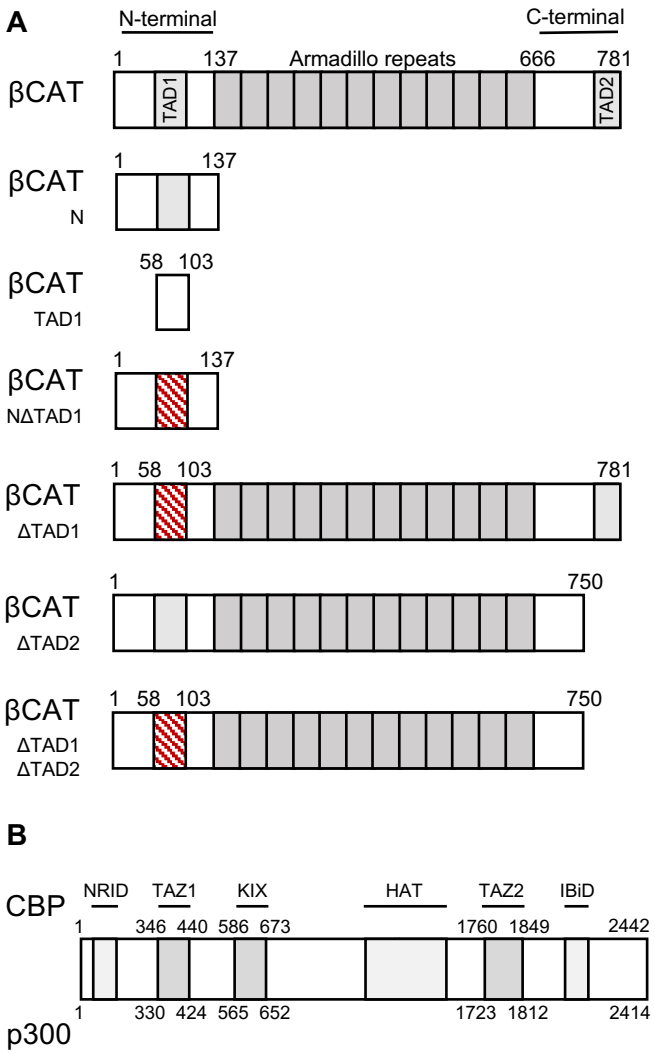

Figure 3.1. Schematic of β-catenin and CBP/p300. (A) β-catenin consists of a central armadillo repeat domain, and two transactivation domains (TAD1 and TAD2) located N-terminal and C-terminal to the armadillo repeat region, protein constructs used in this study are annotated according to native amino acid sequence, dashed areas indicate deleted regions in mutant constructs. (B) Domain architecture of CBP/p300 including catalytic histone acetyltransferase domain (HAT), nuclear receptor interaction domain (NRID), IRF-3 binding domain (IBiD), kinase inducible domain (KIX), and transcription adaptor zinc finger domains (TAZ1/TAZ2), numbering corresponds to CBP amino acid sequence (above) and p300 (below).

3.4 Materials and Methods

3.4.1 Plasmid Preparation

β-catenin plasmids for protein expression were derived from a pET28a plasmid containing full-length human β-catenin gifted by Randall Moon (Addgene plasmid # 17198). Regions comprising of residues 1-137 (N) and residues 58-103 (TAD1), were cloned using restriction enzymes *BamHI* and *SalI* into a pET21b vector modified to contain an upstream His_6 affinity tag, the B1 domain of protein G (GB1), and a TEV protease recognition sequence (pGB1-βCAT_N and pGB1-βCAT_{TAD1}, respectively). To create pGB1-$\beta CAT_{N\Delta TAD1}$, mutagenesis was performed to remove residues 58-103 (TAD1) using a Q5 site-directed mutagenesis kit (New England BioLabs), with pGB1-βCAT_N as a template. Plasmids encoding for the protein-interacting domains of CBP/p300 (KIX, TAZ1, and TAZ2) and the conserved region 1 domain (CR1) of adenovirus early region 1 A (pGB1-$E1A_{CR1}$) were the same as those previously used (58, 179).

For expression in mammalian cells, the $E1A_{CR1}$ sequence was cloned into a pcDNA3-GFP vector gifted by Doug Golenbock (Addgene plasmid # 13031) (pGFP-$E1A_{CR1}$), and full-length p300 (residues 1-2414) was cloned into pcDNA3.1(+) mammalian expression vector (pcDNA-p300). For transactivation assays, constructs consisted of βCAT_N and $\beta CAT_{N\Delta TAD1}$ subcloned into a pCMV-GAL4 vector gifted by Liqun Luo (Addgene plasmid # 24345) (pGAL4-βCAT_N), and full-length β-catenin in pcDNA3 gifted by Eric Fearon (Addgene plasmid # 16828) (pcDNA-βCAT). Constructs pcDNA-$\beta CAT_{\Delta TAD1}$, pcDNA-$\beta CAT_{\Delta TAD2,}$ and pcDNA-$\beta CAT_{\Delta TAD1\Delta TAD2,}$

removing residues 58-103 (TAD1) and/or residues 750-781 (TAD2) were produced using QuikChange site-directed mutagenesis kit (Stratagene), with pcDNA-βCAT used as template. All plasmid constructs were validated using DNA-sequencing.

3.4.2 Cell Culture and Transcription Assays

Luciferase reporter assays were performed using a Dual Luciferase Reporter Assay System (Promega). HEK 293A cells were seeded into 24-well plates and transfected using JetPRIME reagent (Polyplus) according to manufacturer protocols. Each reaction contained 0.5 μg of plasmid including: 0.35 μg luciferase reporter (5xGAL4-Luc or M50 Super 8x TOPFlash), 0.10 μg (pGAL4-βCAT or pcDNA-βCAT construct), and 0.05 μg internal control (pCMV-Renilla). Cell lysate was prepared and tested for luciferase activity 24 hr post transfection using a luminometer, all luciferase values are normalized to *Renilla*-luminescence and represent triplicate-transfections relative to negative controls.

3.4.3 Protein Expression and Purification

Plasmids used for recombinant protein expression (pGB1-βCAT_N and pGB1-$E1A_{CR1}$) were introduced into *E. coli* (BL21 (DE3)) and grown to an optical density of 0.6-0.8 at 600 nm in Lysogeny broth, ^{15}N- or ^{13}C,^{15}N -enriched M9 minimal media (149), at which point expression was induced with the addition of isopropyl β-d-1-thiogalactopyranoside (final concentration 0.5 mM) and left to grow at 37°C for 4 hr. Cell pellets were then harvested and resuspended in lysis buffer (8M urea, 20 mM Tris-HCl pH 8, 250 mM NaCl, 10 mM βME), lysed by sonication, and after centrifugation, the supernatant was applied to a Ni^{2+} affinity-resin (Ni-NTA agarose,

GE healthcare). After washing with lysis buffer containing 10 mM imidazole, proteins were refolded with the addition of lysis buffer lacking urea and eluted from the column with the same buffer containing 300 mM imidazole. Proteins were then dialyzed overnight at 4°C into native buffer (20 mM Tris-HCl pH 8, 50 mM NaCl, 10 mM βME) with 150 µg of TEV protease to remove the GB1 affinity-tag. Cleaved proteins were separated from their tag by Ni^{2+}-affinity chromatography and Fast Flow Q Sepharose anion exchange chromatography (GE healthcare) using native buffer to wash, and native buffer containing 500 mM NaCl to elute. The KIX, TAZ1, and TAZ2 domains were expressed and purified as per previously described methods (58). All protein fractions were monitored throughout the purification using SDS-PAGE.

3.4.4 Pulldown Experiments

For pulldown assays, GB1-βCAT_N or GB1-βCAT_{TAD1} were added to 20 µL IgG agarose beads (GE Healthcare) for 15 min in assay buffer (20 mM Tris-HCl pH 8, 25 mM NaCl, 10 µM $ZnCl_2$, 5 mM βME). Following two washes with assay buffer, 1 mL of prey protein consisting of 20 µM isolated KIX, TAZ1, or TAZ2 was added to the beads and incubated for 30 min with gentle spinning. Beads were then washed three times with assay buffer, or assay buffer containing 20 µM of purified $E1A_{CR1}$ (for competition assays), to remove any unbound protein. The final protein bound beads were then analyzed by SDS-PAGE.

3.4.5 Isothermal Titration Calorimetry

ITC experiments were conducted at 30°C in buffer (20 mM MES pH 6, 25 mM NaCl, 1 μM $ZnCl_2$, and 5 mM βME) with 400 μM of βCAT construct (βCAT_N, βCAT_{TAD1}, or $\beta CAT_{N\Delta TAD1}$) in the syringe (total volume 400 μL) and 40 μM TAZ2 in the in the reaction cell (total volume 1400 μL). Experiments were carried out using a VP-ITC Microcalorimeter with the following specifications: 30 injections of 10 μL with 300 sec spacing, reference power of 20 μCal/sec, and a stirring speed 300. Experimental data was performed in duplicate and thermograms were fit to a single binding-site model using MicroCal Origin 7.0.

3.4.6 NMR Spectroscopy

NMR experiments were performed in 20 mM MES pH 6, 25 mM NaCl, 1 μM $ZnCl_2$, 5 mM DTT and 5% D_2O at 25 °C on a 700 MHz Bruker Advance III spectrometer equipped with a cryogenic probe at the National Research Council (Halifax, NS). For backbone assignments, uniformly ^{13}C,^{15}N-labelled samples of βCAT_N (513 μM) and βCAT_{TAD1} (500 μM) were prepared and resonances were assigned using standard heteronuclear multidimensional NMR experiments (^1H-^{15}N HSQC, HNCACB, CBCACONH, H(CCO)NH, (H)C(CO)NH, HNCO, and HN(CA)CO). Secondary structure propensity (SSP) was then calculated per residue based on the determined Cα and Cβ chemical shifts (157). NMR datasets were processed using NMRPipe and analyzed using the program CCPNMR Analysis (150, 151).

To assess binding between β-catenin and TAZ2, ^{15}N-labelled βCAT_N or βCAT_{TAD1} (100 μM each) were prepared and titrated with up to 400 μM of unlabelled TAZ2 (for competition experiments, 100 μM of TAZ2 with or without 100 μM $E1A_{CR1}$ was used). Heteronuclear NOE values and backbone assignments were obtained from the bound βCAT_{TAD1}: TAZ2 complex. Chemical shift perturbations (Δδ) of ^{1}H-^{15}N-HSQC resonances were quantified as $\Delta\delta = [(0.17\Delta\delta_N)^2 + (\Delta\delta_{HN})^2]^{1/2}$ (153). To map the βCAT_{TAD1} binding site onto TAZ2, ^{15}N-labelled TAZ2 (100 μM) was prepared with up to 400 μM of unlabelled βCAT_{TAD1} and the residues which underwent the largest chemical shift changes (> mean Δδ) were mapped onto the surface structure of the TAZ2: E1A complex (PDBID: 2KJE) (180).

3.5 Results

3.5.1 β-catenin N-terminal binds promiscuously to CBP/p300

To examine the role of N-terminal β-catenin in the regulation of gene transcription, I conducted a luciferase-based transcriptional assay where HEK 293A cells were transfected with βCAT_N fused to a GAL4 DNA-binding domain. Normalized luminescent values from triplicate experiments showed that the fusion of βCAT_N activated luciferase activity 60-fold more than GAL4 alone, highlighting the importance of this region for transactivation (Figure 3.2A). Since the presence of CBP/p300 is known in part to modulate β-catenin activity, I also tested its impact on βCAT_N transcription by co-transfecting an increasing amount of p300 (up to 50 ng). Here I found that the addition of p300 enhanced βCAT_N transcriptional activity up to

83-fold more than the GAL4 control suggesting a functional relationship between these two proteins, the difference of only 1.4-fold more activation than βCAT_N without p300 present may be attributed to the fact p300 is a chromatin modifying protein and luciferase assays were performed using plasmid DNA.

To gain better understanding of the observed functional interaction between βCAT_N and CBP/p300, I next investigated how they associate with one another. I first conducted a protein pulldown assay where immobilized GB1-tagged βCAT_N was used to pulldown candidate protein-interacting domains of CBP/p300: KIX, TAZ1, and TAZ2. βCAT_N was not observed to interact with the purified KIX domain, since no KIX was present in comparison to the input control (Figure 3.2B). Although βCAT_N demonstrated weak binding to the TAZ1 domain of CBP/p300, the most notable interaction occurred between βCAT_N and the TAZ2 domain where a significant amount of TAZ2 was retained by βCAT_N. To confirm a direct association between these domains, ITC analysis of these protein interactions was conducted and revealed that βCAT_N binds TAZ2 at one-site (N: 0.98) with a measured dissociation constant (K_d) of 312 ± 23 nM (Figure 3.2C).

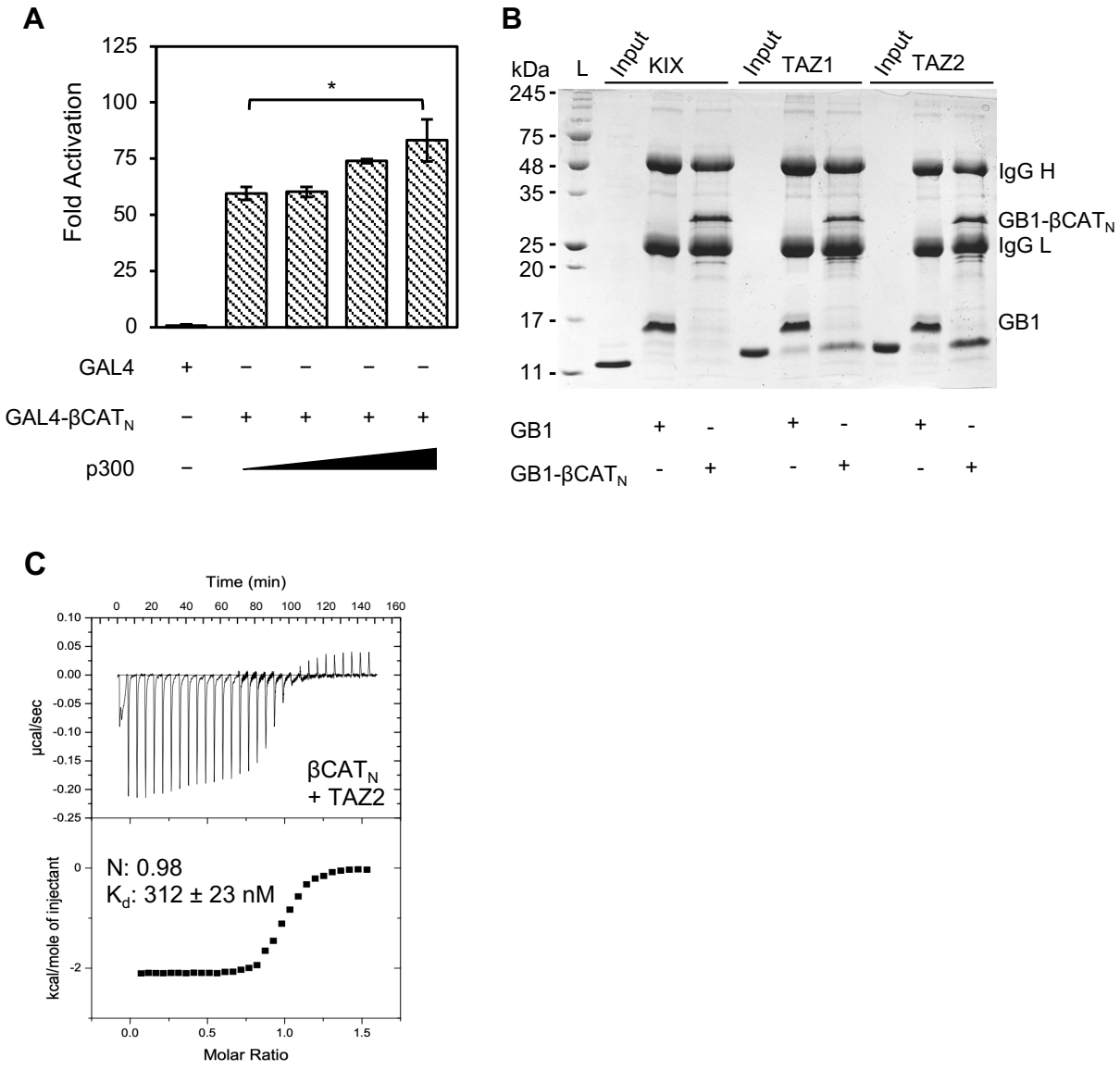

Figure 3.2. N-terminal β-catenin mediates promiscuous CBP/p300 interactions. (A) Luciferase gene reporter assay of GAL4-βCAT$_N$ co-transfected with increasing amount of p300. Data represents mean fold activation over negative control, error bars are standard error from three separate experiments. Statistical significance measured using one-way ANOVA and Dunnetts multiple comparison test (* p value < 0.05, n=3 technical replicates). (B) SDS-PAGE analysis of protein pulldown assay of GB1-βCAT$_N$ tested for its ability to pulldown and interact with purified KIX, TAZ1, or TAZ2 domains of CBP/p300. Lanes 2, 5, and 8 contain CBP/p300 domain only and represents 10% total pulldown input, protein constructs (GB1, GB1-βCAT$_N$) and immunoglobulin G antibody chains (IgG H/L) are labelled. (C) Isothermal titration calorimetry thermogram of βCAT$_N$ titrated into cell containing TAZ2, the resulting curve is fit to a single binding-site with dissociation constant (K$_d$) 312 ± 23 nM (n=2 biological replicates, error reported as SD).

3.5.2 Structural features of β-catenin N-terminal Region

To assign the backbone resonances of the β-catenin N-terminal region a ^{1}H-^{15}N-heteronuclear single quantum coherence (HSQC) spectrum was collected on a ^{13}C,^{15}N-uniformly labelled sample of βCAT_N (Figure 3.3A). Using triple resonance NMR experiments and sequential assignment, nearly complete backbone assignment of βCAT_N was achieved, including 94% of backbone amide chemical shifts (129/137 residues, 7 of which are proline). The limited dispersion of amide proton resonances indicates the N-terminal of β-catenin is disordered in its unbound state. These structural features were further investigated using secondary structure propensity (SSP) calculations based on the determined $^{13}C\alpha$ and $^{13}C\beta$ chemical shifts for each β-catenin residue (Figure 3.3B). These values consider the propensity of any given amino acid in the polypeptide to form a secondary structure where consecutive positive values (+1) indicate fully formed α-helix and negative values (-1) indicate β-sheet. SSP analysis of βCAT_N showed little deviation from the random coil state, with all values falling within a range of -0.12-0.33. These findings suggest that the N-terminal region of β-catenin has some minor propensity to form α-structure in its native form but still mostly exists in a disordered state.

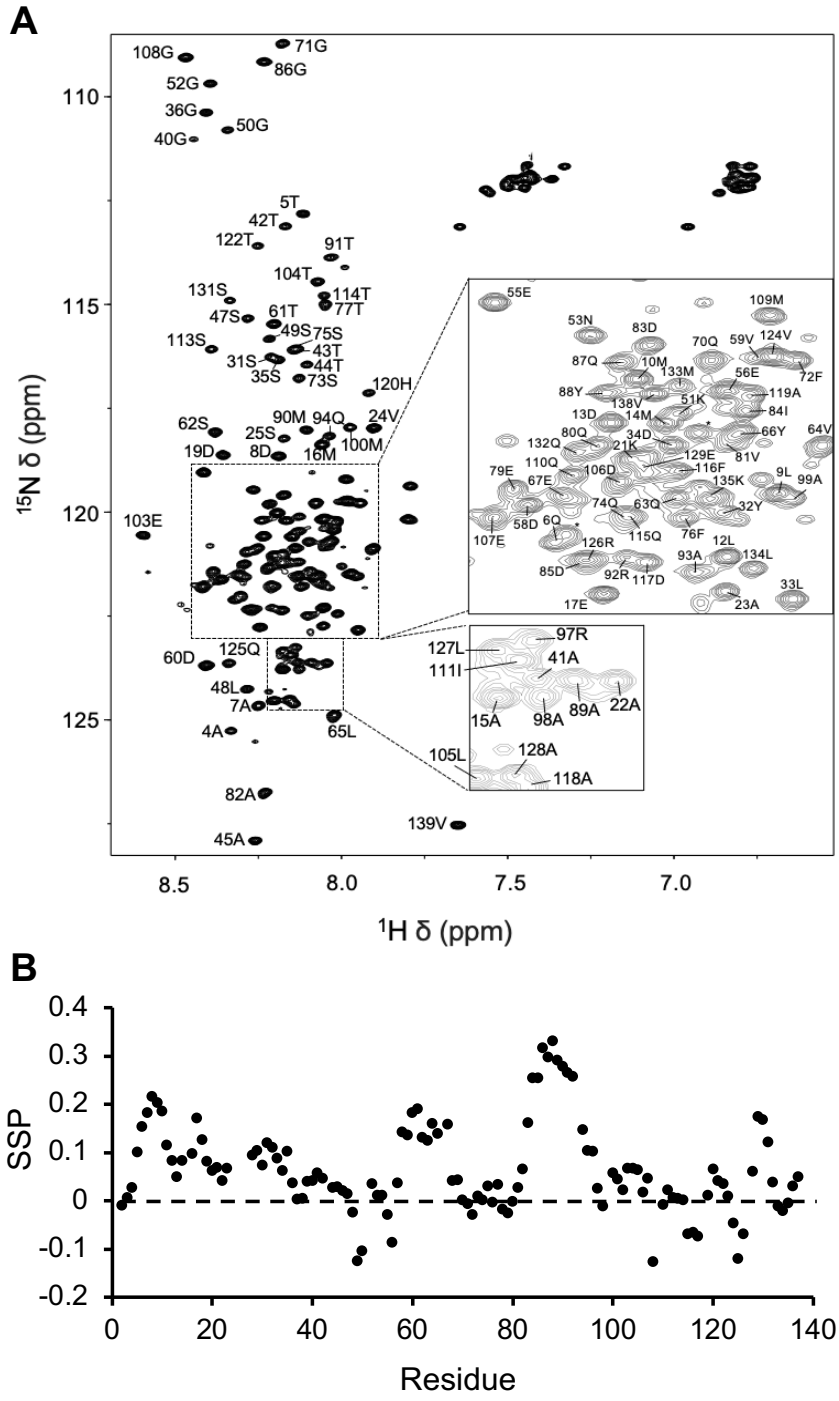

Figure 3.3. The β-catenin N-terminal is structurally disordered. (A) ^{1}H-^{15}N-HSQC spectrum of βCAT_N, with assigned backbone amide resonances labelled based on their amino acid and sequence position. (B) Secondary structure propensity (SSP) values calculated per residue of βCAT_N based on assigned Cα and C_β chemical shifts.

3.5.3 β-catenin TAD1: TAZ2 interaction is functionally important

I next wanted to investigate the binding of N-terminal β-catenin to TAZ2. ^{1}H-^{15}N-HSQC spectra were collected on a ^{15}N-labelled sample of βCAT_N with and without the addition of unlabelled TAZ2 to the sample (1:4 ratio). While many resonances remain unperturbed, those corresponding to a region from D58-L103 experience significant chemical shift perturbation upon addition of TAZ2, indicative of a potential molecular interaction (Figure 3.4). To corroborate these findings, a GB1-βCAT_N mutant was produced, removing D58-L103 (referred to as ΔTAD1), and tested for its ability to pulldown and interact with purified TAZ2. The GB1-$\beta CAT_{N\Delta TAD1}$ mutant diminished binding between N-terminal β-catenin and TAZ2, this coincided with ITC measurements which revealed that the $\beta CAT_{N\Delta TAD1}$ mutant had no detectable affinity for TAZ2 (Figures 3.5A, 3.6). Furthermore, when tested in a luciferase assay, deletion of TAD1 ablated any transcriptional activity by GAL4-βCAT_N, emphasizing the importance of this region to β-catenin function (Figure 3. 5B).

β-catenin contains two transactivation domains, one located at the N-terminal (TAD1, residues 58-103) and the second at the C-terminal (TAD2, residues 750-781) (178), which can function either independently, cooperatively, or redundantly with one another. To test this, I generated three β-catenin mutants which deleted TAD1, TAD2, or both domains and assessed their potential to activate a β-catenin-specific TOPFlash luciferase gene reporter. In comparison to wild-type β-catenin, which measured 35-fold transcriptional activity, removal of either domain $\beta CAT_{\Delta TAD1}$ or $\beta CAT_{\Delta TAD2}$ diminished the ability of β-catenin to activate reporter gene transcription

and was equivalent to that of $\beta CAT_{\Delta TAD1\Delta TAD2}$ which removed both domains, suggesting they are both essential to β-catenin function (Figure 3.5C).

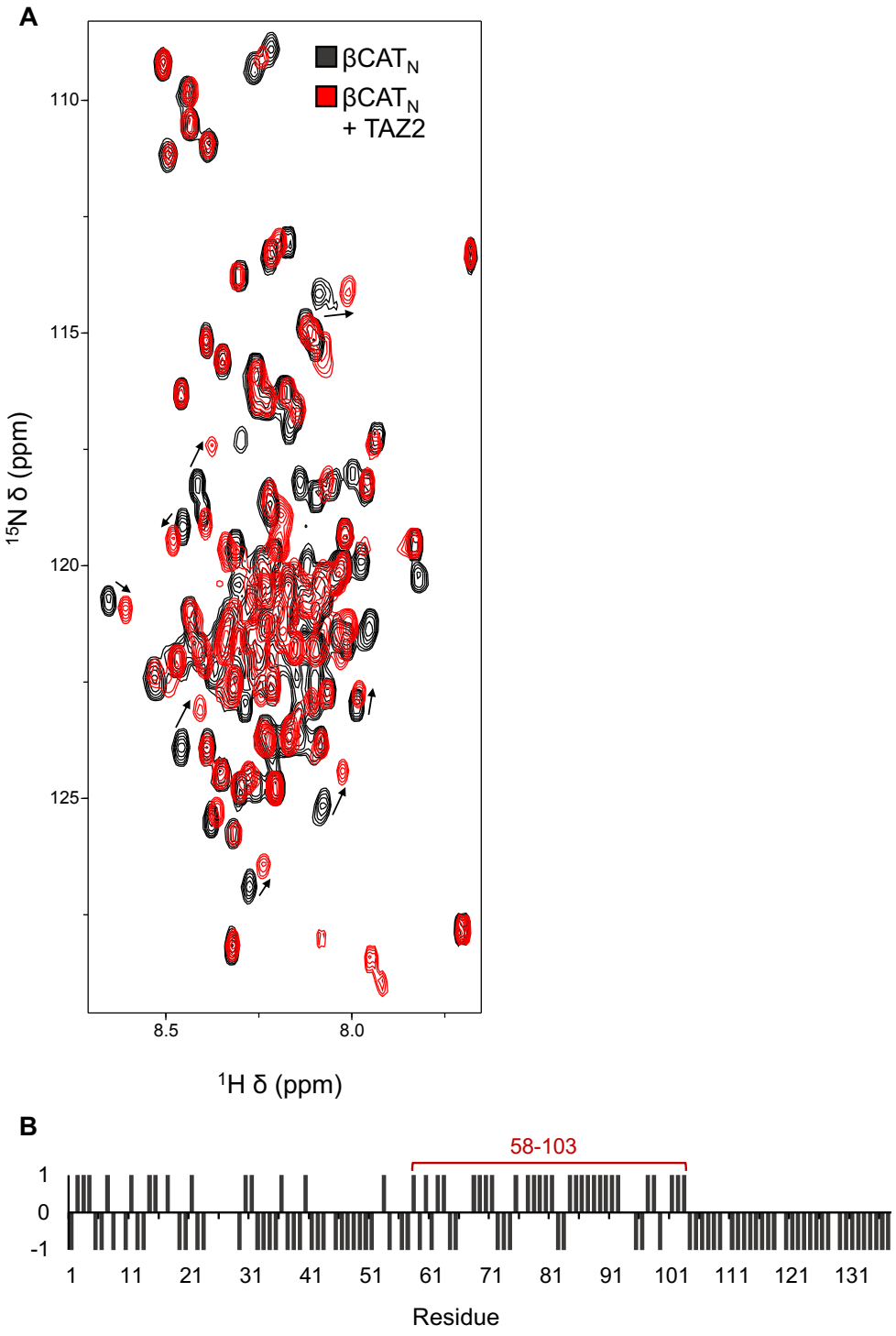

Figure 3.4. NMR analysis of N-terminal β-catenin and TAZ2 interaction. (A) ^{1}H-^{15}N-HSQC spectra of βCAT$_N$ (100 μM) when unbound (black) and saturated with TAZ2 (400 μM) (red). (B) Summary of βCAT$_N$ resonances that are perturbed (+1) or unperturbed (-1) upon addition of TAZ2, labels correspond to native amino acid sequence.

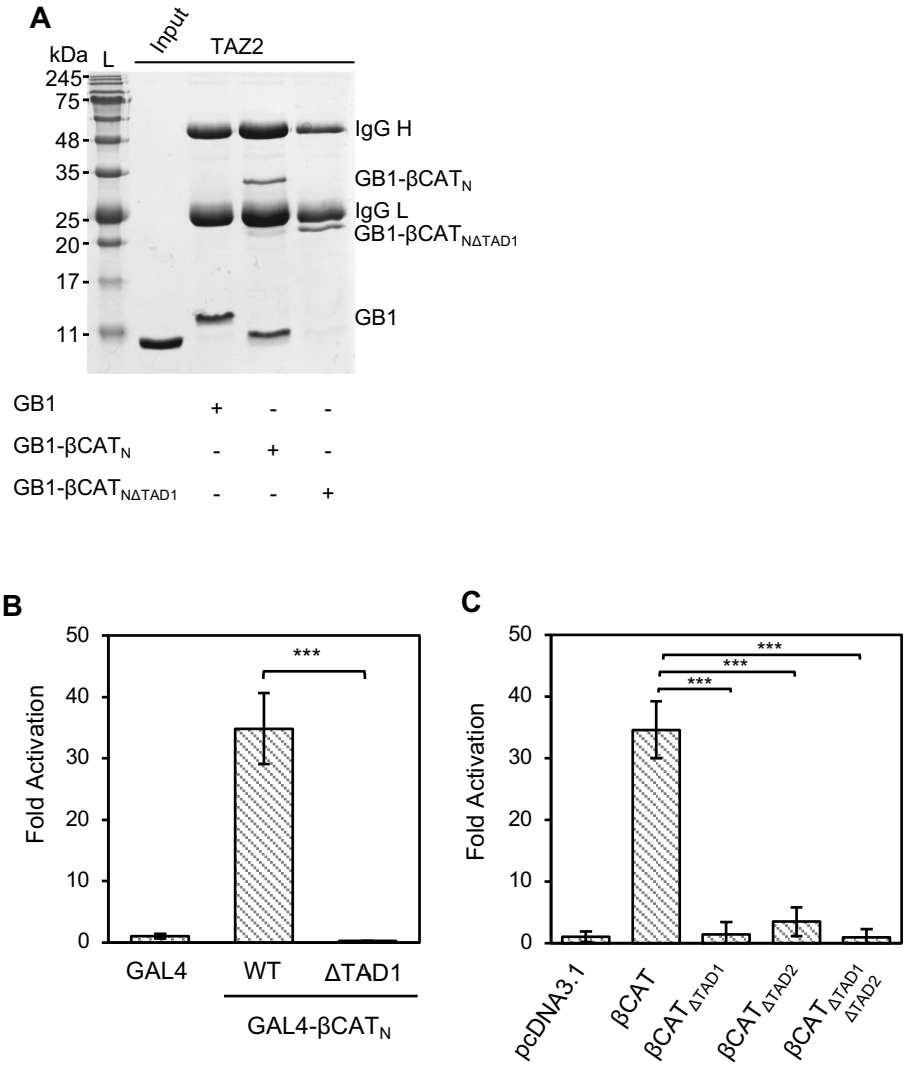

Figure 3.5. β-catenin TAD1 is critical to TAZ2 binding and transactivation. (A) SDS-PAGE of protein pulldown assay of GB1, GB1-βCAT$_N$, and GB1-βCAT$_{NΔTAD1}$ tested to pulldown and interact with purified recombinant TAZ2 of CBP. Lanes 3 contains purified TAZ2 only and represents 10% total pulldown input, protein constructs and antibody chains (IgG H/L) are labelled. (B) Luciferase transactivation assay showing relative activity of GAL4, GAL4-βCAT$_N$ and GAL4-βCAT$_{NΔTAD1}$. (C) TOPFlash luciferase reporter assay measured for full-length β-catenin (βCAT), βCAT$_{ΔTAD1}$, βCAT$_{ΔTAD2}$, and βCAT$_{ΔTAD1ΔTAD2}$. Data represents mean fold activation over negative control, error bars are standard error from three separate experiments. Statistical significance was measured using one-way ANOVA and Dunnetts multiple comparison test (*** p value < 0.001, n=3 technical replicates).

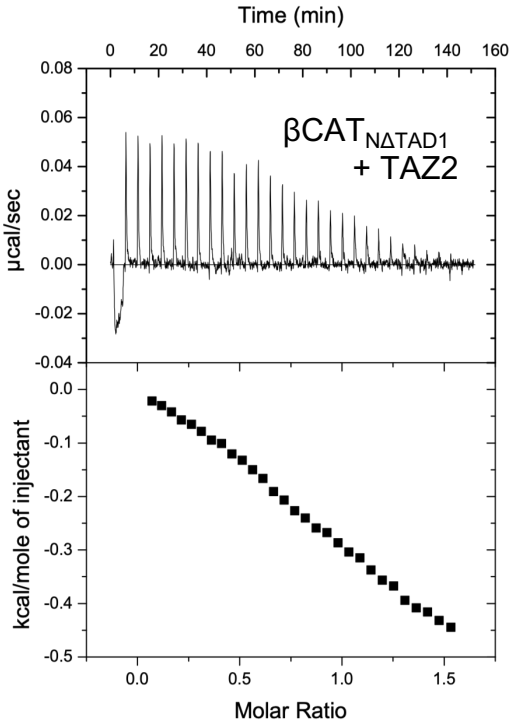

Figure 3.6. ITC analysis of $\beta CAT_{N\Delta TAD1}$ and TAZ2. Isothermal titration calorimetry thermogram of 400 µM $\beta CAT_{N\Delta TAD1}$ titrated into 40 µM TAZ2.

3.5.4 Structural features of βCAT_{TAD1}: TAZ2 complex

To identify the residues involved in the βCAT_{TAD1}: TAZ2 interaction, a $^{13}C,^{15}N$-labelled sample of βCAT_{TAD1} was prepared in complex with unlabelled TAZ2. Using multidimensional NMR experiments and sequential assignment, 97% of backbone proton and ^{15}N-amide resonances (45/46 residues, 1 of which are proline) of βCAT_{TAD1} were identified (Figure 3.7). SSP calculations were determined from assigned βCAT_{TAD1} Cα and Cβ chemical shifts. Binding of TAZ2 to the βCAT_{TAD1} domain caused the largest increase in SSP values from residues T59-F74, suggesting this region is adopting more of a helical conformation. The highest SSP value being only 43% propensity for α-structure suggests that flexibility is still retained by βCAT_{TAD1} in the bound complex (Figure 3.8A). These findings are in accordance with heteronuclear $\{^1H\}$-^{15}N NOE values calculated per βCAT_{TAD1} residue when bound to TAZ2. I observed the highest hetNOE values (~0.6) occur in the same region of βCAT_{TAD1} from residues E65-S71, indicating that they become more ordered when bound. The average $\{^1H\}$-^{15}N NOE of ~0.43 is lower than that of well-structured elements in proteins (typically >0.65), and further evidence of transient rigidity by βCAT_{TAD1} when binding TAZ2 (Figure 3.8B). Interestingly, these βCAT_{TAD1} residues also experienced the largest chemical shift perturbations of resonances in the ^1H-^{15}N-HSQC spectra upon titration of TAZ2 (Figure 3.8C, HSQC titration spectra Figure 3.9, Assignments unbound βCAT_{TAD1} Figure 3.10).

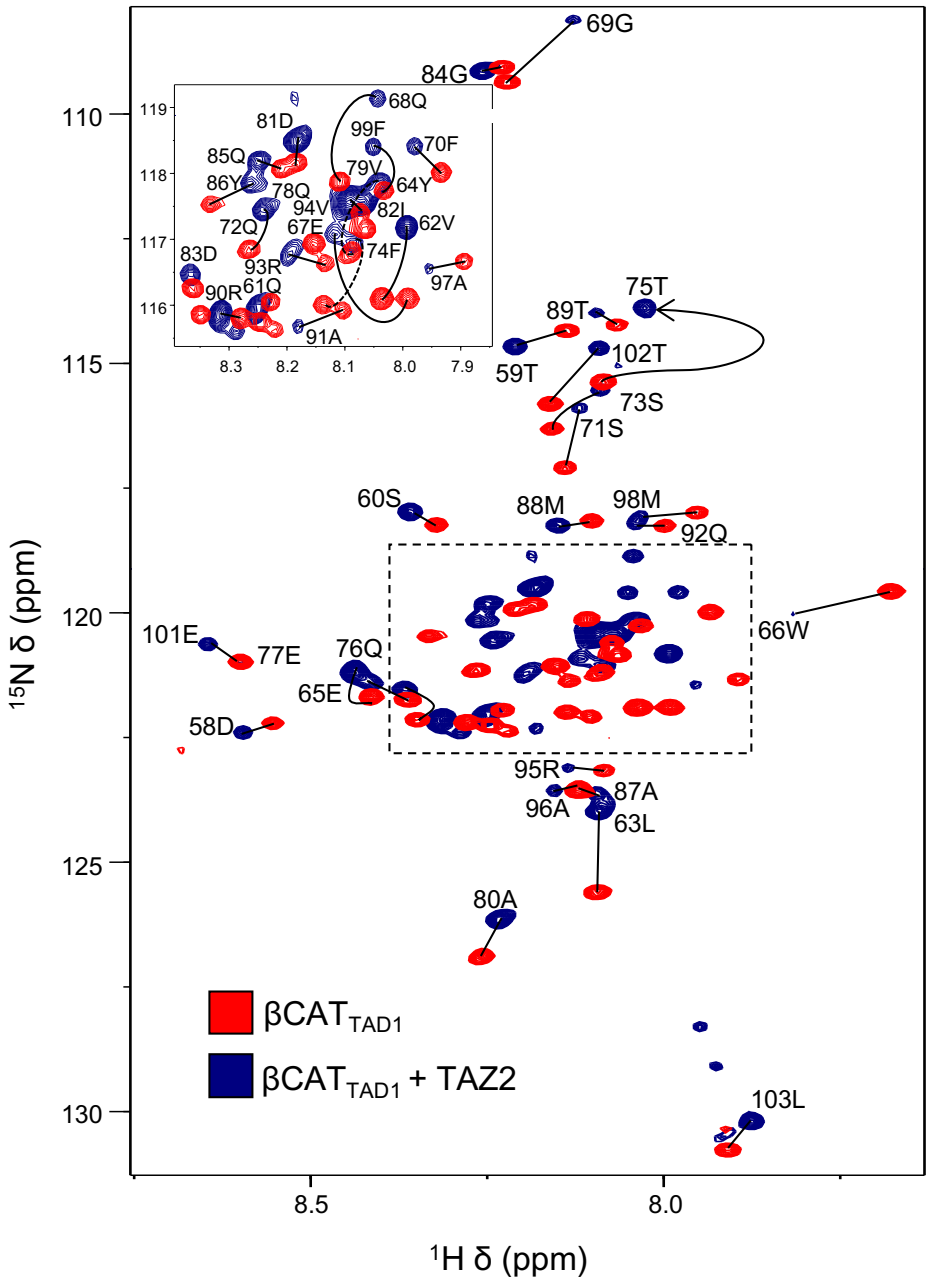

Figure 3.7. Resonance assignments of βCAT$_{TAD1}$: TAZ2 complex. ^{1}H-^{15}N-HSQC of βCAT$_{TAD1}$ (red spectra) and in complex with TAZ2 (blue spectra), assigned resonances of backbone amide peaks for the βCAT$_{TAD1}$: TAZ2 complex are annotated with their corresponding sequence position and amino acid residue.

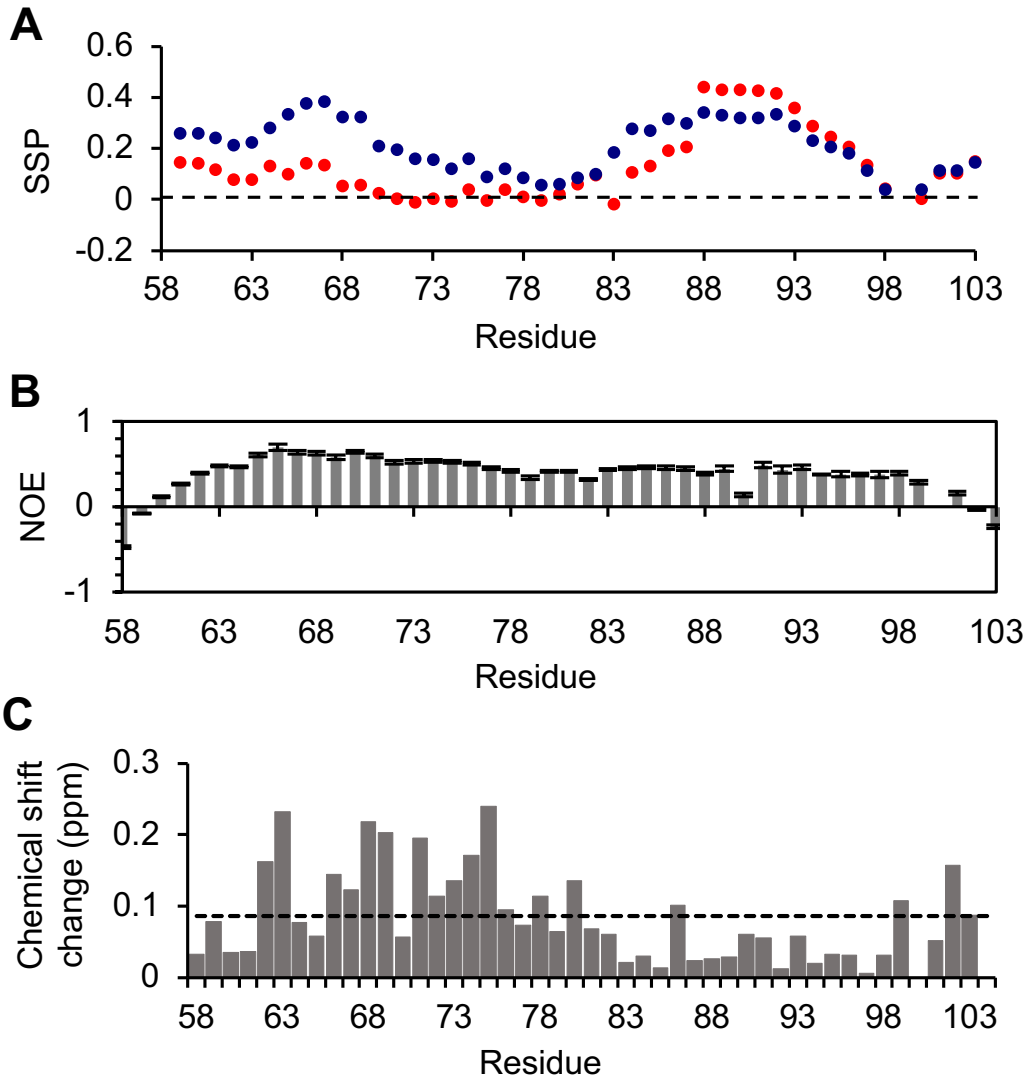

Figure 3.8. Structural features of βCAT_{TAD1}: TAZ2 complex. (A) Calculated secondary structure propensity (SSP) scores for each βCAT_{TAD1} residue when unbound (red) and bound (blue) to TAZ2. (B) $\{^1H\}$-^{15}N NOE values and (C) chemical shift changes ($\Delta\delta = [(0.17\Delta\delta_N)^2 + (\Delta\delta_{HN})^2]^{1/2}$) determined for each βCAT_{TAD1} residue upon formation of the βCAT_{TAD1}:TAZ2 complex, dashed line represents average chemical shift change ($\Delta\delta$).

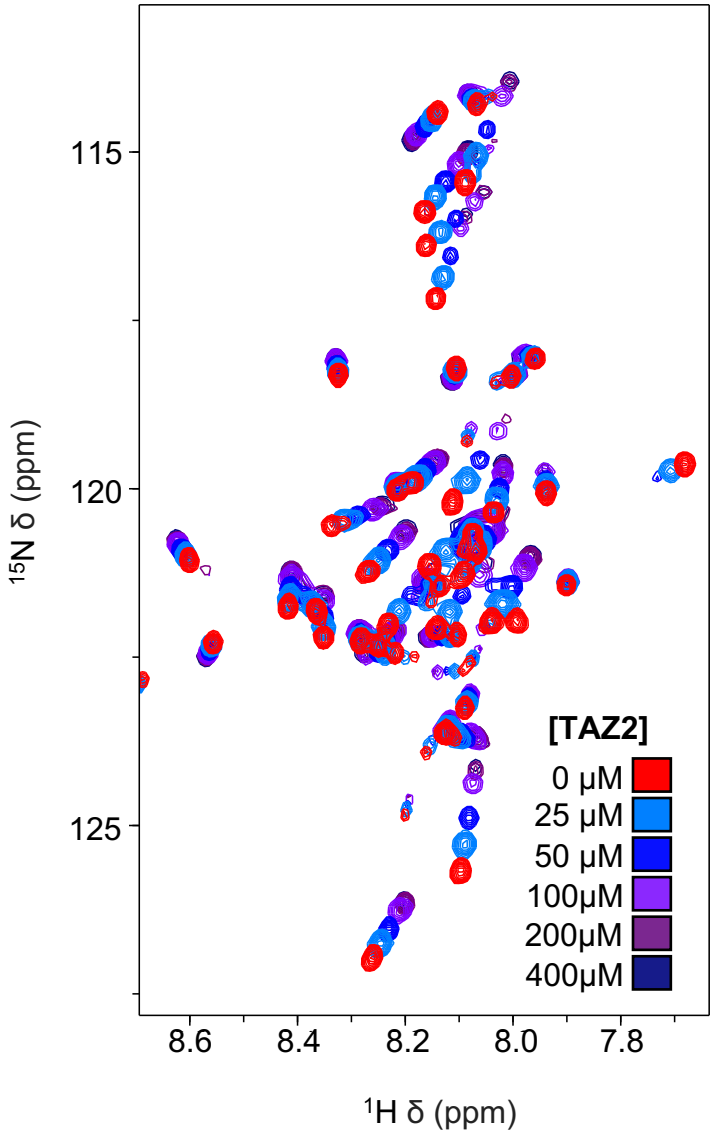

Figure 3.9. HSQC spectra of N-terminal β-catenin TAD upon TAZ2 binding. ^{1}H-^{15}N-HSQC spectra of 100 μM βCAT_{TAD1} (red) overlayed with titration of up to 400 μM unlabeled TAZ2 (dark blue).

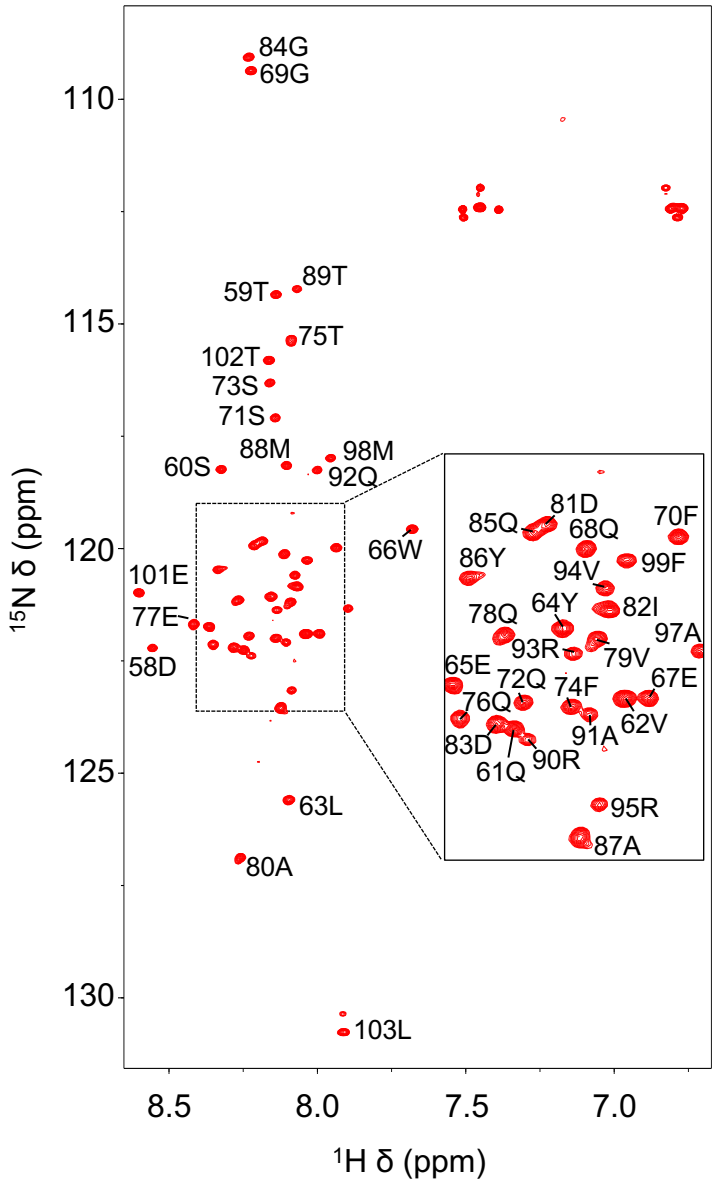

Figure 3.10. Resonance assignments of β-catenin TAD. ^{1}H-^{15}N-HSQC spectra of βCAT_{TAD1} labelled with backbone resonance assignments according to their respective amino acid.

3.5.5 Defining the βCAT_{TAD1}: TAZ2 interaction site

To characterize the βCAT_{TAD1} interaction site of the TAZ2 surface ^{15}N-labelled TAZ2 was titrated with unlabelled βCAT_{TAD1} and analyzed by NMR spectroscopy (Figure 3.11A, Full spectra Figure 3.12). ^{1}H-^{15}N-HSQC spectra of TAZ2 has well dispersed peaks in both the free and bound states, suggesting that TAZ2 remains folded upon binding. Linear chemical shift perturbations of TAZ2 resonances upon the addition of βCAT_{TAD1} suggested 1:1 binding in a fast exchange regime (181), which agrees with our previous ITC findings of a one-site binding interaction (Figure 3.2C). The largest chemical shift perturbations affected only certain TAZ2 resonances around the βCAT_{TAD1} binding site (Figure 3.11B), when quantified and mapped onto the structure of TAZ2 (PDBID: 2KJE), the largest perturbations localized to a hydrophobic groove formed by the α-1, α-2 and α-3, helices (shaded pink) (Figure 3.11C) (180).

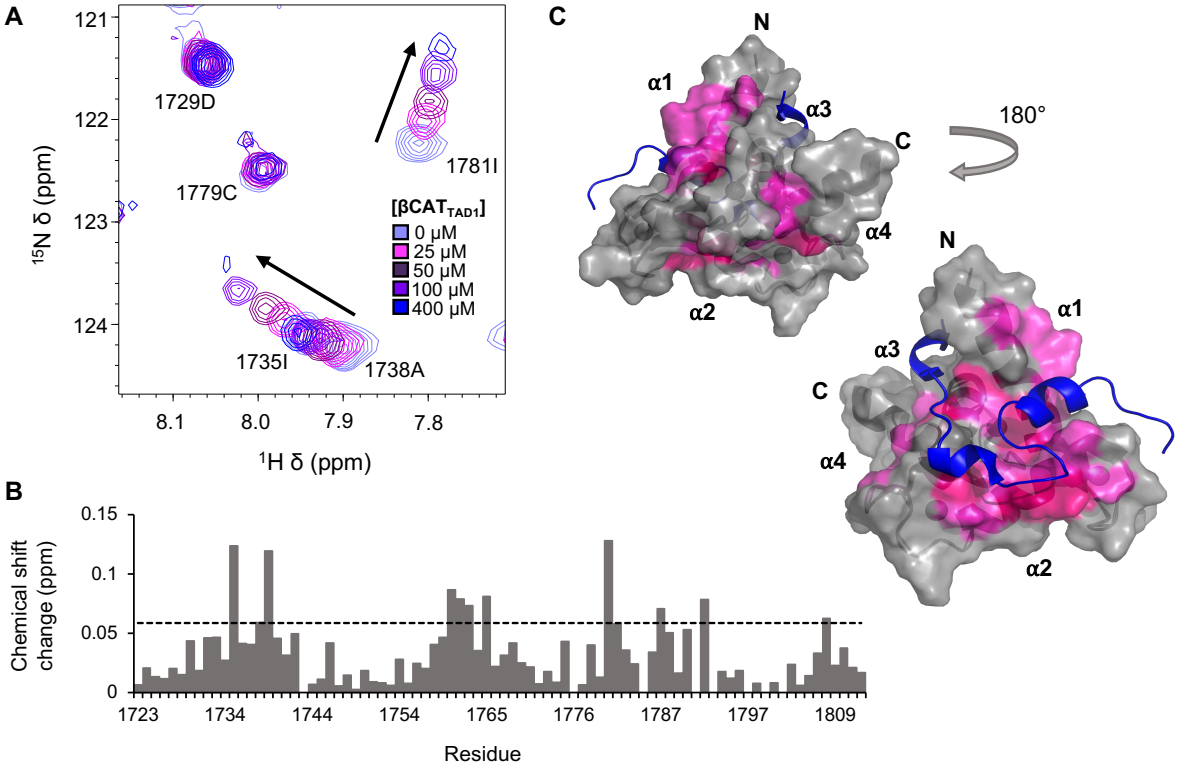

Figure 3.11. NMR chemical shift mapping of the βCAT$_{TAD1}$: TAZ2 binding site. (A) Portion of ^{1}H-^{15}N-HSQC spectra of ^{15}N-labelled TAZ2 titrated with increasing amounts of unlabelled βCAT$_{TAD1}$, full spectra provided in Figure 3.12. (B) Changes in chemical shift were calculated for each TAZ2 residue ($\Delta\delta = [(0.17\Delta\delta_N)^2 + (\Delta\delta_{HN})^2]^{1/2}$) upon binding βCAT$_{TAD1}$, dashed line represents average chemical shift change (Δδ). (C) A surface representation of TAZ2 (grey) in complex with the CR1 domain of adenovirus E1A (blue) (PDBID: 2KJE; (180)) with residues that experienced the largest changes in chemical shift upon titration with βCAT$_{TAD1}$ coloured in pink (> mean Δδ) and dark pink (> mean Δδ + SD).

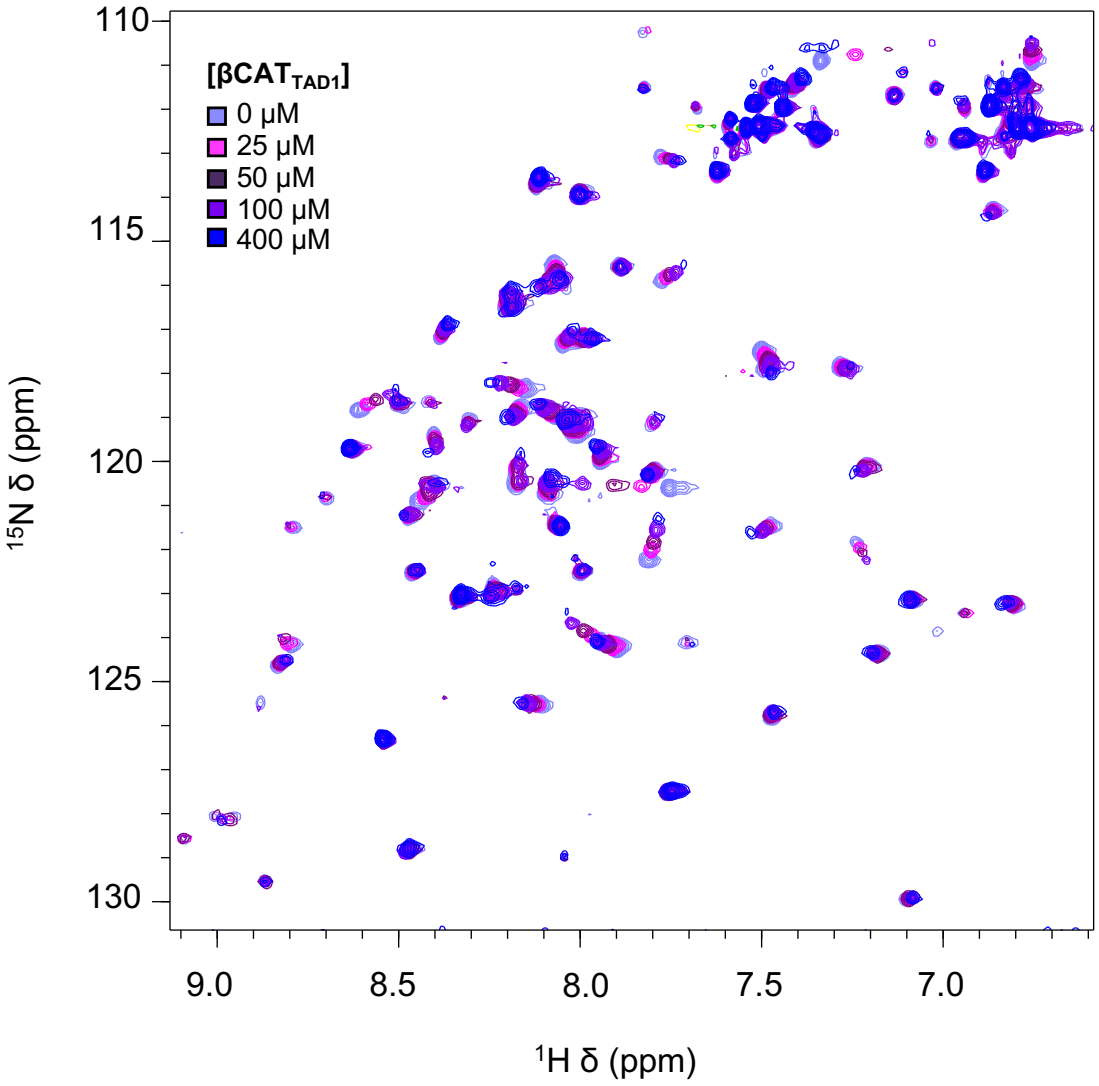

Figure 3.12. Full HSQC spectra of TAZ2 upon β-catenin TAD binding. ^{1}H-^{15}N-HSQC spectra of 100 μM TAZ2 (light purple) overlayed with titration of up to 400 μM unlabeled βCAT$_{TAD1}$ (royal blue).

3.5.6 E1A-derived peptide disrupts the βCAT_{TAD1}:TAZ2 interaction

The adenoviral oncoprotein early region 1 A (E1A) has been shown to functionally impact β-catenin/TCF-regulated gene activity by interfering with its binding to CBP/p300 (182). E1A sequesters CBP/p300 through interactions between its conserved region 1 domain (CR1) which interact with the same TAZ2 binding site as β-catenin TAD1 (Figure 3. 6C). To test this mechanism of inhibition and see if $E1A_{CR1}$ could directly block the association of β-catenin TAD1 with TAZ2 I performed NMR competition experiments on a ^{15}N-labelled sampled of βCAT_{TAD1}. Addition of TAZ2 results in a shift of βCAT_{TAD1} cross peaks in the ^{1}H-^{15}N HSQC spectrum to their characteristic positions of the βCAT_{TAD1}:TAZ2 complex (Figure 3. 13A, Full spectra Figure 3.14). Subsequent addition of equimolar $E1A_{CR1}$ (residues 54-82) causes a shift of βCAT_{TAD1} resonances back towards those of unbound protein, indicating that $E1A_{CR1}$ displaces βCAT_{TAD1} from TAZ2. These findings are in agreement with protein pulldown data, where $E1A_{CR1}$ diminished nearly all ability of GB1-βCAT_{TAD1} to pulldown and interact with TAZ2 (Figure 3.13B).

Given that the βCAT_{TAD1} and $E1A_{CR1}$ domains compete for TAZ2 binding, and that CBP/p300 is required for β-catenin-dependent transactivation, I examined the effect of E1A on β-catenin transcriptional function. To do so, HEK 293A cells were transfected with full-length β-catenin and a TOPFlash luciferase gene reporter that contained multiple TCF-binding sites. Transfection of β-catenin activated luciferase gene activity 40-fold more than pcDNA3.1 controls (Figure 3.13C), while co-transfecting p300 enhanced β-catenin activity up to 55-fold, and co-transfection of

$E1A_{CR1}$ peptide abolishes β-catenin-dependent transcription to only 7-fold more than controls, demonstrating the potential of this peptide in inhibiting β-catenin function.

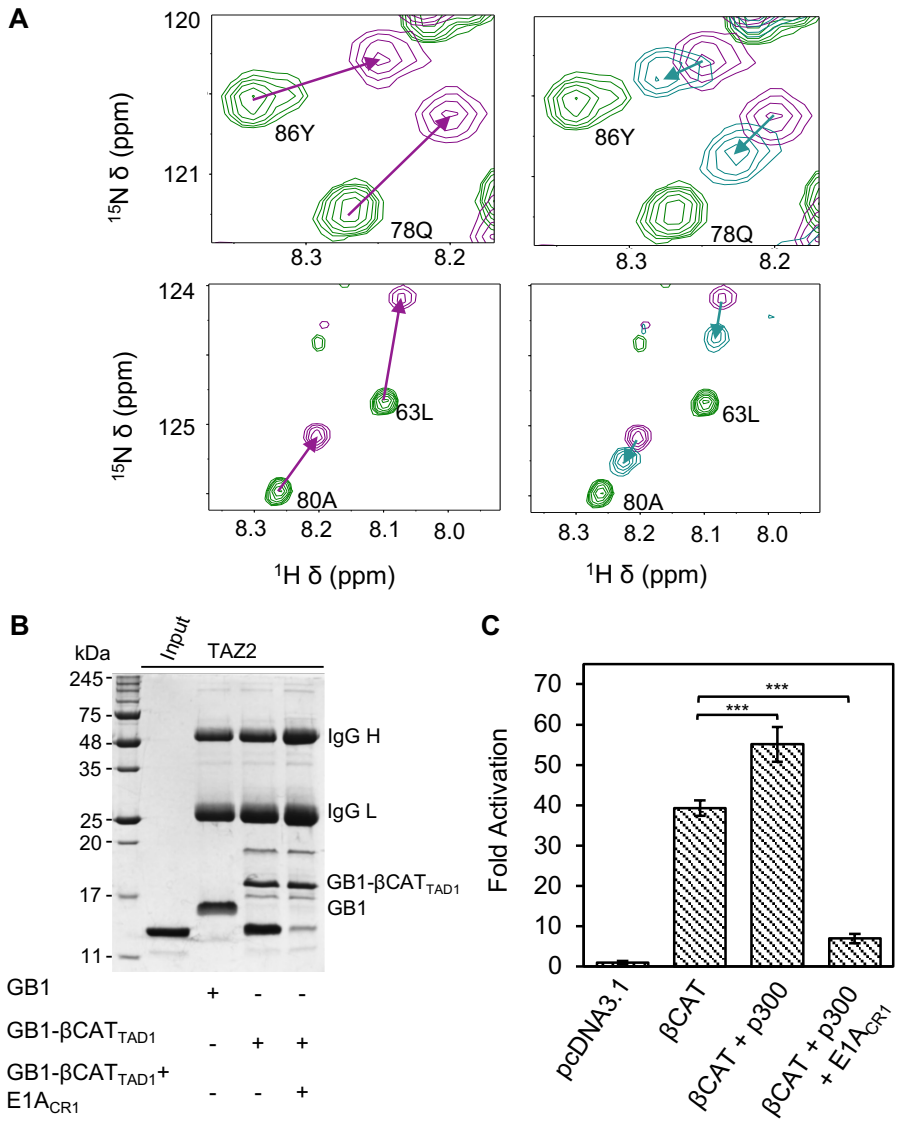

Figure 3.13. E1A$_{CR1}$ competes with βCAT$_{TAD1}$ for TAZ2. (A) Portion of overlayed ^{1}H-^{15}N-HSQC spectra of ^{15}N-labelled βCAT$_{TAD1}$ (green) with arrows indicating change in resonance position of indicated residues upon addition of unlabelled TAZ2 (purple) or TAZ2 and E1A$_{CR1}$ (teal), full spectra provided in Figure 3.14. (B) SDS-PAGE analysis following protein pulldown with GB1 and GB1-βCAT$_{TAD1}$ with or without the presence of E1A$_{CR1}$ in washes following addition of TAZ2. Lanes 2 shows migration of TAZ2 only and represents 10% total input, protein constructs, IgG H and IgG L are annotated. (C) Luciferase transactivation assay using TOPFlash TCF reporter plasmid to measure the activity of β-catenin with and without the cotransfection of p300 or p300 and E1A$_{CR1}$. Mean fold activation relative to pcDNA3.1 is shown, bars represent standard error from three independent experiments. One-way analysis of variance and Dunnett's multiple comparison test were used to determine statistical significance (*** $p < 0.001$, n=3 technical replicates).

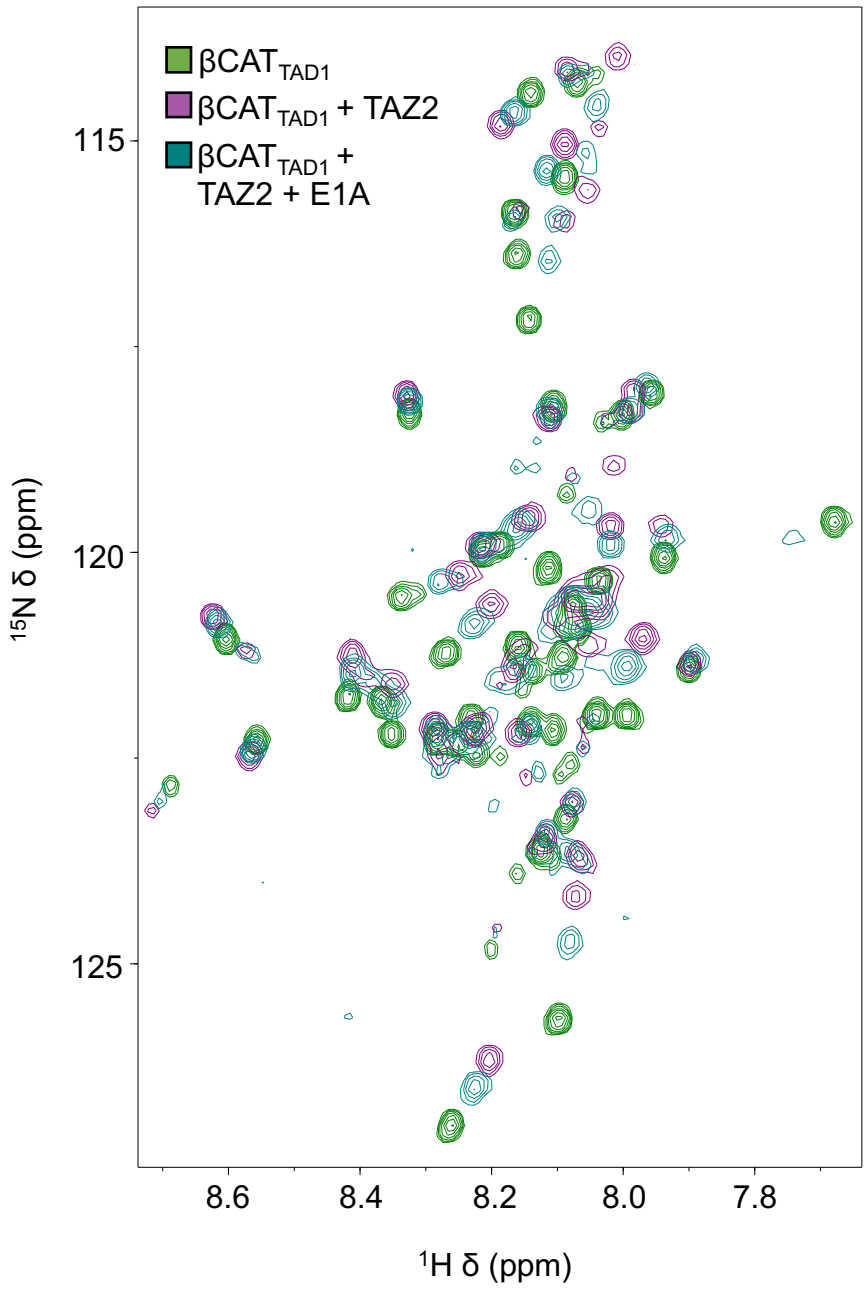

Figure 3.14. Full HSQC spectra of βCAT$_{TAD1}$ competing with E1A for TAZ2. ^{1}H-^{15}N-HSQC spectra of βCAT$_{TAD1}$ (green) in the presence of unlabeled TAZ2 (purple) and TAZ2 with E1A$_{CR1}$ (teal).

3.6 Discussion

Transduction of canonical Wnt-signaling pathway and its downstream gene expression is reliant on the nuclear effector β-catenin. The β-catenin ARM domain and its interactions with DNA-binding transcription factors have been the subject of many previous investigations, however the β-catenin transactivation domains have been studied far less extensively. The N-terminal and C-terminal of β-catenin provide an essential transactivating role by facilitating interactions with co-regulators including B-cell lymphoma 9 protein (BCL9), PCNA-associated factor (PAF), and CBP/p300, which help stimulate the transcriptional response (171, 183). Here I have provided one of the first investigations of the molecular mechanisms of CBP/p300 recruitment by the N-terminal β-catenin TAD1.

I determine that N-terminal β-catenin TAD1 binds to both TAZ1 and TAZ2 of CBP/p300 with high affinity for TAZ2 (K_d ~312 nM) (Figure 3.2). In our previous work I have shown that C-terminal β-catenin TAD2 binds to these same CBP/300 domains, albeit with higher affinity for TAZ1 (K_d ~380 nM) (178). The interactions that I describe raise the potential for a mechanism in which both β-catenin TADs could work together to enhance their affinity for CBP/p300, where TAD1 preferentially binds TAZ2 and TAD2 binds to TAZ1, but both are essential for CBP/p300 recruitment. Our luciferase experiments corroborate this notion that both TADs are essential to β-catenin function, as removal of either one or both domains equally ablate β-catenin-mediated transcription of a TCF luciferase reporter gene (Figure 3.5).

CBP/p300 are critical to the assembly of transcriptional hubs and one of the most highly connected proteins in the interactome, binding to hundreds of different transcriptional regulators (40). Despite this, CBP/p300 are present in the cell in limiting concentrations. In the instance that CBP/p300 could be directed towards specific transcriptional regulators to the exclusion of others, I speculate that multivalent binding could further increase the ability of β-catenin to recruit CBP/p300 to its own transcriptional targets. It would also suggest why other TADs of transcription factors like p53, EKLF, and FOXO3a have been found to interact with multiple different CBP/p300 domains (45, 53, 184, 185).

It is well accepted that abnormal activation of β-catenin signaling plays a significant role in the development and spread of several major types of cancer. Given the therapeutic value of modulating β-catenin function, I wanted to identify ways in which its interactions with CBP/p300 could be targeted. The adenovirus E1A directly effects β-catenin-regulated transcription by sequestering co-activator CBP/p300 from TCF gene promoters (182). Our NMR and protein pulldown studies provide a potential mechanism of this inhibition in which a region of E1A (consisting of residues 54-82 from the CR1 domain) can block β-catenin by direct competition for the TAZ2 domain of CBP (Figure 3.13A, B). This is further supported by our findings that the co-expression of $E1A_{CR1}$ peptide in cells leads to functional inhibition of a β-catenin/ TCF luciferase reporter gene (Figure 3.13C).

In this work I have also provided analysis of the structural features of N-terminal β-catenin TAD1. This region exhibits the hallmarks of being intrinsically disordered, based on both ^{1}H-^{15}N-HSQC chemical shifts and calculated SSP scores

(Figure 3. 3). This is perhaps unsurprising since many well-characterized transcription factors (eg. Sp1, TFIID, c-Myb, and p53) interact with CBP/p300 through unstructured transactivation domains (28, 57, 186). Our complete backbone resonance assignments of the N-terminal region of β-catenin offers an accurate and sensitive representation of conformational preferences of the protein in its native state, and the immediate capability to probe for changes in protein secondary structuring and backbone dynamics for future studies investigating protein-protein interactions with this key domain of β-catenin.

When bound to a partner molecule, structurally disordered TADs can display a wide range of structural propensities. While some exhibit coupled folding and binding of the region, in other instances they can remain disordered and dynamic in what is known as a 'fuzzy complex' (187). I found that there is only minor proclivity for β-catenin TAD1 to form an α-helical structure when interacting with TAZ2, illustrated by low heteronuclear NOE and SSP values calculated from chemical shifts of the bound complex (Figure 3.8). Maintaining some structural plasticity in its interactions might help in allowing β-catenin TAD1 to easily associate/dissociate from transient transcriptional complexes.

Our study outlines the molecular determinants of a newly identified interaction between N-terminal β-catenin TAD1 and CBP/p300, in which β-catenin forms both promiscuous and dynamic interactions with the TAZ1 and TAZ2 domains. Since β-catenin uses both TADS to bind the same CBP/p300 domains, and each individually are essential to β-catenin transcriptional function, this opens the possibility for cooperativity between β-catenin TAD1 and TAD2 to recruit CBP/p300

to TCF/LEF transcription factors at Wnt/ β-catenin target genes. These results provide critical insight on the specific mechanisms by which Wnt/ β-catenin gene activity is regulated by the sequestration of co-activator CBP/p300.

Chapter 4: Structural Basis of CBP/p300 Recruitment by the Microphthalmia-Associated Transcription Factor

4.1 Contributions of Authors

This chapter contains the abstract, introduction, materials and methods, results and discussion sections of the manuscript accepted for publication in Biochimica et Biophysica Acta (BBA) Molecular Cell Research: Brown, A. D., Vergunst, K. L., Branch, M., Blair, C. M., Baillie, G. S., Dupré, D. J., & Langelaan, D. N. (2023). Structural basis of CBP/p300 recruitment by the microphthalmia-associated transcription factor. Previous honours students Kathleen Vergunst and Makenzie Branch prepared NMR samples and collected data found in Figures 4.7A & 4.9A. The peptide array in Figure 4.6A was conducted in the lab of Dr. George Baillie at Glasgow University by graduate student Connor Blair. Calculation of the NMR structure in Figures 4.10 & 4.11 was completed by Dr. David Langelaan. The execution and analysis of all other experiments were performed by me, as well as the written first draft of the manuscript. Resources, supervision, and editing of the manuscript were provided by Dr. Denis Dupré and Dr. David Langelaan.

4.2 Abstract

The microphthalmia-associated transcription factor (MITF) is a master regulator of the melanocyte cell lineage. Aberrant MITF activity can lead to multiple malignancies including skin cancer, where it modulates the progression and

invasiveness of melanoma. MITF-regulated gene expression requires recruitment of the transcriptional co-regulator CBP/p300, but details of this process are not fully defined. In this study, I investigate the structural and functional interaction between the MITF N-terminal transactivation domain ($MITF_{TAD}$) and CBP/p300. Using pulldown assays and nuclear magnetic resonance spectroscopy I determined that $MITF_{TAD}$ is intrinsically disordered and binds to the TAZ1 and TAZ2 domains of CBP/p300 with moderate affinity. The solution-state structure of the $MITF_{TAD}$:TAZ2 complex reveals that MITF interacts with a hydrophobic surface of TAZ2, while remaining somewhat dynamic. Peptide array and mutagenesis experiments determined that an acidic motif is integral to the $MITF_{TAD}$:TAZ2 interaction and is necessary for transcriptional activity of MITF. Peptides that bind to the same surface of TAZ2 as $MITF_{TAD}$, such as the adenoviral protein E1A, are capable of displacing MITF from TAZ2 and inhibiting transactivation. These findings provide insight into co-activator recruitment by MITF that are fundamental to our understanding of MITF targeted gene regulation and melanoma biology.

4.3 Introduction

The microphthalmia family of transcription factors (MiT/TFE) is comprised of four closely related members, the microphthalmia-associated transcription factor (MITF), transcription factor EB (TFEB), TFE3, and TFEC (103). MITF is a master transcriptional regulator of melanocytes, the pigment producing cells of the skin (81), where it is essential for development and differentiation by controlling expression of

many genes involved in growth, metabolism, and cell survival (188). Mutation to MITF can cause the failure of melanocytes to form, resulting in genetic diseases such as Waardenburg Syndrome type 2 and Tietz syndrome, which are characterized by skin, eye, and hearing defects (85, 189). Aberrant MITF activity has also been linked to the melanocyte-derived skin cancer, melanoma, where MITF is critical in modulating the proliferation and invasiveness of the disease (97). MITF is a recognized lineage-specific oncogene in melanoma where it has a pro-survival role. Overexpression of MITF drives melanoma progression while long-term suppression of MITF can lead to cellular senescence (91, 190).

MiT/TFE family members are similar in structure and composed of a characteristic set of domains. The central basic helix-loop-helix (bHLH) leucine zipper domain is highly homologous and responsible for dimerization and DNA-recognition of canonical E-box sequences (CANNTG) in gene promoter regions (191). MiT/TFE family members also share a transactivation domain (TAD) that is N-terminal to the bHLH (Figure 4.1A). While divergent in sequence, these TADs allow MITF and other MiT/TFE members to recruit protein co-activators for enhanced transcription of targeted genes (192). Co-factor recruitment by activation domains is often facilitated by small recognition motifs, including the ΦXXΦΦ motif (with Φ representing a hydrophobic residue and X any amino acid), which is conserved in the MiT/TFE family (Figure 4.1B) and also present in numerous other transcription factors including E2A, p65, and FOXO3a (53, 58, 193).

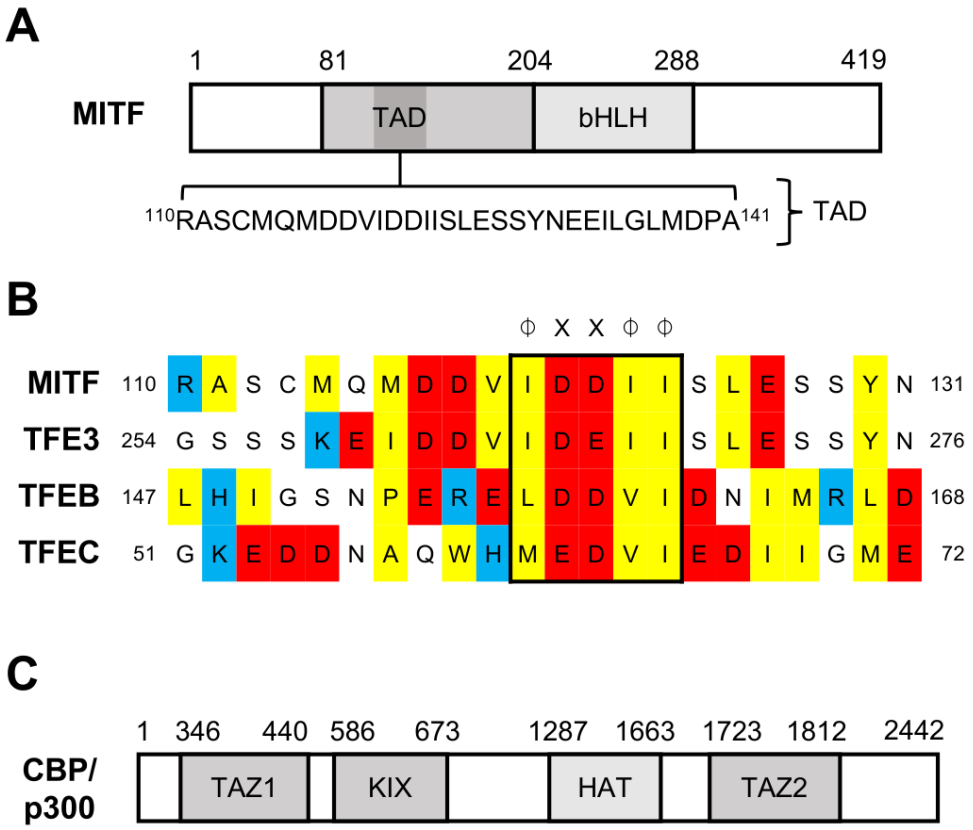

Figure 4.1. Domain architecture of MITF and CBP/p300. (A) Schematic of MITF illustrating the acidic N-terminal transactivation domain (TAD) and basic helix-loop-helix leucine zipper DNA binding domain (bHLH), numbered residues indicate domain boundaries. (B) Alignment of ΦXXΦΦ containing sequences conserved amongst activation domains of MITF, TFE3, TFEB, and TFEC, where Φ represents a hydrophobic amino acid and X any amino acid. (C) Domains of CBP/p300 including the catalytic histone acetyltransferase domain (HAT), and protein-interacting domains KIX, TAZ1, and TAZ2, numbering is in accordance with native protein sequence of p300.

Interacting partners with the $MITF_{TAD}$ most notably includes the histone acetyltransferase cAMP-response element-binding protein (CREB)-binding protein (CBP), and its close homolog E1A-binding protein (p300), which share > 90% sequence identity in their structured domains (107, 194). CBP/p300 are functionally redundant histone acetyltransferases that interact with over 400 known binding partners (195) at the promotors of over 16,000 human genes, making them among the most heavily connected nodes in the mammalian interactome (16). CBP/p300 is a large multimodular protein, with multiple folded domains including a histone acetyltransferase (HAT) domain and several small protein-binding domains that are linked by long disordered regions (Figure 4.1C). The catalytic HAT domain promotes the pre-initiation complex of transcription through its acetylation of relevant histones, as a result chromatin becomes less compact, making DNA more accessible for transcription (196). The transcription adaptor zinc finger (TAZ1/2) and kinase inducible domains (KIX) form interaction sites for intrinsically disordered activation sites of transcription factors, and thus act as a conduit between a variety of transcription factors and transcriptional machinery (25, 197). Transcription factors compete for limited quantities of CBP/p300 (198), and some viral oncoproteins, such as adenovirus early region 1 A (E1A), deregulate the hosts' cell cycle by sequestering CBP/p300 through tight binding interactions with the TAZ2 domain (199, 200).

Despite the importance of MITF for melanocyte differentiation and melanoma biology, the mechanistic details of how MITF interacts with CBP/p300 to induce MITF-target gene expression are not fully understood. Here, I characterize the

structure and function of the $MITF_{TAD}$ and its interactions with different domains of CBP/p300 using a combination of structural biology, pulldown, and transactivation assays. I then evaluate the ability of an E1A-derived peptide to inhibit TAZ2 recruitment by MITF and impede MITF transcriptional activity.

4.4 Materials and Methods

4.3.1 Plasmid Constructs

Full length MITF isoform M cDNA was purchased from ThermoFisher Inc. (Genbank Accession no. BC065243.1). Residues 81-204, 110-161, and 110-141 (TAD) of MITF-M were amplified by PCR and subcloned into a modified pET21 vector containing upstream sequences coding for a hexahistidine tag (His_6), the B1 domain of *Streptococcus* protein G (GB1), and a tobacco etch virus protease cleavage site to create pGB1-$MITF_{81-204}$, pGB1-$MITF_{110-161}$, and pGB1-$MITF_{TAD}$ respectively. Residues 1-204, 81-204, 1-100, and 289-419 of MITF were cloned into pCMV-GAL4 vector gifted by Liqun Luo (Addgene plasmid # 24345) for use in transcriptional activation assays (pGAL4-MITF) (201). Full-length human p300 (residues 1-2414) was subcloned into pcDNA3.1(+) mammalian expression vector (pcDNA-p300) for transfection. Plasmids coding for TAZ1 (residues 346–440 of CBP), TAZ2 (residues 1723-1812 of p300 with four mutations to enhance stability C1738A, C1746A, C1789A, C1790A), and KIX (residues 586–673 of CBP) were provided by Dr. Steven Smith (Queens University, Kingston, ON) (58). A pET21 derived plasmid containing sequences encoding His_6, GB1, TEV, and residues 54-82 (CR1) from

adenovirus early region 1 A (pGB1-E1A$_{CR1}$) was synthesized by BioBasic Inc, and the E1A$_{CR1}$ sequence was then subcloned into pcDNA3-GFP gifted by Doug Golenbock (Addgene plasmid # 13031) (pGFP-E1A$_{CR1}$). MITF deletion mutants (ΔTAD, residues 110-141; ΔDDVIDDII, residues 117-124; ΔIISLE, residues 123-127) were generated from pGB1-MITF$_{81-204}$ and pGAL4-MITF$_{1-204}$ using the Q5 site-directed mutagenesis kit (New England Biolabs) according to the manufacturer's protocol. All plasmids were validated by DNA sequencing.

4.3.2 Protein Expression and Purification

Recombinant proteins were expressed from the plasmids pGB1-MITF, pGB1-TAZ2, and pGB1-E1A$_{CR1}$ in chemically competent *E. coli* BL21 (DE3) cells. Protein expression was induced by adding 0.5 mM isopropyl 1-thio-β-D-galactopyranoside after cultures were grown to an optical density at 600 nm of 0.6-0.8 in LB or ^{15}N- or ^{15}N/^{13}C enriched M9 Minimal Media (149). Following incubation for 4 hours at 37°C or overnight at 20°C, cells were then collected by centrifugation.

TAZ1 and KIX were purified as per previous methods (58). To isolate GB1-TAZ2, 30 mL of denaturing lysis buffer (20 mM Tris-HCl pH 8, 250 mM NaCl, 8 M urea, 100 μM $ZnCl_2$), was added to 1L of cell pellets, followed by sonication, centrifugation (14500 rpm, 20 min) and purification using Ni^{2+}-affinity chromatography. GB1-TAZ2 protein refolding occurred on the column by adding lysis buffer without urea (IMAC Sepharose, Cytiva). After which the eluent was reduced with β-mercaptoethanol (βME) and diluted two-fold with lysis buffer containing 1 mM $ZnCl_2$. For cleavage of GB1, 200 U of thrombin was added, and

samples were left overnight at 4°C. Cleaved TAZ2 was then diluted three-fold in a low-salt buffer (20 mM Tris-HCl pH 8, 5 mM βME, 10 μM $ZnCl_2$) and purified by ion exchange chromatography (SP Sepharose, Cytiva).

For purification of GB1-MITF and GB1-$E1A_{CR1}$, cell pellets were resuspended in native lysis buffer (20 mM Tris-HCl pH 8, 250 mM NaCl, 5 mM βME) and purified by Ni^{2+}-affinity chromatography. The eluent was dialyzed overnight at 4°C (20 mM Tris pH 8, 5 mM βME), and if required 150 μg TEV protease was added to remove the affinity tag. Cleaved MITF and $E1A_{CR1}$ were separated from His_6-GB1 by Ni^{2+}-affinity and ion exchange chromatography (Q Sepharose, Cytiva). All protein purifications were analyzed by SDS-PAGE.

4.3.3 Protein Pulldown Assay

In pulldown solution (20 mM Tris-HCl pH 8, 25 mM NaCl, 5 mM βME, and 10 μM $ZnCl_2$) GB1 and GB1-MITF proteins (20 nmoles) were immobilized onto 20 μL of IgG agarose beads (Cytiva). After being washed two times to remove unbound protein, the beads were then treated with 20 nmoles of TAZ2 for 30 minutes. Samples were rinsed three times with pulldown buffer with or without 20 μM of $E1A_{CR1}$ present. SDS-PAGE was used to analyze protein pulldown by resuspension of the IgG agarose beads in Laemmli buffer.

4.3.4 Isothermal Titration Calorimetry

ITC experiments were conducted using a VP-ITC microcalorimeter at 30°C in buffer containing 20 mM MES pH 6, 50 mM NaCl, 1 mM TCEP, and 10 μM $ZnCl_2$. The syringe contained 500 μM of TAZ1 or TAZ2 which was injected into a

calorimetric reaction cell containing 50 μM of $E1A_{CR1}$, $MITF_{81\text{-}204\ \Delta IISLE}$, $MITF_{81\text{-}204\ \Delta DDVIDDII}$, or $MITF_{81\text{-}204}$ with and without 150 μM TAZ1. A total of 30 injections of 10 μL increments were taken at 300 sec equilibration intervals to obtain ITC data which was performed in duplicate. MicroCal Origin 7.0 software was then used to fit thermograms using a one-site binding model.

4.3.5 NMR Spectroscopy

NMR spectra of $MITF_{81\text{-}204}$ (400 μM) were collected in 20 mM MES pH 6.0, 50 mM NaCl, and 5 mM DTT at 25 °C using a Varian INOVA 600 MHz spectrometer with a room temperature probe (Queen's University, Kingston ON). Resonance assignments of $MITF_{81\text{-}204}$ were determined by interpreting ^{1}H-^{15}N HSQC, HNCACB, CBCACONH, H(CCO)NH, (H)C(CO)NH, HNCO, and HN(CA)CO experiments. To assess binding between MITF and domains of CBP/p300, 10 μM $ZnCl_2$ was added to the sample buffer and ^{1}H-^{15}N HSQC spectra were collected of 100 μM ^{15}N-labelled $MITF_{81\text{-}204}$ or $MITF_{110\text{-}161}$ in the absence and presence of 200 μM TAZ1, or TAZ2.

All other NMR samples were prepared in 20 mM MES pH 6.0, 5 mM βME, 10 μM $ZnCl_2$, and 5% D_2O and data was collected at 35 °C. For competition experiments, samples of 100 μM ^{15}N-labelled $MITF_{110\text{-}161}$ were prepared with or without 100 μM TAZ2 and 150 μM E1A. NMR spectra were acquired on a Bruker Avance III 700 MHz spectrometer equipped with a cryogenically cooled probe at the National Research Council (Halifax, NS). To determine the structure of the $MITF_{TAD}$:TAZ2 complex, samples were prepared containing either 1 mM uniformly $^{13}C/^{15}N$-labelled $MITF_{TAD}$ (residues 110-141) and 1.2 mM TAZ2, or 950 μM uniformly $^{13}C/^{15}N$-

labelled TAZ2 and 1150 μM $MITF_{TAD}$. Resonance assignments were determined using standard triple resonance experiments and distance restraints for the $MITF_{TAD}$:TAZ2 complex and distance restraints were obtained from ^{15}N HSQC-NOESY, aliphatic and aromatic ^{13}C HSQC-NOESY, and $^{12}C/^{14}N$-filtered ^{13}C-edited NOESY experiments. All NOESY experiments were acquired with a 100 ms mixing time.

Raw data were processed using NMRPipe (150) and analyzed using CcpNmr Analysis (151). After resonance assignment, secondary structure propensity (157) was calculated and chemical shift changes (Δδ) upon addition of $MITF_{TAD,}$ TAZ1 or TAZ2 were quantified as $\Delta\delta = [(0.17\Delta\delta_N)^2 + (\Delta\delta_{HN})^2]^{1/2}$ (153). For structure calculation NOESY peak lists and DANGLE-generated dihedral angle predictions (202) were provided to ARIA2 (203). After the initial fold of the $MITF_{TAD}$:TAZ2 complex became apparent, zinc coordination restraints were incorporated for known zinc-binding residues of TAZ2 (46) and hydrogen bond distance restraints ($1.8 \leq d_{OH} \leq 2.2$ Å; $2.7 \leq d_{ON} \leq 3.2$ Å) were applied to helical regions of the complex. In total 100 structures were generated over 8 iterations of automated NOE assignment, with the 20 lowest energy structures being selected for automated water refinement. The quality of the final ensemble of structures was assessed using the protein structure validation suite (204), and the Protein Data Bank validation tools. The $MITF_{TAD}$:TAZ2 ensemble was deposited into the Protein Data Bank (accession no. 8E1D), while the chemical shift assignments of $MITF_{81-204}$ and the $MITF_{TAD}$:TAZ2 complex were deposited into the BMRB (accession nos. 51550 and 31038,

respectively). PyMOL (Schrödinger Inc.) was used to interpret structures and generate figures.

4.3.6 Peptide Array

Peptide array experiments were performed as described previously (205). Briefly, MITF peptides were generated via automatic SPOT synthesis (206, 207). Peptides were synthesised on continuous cellulose membrane supports using 9-fluorenylmethyloxycarbonyl chemistry by the MultiPep RSi Robot (Intavis). Arrays were pre-activated in absolute ethanol, followed by blocking in 5% BSA in 1x Tris-buffered saline with 0.1% tween-20 (TBS-T) for 4 hours at room temperature. GB1-TAZ2 was diluted to 2 μM using 200 mM NaCl, 50 mM Tris Base, 5% glycerol, pH 7.4, and overlaid onto the MITF array overnight at 4 °C. GB1-TAZ2 binding to MITF peptides was determined utilising a polyhistidine monoclonal mouse antibody (1:5000, Sigma, H1029), incubated on the array for 4 hours at 4 °C. Following this, a mouse horse radish peroxidase conjugated secondary antibody (1:5000) was incubated for 1 hour at room temperature. Antibodies were diluted into TBS-T with 1% BSA. Finally, binding signal was determined by enhanced chemiluminescence detection. All protein and antibody incubation steps were carried out under gentle agitation, and arrays washed following protein and antibody incubation steps 3 times in TBS-T.

4.3.7 Transactivation Assays

HEK 293A cells were grown in DMEM containing 10% FBS and maintained at 37°C with 5% CO_2. After being seeded into 24-well plates, cells were transfected

the next day using jetPRIME transfection reagent. The following amounts of plasmid were transfected into each well: 350 ng luciferase reporter (p5xGAL4-luc), 50 ng internal control (pCMV-Renilla), and 100 ng MITF plasmid (pGAL4-MITF). For co-transfections, 50 ng pGAL4-MITF or pGAL4 was transfected with up to 50 ng of pcDNA-p300 or pGFP-E1A$_{CR1}$. Luciferase activity was measured 24 hrs post-transfection using a dual-luciferase reporter assay. All luciferase data are the mean of at least three separate transfections and are expressed as a ratio of *Renilla* normalized luminescence. One-way analysis of variance (ANOVA) and Dunnett's multiple comparison test was performed to determine statistical significance.

4.5 Results and Discussion

4.5.1 MITF Interacts with the TAZ1 and TAZ2 Domains of CBP/p300

A combination of luciferase and pulldown experiments were used to investigate the MITF transactivation domain first characterized by Sato *et al.* (1997). Luciferase-based mammalian one-hybrid assays with MITF regions fused to the GAL4 DNA-binding domain demonstrated that transfection of plasmids containing the N-terminal of MITF, particularly pGAL4-MITF$_{1-204}$ and pGAL4-MITF$_{81-204}$, activated transcription 100-fold and 135-fold, respectively, compared to expression of pGAL4 alone (Figure 4.2A). In contrast pGAL4-MITF$_{1-100}$ and pGAL4-MITF$_{289-419}$ were unable to activate transcription above levels observed for pGAL4. These results are consistent with MITF containing a transactivation domain in its N-terminal sequence (107), and I do not observe evidence for transactivation from C-

terminal fragments of MITF. Since transcriptional activation by MITF is partly mediated by CBP/p300 recruitment (116), I investigated the co-activation potential of p300 by transfecting pGAL4-MITF$_{81-204}$ alone or with increasing amounts of pcDNA-p300. I found co-transfection of pcDNA-p300 potentiated transactivation by pGAL4-MITF$_{81-204}$ up to 5-fold, indicating a functional interaction between MITF and p300, as this effect was not observed by titrating pcDNA-p300 with pGAL4 alone (Figures 4.2B and 4.3).

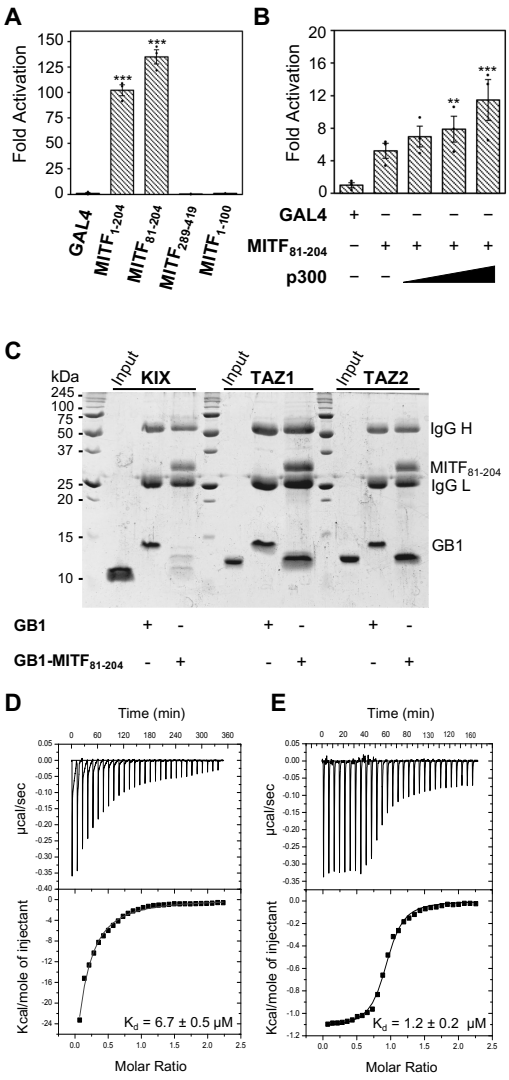

Figure 4.2. MITF interacts with CBP/p300 through TAZ1 and TAZ2. (A) Luciferase-based mammalian one-hybrid transactivation assays performed in HEK 293A cells using 100 ng of indicated pGAL4-MITF fusion proteins. (B) Luciferase-based mammalian one-hybrid transactivation assays performed for 50 ng of pGAL4-$MITF_{81-204}$ with co-transfection of up to 50 ng of p300. Asterisks indicate statistical significance by one-way ANOVA and Dunnetts multiple comparison test (** $p \leq 0.01$, *** $p \leq 0.005$, n=3 technical replicates) compared to pGAL4 and variation is reported as SEM. (C) 15% SDS-PAGE analysis of the ability of immobilized GB1 or GB1-$MITF_{81-204}$ to pulldown and interact with purified recombinant KIX, TAZ1, and TAZ2 stained with Coomassie brilliant blue. The input lane shows purified CBP/p300 domain only and represents 10% of pulldown input. Positions of $MITF_{81-204}$, the heavy and light immunoglobulin G chains (IgG H and IgG L, respectively), and the GB1 protein are annotated. ITC thermograms of 500 µM TAZ1 (D) or TAZ2 (E) titrated into 50 µM $MITF_{81-204}$ and fit to a one-site binding model with measured K_d indicated (n=2 biological replicates, error reported as SD).

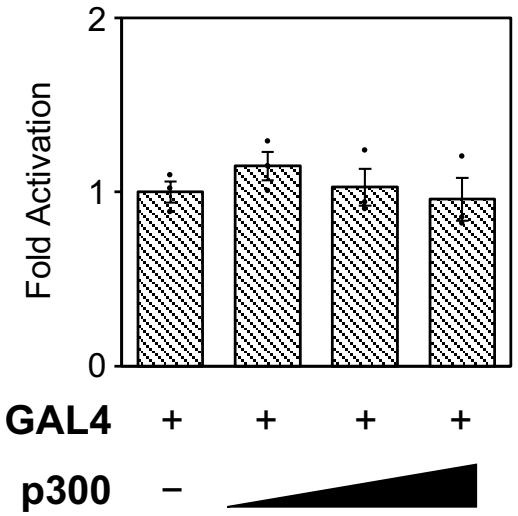

Figure 4.3. Luciferase assay of GAL4 titrated with p300. Luciferase-based one-hybrid assay performed for 50 ng of pGAL4 with co-transfection of up to 50 ng of p300. Asterisks indicate statistical significance by one-way ANOVA and Dunnetts multiple comparison test compared to pGAL4 alone, variation is reported as SEM (n=3 technical replicates).

CBP/p300 is a large protein with multiple protein-interaction domains, and outside of the histone acetyltransferase region, the TAZ1, TAZ2, and KIX domains are common binding sites for intrinsically disordered activation domains of cellular transcription factors including STAT1/2, p53 and *c-Myb* (208–211). To corroborate our transactivation assays and to determine the regions of CBP/p300 that interact with MITF, I completed pulldown assays using various fragments of MITF expressed in *E. coli* as fusion proteins with the B1 binding-domain of *Streptococcus* protein G (GB1). An equal amount of purified KIX, TAZ1, or TAZ2 was then combined with GB1-MITF bound to IgG Sepharose beads. SDS-PAGE analysis of bound protein indicates that GB1-$MITF_{81-204}$ interacts significantly with both the TAZ1 (CBP) and TAZ2 (p300) domains, but very weakly with the KIX domain (CBP) (Figure 4.2C). Using isothermal titration calorimetry, I measured dissociation constants (K_d)'s of 6.7 ± 0.5 μM and 1.24 ± 0.23 μM for the association of $MITF_{81-204}$ with TAZ1 and TAZ2, respectively (Figure 4.2D, E). The association with TAZ2 of p300 is consistent with pulldown studies between larger fragments of CBP/p300 and MITF (107); however, to our knowledge the association between TAZ1 and MITF has not been previously reported. Interestingly, the binding of $MITF_{81-204}$ to these domains is mutually exclusive, where the presence of TAZ1 in the ITC cell impedes any observed interaction with TAZ2 (Figure 4.4).

4.5.2 MITF Interacts with TAZ1 and TAZ2 via a Common Transactivation Domain

Since $MITF_{81-204}$ demonstrated both a functional interaction with p300 in HEK 293A cells and direct binding to TAZ1 and TAZ2 by pulldown assay and ITC, nuclear magnetic resonance (NMR) spectroscopy was used to further characterize the

molecular properties of MITF and its interaction with these domains. The ^{1}H-^{15}N HSQC spectrum of ^{15}N-labelled $MITF_{81-204}$ has the expected number of peaks with sharp linewidths and little chemical shift dispersion (Figure 4.5A), which is indicative of MITF being an intrinsically disordered protein (212). Standard triple resonance experiments were used to assign 122/124 residues and 96% of the backbone resonances of $MITF_{81-204}$. Secondary structure propensity analysis indicates that although disordered, $MITF_{81-204}$ has some propensity to form an α-helix, with residues Met105-Gln115, Ile124-Met144, Gly152-Gly159, and Cys188-Ala198 having the highest SSP scores (Figure 4.5B).

I then used NMR-based chemical shift perturbation studies to clearly define which residues within $MITF_{81-204}$ bind TAZ1 and TAZ2 (Figures 4.6A and 4.7A). When compared to free peptide, most resonances of $MITF_{81-204}$ experienced minor chemical shift perturbations upon the addition of unlabelled TAZ1 or TAZ2 (Figures 4.6B and 4.7B), with no obvious change in linewidth or peak intensity. However, residues Gln115-Ala141 of MITF undergo line broadening to the extent that peaks disappear from the ^{1}H-^{15}N HSQC spectrum upon addition of TAZ2, with similar changes observed for TAZ1. This may be due to slow tumbling of the MITF:TAZ complex or these resonances transitioning from fast to intermediate timescales of chemical exchange upon binding TAZ. This phenomenon has been observed for other transcription factors including p53, which undergoes line broadening when bound to its regulator MDM2 (213).

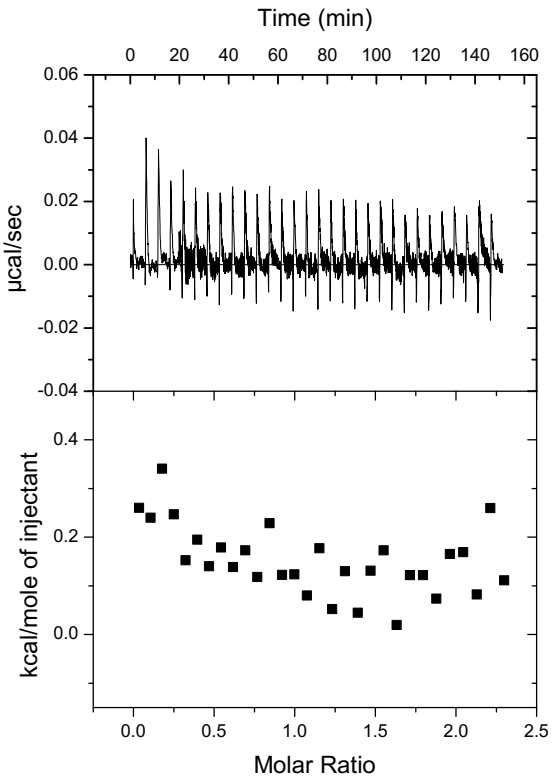

Figure 4.4. ITC of TAZ2 with $MITF_{81-204}$ and TAZ1. Isothermal titration calorimetry thermogram of 500 µM TAZ2 titrated into a cell containing 50 µM $MITF_{81-204}$ and 150 µM TAZ1.

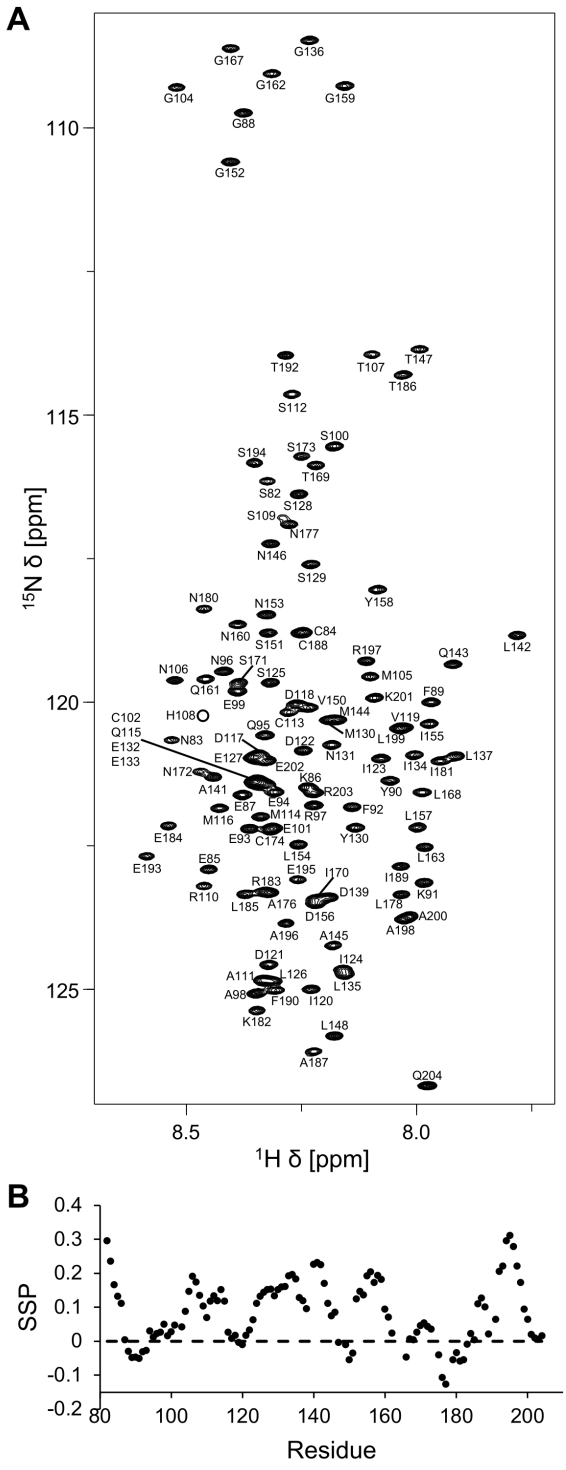

Figure 4.5. Backbone resonance assignments of $MITF_{81-204}$. (A) ^{1}H-^{15}N HSQC of $^{13}C/^{15}N$-labelled $MITF_{81-204}$, residue assignments for backbone resonance peaks are indicated. (B) Secondary structure propensity (SSP) values per residue of $MITF_{81-204}$ calculated from Cα and Cβ chemical shifts.

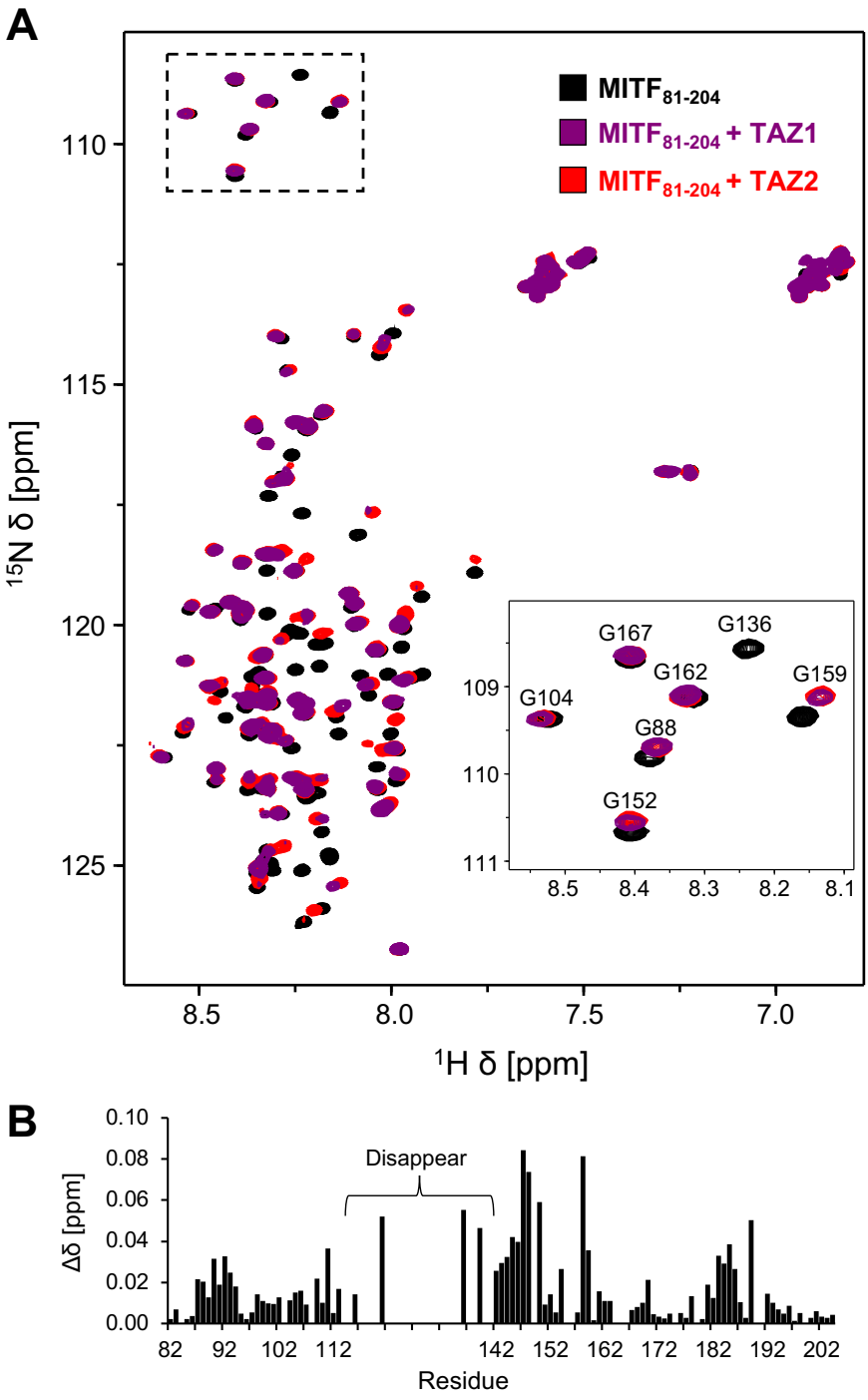

Figure 4.6. HSQC chemical shift analysis of $MITF_{81-204}$ with TAZ2. (A) ^{1}H-^{15}N HSQC of 100 µM ^{15}N-labelled $MITF_{81-204}$ in the absence (black) and presence of 200 µM of unlabelled TAZ1 (purple) or TAZ2 (red). Resonance assignments for a subset of peaks are indicated in the inset. (B) Chemical shift change ($\Delta\delta = [(0.17\Delta\delta_N)^2 + (\Delta\delta_{HN})^2]^{1/2}$) plotted per residue of $MITF_{81-204}$ upon addition of TAZ2.

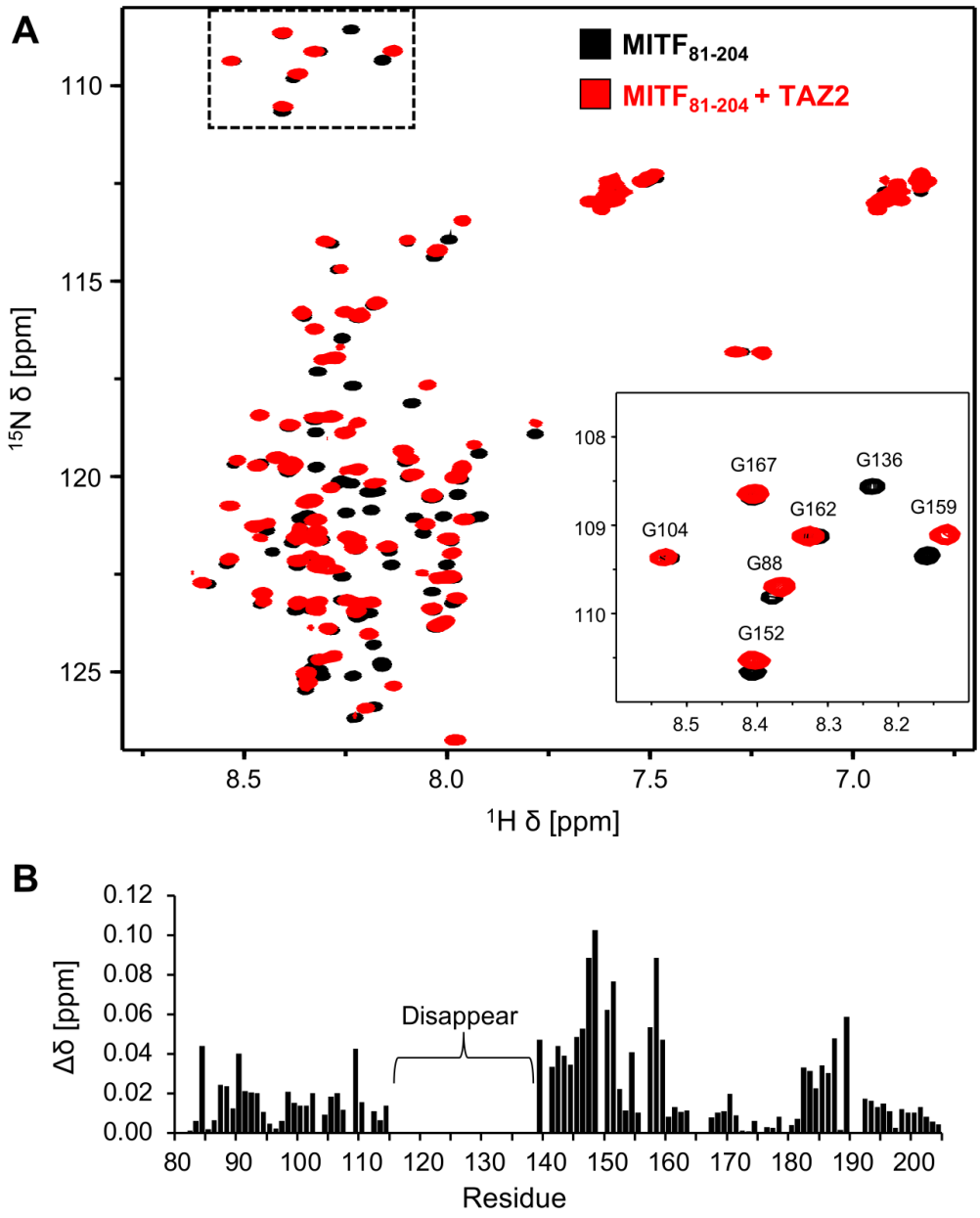

Figure 4.7. MITF binds TAZ2 through $MITF_{TAD}$. (A) ^{1}H-^{15}N HSQC of 100 µM ^{15}N-labelled $MITF_{81-204}$ overlayed in the absence (black) and presence (red) of 200 µM unlabelled TAZ2. Residue assignments of a subset of peaks are indicated in the insert. (B) The chemical shift changes ($\Delta\delta = [(0.17\Delta\delta_N)^2 + (\Delta\delta_{HN})^2]^{1/2}$) that each residue of $MITF_{81-204}$ experienced upon addition of TAZ2 results are plotted, with peaks that disappear upon addition of TAZ2 indicated.

To improve spectral quality by reducing resonance overlap, I titrated ^{15}N-labelled MITF$_{110\text{-}161}$ with TAZ1 and TAZ2. When free in solution MITF$_{110\text{-}161}$ has low peak dispersion and sharp resonances, indicating that it is disordered (Figure 4.8A). By utilizing this smaller construct more MITF resonances remained visible upon the addition of TAZ1 or TAZ2, this is likely due to faster tumbling rates and fast chemical exchange of the MITF:TAZ complex. Interestingly, resonances of MITF experience similar magnitude and direction of chemical shift changes upon the addition of either TAZ1 or TAZ2, suggesting that MITF adopts a similar structure when binding these proteins. Consistent with the peak disappearance observed for MITF$_{81\text{-}204}$, residues Arg110-Ala141 of MITF (hereafter referred to as MITF$_{TAD}$) underwent the most significant chemical shift changes, while the rest of the peptide experienced only minor chemical shift perturbations. Since all resonances of MITF$_{110\text{-}161}$ are observable when bound to TAZ2 but not when bound to TAZ1 (Figure 4.8), I next used NMR spectroscopy to characterize the structure of the MITF$_{TAD}$:TAZ2 complex.

4.5.3 Structure of the MITF$_{TAD}$:TAZ2 Complex

To determine the structure of the MITF$_{TAD}$:TAZ2 complex, resonance assignments were determined for ^{13}C/^{15}N-labelled TAZ2 in complex with MITF$_{TAD}$ (residues 110-141), as well as ^{13}C^{15}N-labelled MITF$_{TAD}$ saturated with TAZ2 (saturation was determined based on the concentration of binding partner at which peaks no longer moved) (Figures 4.9A and 4.10).These spectra were high quality and allowed for assignment of 97%, 81%, and 56% of backbone, sidechain, and aromatic resonances, respectively. When bound to TAZ2, residues Asp118-Asp139 of MITF

have $^{15}N\{^{1}H\}$ NOE values > 0.25, with most of these values ranging from 0.5 to 0.6 (Figure 4.9B). Many of these residues (Asp121, Asp122, and Ser125-Ser129) have chemical shift index (Figure 4.9C) values that suggest this region forms an α-helical turn upon binding TAZ2.

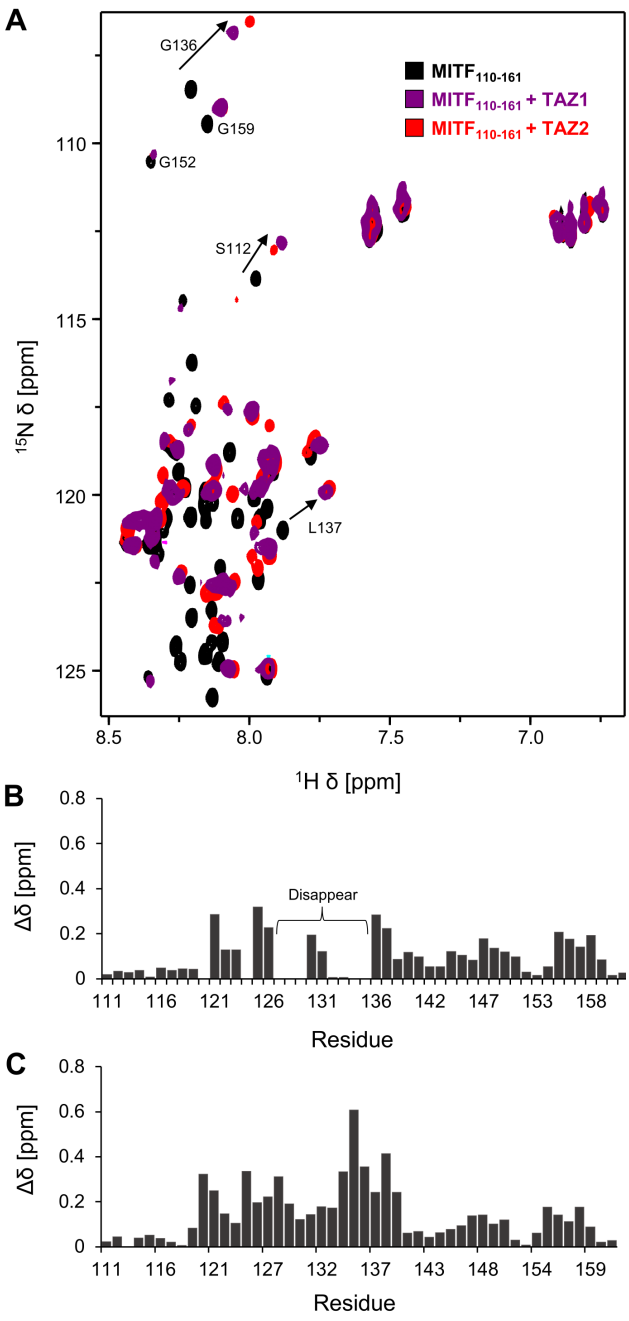

Figure 4.8. HSQC chemical shift analysis of $MITF_{110-161}$ with TAZ1 or TAZ2. (A) ^{1}H-^{15}N HSQC of 100 µM ^{15}N-labelled $MITF_{110-161}$ overlayed in the absence (black) and presence of 200 µM unlabelled TAZ1 (purple) or TAZ2 (red). Resonance assignments are indicated for non-overlapped peaks that shift upon addition of TAZ1 or TAZ2. Plots of chemical shift changes ($\Delta\delta = [(0.17\Delta\delta_N)^2 + (\Delta\delta_{HN})^2]^{1/2}$) that each residue of $MITF_{110-161}$ experienced upon addition of (B) TAZ1 or (C) TAZ2. Regions of MITF where resonances disappear upon addition of TAZ1 are indicated.

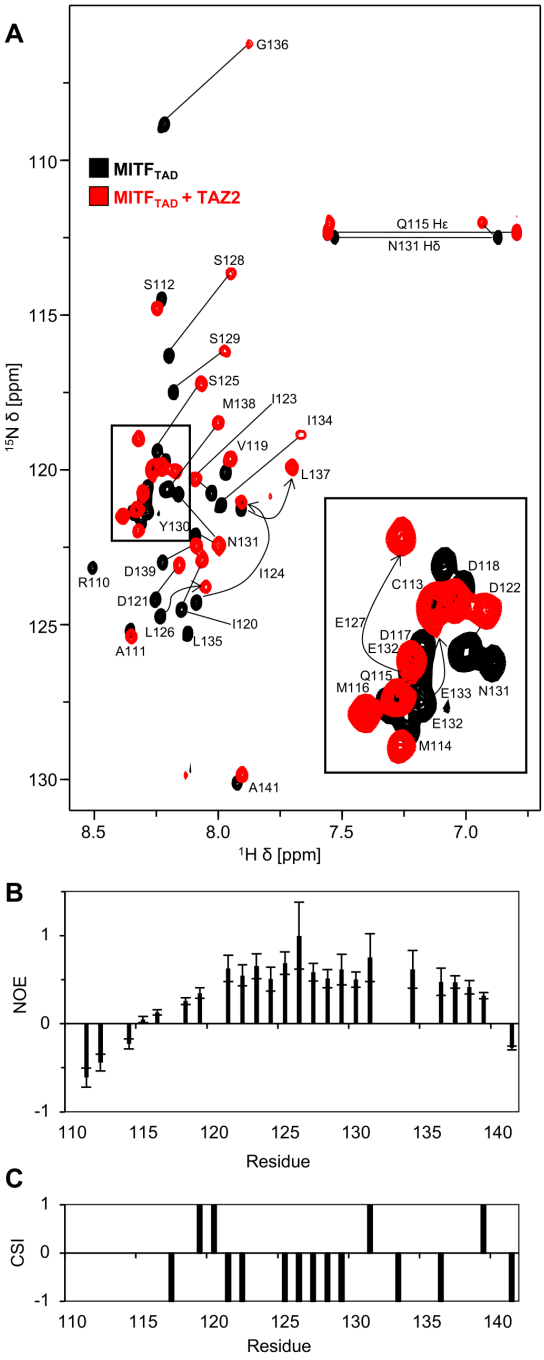

Figure 4.9. Secondary structure and dynamics of $MITF_{TAD}$ bound to TAZ2. (A) Overlay of ^{1}H-^{15}N HSQC of 1 mM $^{13}C/^{15}N$-labelled $MITF_{TAD}$ in the absence (black) and presence (red) of 1.2 mM unlabelled TAZ2 (red). Residue assignments of resonance peaks are indicated, and arrows indicate resonance shifts upon TAZ2 addition. (B) Plot of $^{15}N\{^{1}H\}$ NOE values for reach residue of $MITF_{TAD}$ when bound to TAZ2. (C) Chemical Shift Index (CSI) values per residue of $MITF_{TAD}$ when bound to TAZ2. Negative values indicate α-helical and positive values indicate β-sheet propensity.

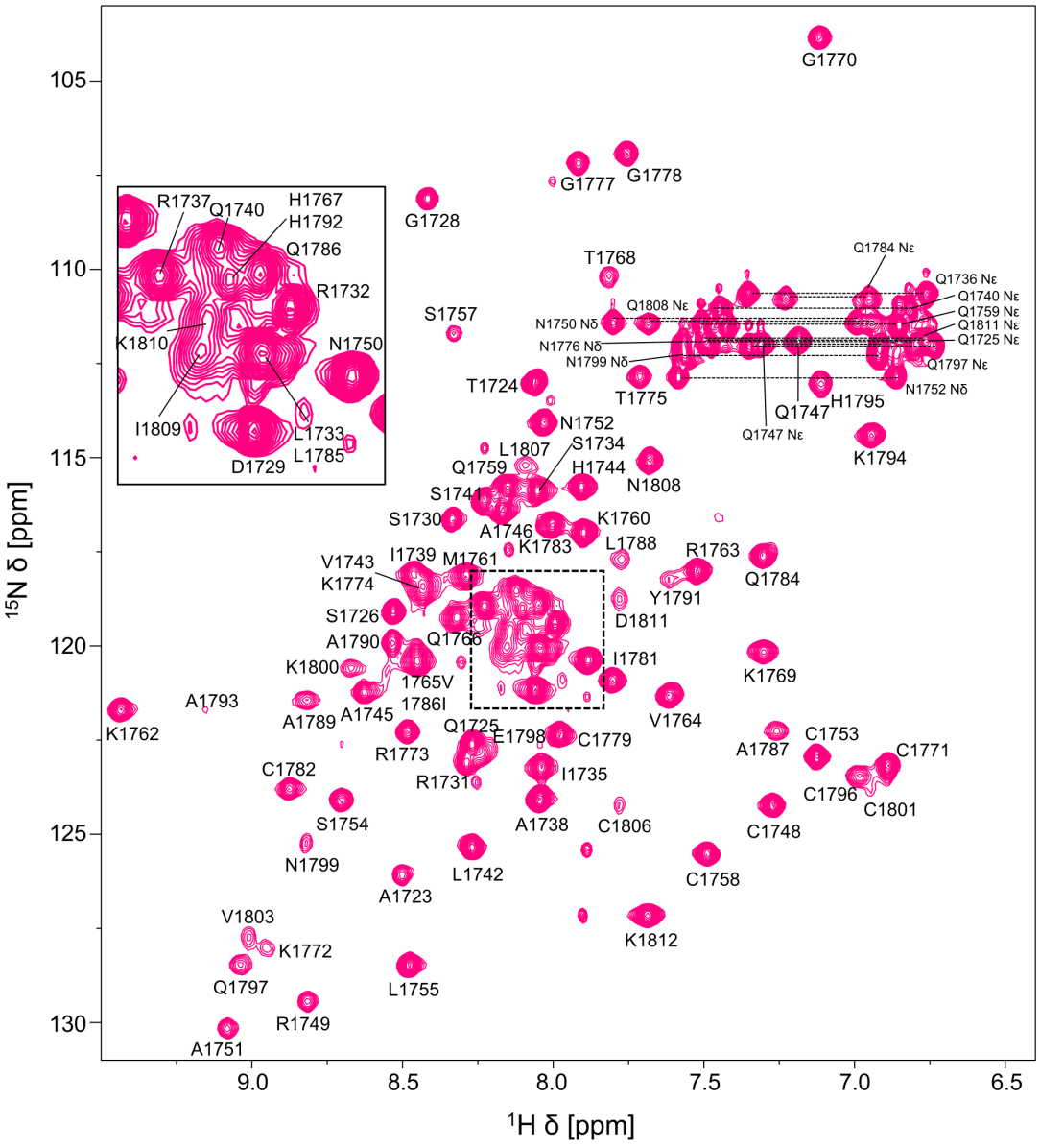

Figure 4.10. HSQC of labelled TAZ2 bound to $MITF_{TAD}$.^{1}H-^{15}N HSQC of 950 µM ^{13}C/^{15}N-labelled TAZ2 in the presence of 1150 µM unlabelled $MITF_{TAD}$. Resonance assignments are indicated.

After resonance assignment of $MITF_{TAD}$:TAZ2, 1783 NOE-derived distance restraints were obtained from ^{13}C-NOESY-HSQC, ^{15}N-NOESY-HSQC, and $^{12}C/^{14}N$-filtered ^{13}C-edited NOESY spectra and with dihedral angle restraints were used to generate a 20-member structural ensemble of the $MITF_{TAD}$:TAZ2 complex (Table 4.1 and Figure 4.11A). The resulting ensemble was high quality with 91.1%, 6.8%, and 2.1% of ordered residues having favoured, allowed, and disallowed dihedral angles, respectively. In this ensemble TAZ2 is well-converged while the structure of MITF is less defined. Analysis using protein data bank validation reports indicate that nearly all TAZ2 and a small region of MITF (residues Pro1727-Gln1811 and Leu126-Ile134, respectively) can be considered the ordered core of this complex, with a root-mean-square deviation (RMSD) of 0.7 Å and 1.1 Å for backbone and heavy atoms, respectively. This positioning of $MITF_{TAD}$ is supported by observed intermolecular NOE contacts between Leu126-Ala1787, Tyr130-Ile1735/Leu1788, and Ile134-Pro1780/Ile1781/Gln1784 (Figure 4.11B). The structure of TAZ2 is consistent with previously determined structures of TAZ2 and consists of four alpha helices (α1- α4) spanning residues Gly1728-Gln1747, Cys1758-Thr1768, Pro1780-Ala1793, and Pro1804-Ile1809, respectively. $MITF_{TAD}$ has two α-helices spanning residues Asp118-Ser129 and Glu132-Gly136 that are supported by both cross peaks in NOESY spectra and the calculated CSI for $MITF_{TAD}$. Although the presence of these α-helices is well-defined there are few intermolecular contacts with TAZ2 in these regions, making the positioning of these α-helices with respect to TAZ2 somewhat variable. $MITF_{TAD}$ binds a hydrophobic surface of TAZ2 created by the intersection of α1-α3 (Figure 4.11C), which is also targeted by other transcription factors, such as

p53 and viral E1A (214, 215). Consistent with the variable positioning of MITF α-helices relative to TAZ2, the $^{15}N\{^{1}H\}$ NOE values of $MITF_{TAD}$ in complex with TAZ2 (most ranging from 0.5 to 0.6) are lower than for a well-ordered protein (typically 0.8). Intrinsically disordered proteins such as MITF often form a dynamic or fuzzy complex when interacting with binding partners, and recently this has been observed for the E7 protein binding to TAZ2 (216).

Table 4.1. Statistics of the NMR-derived ensemble of $MITF_{TAD}$:TAZ2

Completeness of resonance assignments (%)[a]		
Backbone	97	
Side Chain	81	
Aromatic	56	
Number of conformational restraints		
Total NOE restraints	1783	
Intra-residue (i = j)	$MITF_{TAD}$: 210	Taz2: 712
Sequential (|i−j| = 1)	$MITF_{TAD}$: 89	Taz2: 313
Medium range (1 < |i − j| < 5)	$MITF_{TAD}$: 48	Taz2: 201
Long range (|i − j| ≥ 5)	$MITF_{TAD}$: 2	Taz2:152
Intermolecular	41	
Ambiguous	190	
Dihedral angle restraints	90	
Hydrogen bond restraints	13.1	
NOE restraints per residue	1.1	
Long range restraints per residue		
Residual restraint violations[b]		
RMSD NOE restraints (Å)	0.05	
RMSD dihedral angle restraints (°)	0.34	
Mean distance violations per structure		
> 0.3 Å	3.6	
> 0.5 Å	0.15	
Mean dihedral angle violations per structure > 5°	0.05	
Model quality[c]		
RMSD backbone atoms (Å)[d]	0.7	
RMSD heavy atoms (Å)[d]	1.1	
RMSD bond lengths to ideal geometry (Å)	0.006	
RMSD bond angles to ideal geometry (°)	0.8	
Ramachandran plot statistics[de]		
most favored regions (%)	91.1	
allowed regions (%)	6.8	
disallowed regions (%)	2.1	
Global quality scores (Raw / Z-score)[c]		
Verify3D	0.07 / -6.26	
ProsaII	0.64 / -0.04	
ProCheck G-factor (phi-psi)[d]	-0.15 / -0.28	
ProCheck G-factor (all)[d]	-0.39 / -2.31	
MolProbity clash score	45.41 / -6.27	
Model contents		
Ordered residue ranges[f]	1727-1811	
	126-134	
Total no. of residues	136	
BMRB accession no.	31038	
PDB accession no.	8E1D	

[a]Calculated using RCSB validation server
[b]Calculated using CNS version 1.21
[c]Calculated using PSVS version 1.5
[d]Calculated over ordered residue ranges
[e]Calculated using Molprobity through PSVS version 1.5
[f]Based on core residue ranges listed in RCSB validation report.

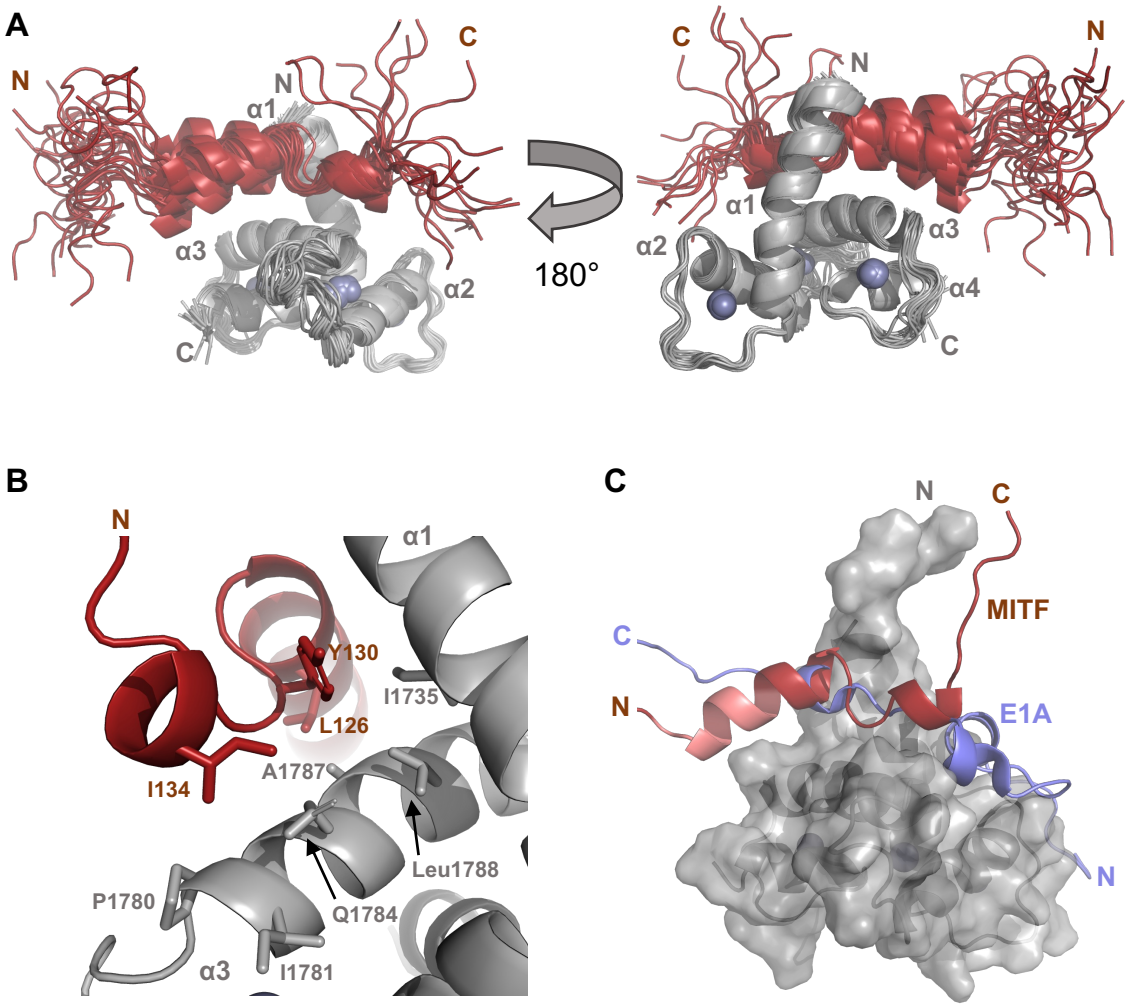

Figure 4.11. Structure of $MITF_{TAD}$:TAZ2 complex. (A) Backbone ribbon illustration of the 20-member structural ensemble of the $MITF_{TAD}$:TAZ2 complex, with TAZ2 coloured grey and $MITF_{TAD}$ shown in red. The disordered N-terminal residues of TAZ2 are omitted for clarity and zinc ions are shown as spheres. (B) Close-up view of the interaction interface between $MITF_{TAD}$ and TAZ2. Residues with observable intermolecular NOE contacts are shown as sticks and labelled. (C) Superposition of E1A (PDB accession no. 2KJE) with the $MITF_{TAD}$:TAZ2 complex. The functionally important MITF motif (DDVIDDII, residues 117-124) is coloured light pink, TAZ2 is shown as a transparent grey surface, and E1A is coloured blue.

4.5.4 An Acidic Motif Mediates Binding of $MITF_{TAD}$ to TAZ2

To identify residues important for the $MITF_{TAD}$:TAZ2 interaction in a high-throughput manner, a peptide array was used to probe for variation in the ability of MITF to pull down TAZ2. Due to technical limitations a shorter MITF peptide, $MITF_{117-135}$, was used for this assay, which corresponds to the region of MITF that associates directly with TAZ2 based on the NMR-derived structure and heteronuclear NOE measurements. Each residue of $MITF_{117-135}$ was sequentially mutated to alanine, probed with GB1-TAZ2, and visualized for GB1-TAZ2 binding using chemiluminescence. Although no point mutations completely ablated GB1-TAZ2 binding, decreased interaction was observed when residues within Asp117-Asp122 (DDVIDD) were mutated to alanine. This overlaps with the ΦXXΦΦ motif that is conserved in MiT/TFE members (Figure 4.1B) and suggests that this motif is necessary for association with TAZ2 (Figure 4.12A).

The peptide array results were consistent with luciferase-based mammalian-one hybrid assays and pulldown experiments (Figure 4.12B, C), where this acidic motif between Asp117-Ile124 (DDVIDDII) was found to be necessary for both transcriptional activation and pulldown of TAZ2 by $MITF_{81-204.}$ Supporting this, mutation of this motif significantly weakened the interaction between TAZ2 and $MITF_{81-204}$ by isothermal titration calorimetry rendering a K_d of 37 ± 3.0 μM (Figure 4.13). Conversely, mutation of individual residues between Ile123-Glu127 (IISLE) did not decrease the observed binding in the peptide array and complete removal of Ile123-Glu127 resulted in only partial disruption of theTAZ2 interaction by ITC (K_d = 9.0 ± 1.1 μM), pulldown, and transactivation by $MITF_{81-204}$ (Figures 4.12 and 4.14).

This is consistent with studies finding deletion of IISLE significantly reduces the function of the MITF activation domain, but retains the ability to activate transcription above the GAL4 reporter alone (107).

It is interesting that the acidic motif Asp117-Ile124 (DDVIDDII), which remains somewhat variable in its orientation when interacting with TAZ2, is a primary modulator of binding and transactivation potential. This may be partly explained by the observed dynamics and difficulties in identifying intermolecular NOE contacts to aspartate, which is a small amino acid without methyl groups. Overall, our NMR and mutagenesis results indicate MITF and TAZ2 utilize both hydrophobic and electrostatic interactions for molecular recognition. Given the negative charge of this acidic motif within $MITF_{TAD}$ and the highly positively charged surface of TAZ2, long-range electrostatic interactions could drive the initial contact between MITF and TAZ2, promoting the formation of additional hydrophobic interactions that enhance complex stability. Several oncogenic transcription factors (e.g., HPVE7, SV40, and E1A) also contain an acidic stretch within the structurally variable region adjacent to their binding motif. These residues participate in favourable electrostatic interactions with complementary charges on the surface surrounding the more ordered binding site (217–219). The presence of these charged motifs helps to maximize binding affinity, and the importance of this region for the $MITF_{TAD}$ is further supported by its conservation amongst other MiT/TFE family members (Figure 4.1B).

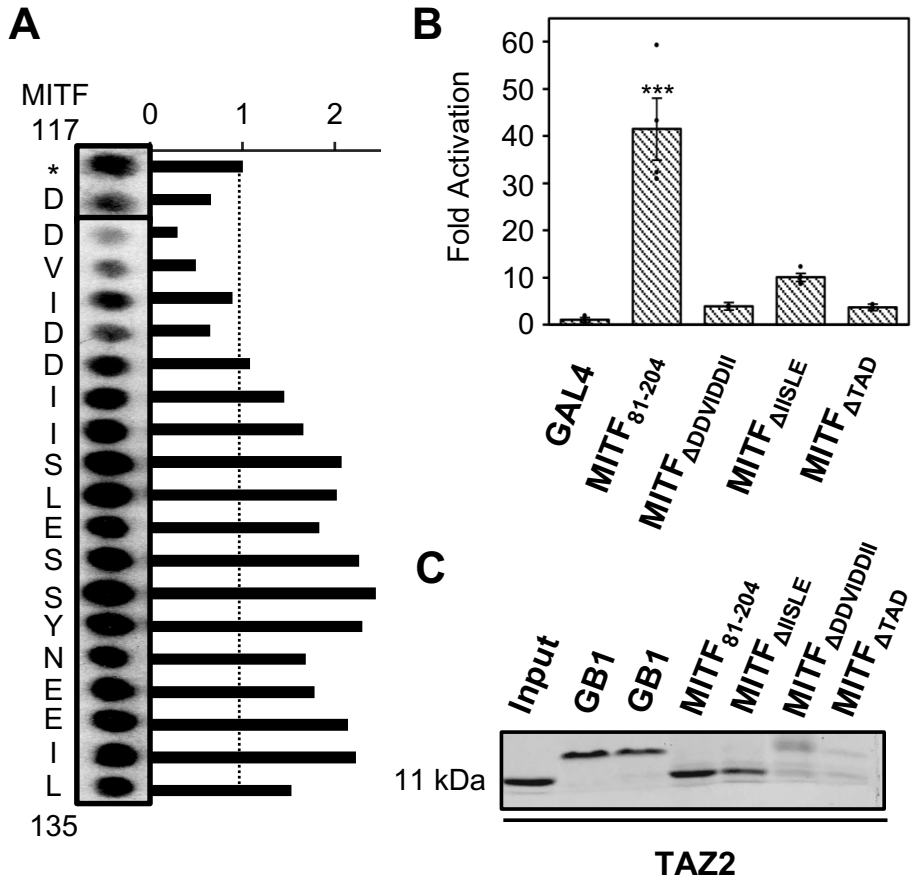

Figure 4.12. $MITF_{TAD}$ mutagenesis ablates TAZ2 binding. (A) Peptide microarray of $MITF_{117-135}$ with each residue sequentially mutated to alanine, probed for its binding affinity with GB1-TAZ2 and visualized by chemiluminescence. * Annotates wildtype $MITF_{117-141}$ to which all peak intensities were normalized. (B) Luciferase-based transcriptional activity after transfection of cells with 100 ng pGAL4-$MITF_{81-204}$ (either wildtype or containing the indicated deletion). Statistical significance by one-way ANOVA and Dunnetts multiple comparison test compared to Gal4 is indicated (*** $p \leq 0.005$, n=3 technical replicates) and variation is reported as SEM. (C) Protein pulldown assay of GB1 and GB1-$MITF_{81-204}$ analyzed by SDS-PAGE and stained with Coomassie blue. The input lane shows TAZ2 domain only and represents 10% of total pulldown input. Reference bands are shown for TAZ2 and GB1, while pulldown of TAZ2 by the indicated GB1-$MITF_{81-204}$ deletion mutants is shown.

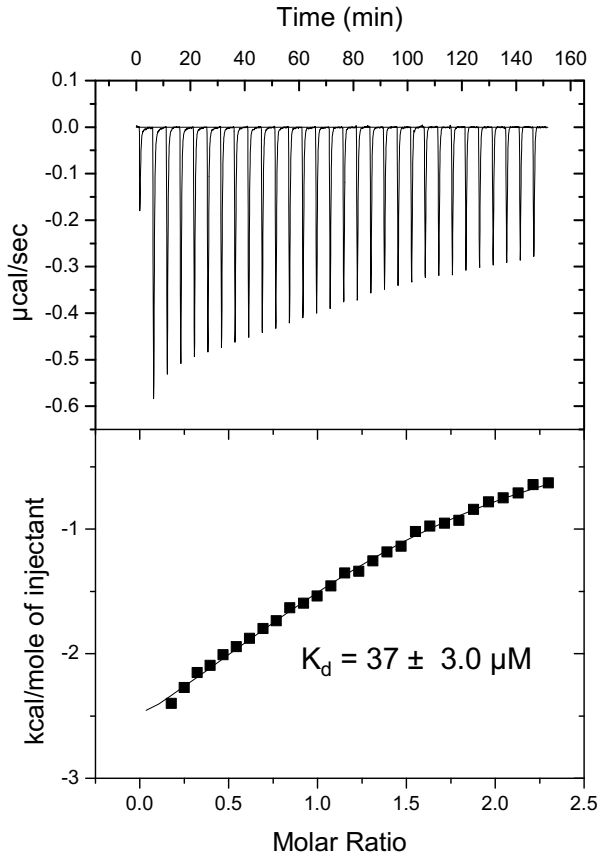

Figure 4.13. ITC of TAZ2 and $MITF_{81\text{-}204\ \Delta DDVIDDII}$. Isothermal titration calorimetry thermogram of 500 µM TAZ2 titrated into 50 µM $MITF_{81\text{-}204\ \Delta DDVIDDII}$. Data were fit to a one-site binding model yielding K_d = 37 ± 3.0 µM (n=2 biological replicates, error reported as SD).

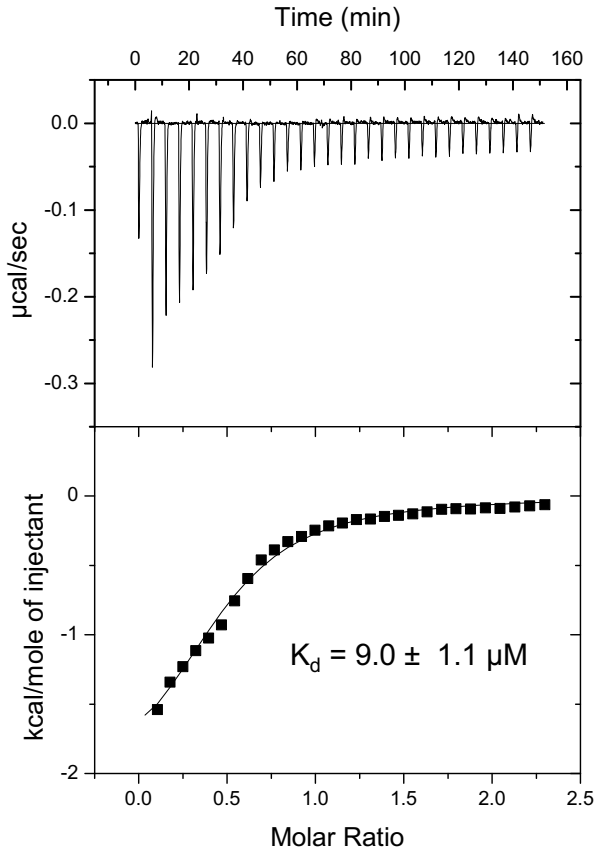

Figure 4.14. ITC of TAZ2 and $MITF_{81\text{-}204\ \Delta IISLE}$. Isothermal titration calorimetry thermogram of 500 µM TAZ2 titrated into 50 µM $MITF_{81\text{-}204\ \Delta IISLE}$. Data were fit to a one-site binding model yielding K_d = 9.0 ± 1.1 µM (n=2 biological replicates, error reported as SD).

4.5.5 E1A-peptide competes with MITF for the TAZ2 binding surface

Since MITF interacts with TAZ2 through a large interaction surface instead of a distinct binding pocket, the ability of a peptide to block the MITF:TAZ2 interaction was evaluated. The adenovirus early region 1 A (E1A) plays a critical role in viral infections by deregulating the hosts' cell cycle through interactions with essential cellular proteins including CBP/p300 (199). The interaction between CBP/p300 and E1A is mediated by the TAZ2 domain and a region within conserved region 1 of E1A (residues 54-82; $E1A_{CR1}$) binds the same surface of TAZ2 as $MITF_{TAD}$ (Figure 4.11C), suggesting that E1A, MITF, and other transcription factors may potentially compete for the TAZ2 domain of CBP/p300 to mediate viral infection (107, 116, 180, 220).

To test if E1A competes with MITF for TAZ2, an NMR-based displacement experiment was performed. Unlabelled TAZ2 was initially titrated into ^{15}N-labelled $MITF_{110-161}$ and HSQC spectra were collected. The presence of TAZ2 resulted in significant chemical shifts of many of the backbone ^{1}H-^{15}N resonances in the spectrum consistent with the formation of a TAZ2:MITF complex (Figure 4.15A). Upon the subsequent addition of unlabelled $E1A_{CR1}$ to this sample, the chemical shifts of $MITF_{110-161}$ became more like those of the unbound peptide, indicating that $E1A_{CR1}$ can displace $MITF_{110-161}$ from TAZ2. These findings are supported by pulldown experiments, where incorporating $E1A_{CR1}$ into the washes was sufficient to abrogate the ability of $MITF_{81-204}$ to pulldown TAZ2 (Figure 4.15B). This also reflects isothermal titration calorimetry data that shows $E1A_{CR1}$ can bind TAZ2 of p300 (K_d 0.21 ± 0.02 μM) with ~6-fold higher affinity than $MITF_{81-204}$ (Figure 4.16).

To assess whether MITF-dependent transcriptional activation could be suppressed by $E1A_{CR1}$, I performed luciferase-based one-hybrid assays in which pGAL4-$MITF_{81-204}$ was co-transfected with increasing amounts of pGFP-$E1A_{CR1}$ in HEK 293A cells. The addition of $E1A_{CR1}$ reduced luciferase activation by 5-fold, providing functional inhibition of MITF-dependent transcriptional activation (Figure 4.15C) and indicating peptides that bind tightly to the α1-α3 surface of TAZ2 can act as effective inhibitors of MITF function.

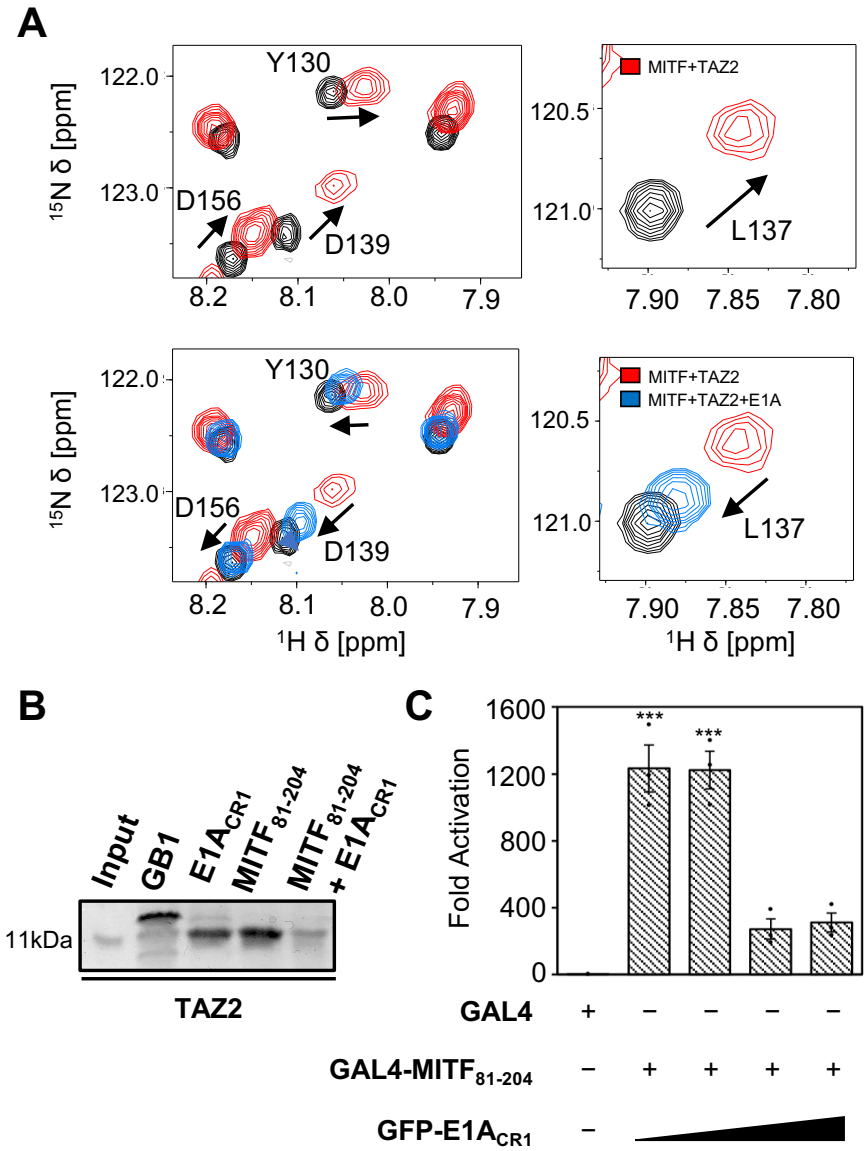

Figure 4.15. E1A$_{CR1}$ competes with MITF for TAZ2. (A) Overlay of ^{1}H-^{15}N HSQC spectra of 100 µM ^{15}N-labelled MITF$_{110-161}$ (black), 100 µM MITF$_{110-161}$ in the presence of 100 µM TAZ2 (red), and 100 µM MITF$_{110-161}$ in the presence of both 100 µM TAZ2 and 150 µM E1A$_{CR1}$ (blue). (B) TAZ2 pulldown by immobilized GB1, GB1-E1A$_{CR1}$ and GB1-MITF$_{81-204}$ as visualized using SDS-PAGE and stained with Coomassie blue. The input lane shows purified TAZ2 alone and represents 10% of total pulldown input. Pulldown of TAZ2 by MITF$_{81-204}$ when E1A$_{CR1}$ is included in wash steps is shown in the righthand lane. (C) Luciferase-based transactivation assay of HEK 293A cells co-transfected with 50 ng pGAL4-MITF$_{81-204}$ and up to 50 ng of pGFP-E1A$_{CR1}$. Statistical significance by one-way ANOVA and Dunnetts multiple comparison test (*** $p \leq 0.005$, n=3 technical replicates) is compared to activation from pGAL4, and variation is reported as SEM

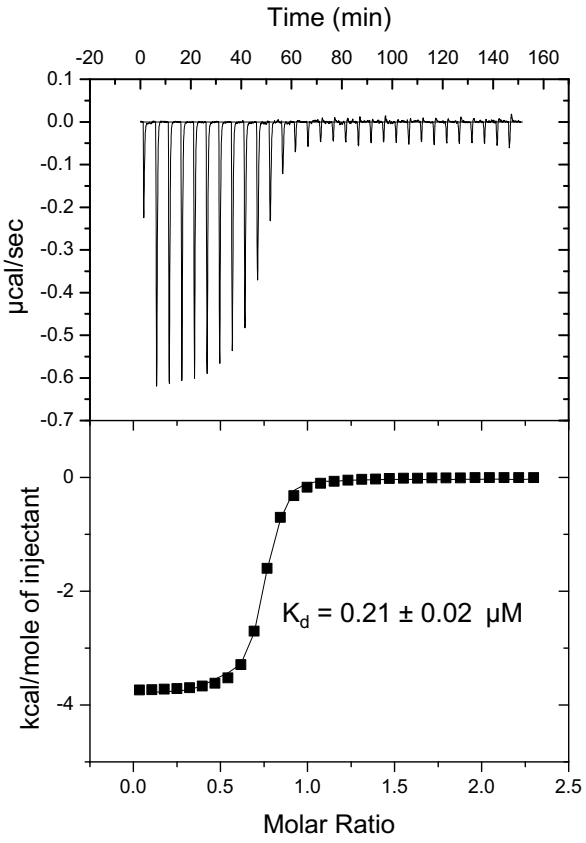

Figure 4.16. ITC of TAZ2 and E1A$_{CR1}$. Isothermal titration calorimetry thermogram of 500 µM TAZ2 titrated into 50 µM E1A$_{CR1}$, fit to a one-site binding model yielding K_d = 0.21 ± 0.02 µM (n=2 biological replicates, error reported as SD).

4.5.6 Plasticity of transcriptional co-activator recruitment by MITF

CBP/p300 is recruited to promoters where it may simultaneously bind different transcription factors at nearby binding sites. Long disordered regions linking the multiple domains of CBP/p300 provide conformational flexibility to interact with binding partners through several protein-interaction domains. The KIX, TAZ1, and TAZ2 domains particularly facilitate activation domain binding with a broad range of affinity and specificities. For example, the tumor suppressor p53 activation domain binds promiscuously to CBP/p300 with affinity for KIX, TAZ1 and TAZ2 (185). I have found that the MITF activation domain also recruits CBP/p300 by binding to multiple domains, with a moderate binding affinity for both TAZ1 (K_d 6.7 ± 0.5 μM) and TAZ2 (K_d 1.24 ± 0.23 μM) (Figure 4.17). Multivalent binding of CBP/p300 domains to MITF may be biologically relevant in facilitating cooperative interactions between MITF homodimers and/or and other transcriptional regulators that interact with TAZ1 or TAZ2. This promiscuous transcription factor binding by CBP/p300 provides a rationale for how the functional outcome of MITF overexpression/suppression depends in part on the cellular context and which transcription factors other than MITF are present (3).

The disordered nature of activation domains within transcriptional complexes allows for recognition of a variety of different sequences, where a small number of residues can mediate interactions with a high specificity. This study identifies a small acidic motif (DDVIDDII) that overlaps with the ΦXXΦΦ motif within the MITF activation domain that facilitates TAZ2 binding and MITF transcription. Given the proximity of serine residues to this motif, and that phosphorylation occurs within the

activation domain promoting CBP/p300 interactions (221), it is possible that post-translational modifications could further modulate MITF affinity for TAZ2 (through the addition of more negative charge), thereby modulating MITF activity. Binding to TAZ2 also brings MITF near the catalytic HAT domain, which may provide an additional method of regulation through post-translational mechanisms of acetylation, where CBP/p300 may directly regulate the affinity of MITF for DNA (222).

In summary, I have determined that the MITF transactivation domain binds both TAZ1 of CBP and TAZ2 of p300 and interacts with TAZ2 via a hydrophobic surface that coincides with the adenoviral E1A binding site. The $MITF_{TAD}$:TAZ2 complex maintains some conformational flexibility and is modulated primarily by an acidic motif and hydrophobic contacts, which can be disrupted by peptides that bind TAZ2 with high affinity. This work provides a detailed characterization of how MITF binds to CBP/p300 and outlines how peptides that target TAZ2 can inhibit MITF function.

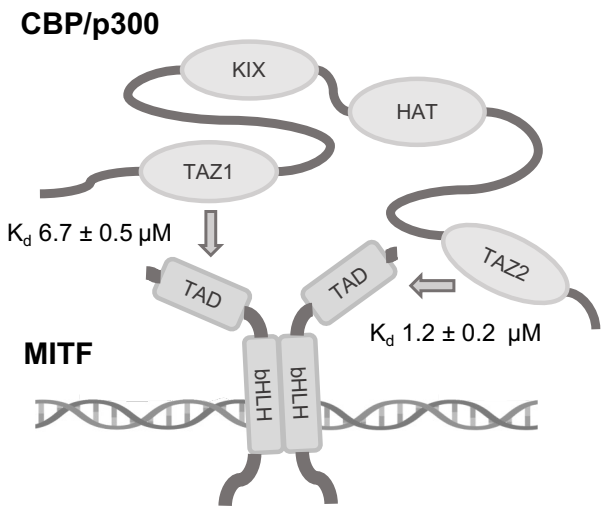

Figure 4.17. Schematic showing plasticity in CBP/p300 recognition by MITF. MITF can homo- or hetero-dimerize with other MiT/TFE proteins at gene promoters. The transactivation domains may then interact with both TAZ1 and TAZ2 domains to enhance recruitment of CBP/p300 to gene promotors. Binding affinities (K_d) determined in this study are annotated.

Chapter 5: The C-terminal transactivation domain of MITF interacts promiscuously with co-activator CBP/p300

5.1 Contributions of Authors

This chapter is composed of the abstract, introduction, materials and methods, results and discussion sections of a manuscript intended for submission to Scientific Reports: Brown, A. D., Lynch, K., Dupré, D. J., & Langelaan, D. N. The C-terminal transactivation domain of MITF interacts promiscuously with co-activator CBP/p300. The NMR data in Figures 5.2A and 5.4A were acquired by former honours student Kyle Lynch. All other experiments were performed and analyzed by me, as well as the first written draft of the manuscript. Dr. Denis Dupré and Dr. David Langelaan provided support in the forms of materials, guidance, and editing of this work.

5.2 Abstract

The microphthalmia-associated transcription factor (MITF) is one of four closely related members of the MiT/TFE family (TFEB, TFE3, TFEC) that regulate a wide range cellular processes. MITF is a key regulator of melanocyte-associated genes, and essential to proper development of the melanocyte cell lineage. Abnormal MITF activity can contribute to the onset of several diseases including melanoma, where MITF is an amplified oncogene. To enhance transcription, MITF recruits the co-activator CREB-binding protein (CBP) and its homolog p300 to gene promoters, however the molecular determinants of their interaction are not yet fully understood.

Here, I characterize the interactions between the C-terminal transactivation domain (TAD2) of MITF and CBP/p300. Using NMR spectroscopy, protein pulldown assays, and isothermal titration calorimetry I determine C-terminal MITF is intrinsically disordered and binds with moderate-affinity to both TAZ1 and TAZ2 of CBP/p300. Mutagenesis studies revealed two conserved motifs within MITF TAD2 that are necessary for TAZ2 binding and critical for MITF-dependent transcription of a reporter gene. Finally, I observe MITF TAD2 works together with TAD1 to activate transcription. Taken together, our study helps elucidate the molecular details of how MITF interacts with CBP/p300 through multiple redundant interactions that lend insight into MITF function in melanocytes and melanoma.

5.3 Introduction

The microphthalmia transcription factor family (MiT/TFE) is comprised of four closely related DNA-binding proteins: transcription factor EB (TFEB), transcription factor E3 (TFE3), transcription factor EC (TFEC), and the microphthalmia-associated transcription factor (MITF) (223, 224). These transcription factors are highly evolutionarily conserved and homo/heterodimerize through a shared basic helix-loop-helix leucine zipper (bHLH) domain that recognizes and binds to E-box (CANNTG) and M-box (TCATGTG) binding sites in promoter regions of target genes (225). The structural similarities between MiT transcription factors allows them to control numerous cellular processes including organelle biogenesis, energy homeostasis, and cell fate determination (103, 226).

Despite their similarities, the expression patterns of MiT/TFE family members differ significantly, while TFEB and TFE3 are ubiquitously expressed in most cell types, TFEC is restricted to myeloid cells, and MITF is predominantly found in melanocytes where it is widely regarded as the master regulator of the melanocytic cell-lineage (192, 227).

Mutation to the *MITF* gene results in the failure of melanocytes to form, and is found in conditions including Waardenburg Type 2 and Tietz syndrome, which cause varying degrees of hearing loss and pigmentation deficiencies (189, 228). In melanocytes, MITF plays a critical role in regulating melanogenesis by directly controlling the expression of pigmentation enzymes including tyrosinase which in turn initiates melanin production (229). Aside from this function, MITF also regulates the expression of almost one hundred genes involved in melanocyte growth, migration, and cell survival (188, 230). For these reasons, MITF activity is also utilized by malignant cells and MITF has been identified as a lineage-specific oncogene for melanoma (81).

The ability of MITF to activate gene expression is in part attributed to its interactions with co-regulating proteins within transcriptional complexes. This includes the histone acetyltransferases CREB-binding protein and its homolog p300 (CBP/p300), which potentiate MITF transactivation by remodeling chromatin structure and making DNA more accessible to transcriptional machinery (107, 143). MITF recruits CBP/p300 through interactions facilitated by its N-terminal transactivation domain (TAD1) (179). While many studies have focused on the importance of MITF TAD1, evidence has suggested that the C-terminal region of

MITF also contains a transcriptionally competent domain, which when removed significantly impacts MITF-regulated transcription (Figure 5.1) (231). Despite the potential importance of the MITF C-terminal TAD2 for gene transcription, the molecular details defining this domain or how it might interact with CBP/p300 remain unknown.

In this study, I utilize a combination of nuclear magnetic spectroscopy (NMR), isothermal titration calorimetry (ITC), and protein pulldown assays to determine the structural features of the C-terminal MITF TAD2 and define its interactions CBP/p300. I determine that the disordered MITF C-terminal interacts promiscuously with both transcriptional adaptor zinc finger domains (TAZ1 and TAZ2) of CBP/p300. Furthermore, I identify acidic and serine-rich motifs within the MITF TAD2 that are essential to maintain its interaction with TAZ2, and when removed significantly reduce the ability of MITF to activate reporter gene transcription. Finally, I remark that the MITF TAD2 appears to work in cooperation with the MITF TAD1 to activate gene transcription.

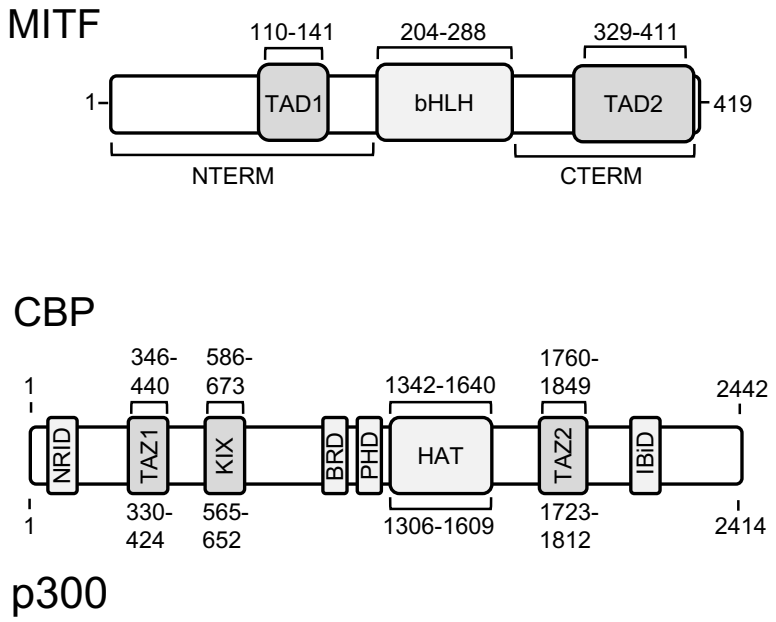

Figure 5.1. Schematic of MITF and CBP/p300 domains. MITF contains a basic helix-loop-helix DNA-binding domain (bHLH), N-terminal (NTERM) and C-terminal (CTERM) regions, and transactivation domains (TAD1 and TAD2). CBP/p300 has a catalytic histone acetyltransferase domain (HAT) and several protein-binding domains: nuclear receptor interaction domain (NRID), kinase inducible domain (KIX), IRF-3 binding domain (IBiD), and transcription adapter zinc finger domains (TAZ1 and TAZ2), domain boundaries are numbered according to native amino acid sequence.

5.4 Materials and Methods

5.4.1 Plasmid Constructs

The cDNA of MITF isoform M (Genbank: Accession no. BC065243.1) was purchased from ThermoFisher Inc. and a region encoding for C-terminal MITF (residues 289-419, CTERM) was cloned into restriction sites *BglII/SalI* of a pET21b derived vector modified to include a hexahistidine tag, the B1 domain of *Streptococcal* protein G (GB1), and a tobacco-etch virus recognition site, to derive pGB1-$MITF_{CTERM}$. MITF variants ($MITF_{\Delta Thr\text{-}rich}$ (Δ334-354), $MITF_{\Delta Acidic}$ (Δ372-381), $MITF_{\Delta Ser\text{-}rich}$ (Δ394-411)) were produced by site-directed mutagenesis of pGB1-$MITF_{CTERM}$ using *in vivo* assembly cloning where deletions were incorporated into primers(232). Expression constructs for the domains of CBP/p300 (TAZ1, TAZ2, and KIX) were as previously described(58). For transcriptional assays, a pGL3 luciferase reporter plasmid was purchased from BioBasic Inc. and modified to include 7 E-box (CACGTG) binding sites upstream a luciferase reporter gene (p7xE-box). Constructs for mammalian expression of full-length MITF were provided by Yardena Samuels (Addgene plasmid #31151; pCMV-MITF-WT), and mutant constructs were produced from full-length pCMV-MITF-WT using Q5 site-directed mutagenesis (New England Biolabs). The validity of all constructs was confirmed using DNA sequencing.

5.4.2 Protein Expression and Purification

MITF constructs (GB1-$MITF_{CTERM}$, GB1-$MITF_{\Delta Thr\text{-}rich}$, GB1-$MITF_{\Delta Acidic}$, GB1-$MITF_{\Delta Ser\text{-}rich}$) were expressed in *Escherichia coli* BL21 (DE3). Cells were grown in Lysogeny Broth under ampicillin selection until a mid-log phase and optical

density of 0.6-0.8 was reached and then expression was induced with the addition of 0.5 mM isopropyl-β-d-thiogalactopyranoside at 37°C for 4 hrs. Isotopically labelled samples were produced by cells grown in ^{15}N- or ^{13}C,^{15}N enriched M9 minimal media(149). Cells (1 L) were harvested by centrifugation and resuspended in 30 mL lysis buffer (20 mM Tris-HCl pH 8, 250 mM NaCl, 8 M urea), sonicated for 3 min, centrifuged in SS-34 rotor (Sorvall) at 14500 rpm to clarify lysate which was then applied to a Ni-NTA affinity column (Cytiva) and washed with lysis buffer containing 10 mM imidazole. Proteins were refolded on column with the addition of native buffer (20 mM Tris-HCL pH 8, 250 mM NaCl, 5 mM βME) and eluted with native buffer containing 300 mM imidazole. Refolded protein was then dialyzed overnight at 4°C into dialysis buffer (20 mM Tris-HCl pH 8, 50 mM NaCl, 5 mM βME) in the presence of TEV protease (150 µg). The GB1 affinity tag was removed using another round of Ni-NTA chromatography, and the flowthrough containing cleaved MITF constructs was further purified using Q-Sepharose anion exchange column (Cytiva) equilibrated with IEC buffer (20 mM Tris-HCl pH 8, 5 mM βME). The column was washed with IEC buffer containing 50 mM NaCl, and the final protein was eluted using IEC buffer containing 500 mM NaCl. Protein fractions were analyzed by SDS-PAGE and quantified using UV-Vis spectroscopy.

5.4.3 NMR Spectroscopy

A ^{13}C,^{15}N-labelled sample of $MITF_{CTERM}$ (700 µM) was prepared in NMR buffer (20 mM MES pH 6, 25 mM NaCl, 5 mM DTT, 5% D_2O). Backbone resonances were then assigned using ^{1}H-^{15}N HSQC, HNCO, HN(CA)CO, CBCACONH, and HNCACB spectra, and following resonance assignment secondary

structure propensity (SSP) was calculated based on Cα and Cβ chemical shifts (157). All NMR experiments were collected at 35°C on a Bruker Avance III 700 MHz spectrometer at the National Research Council (Halifax, NS). Data was processed using NMRPipe and assigned using CcpNmr Analysis (150, 151).

Chemical shift assignments for $MITF_{CTERM}$ have been deposited at the Biological Magnetic Resonance Data Bank under accession no. 51763. To assess binding between $MITF_{CTERM}$ and TAZ2, a sample of ^{15}N-labelled $MITF_{CTERM}$ (100 μM) was prepared in NMR buffer and ^{1}H-^{15}N HSQC spectra were collected in the absence or presence of increasing amounts of unlabelled TAZ2 (up to 300 μM). Chemical shift perturbations (Δδ) of MITF resonances were then measured upon addition of TAZ2 ($\Delta\delta = [(0.17\Delta\delta_N)^2 + (\Delta\delta_{HN})^2]^{1/2}$) (153).

5.4.4 Pulldown Assays

Indicated GB1-tagged fusion proteins or GB1 as a control (20 nmoles), were incubated with 20 μL IgG agarose beads (Cytiva) in binding buffer (20 mM Tris-HCl pH 8, 50 mM NaCl, 5 mM βME, 10 μM $ZnCl_2$) and rotated end-over-end at room temperature for 15 min. Beads were then collected by microcentrifugation (1 min at 2000 rpm), washed two times with binding buffer, before an equimolar amount of TAZ1 or TAZ2 was added and rotated for 30 min. The protein complexes bound to the beads were washed three more times with binding buffer, and the total protein present was then analyzed by SDS-PAGE.

5.4.5 Isothermal Titration Calorimetry

All ITC experiments were performed in buffer containing 20 mM TRIS pH 8, 25 mM NaCl, 5 mM βME, 10 μM $ZnCl_2$. A total concentration of 400 μM TAZ1 or TAZ2 was loaded into the ITC syringe and incrementally injected into the sample cell containing 16-30 μM of purified MITF construct. Experiments were carried out using a VP-ITC Microcalorimeter with the following parameters: 30 injections of 10 μL with 300 sec equilibration intervals, reference power 20 μCal/sec, and stirring speed of 300 at 30°C. Thermograms were fit assuming a single-binding site using MicroCal Origin 7.0 software and each experiment was performed in duplicate.

5.4.6 Transcriptional Assays

For all luciferase-based transcriptional assays, HEK 293A cells were cultured in DMEM supplemented with 10% FBS and incubated at 37°C with 5% CO_2. Cells were seeded 24-hours prior to transfection into 24-well plates and transfected with jetPRIME reagent. To each well, 0.5 μg of plasmid was added including: 0.35 μg p7xE-box reporter, 0.05 μg pCMV-Renilla, and 0.1 μg of pCMV-MITF expression plasmid. Cells were harvested 24 hrs after transfection at which point luminescence was measured from cell lysate using a Dual-Luciferase Reporter Assay System (Promega). Each experiment is a representation of *Renilla*-normalized luminescence from triplicate experiments and shown as fold activation relative to pcDNA3.1 negative control. Statistical significance was measured using one-way AVONA and Dunnett's multiple comparison test compared to pCMV-MITF-WT.

5.5 Results and Discussion

5.5.1. The MITF C-terminal is intrinsically disordered

To analyze the structural features of the MITF C-terminal region, NMR experiments were collected on a $^{13}C,^{15}N$-labelled sample of $MITF_{CTERM}$. The resulting ^{1}H-^{15}N HSQC spectrum was of high-quality with strong signal-to-noise intensities and the expected number of cross-peaks based on the number of non-proline MITF residues and (Figure 5.2A). Utilizing standard triple resonance experiments, I achieved unambiguous assignment of 91% of backbone amide ^{1}H and ^{15}N resonances for $MITF_{CTERM}$ (119/131 residues). This nearly complete assignment provided an excellent basis for both this study and future investigations of protein-protein interactions involving the MITF C-terminal.

The proton chemical shifts of the ^{1}H-^{15}N HSQC spectrum of $MITF_{CTERM}$ fell within a narrow range of 0.6 ppm, a hallmark feature of intrinsically disordered proteins, where both sequence biases and conformational plasticity contribute to this limited chemical shift dispersion (233, 234). I also calculated residue-specific secondary-structure propensity scores (SSP) based on the assigned backbone Cα and C_β chemical shifts, where a score of +1 indicates the formation of a fully-formed α-helix, -1 a β-sheet, and values in between roughly corresponding to the fraction or propensity to adopt secondary structure at that position (157). Along the entire sequence of $MITF_{CTERM}$ residues had SSP scores ranging from -0.2 to +0.25, I calculated an overall total of 11.6% proclivity for forming α-structure and 5.3% β-structure (Figure 5.2B). This suggests that this region of MITF has significant

random-coil propensity, with minor tendency to form secondary structure, consistent with the narrow peak dispersion observed in the ^{1}H-^{15}N HSQC spectrum.

Intrinsically disordered proteins are abundant in the eukaryotic proteome, and particularly important to processes like signaling and regulation (6, 235). Disordered regions are prevalent amongst transactivation domains including those of the well-characterized p53 and c-Myc transcription factors (236, 237). Their conformational flexibility helps to facilitate binding of these transactivation domains to a variety of structurally diverse co-regulators within transcriptional complexes. These regions can undergo a disorder-to-order transition to fine-time their affinity for a particular binding partner, but many retain some structural ambiguity in their molecular recognition, termed ‘fuzzy’ complexes which can mediate highly specific but transient interactions (187, 238).

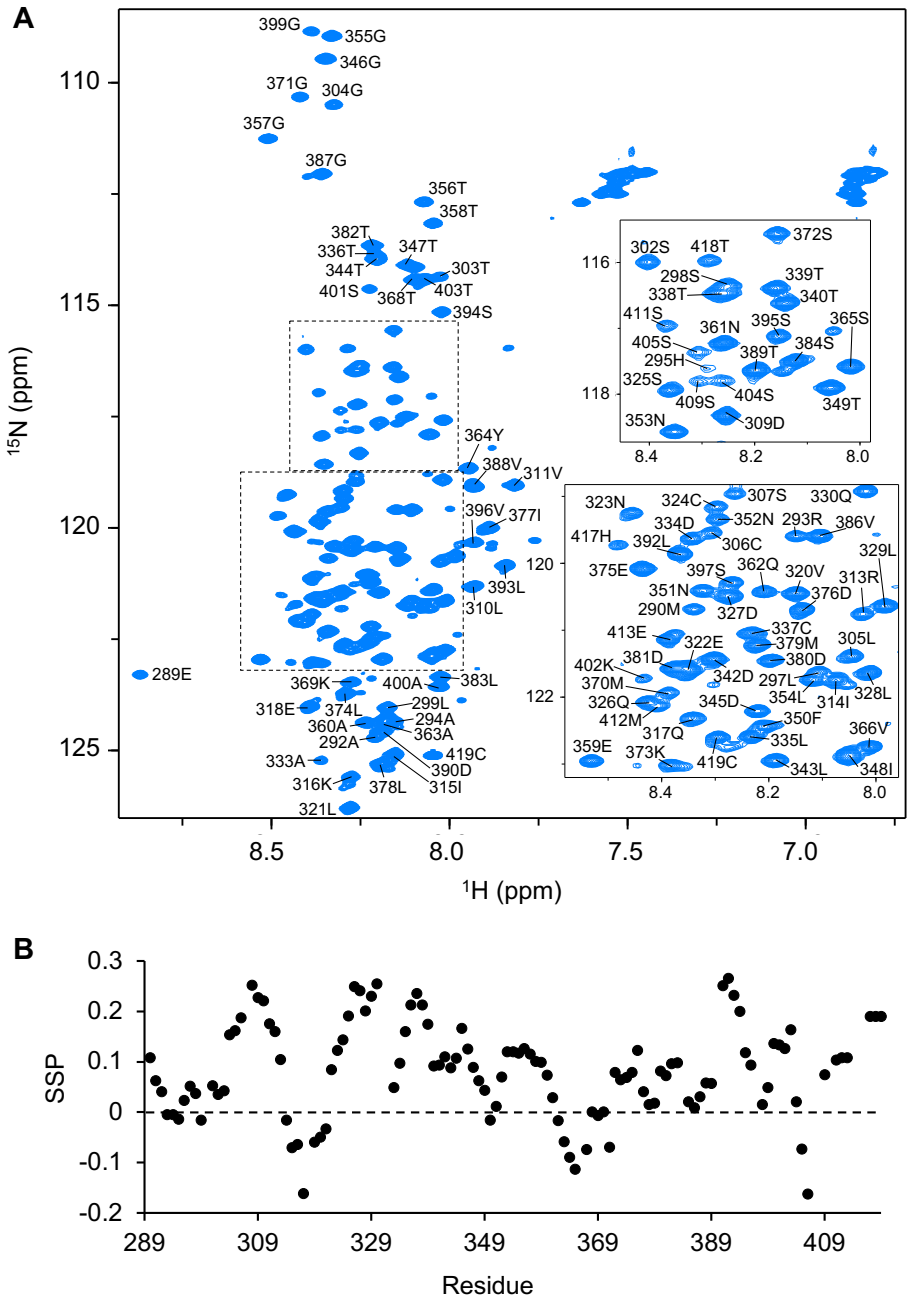

Figure 5.2. Structural Analysis of MITF$_{CTERM}$. (A) ^{1}H-^{15}N-HSQC of ^{13}C,^{15}N-labelled MITF$_{CTERM}$, backbone amide resonance peaks are labelled based on their assigned residue. (B) Secondary structure propensity (SSP) values per residue of MITF$_{CTERM}$ calculated from Cα and Cβ chemical shifts.

5.5.2 The C-terminal of MITF binds both TAZ domains of CBP/p300

CBP/p300 are large multi-domain proteins that play an important role connecting numerous independent cell-signaling pathways through interactions with hundreds of regulators from all major transcription factor families (34, 239). Within transcriptional complexes, CBP/p300 provide a scaffold to coordinate various sequence-specific transcription factors through interactions with their multiple conserved protein-binding domains. These include the kinase inducible domain (KIX) and transcriptional adaptor zinc finger domains (TAZ1 and TAZ2) (Figure 5.1B), which facilitate binding of CBP/p300 to transcription factors including p53, E2A, and STAT1/2 (31, 40, 58, 210). To test if any of these domains interact with the MITF C-terminal, I performed a protein pulldown assay where GB1-$MITF_{CTERM}$ was immobilized and incubated with purified KIX, TAZ1, or TAZ2. SDS-PAGE analysis of total protein following these experiments indicated that GB1-$MITF_{CTERM}$ did not interact with the KIX domain of CBP/p300 but did interact with both the TAZ1 and TAZ2 domains (Figure 5.3A).

To quantitatively assess these interactions, I next performed isothermal titration calorimetry, where isolated TAZ1 or TAZ2 was injected into a reaction cell containing purified $MITF_{CTERM}$. The resulting thermograms indicated that $MITF_{CTERM}$ interacts with TAZ1 with a binding affinity (K_d) of 5.0 ± 0.31 μM, and with TAZ2 with a ~6x higher affinity (K_d = 0.76 ± 0.05 μM) (Figure 5.3B, C). These findings correlate with our protein pulldown data which suggested that MITF binds promiscuously to both domains. They are also comparable to the MITF N-terminal TAD1 which binds TAZ1 with a K_d ~6.7 μM and TAZ2 with a K_d ~1.2 μM, and to

the p53 transactivation domain which similarly binds TAZ1 with a K_d ~ 0.9 μM and TAZ2 with a K_d ~ 26 nM (160, 179). Given that the availability of transcriptional co-regulators can directly influence MITF activity, and that CBP/p300 is a hub for a multitude of transcription factor interactions across many different signaling cascades, the ability of MITF to bind multiple CBP/p300 domains may help with its potential to re-direct the co-activator from other signaling pathways to enhance its own function.

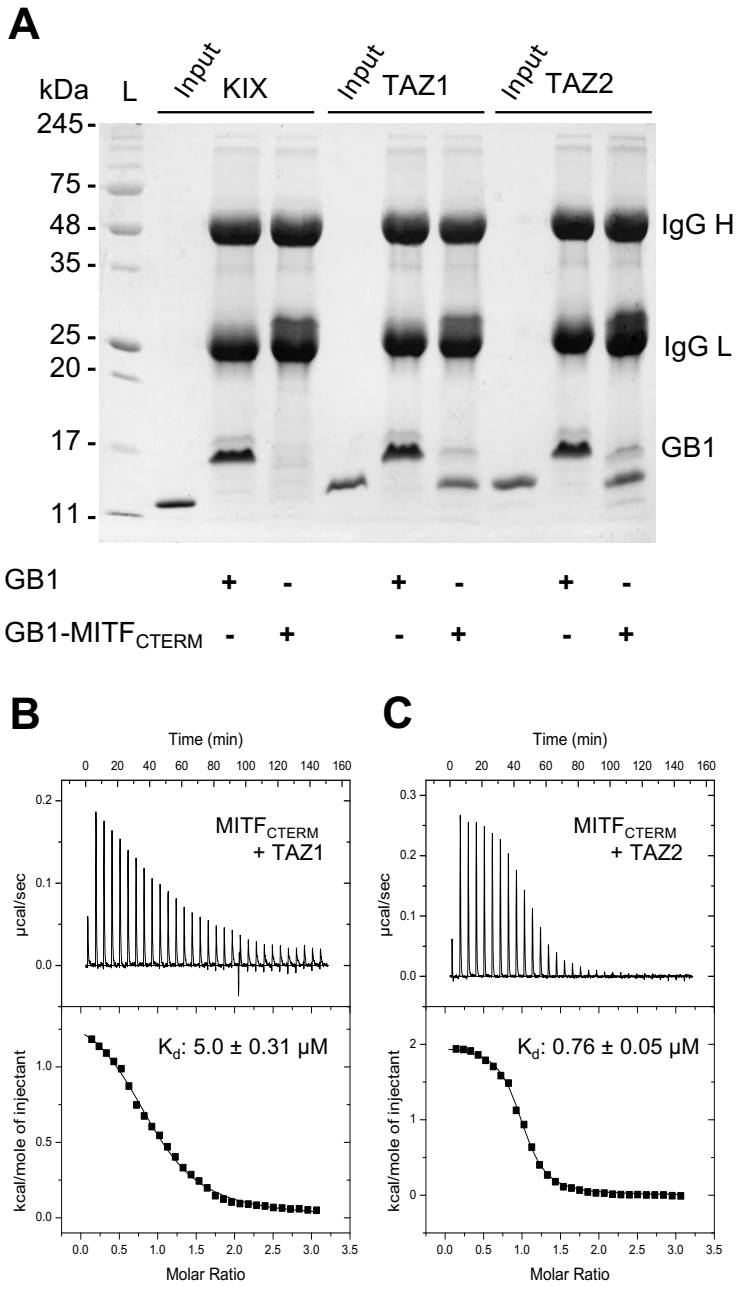

Figure 5.3. MITF$_{CTERM}$ binds TAZ1 and TAZ2 of CBP/p300 (A) SDS-PAGE analysis of the total amount of KIX, TAZ1, or TAZ2 pulled down by immobilized GB1 or GB1-MITF$_{CTERM.}$ Lanes 2, 5, and 8 show migration of each isolated CBP/p300 domain and represents 10% of total pulldown input, the immunoglobulin heavy and light chains (IgG H and IgG L) are also denoted. (B) ITC thermogram following titration of TAZ1 (400 µM) or (C) TAZ2 (400 µM) into MITF$_{CTERM}$ (30 µM). Data were fit to one-site binding curves, determining dissociation constants (K_d) of 5.0 ± 0.31 µM and 0.76 ± 0.05 µM for the interaction of MITF$_{CTERM}$ with TAZ1 and TAZ2, respectively) (n=2 biological replicates, error reported as SD).

5.5.3 Identification of functionally important $MITF_{TAD2}$ residues

I decided to further characterize how TAZ2 binds $MITF_{CTERM}$, given its higher affinity to $MITFC_{TERM}$ than TAZ1. To determine which residues of the MITF C-terminal were involved in binding TAZ2, a ^{15}N-labelled $MITF_{CTERM}$ sample was prepared, and sequential ^{1}H-^{15}N-HSQC spectra were collected upon titration with unlabelled TAZ2 (Figure 5.4A). Once saturated with TAZ2, chemical shift changes ($\Delta\delta$) experienced by $MITF_{CTERM}$ backbone resonance peaks were then calculated (Figure 5.4B). From these calculations it was determined that most $MITF_{CTERM}$ residues experienced only minor changes in chemical shift (<0.15 ppm). While there appears to be a larger number of chemical shift perturbations located between the regions L329-I348 and K369-T389, other resonances throughout the protein sequence disappeared entirely. This disappearance of resonance peaks can be caused by intermediate chemical exchange leading to line broadening and signifies that these residues could be involved in the intermolecular interaction with TAZ2 (240, 241).

The transactivation domain architecture of MiT/TFE transcription factors include either acidic or serine/threonine/proline-rich regions which can work synergistically with one another (242). For example, TFE3 the closest relative to MITF, contains two activation domains, a C-terminal proline-rich TAD2 that both contributes to transactivation and potentiates the function of its N-terminal acidic TAD1 (243, 244). Given the homology between MITF and TFE3 (58% sequence identity), it is reasonable to believe the MITF C-terminal TAD2 may function in a similar synergistic fashion to enhance the activity of the MITF N-terminal TAD1. Taking into consideration sequence homology and our NMR perturbation studies,

three mutants of $MITF_{CTERM}$ were generated to remove a threonine-rich region from residues D334-D345, an acidic region from residues S372-D381, and a serine-rich region from residues S394-S411 (Figures 5.4B). To determine if any of these regions are important for transactivation, a luciferase-based transcriptional assay was performed where HEK 293A cells were transfected with wildtype or deletion mutants of MITF and a reporter containing 7 E-box binding sites upstream a luciferase gene. Normalized luminescence values were determined, and MITF was seen to activate transcription 40-fold higher than negative controls. Comparatively, deletion of the threonine-rich region (Δ334-345) reduced the transcriptional ability of MITF by half while deletion of the acidic (Δ372-381) or serine-rich (Δ394-411) regions diminished activation eight-times less than wild-type (Figure 5.5A). These findings coincide with previous studies which have shown that removal of the entire MITF TAD2 (residues 324-419) notably decreases MITFs ability to activate transcription of the tyrosinase gene, but a region containing only the threonine-rich motif (residues 324-369) still retains modest activation potential when fused to a GAL4 DNA-binding domain (108).

To identify if the MITF C-terminal transactivation domain functions independently, redundantly, or cooperatively with the MITF N-terminal TAD1, two ΔTAD1 mutants (removing residues 110-141) were generated from MITF and $MITF_{\Delta Thr\text{-}rich}$ upon which any transcriptional activity occurred by either construct was ablated (Figure 5.5A). Given that the removal of either transactivation domain disrupts MITF-dependent transcription, this suggests a cooperative mechanism

similar to TFE3 where both domains are required for MITF to be fully functional (243).

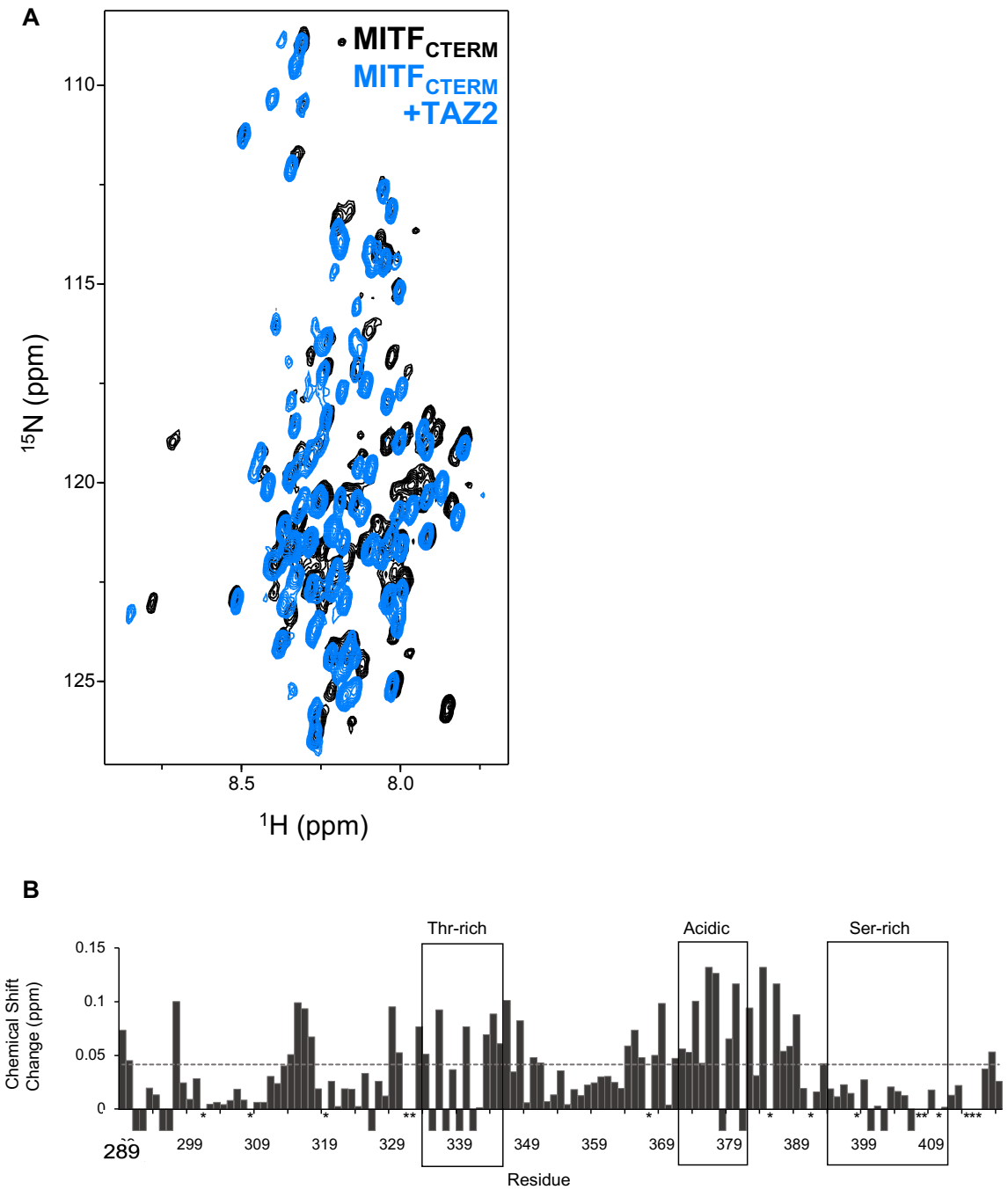

Figure 5.4. NMR Analysis of $MITF_{CTERM}$: TAZ2 Interaction. (A) ^{1}H-^{15}N HSQC of 100 µM ^{15}N-labelled$MITF_{CTERM}$ in the absence (black) and presence (blue) of 300 µM unlabeled TAZ1. (B) Chemical shift perturbations ($\Delta\delta = [(0.17\Delta\delta_N)^2 + (\Delta\delta_{HN})^2]^{1/2}$) of backbone resonances per residue of ^{15}N-labelled $MITF_{CTERM}$ (100 µM) upon the addition of TAZ2 (300 µM). Negative values indicate disappearance of a resonance peak, and * denotes a proline or unassigned resonance. Average chemical shift change (0.04 ppm) is shown as dashed line, boxes denote regions chosen for mutation.

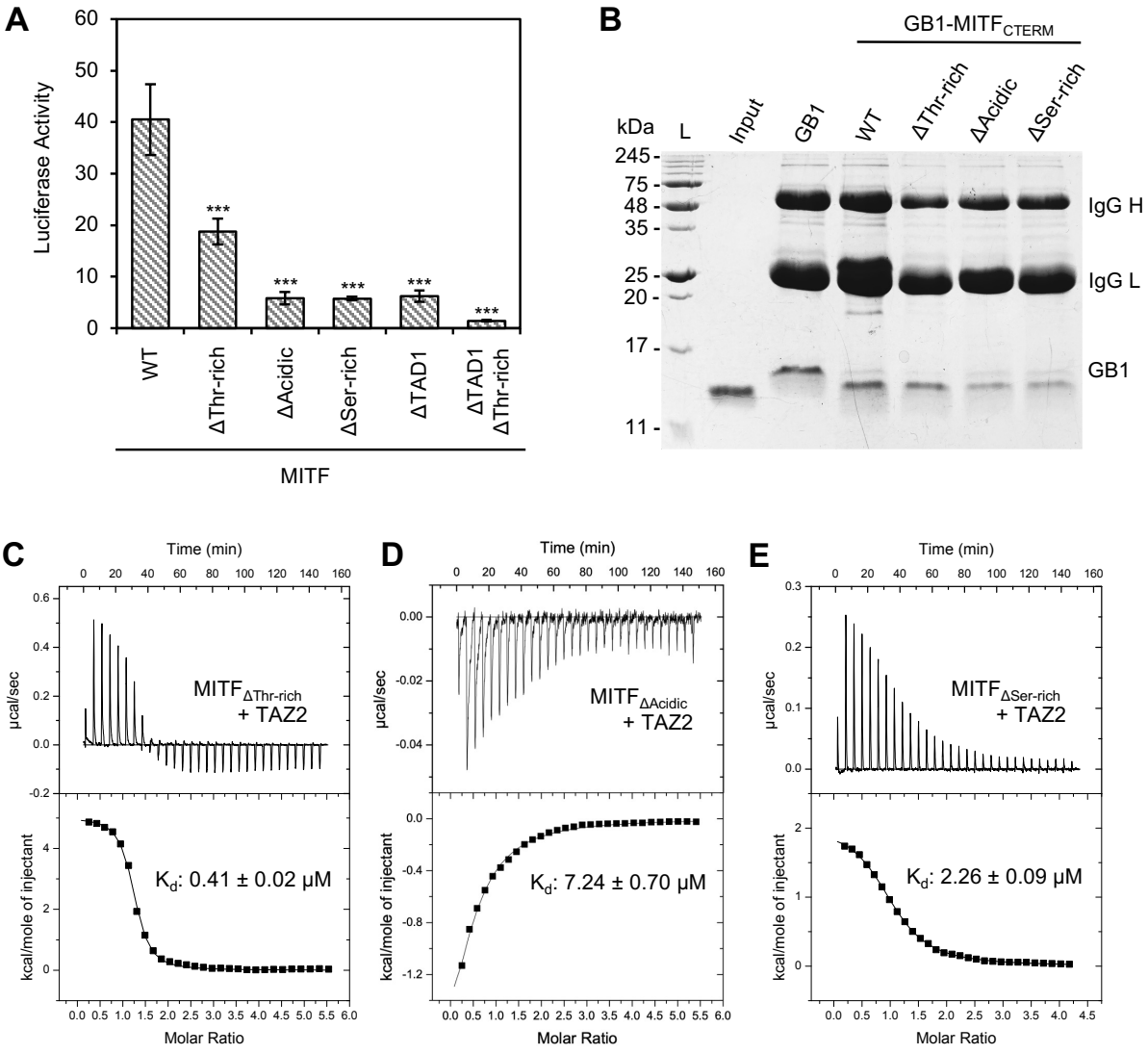

Figure 5.5. MITF mutagenesis studies. (A) Average luciferase activation of MITF constructs, reported as fold activation of pcDNA3.1 negative control. Error bars represent standard error, statistical analysis performed using one-way ANOVA followed by Dunnett's multiple comparison test (*** $p \leq 0.001$, n=3 technical replicates). (B) SDS-PAGE analysis of total TAZ2 pulled down by immobilized GB1-MITF$_{CTERM}$ or GB1-tagged MITF mutant constructs MITF$_{\Delta Thr\text{-}rich}$ (Δ334-345), MITF$_{\Delta Acidic}$ (Δ372-381), and MITF$_{\Delta Ser\text{-}rich}$ (Δ394-411). Lane 2 shows migration of isolated TAZ2 domain and represents 10% total pulldown input, immunoglobulin heavy and light chains (IgG H and IgG L) are also labelled. (C-E) ITC thermograms of MITF$_{\Delta Thr\text{-}rich}$ (16 μM), MITF$_{\Delta Acidic}$ (17 μM), and MITF$_{\Delta Ser\text{-}rich}$ (22 μM), following titration with TAZ2 (400 μM) each fit to a one-site binding curve (K_d = 0.41 ± 0.02 μM, 7.24 ± 0.70 μM, and 2.26 ± 0.09 μM, respectively) (n=2 biological replicates, error reported as SD).

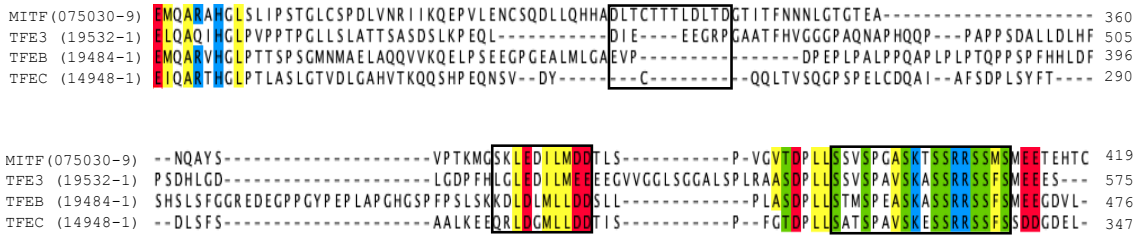

Figure 5.6. Sequence Alignment of MiT/TFE Family. Multiple protein sequence alignment of MITF Isoform M and other MiT family members (TFE3, TFEB, TFEC) showing conservation of the C-terminal region. Residues with amino acid similarity (≥75%) are indicated by coloured shading, hydrophobic (yellow), positive (blue), negative (red), or polar uncharged (green). Boxes denote mutants used in this study labels correspond to positions in native amino acid sequences.

5.5.4 MITF $_{TAD2}$ function correlates to TAZ2 binding

To test which regions of the $MITF_{CTERM}$ are involved in mediating the interaction with TAZ2 of CBP/p300, I performed a protein pulldown assay where GB1-tagged $MITF_{CTERM}$ or deletion mutants were tested for their ability to interact with purified TAZ2 (Figure 5.5B). While all mutants showed some ability to interact with TAZ2, mutants which removed either the acidic (Δ372-381), or serine-rich (Δ394-411) regions greatly reduced the amount of TAZ2 that was bound in comparison to the wild-type domain. Consistent with these results, ITC studies revealed that deletion of the threonine-rich region (Δ334-345) did not have any significant impact on the affinity of the $MITF_{CTERM}$ for TAZ2 (K_d 0.41 ± 0.02 μM; Figure 5.5C), whereas deletion of the acidic region, or serine-rich region impacted TAZ2 binding by 10-fold and 3-fold, respectively (K_d = 7.24 ± 0.70 μM and 2.26 ± 0.09 μM; Figure 5.5D, E). Interestingly, the shape of the ITC curves upon deletion of the threonine-rich region or serine-rich region were characteristic of an endothermic interaction, whereas in contrast deletion of the acidic region was typical of an exothermic interaction. These differences may be attributed to the disruption or formation of favourable non-covalent bonds between the $MITF_{CTERM}$ and TAZ2 or between protein and solvent during the titration.

Interestingly, removal of the threonine-rich region, which had the smallest impact on MITF transcription activity and TAZ2 binding, is the least conserved amongst all MiT family members (Figure 5.6). On the other hand, the acidic region shares considerable homology with conserved aspartic acid and glutamic acid residues at positions E375, D380, and D381. Removal of this region from

$MITF_{CTERM}$ caused the greatest disruption TAZ2 binding, likely due to the loss of these negatively charged residues which would mediate interactions with the highly electropositive surface of TAZ2. The serine-rich region contains eight evolutionarily conserved serine residues present in all other MiT family members including S397, S401, S405, which are known phosphorylation targets of glycogen synthase kinase 3, and S409 a previously identified target of AKT and RSK mediated phosphorylation (118, 221, 245). Evidence for such post-translational modifications may influence the charge of this motif and directly impact the electrostatic interactions between MITF and CBP/p300, though further studies will need to be conducted to test the role of post-translational modifications on MITF: CBP/p300 interactions.

I have determined that the $MITF_{CTERM}$ is intrinsically disordered and interacts with both the TAZ1 and TAZ2 domains of CBP/p300. I have identified an acidic and a serine-rich motif of MITF TAD2 that are essential to both MITF transcriptional function and TAZ2-recruitment of CBP/p300. Finally, I observe that the MITF TAD1 and TAD2 cooperate to activate gene transcription. These finding advance overall understanding of MITF-mediated transcription and are fundamental to our knowledge of co-activator recruitment in gene regulation.

Chapter 6: Conclusion

6.1 Models of CBP/p300 Recruitment by MITF and β-catenin

The results I have presented in this work indicate that CBP/p300 engages in promiscuous binding interactions with the activation domains of MITF and β-catenin via its TAZ1 and TAZ2 domains. The interactions I have observed between these transcription regulators are variable and dynamic, and the possibility for numerous points of contact with CBP/p300 has implications for how these proteins may operate *in vivo*. My findings, taken into context with previous investigations (70), allow me to propose three potential scenarios of CBP/p300 recruitment by MITF and β-catenin that may occur at gene promoters.

Considering that MITF binds DNA as a dimer, this raises the possibility that multiple interactions may be occurring between the MITF activation domains and CBP/p300 at the same time (Figure 6.1A). Similar mechanisms have been proposed for transcription factor p53, which interacts with all four CBP/p300 domains (TAZ1, TAZ2, KIX, and IBiD) via its activation domain, and binds DNA as a tetramer (185). The affinity of the p53 tetramer for CBP/p300 is synergistically enhanced by cooperative binding of each monomer to an individual CBP/p300 domain (185). Like MITF, p53 displays variable affinities for each domain, with the predominant interaction occurring via TAZ2 and the others playing a more supportive role. As a result, additional co-regulators are then able to outcompete these lower-affinity contacts to assemble larger multi-protein transcriptional complexes.

Indeed, I have found the MITF transcriptional co-regulator β-catenin binds to the same TAZ1 and TAZ2 domains of CBP/p300 with even tighter binding affinities (Figure 6.1B). Where low levels of CBP/p300 are competed for in the cell, MITF binding to β-catenin could promote a more stable ternary complex and/or facilitate the recruitment of even more CBP/p300 molecules via multi-site interactions. This is substantiated by my findings that the C-terminal β-catenin activation domain has two TAZ2 binding sites and can interact with multiple molecules of CBP/p300. Finally, my findings can be extended to provide a representation of how β-catenin might act as a transcriptional co-regulator to other transcription factors like TCF/LEF by recruiting CBP/p300 to activate the expression of Wnt-related genes (Figure 6.1C).

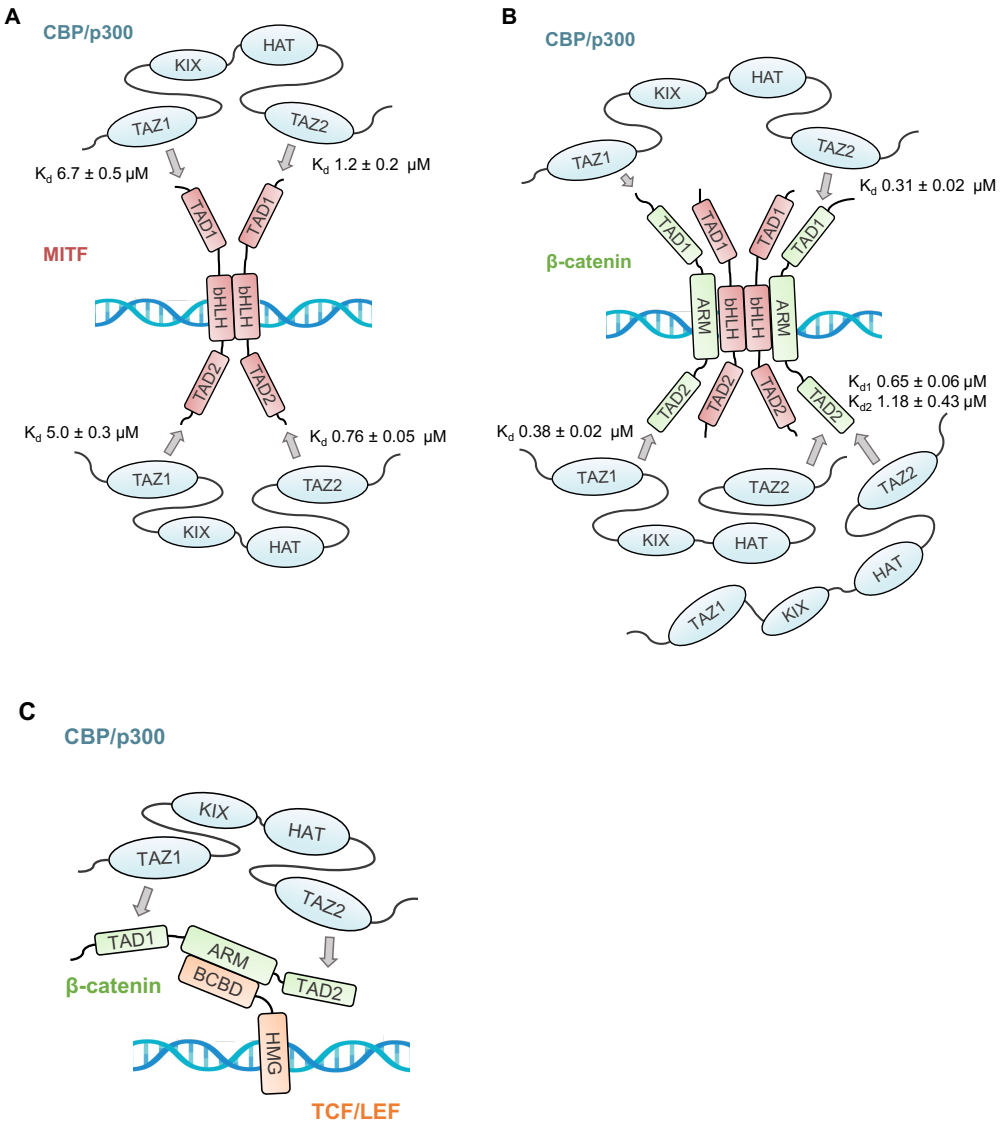

Figure 6.1. Various models of CBP/p300 recruitment by MITF and β-catenin. (A) MITF dimers bind to specific DNA recognition sequences (E-box/M-box) through a basic helix-loop-helix domain (bHLH). The MITF transactivation domains (TAD) then interact with CBP/p300 via simultaneous interactions with TAZ1 and TAZ2. (B) The MITF bHLH domain facilitates binding to the armadillo domain (ARM) of co-regulator β-catenin (as previously described) (70), β-catenin transactivation domains then form promiscuous interactions with TAZ1 and TAZ2, and may promote further CBP/p300 recruitment through multivalent interactions with TAZ2. Binding affinities (K_d) calculated in previous chapters are annotated. (C) β-catenin also recruits CBP/p300 to other transcription factors including T-cell factor and lymphoid enhancer factor (TCF/LEF). TCF/LEF target Wnt-response elements in promoters using a high mobility group DNA-binding domain (HMG) and interact with β-catenin through an N-terminal β-catenin binding domain (BCBD) (136).

6.2 Therapeutic Potential and Impact

Approximately twenty percent of all identified oncogenes are transcription factors, making these proteins direct targets for anticancer drugs (246, 247). Despite the therapeutic potential of controlling transcriptional function, transcription factors and their co-regulators are one of the most underutilized families of pharmaceutical targets and have historically been described as an ‘undruggable’ protein class (247). One of the most significant difficulties to overcome in terms of drug design is the large degree of inherent disorder and structural variation that is maintained in 'fuzzy' transcriptional complexes (248). These interaction surfaces are broad and shallow, without a particularly deep binding pocket or ‘druggable’ site for the effective use of small-molecule inhibitors. Although the implementation of effective and widely utilized medications targeting transcriptional complexes requires further advancements in the field, this outlook has changed dramatically in recent years due to improvement in their structural characterization paving the way for the emergence of new therapeutic techniques.

The results presented in this thesis outline the necessary atomic-resolution structural information that will be required for the rational design of targeted compounds to disrupt CBP/p300 interactions with MITF and β-catenin, including the first ever solution-state NMR structure of the MITF activation domain in complex with TAZ2. Designing ligands that bind to transcription factors directly is likely less feasible than targeting their binding partners. DNA-binding domains are typically avoided as pharmaceutical targets due to their convex shape and highly positive charge, lending to the severe lack of inhibitors targeted towards protein-DNA binding

interfaces (249). Targeting activation domains also provides a unique set of challenges, and further research is still needed in the area of targeting disordered proteins, where current well-characterized IDP-binding molecules are either too reactive or too non-specific to produce a desirable drug (249).

Over the past decade, efforts have been made to instead target transcription factor co-regulators, including CBP/p300. Small-molecule inhibitors have been developed against the bromodomain and catalytic HAT domains, with one compound (Inobrodib) currently undergoing clinical testing in some applications for patients with advanced forms of hematologic cancers (250). While targeting and completely inhibiting all CBP/p300 activity via the active site is one method of pharmaceutical intervention, it might also be beneficial to target and block CBP/p300 protein interactions to fine tune CBP/p300 function.

A feasible strategy to disrupt CBP/p300 protein interactions would be orthosteric inhibition, where peptide inhibitors designed to mimic critical binding residues of transactivation domains target and block the CBP/p300 interface. This approach has been proven successful for transcription factor c-Myb which binds the KIX domain of CBP/p300. Peptide mimics of the c-Myb TAD binding region effectively dissociate the transcription factor/co-activator complex, downregulating oncogenes involved in the growth and angiogenesis of solid tumors (251). Further peptidomimetics have been designed based on the transcription factor HIF1-α TAD, successfully disrupting its interactions with TAZ1 of CBP/p300 leading to apoptosis of acute myeloid leukemia cells and increasing survival in preclinical mouse models with mixed-lineage leukemia (252). The mutagenesis studies outlined in previous

chapters uncovered regions of the MITF and β-catenin TADs that are necessary for CBP/p300 binding and would be instrumental for the structure-guided design of these types of inhibitors.

Regarding clinical applications, the potency and delivery of therapeutic peptides are fundamental issues to overcome. The moderate micromolar affinity of native activation domains (or their analogs) for their targets continues to be a major challenge for this pharmacological strategy. The work I have presented in chapters 3 and 4 provides valuable insight into how this issue may be remedied. By designing a peptide based on the adenoviral protein E1A, which directly targets the same TAZ2 binding region as MITF and β-catenin with inherent nanomolar affinity, I was able to effectively inhibit TAZ2 binding interactions and functionally impede MITF and Wnt/β-catenin regulated transcription. Should no other biologically related inhibitor exist, an alternative method would include the use of high-throughput molecular screening techniques to better refine the binding of these peptide analogs to their target molecules (253).

The use of peptides as therapeutics has been shown to have higher efficacy and lower toxicity than other chemically based drugs, but they present unique challenges in terms of drug delivery (254). Peptides typically cannot penetrate cell membranes because of their size and chemical composition. Several different methods have been developed to help circumvent this issue, including the use of cell penetrating tags, absorption enhancers, nanoparticle carriers, and chemical modifications to the peptide structure, improving their stability and penetration (255, 256). All things considered, the development of a final efficacious drug goes beyond

the discovery of a ligand producing a desirable outcome *in vitro* or in cells but must also take into account further methods of validation that phenotypic effects are generated based on their target mechanisms. Whether the presented findings in this thesis provide a framework for future therapeutic design or not, they do provide a fundamental understanding of gene regulation by MITF and β-catenin via the recruitment of CBP/p300.

6.3 Future Directions

The results of my research raise several new and compelling questions that can help to direct future studies. Given the importance of post-translational modifications in regulating protein function, and that both MITF and β-catenin are phosphorylated by numerous different kinases, it is critical to investigate how phosphorylation of certain residues may impact these proteins' affinity for the domains of CBP/p300. Additionally, the role of electrostatics and the impact of salt in disrupting/driving these interactions could be further investigated.

While this work provides extensive biophysical information on individual protein domains and their interactions, it would also be beneficial to confirm these findings in the context of full-length molecules. In this case, I continue to work towards using co-immunoprecipitation to verify the impact of the identified MITF and β-catenin activation domains on CBP/p300 interactions in cells. These studies can also help determine whether these activation domains function independently or cooperatively of one another when recruiting CBP/p300 in cells.

A long-term goal would be the structural characterization of the CBP/p300: MITF: β-catenin transcriptional complex. Considering the relative sizes of all proteins, this could be an excellent candidate for cryo-EM which can provide global structural details of the overall complex. This information could then be used in conjunction with complementary NMR-derived structures to yield local high-resolution information regarding the individual domains. Further NMR cross saturation experiments could also be conducted to directly discern interaction sites from binding induced conformational changes. Finally, methods such as chromatin immunoprecipitation sequencing (ChIP-Seq) can also be used to supplement these findings and give further biological context as to where and in what various combinations these transcription regulators co-localize in the genome.

Having designed a peptide that significantly effects the transcriptional ability of MITF and β-catenin and inhibits their binding to TAZ2 of CBP/p300 *in vitro*, a logical next step would be to test the biological effects of the peptide inhibitor in cancer cell lines. This inhibitor could be delivered to cells via plasmid coding the peptide or by recombinantly producing it with a cell penetrating tag, to then measure the physiological effects of blocking these interactions. These studies can then be extended to *in vivo* testing using preclinical animal models to work towards therapeutics targeting these interactions in the future.

Bibliography

1. Wright, P. E. and Dyson, H. J. (1999) Intrinsically unstructured proteins: re-assessing the protein structure-function paradigm. *J Mol Biol*. **293**, 321–331

2. Serçinoğlu, O., and Ozbek, P. (2020) Sequence-structure-function relationships in class I MHC: A local frustration perspective. *PLoS One*. **15**, e0232849

3. Liberles, D. A., Teichmann, S. A., Bahar, I., Bastolla, U., Bloom, J., Bornberg-Bauer, E., Colwell, L. J., de Koning, A. P. J., Dokholyan, N. V., Echave, J., Elofsson, A., Gerloff, D. L., Goldstein, R. A., Grahnen, J. A., Holder, M. T., Lakner, C., Lartillot, N., Lovell, S. C., Naylor, G., Perica, T., Pollock, D. D., Pupko, T., Regan, L., Roger, A., Rubinstein, N., Shakhnovich, E., Sjölander, K., Sunyaev, S., Teufel, A. I., Thorne, J. L., Thornton, J. W., Weinreich, D. M., and Whelan, S. (2012) The interface of protein structure, protein biophysics, and molecular evolution. *Protein Sci*. **21**, 769–785

4. Ward, J. J., Sodhi, J. S., McGuffin, L. J., Buxton, B. F., and Jones, D. T. (2004) Prediction and functional analysis of native disorder in proteins from the three kingdoms of life. *J Mol Biol*. **337**, 635–645

5. Alshehri, M. A., Manee, M. M., Al-Fageeh, M. B., and Al-Shomrani, B. M. (2020) Genomic Analysis of intrinsically disordered proteins in the genus camelus. *Int J Mol Sci*. **21**, 4010

6. Babu, M. M. (2016) The contribution of intrinsically disordered regions to protein function, cellular complexity, and human disease. *Biochem Soc Trans*. **44**, 1185–1200

7. Dunker, A. K., Brown, C. J., Lawson, J. D., Iakoucheva, L. M., and Obradović, Z. (2002) Intrinsic disorder and protein function. *Biochem*. **41**, 6573–6582

8. Tompa, P. and Fuxreiter, M. (2008) Fuzzy complexes: polymorphism and structural disorder in protein–protein interactions. *Trends Biochem Sci*. **33**, 2–8

9. Liu, Z. and Huang, Y. (2014) Advantages of proteins being disordered. *Protein Sci*. **23**, 539–550

10. Eick, D., Wedel, A., and Heumann, H. (1994) From initiation to elongation: comparison of transcription by prokaryotic and eukaryotic RNA polymerases. *Trends Genet*. **10**, 292–296

11. Zheng, X.-M., Moncollin, V., Egly, J.-M., and Chambon, P. (1987) A general transcription factor forms a stable complex with RNA polymerase B (II). *Cell*. **50**, 361–368

12. Buratowski, S., Hahn, S., Guarente, L., and Sharp, P. A. (1989) Five intermediate complexes in transcription initiation by RNA polymerase II. *Cell*. **56**, 549–561

13. Cosma, M. P. (2002) Ordered recruitment: gene-specific mechanism of transcription activation. *Mol Cell*. **10**, 227–236

14. Liu, J., Perumal, N. B., Oldfield, C. J., Su, E. W., Uversky, V. N., and Dunker, A. K. (2006) Intrinsic disorder in transcription factors. *Biochem*. **45**, 6873–6888

15. Már, M., Nitsenko, K., and Heidarsson, P. O. (2023) Multifunctional intrinsically disordered regions in transcription factors. *Chem Eur J*. **29**, e202203369

16. Ramos, Y. F. M., Hestand, M. S., Verlaan, M., Krabbendam, E., Ariyurek, Y., van Galen, M., van Dam, H., van Ommen, G.-J. B., den Dunnen, J. T., Zantema, A., and 't Hoen, P. A. C. (2010) Genome-wide assessment of differential roles for p300 and CBP in transcription regulation. *Nucleic Acids Res*. **38**, 5396–5408

17. Moosavi, A. and Ardekani, A. M. (2016) Role of epigenetics in biology and human diseases. *Iran Biomed J*. **20**, 246–258

18. Quina, A. S., Buschbeck, M., and Di Croce, L. (2006) Chromatin structure and epigenetics. *Biochem Pharmacol*. **72**, 1563–1569

19. Kornberg, R. D. (1974) Chromatin structure: a repeating unit of histones and DNA. *Science*. **184**, 868–871

20. Grunstein, M. (1990) Nucleosomes: regulators of transcription. *Trends Genet*. **6**, 395–400

21. Bradbury, E. M. (1992) Reversible histone modifications and the chromosome cell cycle. *Bioessays*. **14**, 9–16

22. Allfrey, V. G., Faulkner, R., and Mirsky, A. E. (1964) Acetylation and methylation of histones and their possible role in the regulation of RNA synthesis. *Proc Natl Acad Sci U S A*. **51**, 786–794

23. Chakraborty, R., Ostriker, A. C., Xie, Y., Dave, J. M., Gamez-Mendez, A., Chatterjee, P., Abu, Y., Valentine, J., Lezon-Geyda, K., Greif, D. M., Schulz, V. P., Gallagher, P. G., Sessa, W. C., Hwa, J., and Martin, K. A. (2022) Histone acetyltransferases p300 and CBP coordinate distinct chromatin remodeling programs in vascular smooth muscle plasticity. *Circulation*. **145**, 1720–1737

24. Kalkhoven, E. (2004) CBP and p300: HATs for different occasions. *Biochem Pharm*. **68**, 1145–1155

25. Wang, F., Marshall, C. B., and Ikura, M. (2013) Transcriptional/epigenetic regulator CBP/p300 in tumorigenesis: structural and functional versatility in target recognition. *Cell Mol Life Sci*. **70**, 3989–4008

26. Dancy, B. M. and Cole, P. A. (2015) Protein lysine acetylation by p300/CBP. *Chem Rev.* **115**, 2419–2452

27. Lee, C. W., Arai, M., Martinez-Yamout, M. A., Dyson, H. J., and Wright, P. E. (2009) Mapping the interactions of the p53 transactivation domain with the KIX domain of CBP. *Biochem*. **48**, 2115–2124

28. Zor, T., De Guzman, R. N., Dyson, H. J., and Wright, P. E. (2004) Solution structure of the KIX domain of CBP bound to the transactivation domain of c-Myb. *J Mol Biol*. **337**, 521–534

29. Toto, A., Giri, R., Brunori, M., and Gianni, S. (2014) The mechanism of binding of the KIX domain to the mixed lineage leukemia protein and its allosteric role in the recognition of c-Myb. *Protein Sci*. **23**, 962–969

30. Bhattacharya, S., Michels, C. L., Leung, M.-K., Arany, Z. P., Kung, A. L., and Livingston, D. M. (1999) Functional role of p35srj, a novel p300/CBP binding protein, during transactivation by HIF-1. *Genes Dev.* **13**, 64–75

31. Wojciak, J. M., Martinez-Yamout, M. A., Dyson, H. J., and Wright, P. E. (2009) Structural basis for recruitment of CBP/p300 coactivators by STAT1 and STAT2 transactivation domains. *EMBO J*. **28**, 948–958

32. von Mikecz, A., Zhang, S., Montminy, M., Tan, E. M., and Hemmerich, P. (2000) Creb-Binding Protein (Cbp/P300) and RNA polymerase II colocalize in transcriptionally active domains in the nucleus. *J Cell Biol*. **150**, 265–274

33. Boija, A., Mahat, D. B., Zare, A., Holmqvist, P.-H., Philip, P., Meyers, D. J., Cole, P. A., Lis, J. T., Stenberg, P., and Mannervik, M. (2017) CBP regulates recruitment and release of promoter-proximal RNA polymerase II. *Mol Cell*. **68**, 491-503.e5

34. Chan, H. M. and La Thangue, N. B. (2001) p300/CBP proteins: HATs for transcriptional bridges and scaffolds. *J Cell Sci*. **114**, 2363–2373

35. Arany, Z., Newsome, D., Oldread, E., Livingston, D. M., and Eckner, R. (1995) A family of transcriptional adaptor proteins targeted by the E1A oncoprotein. *Nature*. **374**, 81–84

36. Van Orden, K. and Nyborg, J. K. (2018) Insight into the tumor suppressor function of CBP through the viral oncoprotein tax. *Gene Expr*. **9**, 29–36

37. Eckner, R., Ludlow, J. W., Lill, N. L., Oldread, E., Arany, Z., Modjtahedi, N., DeCaprio, J. A., Livingston, D. M., and Morgan, J. A. (1996) Association of p300 and CBP with simian virus 40 large T antigen. *Mol Cell Biol*. **16**, 3454–3464

38. Patel, D., Huang, S.-M., Baglia, L. A., and McCance, D. J. (1999) The E6 protein of human papillomavirus type 16 binds to and inhibits co-activation by CBP and p300. *EMBO J*. **18**, 5061–5072

39. Smith, J. L., Freebern, W. J., Collins, I., De Siervi, A., Montano, I., Haggerty, C. M., McNutt, M. C., Butscher, W. G., Dzekunova, I., Petersen, D. W., Kawasaki, E., Merchant, J. L., and Gardner, K. (2004) Kinetic profiles of p300 occupancy in vivo predict common features of promoter structure and coactivator recruitment. *Proc Natl Acad Sci*. **101**, 11554–11559

40. Dyson, H. J. and Wright, P. E. (2016) Role of intrinsic protein disorder in the function and interactions of the transcriptional coactivators CREB-binding protein (CBP) and p300. *J Biol Chem*. **291**, 6714–6722

41. Ragvin, A., Valvatne, H., Erdal, S., Årskog, V., Tufteland, K. R., Breen, K., Øyan, A. M., Eberharter, A., Gibson, T. J., Becker, P. B., and Aasland, R. (2004) Nucleosome binding by the bromodomain and PHD finger of the transcriptional cofactor p300. *J Mol Biol*. **337**, 773–788

42. Chakravarti, D., LaMorte, V. J., Nelson, M. C., Nakajima, T., Schulman, I. G., Juguilon, H., Montminy, M., and Evans, R. M. (1996) Role of CBP/P300 in nuclear receptor signaling. *Nature*. **383**, 99–103

43. Kjaergaard, M., Teilum, K., and Poulsen, F. M. (2010) Conformational selection in the molten globule state of the nuclear coactivator binding domain of CBP. *Proc Natl Acad Sci*. **107**, 12535–12540

44. De Guzman, R. N., Wojciak, J. M., Martinez-Yamout, M. A., Dyson, H. J., and Wright, P. E. (2005) CBP/p300 TAZ1 domain forms a structured scaffold for ligand binding. *Biochem*. **44**, 490–497

45. Radhakrishnan, I., Pérez-Alvarado, G. C., Parker, D., Dyson, H. J., Montminy, M. R., and Wright, P. E. (1997) Solution structure of the KIX domain of CBP bound to the transactivation domain of CREB: a model for activator: coactivator Interactions. *Cell*. **91**, 741–752

46. De Guzman, R. N., Liu, H. Y., Martinez-Yamout, M., Dyson, H. J., and Wright, P. E. (2000) Solution structure of the TAZ2 (CH3) domain of the transcriptional adaptor protein CBP. *J Mol Biol*. **303**, 243–253

47. Lin, C. H., Hare, B. J., Wagner, G., Harrison, S. C., Maniatis, T., and Fraenkel, E. (2001) A small domain of CBP/p300 binds diverse proteins: solution structure and functional studies. *Mol Cell*. **8**, 581–590

48. Ghosh, S., Taylor, A., Chin, M., Huang, H.-R., Conery, A. R., Mertz, J. A., Salmeron, A., Dakle, P. J., Mele, D., Cote, A., Jayaram, H., Setser, J. W., Poy, F., Hatzivassiliou, G., DeAlmeida-Nagata, D., Sandy, P., Hatton, C., Romero, F. A., Chiang, E., Reimer, T., Crawford, T., Pardo, E., Watson, V. G., Tsui, V., Cochran, A. G., Zawadzke, L., Harmange, J.-C., Audia, J. E., Bryant, B. M., Cummings, R. T., Magnuson, S. R., Grogan, J. L., Bellon, S. F., Albrecht, B. K., Sims, R. J., and Lora, J. M. (2016) Regulatory T cell modulation by CBP/P300 bromodomain inhibition. *J Biol Chem*. **291**, 13014–13027

49. Park, S., Stanfield, R. L., Martinez-Yamout, M. A., Dyson, H. J., Wilson, I. A., and Wright, P. E. (2017) Role of the CBP catalytic core in intramolecular SUMOylation and control of histone H3 acetylation. *Proc Natl Acad Sci*. **114**, 5335–5342

50. Parker, D., Ferreri, K., Nakajima, T., Lamorte, V. J., Evans, R., Koerber, S. C., Hoeger, C., and Montminy, M. R. (1996) Phosphorylation of CREB at ser-133 induces complex formation with CREB-binding protein via a direct mechanism. *Mol Cell Biol*. **16**, 694–703

51. De Guzman, R. N., Goto, N. K., Dyson, H. J., and Wright, P. E. (2006) Structural basis for cooperative transcription factor binding to the CBP coactivator. *J Mol Biol*. **355**, 1005–1013

52. Goto, N. K., Zor, T., Martinez-Yamout, M., Dyson, H. J., and Wright, P. E. (2002) Cooperativity in transcription factor binding to the coactivator CREB-binding protein (CBP). The mixed lineage leukemia protein (MLL) activation domain binds to an allosteric site on the KIX domain. *J Biol Chem.* **277**, 43168–43174

53. Wang, F., Marshall, C. B., Yamamoto, K., Li, G.-Y., Gasmi-Seabrook, G. M. C., Okada, H., Mak, T. W., and Ikura, M. (2012) Structures of KIX domain of CBP in complex with two FOXO3a transactivation domains reveal promiscuity and plasticity in coactivator recruitment. *Proc Natl Acad Sci U S A*. **109**, 6078–6083

54. Kluska, K., Adamczyk, J., and Krężel, A. (2018) Metal binding properties, stability and reactivity of zinc fingers. *Coord Chem Rev*. **367**, 18–64

55. De Guzman, R. N., Martinez-Yamout, M. A., Dyson, H. J., and Wright, P. E. (2004) Interaction of the TAZ1 domain of the CREB-binding protein with the activation domain of CITED2. *J Biol Chem*. **279**, 3042–3049

56. Mukherjee, S. P., Behar, M., Birnbaum, H. A., Hoffmann, A., Wright, P. E., and Ghosh, G. (2013) Analysis of the RelA:CBP/p300 interaction reveals its involvement in NF-κB-driven transcription. *PLoS Biol*. **11**, e1001647

57. Krois, A. S., Ferreon, J. C., Martinez-Yamout, M. A., Dyson, H. J., and Wright, P. E. (2016) Recognition of the disordered p53 transactivation domain by the transcriptional adapter zinc finger domains of CREB-binding protein. *Proc Natl Acad Sci U S A*. **113**, E1853–E1862

58. Lochhead, M. R., Brown, A. D., Kirlin, A. C., Chitayat, S., Munro, K., Findlay, J. E., Baillie, G. S., LeBrun, D. P., Langelaan, D. N., and Smith, S. P. (2020) Structural insights into TAZ2 domain-mediated CBP/p300 recruitment by transactivation domain 1 of the lymphopoietic transcription factor E2A. *J Biol Chem.*

59. Dames, S. A., Martinez-Yamout, M., De Guzman, R. N., Dyson, H. J., and Wright, P. E. (2002) Structural basis for Hif-1 alpha /CBP recognition in the cellular hypoxic response. *Proc Natl Acad Sci U S A*. **99**, 5271–5276

60. Holstein, T. W. (2012) The evolution of the Wnt pathway. *Cold Spring Harb Perspect Biol*. **4**, a007922

61. Komiya, Y. and Habas, R. (2008) Wnt signal transduction pathways. *Organogenesis*. **4**, 68–75

62. Liu, J., Xiao, Q., Xiao, J., Niu, C., Li, Y., Zhang, X., Zhou, Z., Shu, G., and Yin, G. (2022) Wnt/β-catenin signaling: function, biological mechanisms, and therapeutic opportunities. *Sig Transduct Target Ther*. **7**, 1–23

63. Ren, Q., Chen, J., and Liu, Y. (2021) LRP5 and LRP6 in Wnt signaling: similarity and divergence. *Front Cell Dev Biol*.

64. Logan, C. Y. and Nusse, R. (2004) The Wnt signaling pathway in development and disease. *Annu Rev Cell Dev Biol*. **20**, 781–810

65. Li, Y.-J., Wei, Z.-M., Meng, Y.-X., and Ji, X.-R. (2005) β-catenin up-regulates the expression of cyclinD1, c-myc and MMP-7 in human pancreatic cancer: Relationships with carcinogenesis and metastasis. *World J Gastroenterol*. **11**, 2117–2123

66. Zhang, T., Otevrel, T., Gao, Z., Gao, Z., Ehrlich, S. M., Fields, J. Z., and Boman, B. M. (2001) Evidence that APC regulates survivin expression: a possible mechanism contributing to the stem cell origin of colon cancer. *Cancer Res*. **61**, 8664–8667

67. Shang, S., Hua, F., and Hu, Z.-W. (2017) The regulation of β-catenin activity and function in cancer: therapeutic opportunities. *Oncotarget*. **8**, 33972–33989

68. White, B. D., Chien, A. J., and Dawson, D. W. (2012) Dysregulation of Wnt/β-catenin signaling in gastrointestinal cancers. *Gastroenterology*. **142**, 219–232

69. Khramtsov, A. I., Khramtsova, G. F., Tretiakova, M., Huo, D., Olopade, O. I., and Goss, K. H. (2010) Wnt/beta-catenin pathway activation is enriched in basal-like breast cancers and predicts poor outcome. *Am J Pathol*. **176**, 2911–2920

70. Schepsky, A., Bruser, K., Gunnarsson, G. J., Goodall, J., Hallsson, J. H., Goding, C. R., Steingrimsson, E., and Hecht, A. (2006) The microphthalmia-associated transcription factor Mitf interacts with beta-catenin to determine target gene expression. *Mol Cell Biol.* **26**, 8914–8927

71. Xing, Y., Clements, W. K., Le Trong, I., Hinds, T. R., Stenkamp, R., Kimelman, D., and Xu, W. (2004) Crystal structure of a beta-catenin/APC complex reveals a critical role for APC phosphorylation in APC function. *Mol Cell*. **15**, 523–533

72. Städeli, R., Hoffmans, R., and Basler, K. (2006) Transcription under the Control of Nuclear Arm/β-Catenin. *Current Biology*. **16**, R378–R385

73. Xing, Y., Takemaru, K.-I., Liu, J., Berndt, J. D., Zheng, J. J., Moon, R. T., and Xu, W. (2008) Crystal structure of a full-length β-Catenin. *Structure*. **16**, 478–487

74. Dar, M. S., Singh, P., Singh, G., Jamwal, G., Hussain, S. S., Rana, A., Akhter, Y., Monga, S. P., and Dar, M. J. (2016) Terminal regions of β-catenin are critical for regulating its adhesion and transcription functions. *Biochim Biophys Acta Mol Cell Res*. **1863**, 2345–2357

75. Barker, N., Hurlstone, A., Musisi, H., Miles, A., Bienz, M., and Clevers, H. (2001) The chromatin remodelling factor Brg-1 interacts with beta-catenin to promote target gene activation. *EMBO J.* **20**, 4935–4943

76. Hecht, A., Vleminckx, K., Stemmler, M. P., van Roy, F., and Kemler, R. (2000) The p300/CBP acetyltransferases function as transcriptional coactivators of beta-catenin in vertebrates. *EMBO J.* **19**, 1839–1850

77. Takemaru, K.-I. and Moon, R. T. (2000) The transcriptional coactivator CBP interacts with β-catenin to activate gene expression. *J Cell Biol*. **149**, 249–254

78. Kimbrel, E. A. and Kung, A. L. (2009) The F-box protein beta-TrCp1/Fbw1a interacts with p300 to enhance beta-catenin transcriptional activity. *J Biol Chem*. **284**, 13033–13044

79. Lévy, L., Wei, Y., Labalette, C., Wu, Y., Renard, C.-A., Buendia, M. A., and Neuveut, C. (2004) Acetylation of beta-catenin by p300 regulates beta-catenin-Tcf4 interaction. *Mol Cell Biol*. **24**, 3404–3414

80. Shibahara, S., Takeda, K., Yasumoto, K., Udono, T., Watanabe, K., Saito, H., and Takahashi, K. (2001) Microphthalmia-associated transcription factor (MITF): multiplicity in structure, function, and regulation. *J Investig Dermatol*. **6**, 99–104

81. Kawakami, A., and Fisher, D. E. (2017) The master role of microphthalmia-associated transcription factor in melanocyte and melanoma biology. *Lab Invest.* **97**, 649–656

82. Hertwig, P. (1942) Neue mutationen und koppelungsgruppen bei der hausmaus. *Z.Ver-erbungslehre*. **80**, 220–246

83. Arnheiter, H. (2010) The discovery of the microphthalmia locus and its gene, Mitf. *Pigment Cell Melanoma Res*. **23**, 729–735

84. Liu, X. Z., Newton, V. E., and Read, A. P. (1995) Waardenburg syndrome type II: phenotypic findings and diagnostic criteria. *Am J Med Genet*. **55**, 95–100

85. Smith, S., Kelley, P., Kenyon, J., and Hoover, D. (2000) Tietz syndrome (hypopigmentation/deafness) caused by mutation of MITF. *J Med Genet*. **37**, 446–448

86. Yasumoto, K., Yokoyama, K., Shibata, K., Tomita, Y., and Shibahara, S. (1994) Microphthalmia-associated transcription factor as a regulator for melanocyte-specific transcription of the human tyrosinase gene. *Mol Cell Biol*. **14**, 8058–8070

87. Du, J., Widlund, H. R., Horstmann, M. A., Ramaswamy, S., Ross, K., Huber, W. E., Nishimura, E. K., Golub, T. R., and Fisher, D. E. (2004) Critical role of CDK2 for melanoma growth linked to its melanocyte-specific transcriptional regulation by MITF. *Cancer Cell*. **6**, 565–576

88. McGill, G. G., Horstmann, M., Widlund, H. R., Du, J., Motyckova, G., Nishimura, E. K., Lin, Y.-L., Ramaswamy, S., Avery, W., Ding, H.-F., Jordan, S. A., Jackson, I. J., Korsmeyer, S. J., Golub, T. R., and Fisher, D. E. (2002) Bcl2 regulation by the melanocyte master regulator MITF modulates lineage survival and melanoma cell viability. *Cell*. **109**, 707–718

89. McGill, G. G., Haq, R., Nishimura, E. K., and Fisher, D. E. (2006) c-Met expression is regulated by MITF in the melanocyte lineage. *J Biol Chem*. **281**, 10365–10373

90. Buscà, R., Berra, E., Gaggioli, C., Khaled, M., Bille, K., Marchetti, B., Thyss, R., Fitsialos, G., Larribère, L., Bertolotto, C., Virolle, T., Barbry, P., Pouysségur, J., Ponzio, G., and Ballotti, R. (2005) Hypoxia-inducible factor 1alpha is a new target of microphthalmia-associated transcription factor (MITF) in melanoma cells. *J Cell Biol*. **170**, 49–59

91. Garraway, L. A., Widlund, H. R., Rubin, M. A., Getz, G., Berger, A. J., Ramaswamy, S., Beroukhim, R., Milner, D. A., Granter, S. R., Du, J., Lee, C., Wagner, S. N., Li, C., Golub, T. R., Rimm, D. L., Meyerson, M. L., Fisher, D. E., and Sellers, W. R. (2005) Integrative genomic analyses identify MITF as a lineage survival oncogene amplified in malignant melanoma. *Nature*. **436**, 117–122

92. Canadian Cancer Statistics Advisory Committee in collaboration with the Canadian Cancer Society, Statistics Canada and the Public Health Agency of Canada. (2021) *Can J Stat.*

93. Saginala, K., Barsouk, A., Aluru, J. S., Rawla, P., and Barsouk, A. (2021) Epidemiology of melanoma. *Med Sci*. **9**, 63

94. Sandru, A., Voinea, S., Panaitescu, E., and Blidaru, A. (2014) Survival rates of patients with metastatic malignant melanoma. *J Med Life*. **7**, 572–576

95. Carreira, S., Goodall, J., Denat, L., Rodriguez, M., Nuciforo, P., Hoek, K. S., Testori, A., Larue, L., and Goding, C. R. (2006) MITF regulation of Dia1 controls melanoma proliferation and invasiveness. *Genes Dev*. **20**, 3426–3439

96. Hoek, K. S., and Goding, C. R. (2010) Cancer stem cells versus phenotype-switching in melanoma. *Pigment Cell Melanoma Res*. **23**, 746–759

97. Goding, C. R. (2011) Commentary. A picture of Mitf in melanoma immortality. *Oncogene*. **30**, 2304–2306

98. Holderfield, M., Deuker, M. M., McCormick, F., and McMahon, M. (2014) Targeting RAF kinases for cancer therapy: BRAF-mutated melanoma and beyond. *Nat Rev Cancer*. **14**, 455–467

99. Long, G. V., Menzies, A. M., Nagrial, A. M., Haydu, L. E., Hamilton, A. L., Mann, G. J., Hughes, T. M., Thompson, J. F., Scolyer, R. A., and Kefford, R. F. (2011) Prognostic and clinicopathologic associations of oncogenic BRAF in metastatic melanoma. *J Clin Oncol*. **29**, 1239–1246

100. Long, G. V., Stroyakovskiy, D., Gogas, H., Levchenko, E., de Braud, F., Larkin, J., Garbe, C., Jouary, T., Hauschild, A., Grob, J. J., Chiarion Sileni, V., Lebbe, C., Mandalà, M., Millward, M., Arance, A., Bondarenko, I., Haanen, J. B. A. G., Hansson, J., Utikal, J., Ferraresi, V., Kovalenko, N., Mohr, P., Probachai, V., Schadendorf, D., Nathan, P., Robert, C., Ribas, A., DeMarini, D. J., Irani, J. G., Casey, M., Ouellet, D., Martin, A.-M., Le, N., Patel, K., and Flaherty, K. (2014) Combined BRAF and MEK inhibition versus BRAF inhibition alone in melanoma. *N Engl J Med*. **371**, 1877–1888

101. Paton, E. L., Turner, J. A., and Schlaepfer, I. R. (2020) Overcoming resistance to therapies targeting the MAPK pathway in BRAF-mutated tumours. *J Oncol*. **2020**, 1079827

102. Van Allen, E. M., Wagle, N., Sucker, A., Treacy, D., Johannessen, C., Goetz, E. M., Place, C. S., Taylor-Weiner, A., Whittaker, S., Kryukov, G., Hodis, E., Rosenberg, M., McKenna, A., Cibulskis, K., Farlow, D., Zimmer, L., Hillen, U., Gutzmer, R., Goldinger, S. M., Ugurel, S., Gogas, H. J., Egberts, F., Berking, C., Trefzer, U., Loquai, C., Weide, B., Hassel, J. C., Gabriel, S. B., Carter, S. L., Getz, G., Garraway, L. A., and Schadendorf, D. (2014) The genetic landscape of clinical resistance to RAF inhibition in metastatic melanoma. *Cancer Discov*. **4**, 94–109

103. La Spina, M., Contreras, P. S., Rissone, A., Meena, N. K., Jeong, E., and Martina, J. A. (2021) MiT/TFE Family of transcription factors: an evolutionary perspective. *Front Cell Dev Biol*.

104. Pogenberg, V., Ögmundsdóttir, M. H., Bergsteinsdóttir, K., Schepsky, A., Phung, B., Deineko, V., Milewski, M., Steingrímsson, E., and Wilmanns, M. (2012) Restricted leucine zipper dimerization and specificity of DNA recognition of the melanocyte master regulator MITF. *Genes Dev.* **26**, 2647–2658

105. Agostini, F., Agostinis, R., Medina, D. L., Bisaglia, M., Greggio, E., and Plotegher, N. (2022) The regulation of MiTF/TFE transcription factors across model organisms: from brain physiology to implication for neurodegeneration. *Mol Neurobiol*. **59**, 5000–5023

106. Zhao, G. Q., Zhao, Q., Zhou, X., Mattei, M. G., and de Crombrugghe, B. (1993) TFEC, a basic helix-loop-helix protein, forms heterodimers with TFE3 and inhibits TFE3-dependent transcription activation. *Mol Cell Biol*. **13**, 4505–4512

107. Sato, S., Roberts, K., Gambino, G., Cook, A., Kouzarides, T., and Goding, C. R. (1997) CBP/p300 as a co-factor for the Microphthalmia transcription factor. *Oncogene*. **14**, 3083

108. Takeda, K., Takemoto, C., Kobayashi, I., Watanabe, A., Nobukuni, Y., Fisher, D., and Tachibana, M. (2000) Ser298 of MITF, a mutation site in Waardenburg syndrome type 2, is a phosphorylation site with functional significance. *Hum Mol Genet*. **9**, 125–32

109. Watanabe, A., Takeda, K., Ploplis, B., and Tachibana, M. (1998) Epistatic relationship between Waardenburg syndrome genes MITF and PAX3. *Nat Genet*. **18**, 283–286

110. Huber, W. E., Price, E. R., Widlund, H. R., Du, J., Davis, I. J., Wegner, M., and Fisher, D. E. (2003) A tissue-restricted cAMP transcriptional response: SOX10 modulates alpha-melanocyte-stimulating hormone-triggered expression of microphthalmia-associated transcription factor in melanocytes. *J Biol Chem*. **278**, 45224–45230

111. Bondurand, N., Pingault, V., Goerich, D. E., Lemort, N., Sock, E., Le Caignec, C., Wegner, M., and Goossens, M. (2000) Interaction among SOX10, PAX3 and MITF, three genes altered in Waardenburg syndrome. *Hum Mol Genet*. **9**, 1907–1917

112. Wellbrock, C., and Arozarena, I. (2015) Microphthalmia-associated transcription factor in melanoma development and MAP-kinase pathway targeted therapy. *Pigment Cell Melanoma Res*. **28**, 390–406

113. Takeda, K., Yasumoto, K., Takada, R., Takada, S., Watanabe, K., Udono, T., Saito, H., Takahashi, K., and Shibahara, S. (2000) Induction of melanocyte-specific microphthalmia-associated transcription factor by Wnt-3a. *J Biol Chem.* **275**, 14013–14016

114. Colombo, S., Petit, V., Wagner, R. Y., Champeval, D., Yajima, I., Gesbert, F., Aktary, Z., Davidson, I., Delmas, V., and Larue, L. (2022) Stabilization of β-catenin promotes melanocyte specification at the expense of the Schwann cell lineage. *Dev*. **149**, 194407

115. Hemesath, T. J., Price, E. R., Takemoto, C., Badalian, T., and Fisher, D. E. (1998) MAP kinase links the transcription factor microphthalmia to c-Kit signaling in melanocytes. *Nature*. **391**, 298–301

116. Price, E. R., Ding, H.-F., Badalian, T., Bhattacharya, S., Takemoto, C., Yao, T.-P., Hemesath, T. J., and Fisher, D. E. (1998) Lineage-specific signaling in melanocytes c-Kit stimulation recruits p300/CBP to microphthalmia. *J Biol Chem.* **273**, 17983–17986

117. Ngeow, K. C., Friedrichsen, H. J., Li, L., Zeng, Z., Andrews, S., Volpon, L., Brunsdon, H., Berridge, G., Picaud, S., Fischer, R., Lisle, R., Knapp, S., Filippakopoulos, P., Knowles, H., Steingrímsson, E., Borden, K. L. B., Patton, E. E., and Goding, C. R. (2018) BRAF/MAPK and GSK3 signaling converges to control MITF nuclear export. *Proc Natl Acad Sci*. **115**, E8668–E8677

118. Ploper, D., Taelman, V. F., Robert, L., Perez, B. S., Titz, B., Chen, H.-W., Graeber, T. G., von Euw, E., Ribas, A., and De Robertis, E. M. (2015) MITF drives endolysosomal biogenesis and potentiates Wnt signaling in melanoma cells. *Proc Natl Acad Sci*. **112**, E420–E429

119. Oldfield, C. J., Xue, B., Van, Y.-Y., Ulrich, E. L., Markley, J. L., Dunker, A. K., and Uversky, V. N. (2013) Utilization of protein intrinsic disorder knowledge in structural proteomics. *Biochim Biophys Acta*. **1834**, 487–498

120. Musselman, C. A. and Kutateladze, T. G. (2021) Characterization of functional disordered regions within chromatin-associated proteins. *iScience*. **24**, 102070

121. Cheng, Y. (2018) Membrane protein structural biology in the era of single particle cryo-EM. *Curr Opin Struct Biol*. **52**, 58–63

122. Ghosh, R., Kaypee, S., Shasmal, M., Kundu, T. K., Roy, S., and Sengupta, J. (2019) Tumor suppressor p53-mediated structural reorganization of the transcriptional coactivator p300. *Biochem*. **58**, 3434–3443

123. Kosol, S., Contreras-Martos, S., Cedeño, C., and Tompa, P. (2013) Structural characterization of intrinsically disordered proteins by NMR spectroscopy. *Molecules*. **18**, 10802–10828

124. Keeler, J. (2010) Understanding NMR Spectroscopy. *John Wiley and Sons*. Chichester, U.K

125. Szakács, Z. and Sánta, Z. (2015) NMR Methodological Overview. *Anthropic Awareness*. Elsevier, Boston

126. Becker, W., Bhattiprolu, K. C., Gubensäk, N., and Zangger, K. (2018) Investigating protein–ligand interactions by solution nuclear magnetic resonance spectroscopy. *Chem Phys*. **19**, 895–906

127. Arai, M., Ferreon, J. C., and Wright, P. E. (2012) Quantitative analysis of multisite protein-ligand interactions by NMR: binding of intrinsically disordered p53 transactivation subdomains with the TAZ2 domain of CBP. *J Am Chem Soc*. **134**, 3792–3803

128. MacDonald, B. T., Tamai, K., and He, X. (2009) Wnt/β-catenin signaling: components, mechanisms, and diseases. *Dev Cell*. **17**, 9–26

129. Garcin, C. L. and Habib, S. J. (2017) A Comparative Perspective on Wnt/β-catenin signaling in cell fate determination. *Results Probl Cell Differ*. **61**, 323–350

130. Steinhart, Z. and Angers, S. (2018) Wnt signaling in development and tissue homeostasis. *Development.*

131. Valenta, T., Hausmann, G., and Basler, K. (2012) The many faces and functions of β-catenin. *EMBO J*. **31**, 2714–2736

132. Pai, S. G., Carneiro, B. A., Mota, J. M., Costa, R., Leite, C. A., Barroso-Sousa, R., Kaplan, J. B., Chae, Y. K., and Giles, F. J. (2017) Wnt/beta-catenin pathway: modulating anticancer immune response. *J Hemat Oncol*. **10**, 101

133. Giles, R. H., van Es, J. H., and Clevers, H. (2003) Caught up in a Wnt storm: Wnt signaling in cancer. *Biochim Biophys Acta Rev Cancer*. **1653**, 1–24

134. Herbst, A., Jurinovic, V., Krebs, S., Thieme, S. E., Blum, H., Göke, B., and Kolligs, F. T. (2014) Comprehensive analysis of β-catenin target genes in colorectal carcinoma cell lines with deregulated Wnt/β-catenin signaling. *BMC Genomics*. **15**, 74

135. Polakis, P. (1999) The oncogenic activation of beta-catenin. *Curr Opin Genet Dev.* **9**, 15–21

136. Cadigan, K. M. and Waterman, M. L. (2012) TCF/LEFs and Wnt signaling in the nucleus. *Cold Spring Harb Perspect Biol*.

137. Hsu, S. C., Galceran, J., and Grosschedl, R. (1998) Modulation of transcriptional regulation by LEF-1 in response to Wnt-1 signaling and association with β-Catenin. *Mol Cell Biol*. **18**, 4807–4818

138. Hoffmans, R., Städeli, R., and Basler, K. (2005) Pygopus and legless provide essential transcriptional coactivator functions to armadillo/beta-catenin. *Current Biology*. **15**, 1207–1211

139. Sampietro, J., Dahlberg, C. L., Cho, U. S., Hinds, T. R., Kimelman, D., and Xu, W. (2006) Crystal structure of a β-catenin/BCL9/Tcf4 complex. *Mol Cell*. **24**, 293–300

140. Song, H., Spichiger-Haeusermann, C., and Basler, K. (2009) The ISWI-containing NURF complex regulates the output of the canonical Wingless pathway. *EMBO Rep*. **10**, 1140–1146

141. Barker, N., Morin, P. J., and Clevers, H. (1999) The yin-yang of TCF/β-catenin signaling. *Adv Cancer Res*. **77**, 1–24

142. Sun, Y., Kolligs, F. T., Hottiger, M. O., Mosavin, R., Fearon, E. R., and Nabel, G. J. (2000) Regulation of beta-catenin transformation by the p300 transcriptional coactivator. *Proc Natl Acad Sci U S A*. **97**, 12613–12618

143. Ogryzko, V. V., Schiltz, R. L., Russanova, V., Howard, B. H., and Nakatani, Y. (1996) The transcriptional coactivators p300 and CBP are histone acetyltransferases. *Cell*. **87**, 953–959

144. Vo, N., and Goodman, R. H. (2001) CREB-binding protein and p300 in transcriptional regulation. *J Biol Chem*. **276**, 13505–13508

145. Pao, G. M., Janknecht, R., Ruffner, H., Hunter, T., and Verma, I. M. (2000) CBP/p300 interact with and function as transcriptional coactivators of BRCA1. *Proc Natl Acad Sci U.S.A.* **97**, 1020–1025

146. Freedman, S. J., Sun, Z.-Y. J., Poy, F., Kung, A. L., Livingston, D. M., Wagner, G., and Eck, M. J. (2002) Structural basis for recruitment of CBP/p300 by hypoxia-inducible factor-1α. *PNAS*. **99**, 5367–5372

147. Ma, H., Nguyen, C., Lee, K.-S., and Kahn, M. (2005) Differential roles for the coactivators CBP and p300 on TCF/beta-catenin-mediated survivin gene expression. *Oncogene*. **24**, 3619–3631

148. Jeong, J.-Y., Yim, H.-S., Ryu, J.-Y., Lee, H. S., Lee, J.-H., Seen, D.-S., and Kang, S. G. (2012) One-step sequence- and ligation-independent cloning as a rapid and versatile cloning method for functional genomics studies. *Appl Environ Microbiol*. **78**, 5440–5443

149. Studier, F. W. (2005) Protein production by auto-induction in high density shaking cultures. *Protein Expr Purif*. **41**, 207–234

150. Delaglio, F., Grzesiek, S., Vuister, GeertenW., Zhu, G., Pfeifer, J., and Bax, A. (1995) NMRPipe: A multidimensional spectral processing system based on UNIX pipes. *J Biomol NMR*.

151. Vranken, W. F., Boucher, W., Stevens, T. J., Fogh, R. H., Pajon, A., Llinas, M., Ulrich, E. L., Markley, J. L., Ionides, J., and Laue, E. D. (2005) The CCPN data model for NMR spectroscopy: development of a software pipeline. *Proteins: Struct Funct Bioinfo*. **59**, 687–696

152. Farmer, B. T., Constantine, K. L., Goldfarb, V., Friedrichs, M. S., Wittekind, M., Yanchunas, J., Robertson, J. G., and Mueller, L. (1996) Localizing the NADP+ binding site on the MurB enzyme by NMR. *Nat Struct Biol*. **3**, 995–997

153. Chitayat, S., Kanelis, V., Koschinsky, M. L., and Smith, S. P. (2007) Nuclear magnetic resonance (NMR) solution structure, dynamics, and binding properties of the Kringle IV Type 8 Module of Apolipoprotein. *Biochem*. **46**, 1732–1742

154. De Guzman, R. N., Wojciak, J. M., Martinez-Yamout, M. A., Dyson, H. J., and Wright, P. E. (2005) CBP/p300 TAZ1 domain forms a structured scaffold for ligand binding. *Biochem*. **44**, 490–497

155. De Guzman, R. N., Liu, H. Y., Martinez-Yamout, M., Dyson, H. J., and Wright, P. E. (2000) Solution structure of the TAZ2 (CH3) domain of the transcriptional adaptor protein CBP. *J Mol Biol.* **303**, 243–253

156. Ulrich, E. L., Akutsu, H., Doreleijers, J. F., Harano, Y., Ioannidis, Y. E., Lin, J., Livny, M., Mading, S., Maziuk, D., Miller, Z., Nakatani, E., Schulte, C. F., Tolmie, D. E., Kent Wenger, R., Yao, H., and Markley, J. L. (2008) BioMagResBank. *Nucleic Acids Res*. **36**, D402–D408

157. Marsh, J. A., Singh, V. K., Jia, Z., and Forman-Kay, J. D. (2006) Sensitivity of secondary structure propensities to sequence differences between alpha- and gamma-synuclein: implications for fibrillation. *Protein Sci*. **15**, 2795–2804

158. Clevers, H. (2006) Wnt/beta-catenin signaling in development and disease. *Cell*. **127**, 469–480

159. Yu, F., Yu, C., Li, F., Zuo, Y., Wang, Y., Yao, L., Wu, C., Wang, C., and Ye, L. (2021) Wnt/β-catenin signaling in cancers and targeted therapies. *Sig Transduct Target Ther*. **6**, 1–24

160. Ferreon, J. C., Lee, C. W., Arai, M., Martinez-Yamout, M. A., Dyson, H. J., and Wright, P. E. (2009) Cooperative regulation of p53 by modulation of ternary complex formation with CBP/p300 and HDM2. *Proc Natl Acad Sci*. **106**, 6591–6596

161. Emami, K. H., Nguyen, C., Ma, H., Kim, D. H., Jeong, K. W., Eguchi, M., Moon, R. T., Teo, J.-L., Oh, S. W., Kim, H. Y., Moon, S. H., Ha, J. R., and Kahn, M. (2004) A small molecule inhibitor of β-catenin/cyclic AMP response element-binding protein transcription. *Proc Natl Acad Sci*. **101**, 12682–12687

162. Denis, C. M., Langelaan, D. N., Kirlin, A. C., Chitayat, S., Munro, K., Spencer, H. L., LeBrun, D. P., and Smith, S. P. (2014) Functional redundancy between the transcriptional activation domains of E2A is mediated by binding to the KIX domain of CBP/p300. *Nucleic Acids Res*. **42**, 7370–7382

163. Miller Jenkins, L. M., Feng, H., Durell, S. R., Tagad, H. D., Mazur, S. J., Tropea, J. E., Bai, Y., and Appella, E. (2015) Characterization of the p300 Taz2–p53 TAD2 complex and comparison with the p300 Taz2–p53 TAD1 complex. *Biochem*. **54**, 2001–2010

164. Miyagishi, M., Fujii, R., Hatta, M., Yoshida, E., Araya, N., Nagafuchi, A., Ishihara, S., Nakajima, T., and Fukamizu, A. (2000) Regulation of Lef-mediated transcription and p53-dependent pathway by associating β-Catenin with CBP/p300. *J Biol Chem.* **275**, 35170–35175

165. Wolf, D., Rodova, M., Miska, E. A., Calvet, J. P., and Kouzarides, T. (2002) Acetylation of β-Catenin by CREB-binding Protein (CBP). *J Biol Chem*. **277**, 25562–25567

166. Taurin, S., Sandbo, N., Qin, Y., Browning, D., and Dulin, N. O. (2006) Phosphorylation of β-Catenin by cyclic AMP-dependent protein kinase. *J Biol Chem*. **281**, 9971–9976

167. Hino, S., Tanji, C., Nakayama, K. I., and Kikuchi, A. (2005) Phosphorylation of beta-catenin by cyclic AMP-dependent protein kinase stabilizes beta-catenin through inhibition of its ubiquitination. *Mol Cell Biol*. **25**, 9063–9072

168. Lambert, P. F., Kashanchi, F., Radonovich, M. F., Shiekhattar, R., and Brady, J. N. (1998) Phosphorylation of p53 Serine 15 Increases Interaction with CBP. *J Biol Chem*. **273**, 33048–33053

169. Ljungberg, J. K., Kling, J. C., Tran, T. T., and Blumenthal, A. (2019) Functions of the Wnt signaling network in shaping host responses to infection. *Front Immunol.*

170. MacDonald, B. T., Tamai, K., and He, X. (2009) Wnt/β-catenin signaling: components, mechanisms, and diseases. *Dev Cell*. **17**, 9–26

171. Bian, J., Dannappel, M., Wan, C., and Firestein, R. (2020) Transcriptional regulation of Wnt/β-catenin pathway in colorectal cancer. *Cells*. **9**, 2125

172. Kovacs, D., Migliano, E., Muscardin, L., Silipo, V., Catricalà, C., Picardo, M., and Bellei, B. (2016) The role of Wnt/β-catenin signaling pathway in melanoma epithelial-to-mesenchymal-like switching: evidences from patients-derived cell lines. *Oncotarget*. **7**, 43295–43314

173. Li, K., Pan, W.-T., Ma, Y.-B., Xu, X.-L., Gao, Y., He, Y.-Q., Wei, L., and Zhang, J.-W. (2020) BMX activates Wnt/β-catenin signaling pathway to promote cell proliferation and migration in breast cancer. *Breast Cancer*. **27**, 363–371

174. Wen, X., Wu, Y., Awadasseid, A., Tanaka, Y., and Zhang, W. (2020) New advances in canonical Wnt/β-catenin signaling in cancer. *Cancer Manag Res*. **12**, 6987–6998

175. Huber, A. H., Nelson, W. J., and Weis, W. I. (1997) Three-dimensional structure of the armadillo repeat region of β-catenin. *Cell*. **90**, 871–882

176. Felzien, L. K., Farrell, S., Betts, J. C., Mosavin, R., and Nabel, G. J. (1999) Specificity of cyclin E-Cdk2, TFIIB, and E1A interactions with a common domain of the p300 coactivator. *Mol Cell Biol*. **19**, 4241–4246

177. Nakajima, T., Uchida, C., Anderson, S. F., Lee, C. G., Hurwitz, J., Parvin, J. D., and Montminy, M. (1997) RNA helicase A mediates association of CBP with RNA polymerase II. *Cell*. **90**, 1107–1112

178. Brown, A. D., Cranstone, C., Dupré, D. J., and Langelaan, D. N. (2023) β-Catenin interacts with the TAZ1 and TAZ2 domains of CBP/p300 to activate gene transcription. *Int J Biol Macromol*. **238**, 124155

179. Brown, A. D., Vergunst, K. L., Branch, M., Blair, C. M., Dupré, D. J., Baillie, G. S., and Langelaan, D. N. (2023) Structural basis of CBP/p300 recruitment by the microphthalmia-associated transcription factor. *Biochim Biophys Acta Mol Cell Res.***1870**, 119520

180. Ferreon, J. C., Martinez-Yamout, M. A., Dyson, H. J., and Wright, P. E. (2009) Structural basis for subversion of cellular control mechanisms by the adenoviral E1A oncoprotein. *Proc Natl Acad Sci U S A*. **106**, 13260–13265

181. Williamson, M. P. (2018) Chemical Shift Perturbation Modern Magnetic Resonance. *Springer International Publishing*. Cham, Switzerland

182. Fuerer, C. and Iggo, R. (2002) Adenoviruses with Tcf binding sites in multiple early promoters show enhanced selectivity for tumour cells with constitutive activation of the wnt signaling pathway. *Gene Ther*. **9**, 270–281

183. Jung, H.-Y., Jun, S., Lee, M., Kim, H.-C., Wang, X., Ji, H., McCrea, P. D., and Park, J.-I. (2013) PAF and EZH2 induce Wnt/β-catenin signaling hyperactivation. *Mol Cell*. **52**, 193–205

184. Mas, C., Lussier-Price, M., Soni, S., Morse, T., Arseneault, G., Di Lello, P., Lafrance-Vanasse, J., Bieker, J. J., and Omichinski, J. G. (2011) Structural and functional characterization of an atypical activation domain in erythroid Kruppel-like factor (EKLF). *Proc Natl Acad Sci U S A*. **108**, 10484–10489

185. Teufel, D. P., Freund, S. M., Bycroft, M., and Fersht, A. R. (2007) Four domains of p300 each bind tightly to a sequence spanning both transactivation subdomains of p53. *Proc Natl Acad Sci U S A*. **104**, 7009–7014

186. Hibino, E., Inoue, R., Sugiyama, M., Kuwahara, J., Matsuzaki, K., and Hoshino, M. (2016) Interaction between intrinsically disordered regions in transcription factors Sp1 and TAF4. *Protein Sci*. **25**, 2006–2017

187. Sharma, R., Raduly, Z., Miskei, M., and Fuxreiter, M. (2015) Fuzzy complexes: specific binding without complete folding. *FEBS Letters*. **589**, 2533–2542

188. Hartman, M. L. and Czyz, M. (2015) MITF in melanoma: mechanisms behind its expression and activity. *Cell Mol Life Sci.* **72**, 1249–1260

189. Tassabehji, M., Newton, V. E., and Read, A. P. (1994) Waardenburg syndrome type 2 caused by mutations in the human microphthalmia (MITF) gene. *Nat Genet*. **8**, 251–255

190. Reddy, J., Fonseca, M. A. S., Corona, R. I., Nameki, R., Segato Dezem, F., Klein, I. A., Chang, H., Chaves-Moreira, D., Afeyan, L. K., Malta, T. M., Lin, X., Abbasi, F., Font-Tello, A., Sabedot, T., Cejas, P., Rodríguez-Malavé, N., Seo, J.-H., Lin, D.-C., Matulonis, U., Karlan, B. Y., Gayther, S. A., Pasaniuc, B., Gusev, A., Noushmehr, H., Long, H., Freedman, M. L., Drapkin, R., Young, R. A., Abraham, B. J., and Lawrenson, K. (2021) Predicting master transcription factors from pan-cancer expression data. *Sci Adv*. **7**, 6123

191. Yang, M., Liu, E., Tang, L., Lei, Y., Sun, X., Hu, J., Dong, H., Yang, S.-M., Gao, M., and Tang, B. (2018) Emerging roles and regulation of MiT/TFE transcriptional factors. *Cell Commun Signal*. **16**, 31

192. Steingrímsson, E., Copeland, N. G., and Jenkins, N. A. (2004) Melanocytes and the microphthalmia transcription factor network. *Annu Rev Genet*. **38**, 365–411

193. Lecoq, L., Raiola, L., Chabot, P. R., Cyr, N., Arseneault, G., Legault, P., and Omichinski, J. G. (2017) Structural characterization of interactions between transactivation domain 1 of the p65 subunit of NF-κB and transcription regulatory factors. *Nucleic Acids Res*. **45**, 5564–5576

194. Arany, Z., Sellers, W. R., Livingston, D. M., and Eckner, R. (1994) E1A-associated p300 and CREB-associated CBP belong to a conserved family of coactivators. *Cell*. **77**, 799–800

195. Bedford, D. C., and Brindle, P. K. (2012) Is histone acetylation the most important physiological function for CBP and p300. *Aging*. **4**, 247–255

196. Zhang, P., Torres, K., Liu, X., Liu, C.-G., and Pollock, R. E. (2016) An overview of chromatin-regulating proteins in cells. *Curr Protein Pept Sci*. **17**, 401–410

197. Dyson, J. H. and Wright, P. E. (2016) Role of intrinsic protein disorder in the function and interactions of the transcriptional coactivators CREB-binding protein (CBP) and p300. *J Biol Chem*. **10**, 692020

198. Lee, C. W., Ferreon, J. C., Ferreon, A. C. M., Arai, M., and Wright, P. E. (2010) Graded enhancement of p53 binding to CREB-binding protein (CBP) by multisite phosphorylation. *Proc Natl Acad Sci U S A*. **107**, 19290–19295

199. Green, M., Panesar, N. K., and Loewenstein, P. M. (2008) The transcription-repression domain of the adenovirus E1A oncoprotein targets p300 at the promoter. *Oncogene*. **27**, 4446–4455

200. Drdová, B. and Vachtenheim, J. (2004) Repression of the melanocyte-specific promoter of the microphthalmia-associated transcription factor by the adenoviral E1A 12S oncoprotein. *Folia Biol (Praha)*. **50**, 159–166

201. Potter, C. J., Tasic, B., Russler, E. V., Liang, L., and Luo, L. (2010) The Q system: a repressible binary system for transgene expression, lineage tracing, and mosaic analysis. *Cell*. **141**, 536–548

202. Cheung, M.-S., Maguire, M. L., Stevens, T. J., and Broadhurst, R. W. (2010) DANGLE: A Bayesian inferential method for predicting protein backbone dihedral angles and secondary structure. *J Magn Reson*. **202**, 223–233

203. Rieping, W., Habeck, M., Bardiaux, B., Bernard, A., Malliavin, T. E., and Nilges, M. (2007) ARIA2: automated NOE assignment and data integration in NMR structure calculation. *Bioinformatics*. **23**, 381–382

204. Bhattacharya, A., Tejero, R., and Montelione, G. T. (2007) Evaluating protein structures determined by structural genomics consortia. *Proteins*. **66**, 778–795

205. Brown, K. M., Day, J. P., Huston, E., Zimmermann, B., Hampel, K., Christian, F., Romano, D., Terhzaz, S., Lee, L. C. Y., Willis, M. J., Morton, D. B., Beavo, J. A., Shimizu-Albergine, M., Davies, S. A., Kolch, W., Houslay, M. D., and Baillie, G. S. (2013) Phosphodiesterase-8A binds to and regulates Raf-1 kinase. *Proc Natl Acad Scis*. **110**, E1533–E1542

206. Frank, R. (1992) Spot-synthesis: an easy technique for the positionally addressable, parallel chemical synthesis on a membrane support. *Tetrahedron*. **48**, 9217–9232

207. Amartely, H., Iosub-Amir, A., and Friedler, A. (2014) Identifying protein-protein interaction sites using peptide arrays. *J Vis Exp*. **10**, 3791-52097

208. Zhang, J. J., Vinkemeier, U., Gu, W., Chakravarti, D., Horvath, C. M., and Darnell, J. E. (1996) Two contact regions between Stat1 and CBP/p300 in interferon gamma signaling. *Proc Natl Acad Sci U S A*. **93**, 15092–15096

209. Paulson, M., Pisharody, S., Pan, L., Levy, D. E., Guadagno, S., and Mui, A. L. (1999) Stat protein transactivation domains recruit p300/CBP through widely divergent sequences. *J Biol Chem*. **274**, 25343–25349

210. Lee, C. W., Martinez-Yamout, M. A., Dyson, H. J., and Wright, P. E. (2010) Structure of the p53 transactivation domain in complex with the nuclear coactivator binding domain of CBP. *Biochem*. **49**, 9964–9971

211. Dai, P., Akimaru, H., Tanaka, Y., Hou, D. X., Yasukawa, T., Kanei-Ishii, C., Takahashi, T., and Ishii, S. (1996) CBP as a transcriptional coactivator of c-Myb. *Genes Dev.* **10**, 528–540

212. Gibbs, E. B., Cook, E. C., and Showalter, S. A. (2017) Application of NMR to studies of intrinsically disordered proteins. *Arch Biochem Biophys*. **628**, 57–70

213. D'Silva, L., Ozdowy, P., Krajewski, M., Rothweiler, U., Singh, M., and Holak, T. A. (2005) Monitoring the effects of antagonists on protein−protein interactions with NMR spectroscopy. *J Am Chem Soc.* **127**, 13220–13226

214. Feng, H., Miller Jenkins, L. M., Durell, S. R., Hayashi, R., Mazur, S. J., Cherry, S., Tropea, J. E., Miller, M., Wlodawer, A., Appella, E., and Bai, Y. (2009) Structural basis for p300 Taz2/p53 TAD1 binding and modulation by phosphorylation. *Structure*. **17**, 202–210

215. Miller, M., Dauter, Z., Cherry, S., Tropea, J. E., and Wlodawer, A. (2009) Structure of the TAZ2 domain of p300: insights into ligand binding. *Acta Crystallogr D Biol Crystallogr*. **65**, 1301–1308

216. Risør, M. W., Jansma, A. L., Medici, N., Thomas, B., Dyson, H. J., and Wright, P. E. (2021) Characterization of the high-affinity fuzzy complex between the disordered domain of the E7 oncoprotein from high-risk HPV and the TAZ2 domain of CBP. *Biochem*. **60**, 3887–3898

217. Palopoli, N., González Foutel, N. S., Gibson, T. J., and Chemes, L. B. (2018) Short linear motif core and flanking regions modulate retinoblastoma protein binding affinity and specificity. *Protein Eng Des Sel*. **31**, 69–77

218. Chemes, L. B., Sánchez, I. E., Smal, C., and de Prat-Gay, G. (2010) Targeting mechanism of the retinoblastoma tumor suppressor by a prototypical viral oncoprotein. *FEBS J*. **277**, 973–988

219. Murrali, M. G., Felli, I. C., and Pierattelli, R. (2020) Adenoviral E1A exploits flexibility and disorder to target cellular proteins. *Biomolecules*. **10**, 1541

220. Bismuth, K., Maric, D., and Arnheiter, H. (2005) MITF and cell proliferation: the role of alternative splice forms. *Pigment Cell Res*. **18**, 349–359

221. Wu, M., Hemesath, T. J., Takemoto, C. M., Horstmann, M. A., Wells, A. G., Price, E. R., Fisher, D. Z., and Fisher, D. E. (2000) c-Kit triggers dual phosphorylations, which couple activation and degradation of the essential melanocyte factor Mi. *Genes Dev*. **14**, 301–312

222. Louphrasitthiphol, P., Siddaway, R., Loffreda, A., Pogenberg, V., Friedrichsen, H., Schepsky, A., Zeng, Z., Lu, M., Strub, T., Freter, R., Lisle, R., Suer, E., Thomas, B., Schuster-Böckler, B., Filippakopoulos, P., Middleton, M., Lu, X., Patton, E. E., Davidson, I., Lambert, J.-P., Wilmanns, M., Steingrímsson, E., Mazza, D., and Goding, C. R. (2020) Tuning transcription factor availability through acetylation-mediated genomic redistribution. *Mol Cell*. **79**, 472-487.e10

223. Kim, S., Song, H.-S., Yu, J., and Kim, Y.-M. (2021) MiT Family Transcriptional factors in immune cell functions. *Mol Cells*. **44**, 342–355

224. Goding, C. R., and Arnheiter, H. (2019) MITF—the first 25 years. *Genes Dev.* **33**, 983–1007

225. Hemesath, T. J., Steingrímsson, E., McGill, G., Hansen, M. J., Vaught, J., Hodgkinson, C. A., Arnheiter, H., Copeland, N. G., Jenkins, N. A., and Fisher, D. E. (1994) Microphthalmia, a critical factor in melanocyte development, defines a discrete transcription factor family. *Genes Dev*. **8**, 2770–2780

226. Ballesteros-Álvarez, J., Dilshat, R., Fock, V., Möller, K., Karl, L., Larue, L., Ögmundsdóttir, M. H., and Steingrímsson, E. (2020) MITF and TFEB cross-regulation in melanoma cells. *PLOS ONE*. **15**, e0238546

227. Martina, J. A., Diab, H. I., Li, H., and Puertollano, R. (2014) Novel roles for the MiTF/TFE family of transcription factors in organelle biogenesis, nutrient sensing, and energy homeostasis. *Cell Mol Life Sci*. **71**, 2483–2497

228. Amiel, J., Watkin, P. M., Tassabehji, M., Read, A. P., and Winter, R. M. (1998) Mutation of the MITF gene in albinism-deafness syndrome (Tietz syndrome). *Clinical Dysmorphology*. **7**, 17

229. Yu, F., Lu, Y., Zhong, Z., Qu, B., Wang, M., Yu, X., and Chen, J. (2021) MITF involved in innate immunity by activating tyrosinase-mediated melanin synthesis in Pteria penguin. *Front Immunol*. **12**, 626493

230. Hoek, K. S., Schlegel, N. C., Eichhoff, O. M., Widmer, D. S., Praetorius, C., Einarsson, S. O., Valgeirsdottir, S., Bergsteinsdottir, K., Schepsky, A., Dummer, R., and Steingrimsson, E. (2008) Novel MITF targets identified using a two-step DNA microarray strategy. *Pigment Cell Melanoma Res*. **21**, 665–676

231. Vachtenheim, J., and Drdová, B. (2004) A dominant negative mutant of microphthalmia transcription factor (MITF) lacking two transactivation domains suppresses transcription mediated by wild type MITF and a hyperactive MITF derivative. *Pigment Cell Res*. **17**, 43–50

232. García-Nafría, J., Watson, J. F., and Greger, I. H. (2016) IVA cloning: A single-tube universal cloning system exploiting bacterial In Vivo Assembly. *Sci Rep*. **6**, 27459

233. Dyson, H. J. (2016) Making sense of intrinsically disordered proteins. *Biophys J*. **110**, 1013–1016

234. Chhabra, S., Fischer, P., Takeuchi, K., Dubey, A., Ziarek, J. J., Boeszoermenyi, A., Mathieu, D., Bermel, W., Davey, N. E., Wagner, G., and Arthanari, H. (2018) ^{15}N detection harnesses the slow relaxation property of nitrogen: Delivering enhanced resolution for intrinsically disordered proteins. *Proc. Natl. Acad. Sci. U.S.A.* **10**, 1073

235. Dunker, A. K., Obradovic, Z., Romero, P., Garner, E. C., and Brown, C. J. (2000) Intrinsic protein disorder in complete genomes. *Genome Inform Ser Workshop Genome Inform*. **11**, 161–171

236. Raj, N., and Attardi, L. D. (2017) The transactivation domains of the p53 protein. *Cold Spring Harb Perspect Med*. **7**, a026047

237. Andresen, C., Helander, S., Lemak, A., Farès, C., Csizmok, V., Carlsson, J., Penn, L. Z., Forman-Kay, J. D., Arrowsmith, C. H., Lundström, P., and Sunnerhagen, M. (2012) Transient structure and dynamics in the disordered c-Myc transactivation domain affect Bin1 binding. *Nucleic Acids Res*. **40**, 6353–6366

238. Brodsky, S., Jana, T., and Barkai, N. (2021) Order through disorder: The role of intrinsically disordered regions in transcription factor binding specificity. *Curr Opin Struct Biol*. **71**, 110–115

239. Philip, P., Boija, A., Vaid, R., Churcher, A. M., Meyers, D. J., Cole, P. A., Mannervik, M., and Stenberg, P. (2015) CBP binding outside of promoters and enhancers in Drosophila melanogaster. *Epigenetics Chromatin*. **8**, 48

240. Maity, S., Gundampati, R. K., and Suresh Kumar, T. K. (2019) NMR methods to characterize protein-ligand interactions. *Natural Product Communications*. **14**, 1934578-19849296

241. Teilum, K., Kunze, M. B. A., Erlendsson, S., and Kragelund, B. B. (2017) Spinning down protein interactions by NMR. *Protein Sci*. **26**, 436–451

242. Chin, K.-C., Li, G. G.-X., and Ting, J. P.-Y. (1997) Importance of acidic, proline/serine/threonine-rich, and GTPbinding regions in the major histocompatibility complex class II transactivator: generation of transdominant-negative mutants. *Proc Natl Acad Sci*. **94**, 2501–2506

243. Artandi, S. E., Merrell, K., Avitahl, N., Wong, K. K., and Calame, K. (1995) TFE3 contains two activation domains, one acidic and the other proline-rich, that synergistically activate transcription. *Nucleic Acids Res*. **23**, 3865–3871

244. Kawata, Y., Suzuki, H., Higaki, Y., Denisenko, O., Schullery, D., Abrass, C., and Bomsztyk, K. (2002) BCN-1 element-dependent activation of the laminin γ1 chain gene by the cooperative action of transcription factor E3 (TFE3) and smad proteins. *J Biol Chem*. **277**, 11375–11384

245. Wang, C., Zhao, L., Su, Q., Fan, X., Wang, Y., Gao, S., Wang, H., Chen, H., Chan, C. B., and Liu, Z. (2016) Phosphorylation of MITF by AKT affects its downstream targets and causes TP53-dependent cell senescence. *Int J Biochem Cell Biol*. **80**, 132–142

246. Lambert, M., Jambon, S., Depauw, S., and David-Cordonnier, M.-H. (2018) Targeting transcription factors for cancer treatment. *Molecules*. **23**, 1479

247. Darnell, J. E. (2002) Transcription factors as targets for cancer therapy. *Nat Rev Cancer*. **2**, 740–749

248. Su, B. G. and Henley, M. J. (2021) Drugging fuzzy complexes in transcription. *Front Mol Biosci*.

249. Bushweller, J. H. (2019) Targeting transcription factors in cancer - from undruggable to reality. *Nat Rev Cancer*. **19**, 611–624

250. He, Z.-X., Wei, B.-F., Zhang, X., Gong, Y.-P., Ma, L.-Y., and Zhao, W. (2021) Current development of CBP/p300 inhibitors in the last decade. *Euro J Med Chem*. **209**, 112861

251. Henchey, L. K., Kushal, S., Dubey, R., Chapman, R. N., Olenyuk, B. Z., and Arora, P. S. (2010) Inhibition of hypoxia inducible factor 1–transcription coactivator interaction by a hydrogen bond surrogate α-helix. *J Am Chem Soc*. **132**, 941–943

252. Ramaswamy, K., Forbes, L., Minuesa, G., Gindin, T., Brown, F., Kharas, M. G., Krivtsov, A. V., Armstrong, S. A., Still, E., de Stanchina, E., Knoechel, B., Koche, R., and Kentsis, A. (2018) Peptidomimetic blockade of MYB in acute myeloid leukemia. *Nat Commun*. **9**, 110

253. Schulte, C., Khayenko, V., Nordblom, N. F., Tippel, F., Peck, V., Gupta, A. J., and Maric, H. M. (2021) High-throughput determination of protein affinities using unmodified peptide libraries in nanomolar scale. *iScience*. **24**, 101898

254. Wang, L., Wang, N., Zhang, W., Cheng, X., Yan, Z., Shao, G., Wang, X., Wang, R., and Fu, C. (2022) Therapeutic peptides: current applications and future directions. *Sig Transduct Target Ther*. **7**, 1–27

255. Giri, N. C. (2022) Protein and peptide drug delivery. *Drug Deliv.* **10**, 5772

256. Dan, N., Samanta, K., and Almoazen, H. (2020) An update on pharmaceutical strategies for oral delivery of therapeutic peptides and proteins in adults and pediatrics. *Children*. **7**, 307